

A role for mitotic SUMOylation in establishing nuclear envelope structure

by

Natasha Olivia Saik

A thesis submitted in partial fulfillment of the requirements for the degree of

Doctor of Philosophy

Department of Cell Biology
University of Alberta

© Natasha Olivia Saik, 2022

Abstract

The compartmentalization of subcellular functions facilitates the regulation of biochemical reactions and cellular processes. The compartmentalization of the eukaryotic genome into the nucleus by the nuclear envelope (NE), for example, facilitates various DNA metabolic activities. The NE is composed of two lipid bilayers: an outer nuclear membrane (ONM) and an inner nuclear membrane (INM). The INM provides an environment for the proper regulation and organization of interacting chromatin. In *Saccharomyces cerevisiae*, INM-associated chromatin includes telomeres and specific transcriptionally active genes. Multiple mechanisms are employed to tether these chromatin regions to the INM, including post-translational modifications. SUMOylation is a post-translational modification linked to regulating the spatial organization of chromatin relative to the nuclear periphery. Therefore, we investigated the contributions of SUMOylation in mediating chromatin interactions with the INM in response to specific cellular events. We observed that activation of an inducible gene, *INO1*, is accompanied by alterations in the SUMOylation of proteins associated with specific regions along the *INO1* locus. Furthermore, we show that the E3 SUMO ligase, Siz2, is required to facilitate these SUMOylation events and target the *INO1* locus to the INM. Following these analyses, we further investigated Siz2 and Siz2-mediated SUMOylation events at the INM.

We found that Siz2 is predominantly distributed throughout the nucleoplasm during interphase but is recruited to the INM during mitosis, where it binds and SUMOylates several proteins, including Scs2. Scs2 is an integral

membrane protein found throughout the endoplasmic reticulum (ER), and by analyses here, the INM. We show that a putative FFAT motif in Siz2 is required to interact with the MSP domain of Scs2. These interactions are further supported by the mitotic phosphorylation of Siz2 and the SUMOylation of Scs2 by Siz2. Formation of the Scs2-Siz2 complex at the INM during mitosis drives the accumulation of SUMO conjugates at the INM, including SUMOylated Scs2 and other specific proteins. The mitotic SUMOylation of these proteins supports the assembly and anchorage of subtelomeric chromatin and the activated *INO1* at the INM during the later stages of mitosis and the subsequent G1-phase. The mitotic SUMOylation of these specific proteins is also required for the proliferation of the NE. These SUMOylation events facilitate the accumulation of phosphatic acid (PA) at the INM during mitosis by altering specific protein interactions of PA metabolism regulators. In summary, we have uncovered previously undefined spatial and temporally regulated SUMOylation events mediated by Siz2 at the NE during mitosis. These events function to support and coordinate multiple processes necessary for establishing nuclear envelope structure, including chromatin association with the NE and membrane proliferation.

Preface

A version of Chapter III of this thesis has been previously published in: **Saik, N.O., Park, N., Ptak, C., Adames, N., Aitchison, J.D., and R.W. Wozniak. (2020) Recruitment of an Activated Gene to the Yeast Nuclear Pore Complex Requires Sumoylation. Front Genet. 2020 11:174.** I was responsible for concept formation, data collection and analysis, and manuscript composition. N. Park, C. Ptak, and myself contributed equally to this work as co-first authors. I have indicated their data contributions in the corresponding figures. N. Adames contributed to original observations and concept formation. R. Wozniak was the supervisory author. R. Wozniak and J. Aitchison involved with concept formation, manuscript formation, and data analysis. All authors performed editing of the final manuscript.

A version of Chapter IV of this thesis has been previously published in: **Ptak, C., Saik, N.O., Premashankar, A., Lapetina, D.L., Aitchison, J.D., Montpetit, B., and R.W. Wozniak. (2021) Phosphorylation-dependent mitotic SUMOylation drives nuclear envelope-chromatin interactions. J Cell Biol. 2021 6;220(12):e202103036.** I was responsible for concept formation, data collection and analysis, and manuscript composition. C. Ptak and myself contributed equally to this work as co-first authors. I have indicated specific data contributions in the corresponding figures. A. Premashankar assisted with data collection and analysis which I have also indicated in the corresponding figures. D.L. Lapetina contributed to original observations and concept formation. R. Wozniak was the supervisory author. R. Wozniak, B. Montpetit, and J. Aitchison were involved with concept formation, manuscript composition, and data analysis.

Acknowledgments

My time in graduate school and this thesis would not be complete without the support and guidance of my friends, family, and many individuals that I had the privilege to engage and learn from throughout my studies. First and foremost, I would like to acknowledge and thank Dr. Wozniak, or Woz as I will forever address you, for providing me with the opportunity to study and learn in your lab. Under your supervision and mentorship, I have grown as a person and scientist. Your intensity and passion for science have inspired me to question what is known, what can be done better, and what else can be learned. Under your guidance, I truly feel I have become a scientist. I feel incredibly privileged to have learned from you and to have been part of your lab.

I would also like to thank and acknowledge all current and past members of the Wozniak lab who have contributed to my learning and development over the years. The personal and professional support that I received from everyone has provided me with a wonderful graduate school experience. In particular, I would like to thank Dr. Lapetina and Dr. Makio for taking the time to teach me experimental techniques and providing insightful feedback on experimental protocols and results. I would like to particularly thank and extend my utmost gratitude towards Dr. Ptak. I no doubt owe all of my success during my studies to you. Your compelling scientific discussions and input has guided my learning and research. Thank you for taking the time to mentor me throughout the years and allowing me to contribute to the project you started.

I would also like to thank the members of my graduate committee, Dr. Montpetit and Dr. Hendzel. Your guidance and insightful feedback have been enormously helpful throughout my graduate studies. I would also like to extend my gratitude to all the staff, students, and faculty of the Department of Cell Biology. Thank you for providing a collaborative research environment and for the continued support over the years, both professionally and personally.

Finally, I would like to thank my loving family, who have provided me with an abundance of support and guidance over the years. In particular, I would like to thank my parents for looking up everything and anything related to my research and for being willing to do anything for me. I would also like to thank my wonderful partner Arthur who has been the calming force in my life. You always know how to set me back on course and help me refocus. Thank you for late-night and weekend drop-offs at the lab and for always understanding that experiments never end on time. I am eternally grateful to everyone who has supported me through my graduate studies. Thank you.

Table of Contents

Abstract.....	ii
Preface	iv
Acknowledgments.....	v
Table of Contents.....	vii
List of Tables	xi
List of Figures.....	xii
List of Symbols, Abbreviations and Nomenclature	xv
Chapter I: Introduction	1
1.1 The nuclear envelope	2
1.1.1 Nuclear pore complexes.....	3
1.1.2 The proteome of the INM	5
1.1.3 The NE during mitosis	7
1.2 NE/ER membrane expansion.....	9
1.2.1 Phospholipid synthesis during mitosis.....	9
1.2.2 Pah1 and lipins.....	12
1.2.3 The Nem1/Spo7 complex	14
1.2.4 Pah1-Nem1/Spo7 and membrane expansion	14
1.2.4.1 The Henry regulatory circuit.....	15
1.2.5 Phospholipid synthesis at the INM	16
1.3 Spatial organization of the genome.....	18
1.3.1 The spatial organization of the genome at the nuclear periphery	21
1.4 Transcriptionally active chromatin at NPCs	24
1.4.1 Yeast inducible genes	25
1.5 Telomeres.....	28
1.5.1 Telomere structure in yeast.....	28
1.5.2 Telomere silencing in yeast	31
1.5.3 Telomere anchoring to the INM in yeast	33
1.6 SUMOylation.....	36
1.6.1 SUMO and SUMOylated proteins	36
1.6.2 SUMO Conjugation	38
1.6.3 SUMO E3 ligases.....	40

1.6.4 SUMO Proteases	42
1.6.5 Molecular Consequences of SUMOylation	44
1.6.5.1 SUMO:SIM interactions	45
1.6.6 SUMOylation and the NE	46
1.6.6.1 SUMOylation and transcriptional activation	48
1.6.6.2 SUMOylation and telomeres.....	49
1.7 Thesis focus	50
Chapter II: Experimental Procedures	53
2.1 Yeast strains and media	54
2.2 Plasmids	70
2.3 Antibodies	73
2.5 Affinity purification of His8 SUMO fusion proteins.....	76
2.5 Western Blotting	77
2.6 Phosphatase treatment.....	77
2.8 Cdc20 shutoff.....	79
2.9 <i>INO1</i> induction.....	79
2.10 FACs analysis	79
2.11 RT-qPCR	80
2.12 RNA Seq.....	82
2.13 Subtelomeric gene-silencing assay	83
2.14 Chromatin Immunoprecipitation.....	84
2.14 Immunofluorescence.....	87
2.15 Epifluorescence microscopy	88
2.15.1 Image analysis.....	89
Chapter III: Recruitment of an activated gene to the yeast nuclear pore complex requires SUMOylation*	92
3.1 Overview.....	93
3.2 Results.....	94
3.2.1 Ulp1 interacts with activated <i>INO1</i>	94
3.2.2 NPC recruitment and expression of <i>INO1</i> requires Ulp1 isopeptidase activity at the NPC.....	96
3.2.3 Repression of <i>INO1</i> is maintained by SUMOylation.....	104
3.2.4 The SUMO ligase Siz2 is required for the recruitment of <i>INO1</i> to NPCs.	107
3.2.5 Siz2 protein levels regulate the recruitment of the <i>INO1</i> locus to NPCs.....	112

3.3 Discussion.....	118
Chapter IV: Phosphorylation-dependent mitotic SUMOylation drives nuclear envelope-chromatin interactions*	123
4.1 Overview.....	124
4.2 Results.....	125
4.2.1 NE associated SUMOylation events occur during mitosis.	125
4.2.2 Mitotic SUMOylation events at the NE are dependent on Siz2.....	125
4.2.3 Mitotic phosphorylation facilitates Siz2 enrichment at the NE.	131
4.2.4 Scs2 is an INM-associated receptor of Siz2 during mitosis.....	135
4.2.5 Scs2 is a mitotic SUMOylation target of Siz2.	153
4.2.6 SUMO:SIM interactions enhance the mitotic enrichment of Siz2 at the NE.....	156
4.2.7 Siz2-dependent SUMOylation events at the NE during mitosis re-establish chromatin-NE interactions.	161
4.2.8 Siz2-mediated SUMOylation of Sir4 regulates mitotic tethering of telomeres to the NE.	167
4.2.9 Siz2-mediated SUMOylation of Sir4 stabilizes Sir4 association with subtelomeric chromatin during mitosis.	173
4.2.10 The Scs2-Siz2 complex facilitates the association of subtelomeric chromatin to the NE independently of silencing.....	183
4.2.11 Siz2-dependent SUMOylation events regulate the transcription of transposons.	184
4.3 Discussion.....	191
Chapter V: Nuclear envelope associated SUMOylation events regulate nuclear membrane expansion during mitosis.....	200
5.1 Overview.....	201
5.2.1 NE association of Siz2 during mitosis supports NE expansion.	202
5.2.2 Directing Siz2 to the INM is sufficient to induce NE expansion.....	208
5.2.3 Siz2-mediated SUMOylation increases INM levels of phosphatidic acid during mitosis.	216
5.2.4 Siz2-directed NE expansion is antagonized by the <i>pah1</i> ^{7A} mutation.	220
5.2.5 Siz2 regulates the interactions of Pah1, Nem1, and Spo7.....	226
5.3 Discussion.....	239
Chapter VI: Perspectives	248
6.1 Synopsis.....	249
6.2 Mitotic SUMOylation at the INM may establish the INM proteome.	249

6.3 Siz2-mediated SUMOylation at the INM functionally connects chromatin binding to the INM with NE expansion.	251
6.4 Scs2 is an essential receptor at different subcellular compartments.	253
6.5 SUMOylation at the INM during mitosis may be regulating other biological processes.	256
References	259

List of Tables

Table 2-1. Yeast strains.....	55
Table 2-2. Plasmids.....	71
Table 2-3. Oligonucleotides used in RT-qPCR	82
Table 2-4. Oligonucleotides used in qPCR.....	86
Table 4-1. Genes representing SUMOylated proteins 40-55kDa in size that were deleted to investigate alterations to SUMOylation profiles.....	136
Table 4-2. Up-regulated ORFs in asynchronously grown <i>siz2^{SS22/527A}</i> cells.....	186
Table 4-3. Down-regulated ORFs in asynchronously grown <i>siz2^{SS22/527A}</i> cells.....	188

List of Figures

Figure 1-1. Schematic representation of phosphatic acid regulation in <i>S. cerevisiae</i>	11
Figure 1-2. Schematic representation of telomere tethering mechanisms at the NE in <i>S. cerevisiae</i>	35
Figure 1-3. SUMO maturation and targeting in <i>S. cerevisiae</i>	39
Figure 3-1. Ulp1 interacts with the induced <i>INO1</i> gene.	95
Figure 3-2. Ulp1 association with NPCs is required for NE-association and expression of <i>INO1</i> following induction.	98
Figure 3-3. Tethering of the C-terminal domain of Ulp1 to the NPC supports NE-association and expression of <i>INO1</i> following induction.	101
Figure 3-4. Ulp1 catalytic activity is required at the nuclear periphery to facilitate the NE-association of <i>INO1</i> upon induction.	102
Figure 3-5. Artificially tethering the C-terminal domain of Ulp1 to the NPC rescues the <i>INO1</i> NE-association and transcriptional defects of <i>nup2Δ</i> and <i>nup60Δ</i> cells.	103
Figure 3-6. SUMOylation of <i>INO1</i> -associated proteins is altered upon <i>INO1</i> induction.	106
Figure 3-7. The SUMO E3 ligase Siz2 is required for NE-association of <i>INO1</i> following induction.	108
Figure 3-8. SUMOylation of <i>INO1</i> -associated proteins is dependent on Siz2.	110
Figure 3-9. Siz2 interacts with the induced <i>INO1</i> locus.	111
Figure 3-10. Loss of Ulp1 association with NPCs reduces Siz2 and Siz2-mediated SUMOylation events.....	114
Figure 3-11. Exogenously expressing Siz2 rescues the <i>INO1</i> NE-association defects of <i>ulp1Δ₁₋₃₄₀</i> cells.....	116
Figure 3-12. Model for the role of SUMOylation and deSUMOylation in <i>INO1</i> NE-association and expression following induction.	117
Figure 4-1. SUMOylation events are enriched at the NE during mitosis.	126
Figure 4-2. The mitotic enrichment of SUMO conjugates at the NE is dependent on Siz2.	127
Figure 4-3. The enrichment of specific mitotic SUMOylation events is dependent on Siz2.	129
Figure 4-4. Siz2 is enriched at the NE during mitosis.	130
Figure 4-5. Siz2 is phosphorylated during mitosis.	132
Figure 4-6. The mitotic phosphorylation of Siz2 at residue 522, is required for mitotic SUMOylation events at the NE.....	134
Figure 4-7. Scs2 is required for mitotic SUMOylation events at the NE.	145
Figure 4-8. Scs2 is required for the mitotic enrichment of Siz2 at the NE.	149

Figure 4-9. Interactions between Scs2 and Siz2 are regulated through MSP:FFAT interactions.....	151
Figure 4-10. Scs2 is localized to the INM.	152
Figure 4-11. Scs2 is a mitotic SUMOylation target of Siz2.	155
Figure 4-12. SUMOylation of Scs2 is required for the mitotic enrichment of Siz2 to the INM.....	158
Figure 4-13. Interactions with SUMOylated targets at the INM enhances the mitotic enrichment of Siz2 to the INM.	160
Figure 4-14. Siz2-mediated mitotic SUMOylation events are required for the NPC association of <i>INO1</i> following induction.	162
Figure 4-15. Siz2 and Scs2 are required for NE-association of telomeres during M- and G1-phase.	164
Figure 4-16. Siz2-mediated mitotic SUMOylation events are required for NE-association of telomeres during M- and G1-phase.	166
Figure 4-17. Siz2 does not interact with subtelomeric chromatin.	168
Figure 4-18. Sir4 is required for telomere tethering during M-phase.....	169
Figure 4-19. Mitotic enrichment of Siz2 to the NE facilitates the SUMOylation of Sir4.	171
Figure 4-20. Siz2-mediated SUMOylation of Sir4 regulates telomere tethering to the NE.	172
Figure 4-21. NE-association of Sir4 is unaltered by Siz2-mediated SUMOylation.	176
Figure 4-22. Sir4 association with subtelomeric chromatin requires Siz2.....	177
Figure 4-23. Siz2-mediated mitotic SUMOylation facilitates Sir4 association with subtelomeric chromatin.....	179
Figure 4-24. Siz2-mediated mitotic SUMOylation facilitates Sir3 association with subtelomeric chromatin.....	180
Figure 4-25 Siz2-mediated mitotic SUMOylation re-establishes Sir4 association with subtelomeric chromatin following S-phase.....	182
Figure 4-26. Siz2-dependent SUMOylation events do not regulate subtelomeric gene expression.	185
Figure 4-27. A model for Scs2-Siz2 dependent mitotic SUMOylation at the INM and its role in chromatin recruitment.....	190
Figure 5-1. NE association of Siz2 during mitosis supports NE expansion.	205
Figure 5-2. Siz2 localization and Siz2-mediated SUMOylation events at the NE during mitosis.....	207
Figure 5-3. Constitutive targeting of Siz2 to the NE induces SUMOylation and increases nuclear surface area.....	210

Figure 5-4. Siz2 enrichment at the INM is restricted to mitosis in <i>ulp1</i> ^{K352E/Y583H} mutant cells.	213
Figure 5-5. Siz2-mediated SUMOylation events are enrichment at the INM at all cell cycle stages in <i>ulp1</i> ^{K352E/Y583H} mutant cells.	214
Figure 5-6. Ulp1-dependent deSUMOylation at the INM restricts nuclear membrane expansion.	215
Figure 5-7. The NE association of Siz2 during mitosis supports the enrichment of PA at the INM.	217
Figure 5-8. PA enrichment at the INM is dependent on Siz2-mediated SUMOylation events.	219
Figure 5-9. Pah1 activity antagonizes Siz2-mediated increases in nuclear surface area.	223
Figure 5-10. Effects of <i>pah1</i> ^{7A} on PA and nuclear surface area.	225
Figure 5-11. Mitotic SUMOylation events reduce Pah1 interactions with the Spo7/Nem1 complex.	227
Figure 5-12. Mitotic SUMOylation events reduce interactions between Spo7 and Nem1.	229
Figure 5-13. Siz2-mediated SUMOylation events reduce Spo7 interactions with Pah1 and Nem1.	230
Figure 5-14. Pah1 membrane association can suppress the increased nuclear surface area of mitotically delayed cells.	234
Figure 5-15. Pah1 membrane association can suppress NE expansion phenotypes of <i>ulp1</i> ^{K352E/Y583H} mutant cells.	236
Figure 5-16. Effects of Pah1 membrane association on PA and nuclear surface area.	238

List of Symbols, Abbreviations and Nomenclature

μ	micro
μm	microns/micrometres
μg	micrograms
μL	microlitres
$^{\circ}\text{C}$	degrees celsius
5-FOA	5-fluoroorotic acid
ATP	adenosine triphosphate
bp	base pairs
CDP-DAG	cytidine diphosphate-diacylglycerol
ChIP	chromatin immunoprecipitation
CSDN	catalytically dead
CTP	cytidine triphosphate
DAG	diacylglycerol
DNA	deoxyribonucleic acid
ECL	enhanced chemiluminescence
ER	endoplasmic reticulum
FA	fatty acid
FACs	fluorescence-activated single cell sorting
FFAT	two phenylalanines in an acidic tract
FG	phenylalanine glycine
FI	fluorescence intensity
Fig	figure
g	grams
G1	gap 1 phase
G2	gap 2 phase
GFP	green fluorescent protein
GRS	gene recruitment sequence
h	hours
IgG	immunoglobulin G
IGR	intergenic region
IF	immunofluorescence
INM	inner nuclear membrane
kDa	kilodalton
LacI	lactose repressor
lacO	lactose operator
LAD	lamina-associated domains
m	milli
M	molarity/mega
mCherry	monomeric cherry
mg	milligrams
min	minutes
mL	millilitres
M-phase	mitotic phase
mRNA	messenger ribonucleic acid

MRS	Memory recruitment sequence
MSP	major sperm protein
n	number
NAD	nicotinamide adenine dinucleotide
NE	nuclear envelope
NEBD	nuclear envelope breakdown
NES	nuclear export signal
NDSM	negatively charged amino acid dependent SUMOylation motif
NLS	nuclear localization signal
NPC	nuclear pore complex
Nup	nucleoporin
OD	optical density
ONM	outer nuclear membrane
ORF	open reading frame
PA	phosphatidic acid
PC	phosphatidylcholine
PE	phosphatidylethanolamine
PCR	polymerase chain reaction
PDSM	phosphorylation dependent SUMOylation motif
PI	phosphatidylinositol
PIC	preinitiation complex
PL	phospholipid
POM	pore membrane
Pom	pore membrane protein
Pol	polymerase
PrA	Protein A
PS	phosphatidylserine
qPCR	quantitative real-time PCR
rDNA	ribosomal DNA
RFP	red fluorescent protein
RNA	ribonucleic acid
RT	room temperature
RT-qPCR	real time qPCR
<i>S. cerevisiae</i>	<i>Saccharomyces cerevisiae</i>
<i>S. pombe</i>	<i>Schizosaccharomyces pombe</i>
S-phase	synthesis phase
SC	synthetic complete media
SD	standard deviation
SDS-PAGE	sodium dodecyl sulfate polyacrylamide gel electrophoresis
sec	seconds
SEM	Standard error of the mean
SIM	SUMO interacting motif
SIR	silent information regulator
SPB	spindle pole body

SUMO	small ubiquitin like modifier
TAD	topologically associating domains
TAG	Triacylglycerols
TCA	trichloroacetic acid
Tel	telomere
tRNA	transfer ribonucleic acid
TSF	transcription factor
UAS _{INO}	Inositol-responsive upstream activating sequence
UTR	untranslated region
VAP	vesicle-associated membrane protein (VAMP)- associated protein
WT	wild type
YPD	yeast extract peptone dextrose media

Chapter I: Introduction

1.1 The nuclear envelope

Within eukaryotic cells, specific cellular processes are compartmentalized into membrane-bound organelles. One such organelle is the nucleus, which encapsulates the eukaryotic genome and all DNA dependent processes. The nucleus is bounded by a double lipid membrane termed the nuclear envelope (NE). The NE establishes a barrier between the nucleoplasm and cytoplasm and provides a level of regulatory control over the genome. The two lipid bilayers of the NE include an outer nuclear membrane (ONM) and an inner nuclear membrane (INM), which are separated by a luminal or perinuclear space. The ONM is exposed to the cytosol and is continuous with the endoplasmic reticulum (ER; Watson, 1955). The membrane continuity between the ONM and the ER allows lipids synthesized in the ER to diffuse to the NE. This continuity also results in the ONM having a similar proteome as the ER. However, the ONM also contains proteins not enriched in the ER (Hetzer, Walther, and Mattaj 2005), including those that mediate interactions with the cytoskeleton (Dreger et al., 2001) and interact with proteins at the INM through the NE luminal space (Starr and Han 2003; Wilhelmssen et al., 2006). The INM is exposed to the nucleoplasm and contains a proteome that is largely distinct from the proteome of the ONM. However, the INM proteome can also include proteins that are also distributed through the INM and ER (Deng and Hochstrasser 2006; Smoyer et al., 2016). The proteome of the INM is retained, in part, through interactions with chromatin. Interactions of the INM proteome with chromatin can influence chromatin structure, gene expression, and the spatial organization of the genome (Strambio-De-Castillia, Niepel, and Rout 2010; Van de Vosse et al., 2011).

Factors contributing to the spatial organization of the genome and the functional consequences of this organization will be discussed in 1.3.

Despite functioning as a critical barrier to segregate the genome from the cytoplasm, proper cellular functions also require communication between the nucleoplasm and cytoplasm. Pore membrane domains (POMs) and nuclear pore complexes (NPCs) provide a means to overcome the barrier established by the NE, allowing materials to move into and out of the nucleus. POMs are membranes where the INM and ONM are continuous; this generates a channel across the NE into which NPCs are situated. NPCs regulate the bi-directional transport of macromolecules into and out of the nucleus. The NPCs are discussed in greater detail below (1.1.1).

1.1.1 Nuclear pore complexes

NPCs are large protein complexes that are exceptionally well conserved among eukaryotes (Q. Yang, Rout, and Akey 1998; Rout et al., 2000; Kabachinski and Schwartz 2015). NPCs are composed of approximately 30 different proteins, collectively referred to as nucleoporins or Nups. Nups are present in multiple copies within the NPC and can be broadly partitioned into three groups based on their localization and associated function within NPCs. These include Poms, core scaffold Nups, and FG-Nups. Poms are integral membrane proteins positioned within the POMs that recruit soluble Nups and anchor the NPC to the NE (Aitchison and Rout 2012; Kabachinski and Schwartz 2015; Onischenko et al., 2009). Core scaffold Nups form the eightfold symmetrical framework of the NPC that interacts with FG-Nups and Poms (Rout et al., 2000). Core scaffold Nups stabilize and

anchor the NPC to the NE and facilitate the membrane curvature observed at the POMs (Alber et al., 2007; H. Wang et al., 2016). FG-Nups are unstructured Nups containing phenylalanine-glycine (FG) repeats. FG-Nups line the central channel of NPCs forming a dense barrier which facilitates the selective passage of molecules into and out of the nucleus. Cargos smaller than ~10 nm can freely diffuse through this channel. However, larger macromolecules require specific amino acid sequence motifs, termed nuclear localization sequences (NLSs) or nuclear export sequences (NESs), and nuclear transport factors to overcome the entropic barrier created by FG-Nups (Knockenbauer and Schwartz 2016). Extending from the nucleoplasmic face of the NPCs is a distinct set of filaments which together with specific FG-Nups, and the Mlp1 and Mlp2 proteins (termed Tpr in vertebrates) forms the nuclear basket. The nuclear basket provides an attachment site for various NPC associated proteins involved in a diverse range of processes including, nucleocytoplasmic transport, post-translational processes, genome stability, chromosome segregation, and transcriptional regulation (Galy et al., 2004; Iouk et al., 2002; Scott et al., 2009; Dilworth et al., 2005; Lewis, Felberbaum, and Hochstrasser 2007; Luthra et al., 2007; Niepel et al., 2013; Regot et al., 2013; Ptak, Aitchison, and Wozniak 2014; Palancade et al., 2007; Wälde and Kehlenbach 2010).

Nups themselves are also involved in other nuclear processes beyond nucleocytoplasmic transport, including various chromatin-regulated functions (Ptak and Wozniak 2016). Nups can contribute to these various biological processes within the context of NPCs (Ptak, Aitchison, and Wozniak 2014), as distinct entities

in the nucleoplasm (Kalverda et al., 2010; Buchwalter, Kaneshiro, and Hetzer 2019; Ibarra and Hetzer 2015) and as distinct subcomplexes at the NE (Lapetina et al., 2017). In yeast, genes strongly induced by changes in environmental conditions are localized to NPCs where they interact with specific Nups. The role of NPCs in these interactions will be discussed in 1.4. In mammalian cells, the association of specific Nups with active genes has been shown to occur in the nucleoplasm (Kalverda et al., 2010; Capelson et al., 2010). More recently, a distinct Nup subcomplex, termed the Snup complex, has been shown to regulate interactions with telomeres (Lapetina et al., 2017). Telomeres will be discussed in 1.5. Overall, Nups possess many functions beyond their canonical role in nucleocytoplasmic transport, and these unique functions are not necessarily dependent on their association with NPCs.

1.1.2 The proteome of the INM

The INM harbors a diverse set of membrane proteins involved in many nuclear processes, including intranuclear signaling, chromosome segregation, and, importantly, genome organization (Dreger et al., 2001; Van de Vosse et al., 2011). Lining the nucleoplasmic face of the INM in higher eukaryotes is a polymer network of intermediate filaments called lamins (lamin A/C and lamin B) which form the nuclear lamina. The nuclear lamina is connected to the INM through integral inner membrane proteins (NE transmembrane proteins or NETs) and NPCs. The nuclear lamina provides the nucleus with mechanical rigidity and establishes proper nuclear morphology through its interactions with chromatin (Dechat et al., 2008; Shimi et al., 2010; Gruenbaum and Foisner 2015). By

contrast, most single-cell eukaryotes, such as *S. cerevisiae*, appear to lack a discernable nuclear lamina. However, lamin-like functions have been proposed for several yeast protein-interaction networks (Diffley and Stillman, 1989; Strambio-de-Castilla, Blobel and Rout, 1999; Taddei et al.,2004; Taddei and Gasser, 2012; Niepel et al.,2013; Van De Vosse et al.,2013).

Proteins are proposed to be distributed to the INM by one of two mechanisms: sequence based-targeting or the diffusion-retention pathway. The transport of soluble INM-associated proteins occurs through the NPC by sequence-based targeting and nuclear transport proteins (Katta, Smoyer, and Jaspersen 2014; Ungricht et al., 2015). Lamins are among the soluble proteins imported into the nucleus (Hennekes et al., 1993). Similarly, sequence-based targeting or karyopherin-mediated import of integral membrane proteins along POMs is also utilized (Ohba et al., 2004; King, Lusk, and Blobel 2006). However, most proteins appear to be enriched at the INM by the diffusion-retention mechanism (Powell and Burke 1990; Boni et al., 2015; Ungricht et al., 2015; Smoyer et al., 2016). In the diffusion-retention mechanism, integral membrane proteins below a certain size threshold are distributed to the INM by diffusion across the POM. The likelihood that a protein will diffuse across the POM depends on the size of its cytoplasmic/nucleoplasmic domain; as this domain increases in size, the protein is more likely to encounter the barrier imposed by the NPCs (Soullam and Worman 1995; Ohba et al., 2004; King, Lusk, and Blobel 2006; Lusk, Blobel, and King 2007; Zuleger, Robson, and Schirmer 2011). Proteins that diffuse into the INM are then maintained by interactions with chromatin, the nuclear lamina, or other nuclear

proteins (Soullam and Worman 1995; Gruenbaum et al., 2003; Östlund et al., 2006; Zuleger, Robson, and Schirmer 2011; Ungricht et al., 2015; Boni et al., 2015).

1.1.3 The NE during mitosis

By the end of interphase, a cell will have duplicated its genome, which will then need to be divided between the mother and daughter cell during mitosis. In order to facilitate the segregation of DNA during mitosis, significant morphological changes to the NE must occur. Mitosis can be broadly categorized as open or closed, based on the changes in NE structure that occur.

Many higher eukaryotes undergo open mitosis. In open mitosis, the NE is disassembled in a process termed NE break down (NEBD). NEBD is coordinated with the formation of the mitotic spindle in the cytosol. NEBD is initiated by mitotic phosphorylation events that include modifications to specific Nups, INM proteins, and lamins. These phosphorylation events disrupt NE-interactions with chromatin and result in the dispersion of the NE membrane and NE-associated proteins into the connected ER (Hetzer 2010). Membranes must be separated from chromatin for proper chromosome compaction and segregation to occur during mitosis (Champion et al., 2019). During this time, there is also an increase in phospholipid synthesis, which is essential for progression through mitosis and the expansion of the NE membranes (Lin and Arthur 2007; Scaglia et al., 2014; Rodriguez Sawicki et al., 2019). As cells progress through metaphase and enter anaphase, newly synthesized NE membranes begin to reassociate with and enclose the segregated chromatin. The binding of INM proteins to chromatin mediates the re-assembly of

the NE and the formation of the nuclear compartments (Hetzer 2010). Specific chromatin interactions with the INM ensures the proper spatial organization of the genome in the newly formed nuclei (Falk et al., 2019; Politz, Scalzo, and Groudine 2013; Poleshko et al., 2013; 2019; Crabbe et al., 2012).

Organisms such as *S. cerevisiae* undergo closed mitosis. In closed mitosis, the spindle forms inside the nucleus, with the NE remaining functionally intact. As a result, the NE undergoes extensive changes in nuclear shape and surface area during anaphase as the intranuclear spindle elongates. The intranuclear assembly of the mitotic spindle requires that the microtubule-organizing centers, spindle pole bodies (SPBs) in *S. cerevisiae*, are anchored to the inner side of the NE, and that tubulin dimers are actively transported into the nucleus. Similar to open mitosis, there is an increase in phospholipid synthesis during closed mitosis which facilitates the expansion of the NE (Campbell et al., 2006; Witkin et al., 2012). Likewise, chromatin interactions with the NE are also lost as cells enter mitosis, and then re-established during the later stages of mitosis, similar to open mitosis (Laroche et al., 2000; Ebrahimi and Donaldson 2008; Donna Garvey Brickner and Brickner 2010; Donna G. Brickner and Brickner 2012).

Therefore, as highlighted above, two significant factors contributing to the structure of the NE during mitosis is the expansion of the NE and the establishment of chromatin interactions with the NE. Phospholipid synthesis and the factors known to contribute to the expansion of the NE are discussed in 1.2. Chromatin interactions with the nuclear periphery and the role of these interactions will be discussed in 1.3, 1.4, and 1.5.

1.2 NE/ER membrane expansion

Phospholipids (PL) comprise the majority of membranes in yeast. Phosphatidic acid (PA) is the central metabolite for *de novo* PL synthesis. As a result, PA is an essential regulator of membrane biogenesis.

PA is composed of a glycerol-3-phosphate backbone to which two fatty acids (FAs) are esterified. FAs can be derived either from *de novo* synthesis, the hydrolysis of complex lipids, the delipidation of proteins, or from external sources. *De novo* synthesis of FAs occurs primarily in the cytosol, by the sequential action of the acetyl-CoA carboxylase, Acc1 (Hasslacher et al., 1993) and the FAS complex, which is composed of Fas1 and Fas2 subunits (Stoops and Wakil 1978; Leibundgut et al., 2008). FAs undergo elongation and desaturation in the ER before they are used to produce PA (Klug and Daum 2014). PA is then used as a precursor for the synthesis of PLs with the hydrophilic head group attached to PA defining the PL produced. The major PLs in yeast include phosphatidylcholine (PC), phosphatidylethanolamine (PE), phosphatidylinositol (PI), and phosphatidylserine (PS; Carman and Han 2011; Henry, Kohlwein, and Carman 2012). In yeast, PLs are primarily produced by the cytidine diphosphate-diacylglycerol (CDP-DAG) pathway, which converts PA to CDP-DAG using CTP. The conversion of PA to diacylglycerol (DAG) will channel PA primarily towards lipid storage (Fig. 1-1; Carman and Han, 2011)

1.2.1 Phospholipid synthesis during mitosis

Due to its central role in membrane biogenesis, PA levels are increased to facilitate PL synthesis and the expansion of the NE during mitosis. During mitosis,

PA is increased by enhanced *de novo* fatty acid (FA) synthesis. The mitotic increase in FA (Scaglia et al., 2014; Rodriguez Sawicki et al., 2019; Blank et al., 2017) promotes the production of PA and PLs, which are incorporated into the NE (Walters et al., 2014; Rodriguez Sawicki et al., 2019; Scaglia et al., 2014). In yeast, the increase in FA synthesis is regulated by the increased translation of mRNAs encoding the FA producing enzymes, Acc1, Fas1, and Fas2 (Blank et al., 2017). The mitotic increase of PA is also facilitated by preventing the conversion of PA to DAG. The conversion of PA to DAG diverts PA away from the CDP-DAG pathway (Fig. 1-1). Lipin is the PA phosphatase, which dephosphorylates PA to convert it to DAG. The phosphatase activity of lipins is vital for regulating the NE during mitosis. In *S. cerevisiae* and *S. pombe*, which undergo closed mitosis, lipin activity is inhibited to promote PL synthesis and NE-expansion (Santos-Rosa et al., 2005; Makarova et al., 2016). In mammals, the loss of lipin causes defects in NEBD (Golden, Liu, and Cohen-Fix 2009; Mall et al., 2012). The regulation of lipins is discussed in greater detail below (1.2.2).

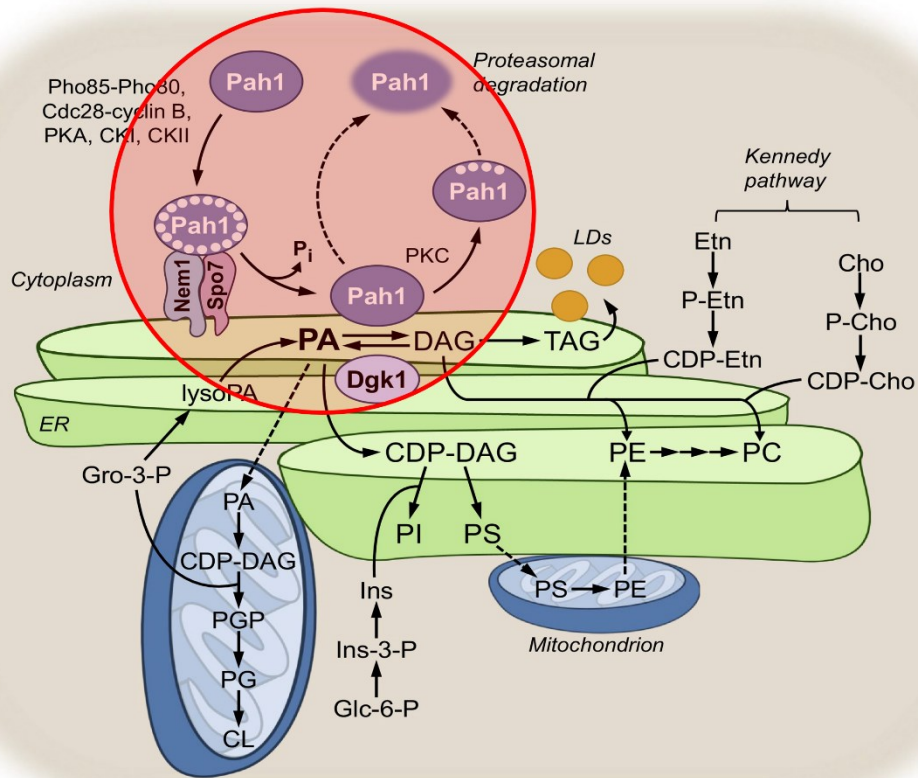


Figure 1-1. Schematic representation of phosphatic acid regulation in *S. cerevisiae*. The figure depicts the pathways for the synthesis of phospholipids and their precursor phosphatidic acid (PA). PA is portioned between the CDP-DAG pathway and the DAG pathway. The CDP-DAG pathway is involved in *de novo* production of phosphatidylserine (PS), phosphatidylethanolamine (PE), and phosphatidylinositol (PI). The DAG pathway can provide the cell with PE and PC through the Kennedy pathway or TAG and lipid droplets (LD), for lipid storage. Conversion of PA to DAG is regulated by the phosphatase Pah1 and its activating complex Nem1/Spo7. Dephosphorylation of Pah1 by the Nem1/Spo7 complex leads to the membrane association and activation of Pah1. The phosphorylated form of Pah1 is indicated by white circles, with kinases directing phosphorylation of Pah1 indicated. Conversion of DAG to PA is regulated by the kinase Dgk1. Gro (glycerol), Ins (inositol), Glc (glucose), Eth (ethanolamine), Cho (choline), P-Etn (phosphoethanolamine), P-Cho (phosphocholine). Adapted from (Kwiattek, Han, and Carman 2020).

1.2.2 Pah1 and lipins

In yeast, multiple lipid-phosphate phosphatases can dephosphorylate PA (Carman 2019). However, the regulation of PA utilized in PL synthesis is attributed solely to the phosphatase, Pah1 (Sorger and Daum 2003; Han, Wu, and Carman 2006; Fakas et al., 2011; Choi et al., 2012). The enzymatic activity of Pah1 was first shown in *S. cerevisiae* (Y. P. Lin and Carman 1989) which, led to the identification of lipin proteins in mammals (Péterfy et al., 2001; Han, Wu, and Carman 2006). There are three lipin paralogs in mammals (Lipin 1-which has three isoforms, Lipin 2 and Lipin 3). These mammalian paralogs have distinct but overlapping functions (Donkor et al., 2007) and can rescue *pah1Δ* phenotypes in yeast (Péterfy et al., 2001). The membrane association and activity of both Pah1 and mammalian lipins are regulated by their phosphorylation (Huffman, Mothe-Satney, and Lawrence 2002; O'Hara et al., 2006; Harris et al., 2007; Grimsey et al., 2008; Choi et al., 2011; Peterson et al., 2011; Choi et al., 2012).

The phosphorylation of Pah1 inhibits its activity, as exemplified by a phosphodeficient Pah1 mutant, which has increased phosphatase activity (O'Hara et al., 2006). Pah1 is phosphorylated at many sites and by numerous kinases. The phosphorylation of Pah1 by Pho85-Pho80, Cdk1 and PKA inhibits Pah1 function by preventing its association with membranes and, therefore, PA (Santos-Rosa et al., 2005; Choi et al., 2011; Han et al., 2012; Su et al., 2012). Phosphorylation of Pah1 by Pho85-86 and PKA reduces its phosphatase activity, and the phosphorylation of Pah1 by PKC promotes the degradation of Pah1 by the 20S proteasome (Hsieh et al., 2015; Su, Han, and Carman 2014). The association of Pah1 with the promoters

of PL synthesizing genes and its role in regulating the transcription of these genes, is also regulated by its phosphorylation (Santos-Rosa et al., 2005). The transcriptional regulation of PL synthesizing genes will be discussed in greater detail below (1.2.4.1). The mitotic phosphorylation of Pah1 by Cdk1 is proposed to inhibit Pah1 activity during mitosis to promote NE expansion (Santos-Rosa et al., 2005).

The reduction of Pah1 and lipin activity causes NE/ER expansion (Tange, Hirata, and Niwa 2002; Golden, Liu, and Cohen-Fix 2009; Gorjánác and Mattaj 2009; Peterson et al., 2011; Bahmanyar et al., 2014). In yeast, the loss of Pah1 activity causes the typically spherical nuclei to become irregularly shaped, with the expansion of the NE/ER membrane occurring at regions adjacent to the nucleolus. The expansion of the NE/ER at these regions results in a nuclear extension or “flare” (Siniosoglou 1998; Santos-Rosa et al., 2005; Campbell et al., 2006; Witkin et al., 2012). It has been proposed that the tethering of DNA to the NE outside of these regions may facilitate their ability to resist expansion (Campbell et al., 2006), with rDNA tethering to the NE not contributing to the formation of the flare (Walters et al., 2014). More recently, however, the tethering of rDNA to the NE in specific mutant backgrounds was shown to be required for the formation of nuclear extensions (Male et al., 2021). Therefore, the formation of nuclear extensions in yeast is likely due to increased PL synthesis and altered protein interactions with membranes. Metazoans do not display these nuclear membrane extensions upon lipin inhibition (Fagone and Jackowski 2009).

1.2.3 The Nem1/Spo7 complex

In yeast, Pah1 is dephosphorylated and activated by the Nem1/Spo7 complex (O'Hara et al., 2006; Choi et al., 2011; 2012; Su, Han, and Carman 2014). Nem1/Spo7 are integral membrane proteins localized to the NE/ER. The Nem1/Spo7 complex dephosphorylates Pah1 and promotes the membrane association of Pah1. Nem1 is the catalytic subunit, while Spo7 is the activator of the holoenzyme (Siniosoglou, 1998; Santos-Rosa et al.,2005). The efficiency of Pah1 dephosphorylation by the Nem1/Spo7 complex is dependent on pH (Antonio Daniel Barbosa et al., 2015), the phosphorylation of the Nem1/Spo7 complex (Dubots et al., 2014; Dey et al., 2019; Su et al., 2018) and the kinase phosphorylation site within Pah1 (Hsieh et al., 2016; Su, Han, and Carman 2014). Membrane association of Pah1 is dependent on both interactions with the Nem1/Spo7 phosphatase complex (Karanasios et al., 2010; Dubots et al., 2014) and the association of its amphipathic helix with membranes (Karanasios et al., 2010). CNEP-1 in *C. elegans* and CTDNEP1 in humans, which are homologues to Nem1, are also enriched at the NE, where they dephosphorylate and regulate the NE-associated pool of lipin (Bahmanyar et al., 2014; Merta et al., 2021).

1.2.4 Pah1-Nem1/Spo7 and membrane expansion

The loss of Pah1 activity, either through the loss of Pah1 (*pah1Δ*) or through the loss of the Nem1/Spo7 complex (*nem1Δ spo7Δ*), results in the expansion of the NE/ER (Siniosoglou et al., 1998; Santos-Rosa et al., 2005; Campbell et al., 2006; Witkin et al., 2012). The expansion of the NE/ER in these mutants is the result of increased PA in the ER (Hassaninasab, Han, and Carman 2017) and increased PL

synthesis (Han, Wu, and Carman 2006; Fakas et al., 2011; Pascual, Soto-Cardalda, and Carman 2013). The increased PA generated by the loss of Pah1 or the Nem1/Spo7 complex serves as a precursor for PL synthesis through the CDP-DAG pathway. As a result, the loss of Dgk1, the kinase that phosphorylates DAG to PA and opposes Pah1 activity, can rescue the NE/ER expansion phenotype of *pah1Δ* cells (Han et al., 2008). The increased PA, caused by the loss of Pah1 activity, also facilitates the derepression of PL synthesizing genes (Han, Wu, and Carman 2006; Han, Siniosoglou, and Carman 2007; Santos-Rosa et al., 2005; Han and Carman 2017) to further promote the increased production of PLs.

1.2.4.1 The Henry regulatory circuit

The transcriptional control of PL synthesizing genes occurs via the Henry regulatory circuit. PL synthesizing genes in the Henry regulatory circuit contains an inositol-responsive upstream activating sequence (UAS_{INO} element). The UAS_{INO} is bound by the Ino2/Ino4 heterodimers, which activates these genes. The Ino2/Ino4 heterodimer themselves are bound by Opi1, which inhibits transcription. Interestingly, Pah1 has also been shown to associate with the promoters of PL synthesizing genes, where it is predicted to have an inhibitory function on the expression of these genes (Santos-Rosa et al., 2005).

In growth conditions where the levels of PA are relatively high, such as during inositol depletion (C. J.R. Loewen et al., 2004) or when Pah1 activity is inhibited, UAS_{INO}-containing genes are derepressed due to the relocalization of Opi1 to the NE/ER membrane. The relocalization of Opi1 to the NE/ER is dependent on the interaction of Opi1 with PA at the ER and the interaction of Opi1

with the integral ER membrane protein, Scs2 (Hofbauer et al., 2014; C. J.R. Loewen et al., 2004; J. H. Brickner and Walter 2004). The interaction of Opi1 with Scs2 is dependent on a FFAT motif (two phenylalanines in an acidic tract) within Opi1 which interacts with the conserved MSP (major sperm protein) domain of Scs2 (Christopher J.R. Loewen, Roy, and Levine 2003). The Scs2-Opi1 complex also interacts with Yet1-Yet3 at the ER (J. D. Wilson, Thompson, and Barlowe 2011). The loss of Scs2-Opi1 interactions or the loss of Yet3 causes the nucleoplasmic localization of Opi1 and the repression of the Henry regulatory circuit (C. J.R. Loewen et al., 2004; J. D. Wilson, Thompson, and Barlowe 2011; Gaspar et al., 2017).

Altering PL synthesis, through the loss of Ino2 or the overexpression of Opi1, rescues the nuclear/ER expansion phenotype of *pah1Δ* cells (Santos-Rosa et al., 2005). These observations suggest that the increased transcription of PL synthesizing genes is partially responsible for expanding the NE/ER membrane. However, the derepression of UAS_{INO} containing genes cannot solely account for the formation of nuclear extensions, and the expansion of the NE/ER membrane as *opi1Δ* mutant cells have round nuclei (O'Hara et al., 2006).

1.2.5 Phospholipid synthesis at the INM

The membranes of various organelles have a distinct lipid composition. This includes the asymmetric distribution of lipids within membranes, which can facilitate customized functions of these membranes (Ferraz et al., 2021; Pomorski and Menon 2006; Klug and Daum 2014). Interestingly, the INM has been shown to have a distinct lipid composition (Haider et al., 2018; Romanuska and Köhler

2018; Antonio D. Barbosa et al., 2019). The unique lipid composition of the INM would require a system to overcome both the lateral and transverse diffusion of lipids from the ONM/ER. This could be established by a physical barrier and/or spatially restricting lipid synthesizing enzymes to specific subcellular compartments (Bahmanyar and Schlieker 2020). POMs may provide a physical barrier to prevent the diffusion of lipids between the INM and the ONM/ER. The positive curvature generated by the NPCs at these regions may favor the diffusion of specific lipids, while sterically hindering the diffusion of lipids with large or charged head groups. The spatial restriction of lipid synthesizing enzymes to specific subcellular compartments such as the nucleus can also contribute to the unique lipid composition at the INM. In yeast, the nuclear localization of Pah1 and Dgk1 promotes the production of PA and DAG at the INM (Romanauska and Köhler 2018). The nuclear localization of CCT α contributes to the unique lipid composition of the INM by controlling PC homeostasis at the INM (Haider et al., 2018). Restricting lipid synthesizing enzymes to other subcellular regions may also facilitate the formation of a unique INM lipid composition. For example, the NE localization of CNEP-1/CTDNEP1 (Nem1 homologues responsible for the dephosphorylation and activation of lipins) increases lipin activity at the NE (Kim et al., 2007; Bahmanyar et al., 2014). This decreases local concentrations of PA at the NE, restricting PI to the peripheral ER and establishing a gradient of high PI levels at the plasma membrane and low PI levels at the NE (Bahmanyar et al., 2014). Interestingly, yeast ER-contact sites at the plasma membrane facilitate local PI production (Stefan et al., 2011), suggesting that the generation of “lipid

concentration gradients” may be a conserved mechanism involved in the production of the unique lipid composition of the INM. Despite the emerging role of the INM in lipid metabolism, it is still unclear what contributions lipid synthesis at the INM has on various aspects of NE biogenesis, including its contributions to the mitotic expansion of the NE.

Lipids not only provide the appropriate environment for membrane proteins, but lipid-protein interactions can contribute to protein structure, folding, stability, and function (Renard and Byrne 2021; Laganowsky et al., 2014). Therefore, investigating what contributions lipids at the INM have on the proteome of the INM and regulating the NE-associated functions of these proteins, including the regulation of the spatial organization of the genome will be an important area of future research.

1.3 Spatial organization of the genome

Early electron micrographs showed that condensed heterochromatin was generally localized along the nuclear periphery, while less dense euchromatin was localized to the nucleoplasm and was adjacent to NPCs (Watson, 1955). These observations demonstrate the non-random 3D distribution of the genome within the nucleus and highlight the importance of the NE as a landmark in this organization.

The 3D distribution of chromatin within the nucleus is determined by the overall functional status of the chromatin and the interactions of chromatin with constraining architectural elements (Misteli 2020). Thus, the clustering of heterochromatin at the nuclear periphery depends on interactions between heterochromatin and the interactions of heterochromatin with the nuclear periphery.

The non-random spatial organization of the genome also appears important for its regulation. This is suggested, in part, by the observations that changes in genome positioning patterns occur in response to developmental and environmental signals (Parada, McQueen, and Misteli 2004; Cremer et al., 2006; Ragoczy et al., 2006; Peric-Hupkes et al., 2010; M. Chen and Gartenberg 2014; Randise-Hinchliff et al., 2016).

Chromatin is a complex of DNA and proteins hierarchically organized across a spectrum of levels. The organization of chromatin at all hierarchical levels affects the regulation and spatial organization of the genome. The first level of chromatin organization is nucleosomes. Nucleosomes consists of ~150 bp of DNA wound around an octamer of histone proteins. The histone tails within nucleosomes are subjected to post-translational modifications such as acetylation, phosphorylation, and methylation, which is proposed to influence the accessibility of DNA to transcription factors (TSFs; Allshire & Madhani, 2018). The next level of organization involves the folding of chromatin loops, which will then assemble into topologically associating domains (TADs). TADs are dynamic chromatin domains correlated with genomic functions, including transcription and replication (Hansen et al., 2018). The genome can then be divided into two broad spatial compartments called compartment A and compartment B. A compartment associated regions or TADs preferentially associated with other A compartment associated regions, and B compartment associated TADs preferentially associate with other B compartment TADs. These different compartments are enriched for specific characteristics that indicate their chromatin state or functional status. For

example, compartment B is generally composed of repetitive DNA sequences, is gene-poor, has a late onset of replication, and is enriched for specific histone modifications that facilitate the higher level of compaction seen in these regions. TADs associated with the B compartment are enriched at the nuclear periphery, while active TADs associated with the A compartment are generally more interior (Rao, Srinivasan, and Rajasekharan 2018; Misteli 2020).

The interactions of chromatin with architectural elements such as the nuclear periphery and nuclear bodies, further establishes the spatial organization of the genome. Nuclear bodies, such as the nucleolus, splicing-factor speckles, and PML bodies, are highly dynamic structures whose structural integrity is mediated by transient interactions (Misteli 2020). These nuclear bodies regulate various cellular processes but can also influence the spatial organization of the genome. The nucleolus, for example, is the site of rDNA transcription and ribosome subunit assembly but, is also an important architectural element involved in the spatial organization of the genome. For example, rDNA is clustered into the nucleolus, and tRNA genes preferentially localize to regions near the nucleolus. Heterochromatin-like regions in mammalian cells are also associated with the periphery of the nucleolus (Németh and Längst 2011). Thus, nuclear bodies, such as the nucleolus are important regulators of the spatial organization of the genome. However, within the context of NE structure, which is the focus of this thesis, the spatial organization of the genome relative to the nuclear periphery and the functional implications of these interactions will only be discussed in greater detail.

1.3.1 The spatial organization of the genome at the nuclear periphery

Interactions of chromatin with the nuclear periphery contribute to the organization of the genome. The nuclear lamina regulates the organization of the genome by interacting with lamina-associated domains (LADs) of chromatin. LADs exhibit heterochromatin features such as low gene density, high AT content, late replication timing, and the enrichment of repressive histone modifications. Histone modifications enriched at LADs include a two (me₂) or three (me₃) methyl group addition to histone H3 lysine 9 (H3K9me_{2/3}) or lysine 27 (H3K27me₃). These histone post-translational modifications facilitate the association of LADs with lamins through the interactions of HP1, the protein that recognizes and binds to methylated H3K, and lamin-associated proteins (Poleshko et al., 2013; 2019; Olins et al., 2010; Makatsori et al., 2004). These interactions ensure that the spatial organization of the genome is inherited during cell division and re-established before mitotic exit (Poleshko et al., 2019). With the loss of lamins altering the spatial organization of the genome, including repositioning peripheral genomic regions to the nuclear interior (Nikolova et al., 2004; Zheng et al., 2018).

Despite lacking a nuclear lamina, the spatial organization of the yeast genome is also dependent on chromatin interactions with the nuclear periphery. In yeast, the spatial organization of the genome is largely regulated by the Rab1-like organization of chromosomes (Rodley et al., 2009; Duan et al., 2010). This Rab1-like configuration is characterized by the tethering of centromeres to the SPB, which results in their rosette pairing or clustering of centromeres at one pole of the nucleus. Chromosome arms then extend outwards from the tethered centromeres towards the opposite pole of the cell (Q. Yang, Rout, and Akey 1998; Zimmer and

Fabre 2011). The ends of chromosomes (telomeres) are clustered into foci and anchored to the NE through two-redundant pathways (Taddei, Schober, and Gasser 2010). The clustering of telomeres into foci is dependent on telomere length and interactions between NE-associated proteins (Therizolsa et al., 2010; Duan et al., 2010; Zimmer and Fabre 2011). Together the tethering and clustering of centromeres and telomeres contribute to the spatial organization of the genome by bringing chromatin from several chromosomes together and anchoring them to distinct regions at the NE. Telomere anchoring to the INM will be discussed in greater detail in 1.5.3.

NPC-genome contacts also contribute to the spatial organization of the genome. Regions underlying NPCs are associated with euchromatin, with specific Nups preventing heterochromatin from invading these areas (Niepel et al., 2013; Krull et al., 2010). Super enhancers, which are regulatory structures that drive the expression of genes involved in specifying cell identity, are also associated with Nups at the nuclear periphery (Ibarra et al., 2016). In yeast, specific transcriptionally active genes are tethered to the NPCs in response to various stimuli (J. H. Brickner and Walter 2004; Cabal et al., 2006; Taddei et al., 2006; Donna Garvey Brickner et al., 2007; Ahmed et al., 2010; Light et al., 2010). These genes will be discussed in greater detail in 1.4.1.

Chromatin interactions with the nuclear periphery have important functional consequences on the genome, including regulating the transcriptional activity of these regions. Artificially tethering genomic regions to the nuclear periphery, for example, can lead to repression (Maillet et al., 1996; Andrulis et al.,

1998; Kumaran and Spector 2008; Finlan et al., 2008; Reddy et al., 2008). Consistently, lamina-genome interactions are lost during the activation of specific chromatin regions (Peric-Hupkes et al., 2010). In yeast, the loss of NE-associated regions of the genome, such as telomeres, has also been associated with the derepression of these regions (Andrulis et al., 1998; Taddei, Schober, and Gasser 2010; Van De Vosse et al., 2013). Telomeres are commonly used to assess chromatin regulation at the NE and will be discussed in greater detail in 1.5. Chromatin interactions with the nuclear periphery can also facilitate the transcriptional activation of associated chromatin. In yeast, for example, coinciding with increased transcription is the association of tRNA with NPCs during M-phase (M. Chen and Gartenberg 2014). Moreover, inducible genes such as *GALI* and *INO1* relocalize from the nucleoplasm to the NPCs upon transcriptional activation. The interactions of these loci with specific Nups can promote robust expression (J. H. Brickner and Walter 2004; Taddei et al., 2006; Donna Garvey Brickner et al., 2007; Ahmed et al., 2010; Texari et al., 2013; Randise-Hinchliff and Brickner 2016). The regulation of yeast inducible genes will be discussed in 1.4.1.

Although organized in a non-random nature, the positioning of the genome is not static, and chromatin undergoes constant local dynamic motion. Live-cell microscopy in yeast (Herbert et al., 2017; Heun et al., 2001) and mammalian cells (Chubb et al., 2002; J. Chen et al., 2014) show the constant motion of chromatin. In yeast, rapid time-lapse imaging and tracking of chromatin show that there are at least two types of chromatin motion: small random movements ($<0.2 \mu\text{m}$ within

1.5 sec) that constantly occur as well as larger movements that occur less frequently over short time intervals ($>0.5 \mu\text{m}$ in a 10.5 sec interval; Heun et al., 2001). Chromatin dynamics appear to be reduced by different constraints, including interactions with the nuclear periphery (Heun et al., 2001; Bystricky et al., 2004; 2005). This chromatin is still dynamic, but becomes constrained to a two-dimensional sliding movement that is restricted to a peripheral zone (Hediger et al., 2002; Gartenberg et al., 2004; Cabal et al., 2006; Taddei et al., 2006; Neumann et al., 2012). As a result, unconstrained chromatin will have an unrestricted subdiffusive movement over time and will therefore, be able to randomly explore the volume of the nucleus more than a constrained locus. As a result, if the nucleus is divided into concentric zones of equal volume, an unconstrained locus will be equally distributed among the zones (Hediger et al., 2002).

1.4 Transcriptionally active chromatin at NPCs

The association of NPCs with euchromatin led to the "gene-gating hypothesis" proposed by G. Blobel in 1985. The "gene-gating hypothesis" stated that patches of euchromatin formed by interactions between NPCs and transcriptionally active portions of the genome may function to coordinate transcription and mRNA export (Blobel 1985). This hypothesis may accurately describe the mechanism for coordinating transcription and mRNA export in *S. cerevisiae* as specific Nups (Ahmed et al., 2010; Brickner & Brickner, 2010; Cabal et al., 2006; Light, Brickner, Brand, & Brickner, 2010), mRNA export factors (Cabal et al., 2006; Dieppois & Stutz, 2010; Köhler & Hurt, 2007), and

transcriptional coactivators (Lo et al., 2005; Cabal et al., 2006; Luthra et al., 2007) are associated with NPCs.

1.4.1 Yeast inducible genes

The localization of active genes to the NPCs has been shown for various inducible genes in yeast. Coinciding with the activation of these inducible genes is the relocalization of these genes from the nucleoplasm to NPCs where their mobility is constrained (Cabal et al., 2006; Taddei et al., 2006). Interactions with specific Nups and NPC associated factors can then promote robust expression (Taddei et al., 2006; Donna Garvey Brickner et al., 2007; Ahmed et al., 2010; Light et al., 2010; Texari et al., 2013; Donna Garvey Brickner et al., 2016).

The NPC association of inducible genes, such as *GALI* or *INO1* requires a DNA element known as a gene recruitment sequence (GRS). A GRS is sufficient to target an ectopic locus to NPCs (Ahmed et al., 2010). However, additional TSFs are required to facilitate the appropriate relocation of inducible genes upon activation (Randise-Hinchliff et al., 2016). Several of these TSFs are modified by a post-translational modification known as SUMOylation. Regulating the SUMOylation state of these TSFs has been shown to be important for the appropriate relocalization and activation of the induced *GALI* locus (Rosonina, Duncan, and Manley 2010; 2012; Texari et al., 2013). SUMOylation and its role in transcriptional activation will be discussed in greater detail below (1.6). GRS sequences also facilitate the interchromosomal clustering of loci containing the same GRS (Brickner & Brickner, 2012). Therefore, a GRS regulates the spatial organization of chromatin on multiple levels.

INO1 targeting to the nuclear periphery requires either a GRS I or GRS II sequence, which is bound by the repressors Put3 and Cbf1, respectively (Brickner & Brickner, 2012). Cells must lack both GRS I and GRS II sequences to prevent *INO1* targeting to the NPC upon activation. Under repressive conditions (presence of inositol), *INO1* is bound by Opi1, Ume6, and Rpd3(L), which blocks Put3 binding to the GRS I sequence (Randise-Hinchliff et al., 2016). Upon activation (depletion of exogenous inositol), the repressors dissociate, allowing Put3 and Cbf1 to bind to the GRSs resulting in the relocalization of *INO1* to the NPCs. Put3 and Cbf1 are required for the localization but not for the transcriptional activation of *INO1* (Brickner & Brickner, 2012; Graves & Henry, 2000). Thus, gene position and transcription are coupled, but distinct elements and factors mediate them. Consistently, the association of active inducible loci with NPCs is not necessary for expression (Cabal et al., 2006; Taddei et al., 2006; Saik et al., 2020), and the loss of loci association with NPCs upon activation does not result in the nuclear accumulation of mRNAs (Ahmed et al., 2010; Brickner et al., 2016). These results indicate that the “gating” of a transcriptionally active gene is not necessary for efficient mRNA production and export.

Interestingly, upon activation the subnuclear distribution of these inducible loci are regulated in a cell cycle dependent manner. Activated *INO1* and *GAL1* are released from the periphery in S-phase, with chromatin interactions being re-established during mitosis. The phosphorylation of specific NPC components by cyclin-dependent kinases regulates the cell cycle dependent interactions of these active genes with NPCs (Brickner & Brickner, 2012; Brickner & Brickner, 2010).

The cell cycle dependent localization of these genes to the NPCs is reminiscent of the cell cycle dependent anchoring of subtelomeric chromatin to the NE. Whereby subtelomeric chromatin association with the NE is also proposed to be re-established during mitosis (Laroche et al., 2000; Ebrahimi and Donaldson 2008). Although the anchoring mechanisms for telomeres and active genes are distinct, the similarity in their temporal localization suggests a common regulatory mechanism may exist to facilitate cell cycle dependent chromatin interactions at the NE. Telomere tethering mechanisms will be discussed in (1.5.3).

Inducible loci will remain bound to the NPCs for several hours following inactivation. The NPC association of these loci following inactivation allows the loci to reactivate with faster kinetics in a process known as transcriptional memory (Light et al., 2010; D'Urso and Brickner 2017). During transcriptional memory, poised RNA Pol II PIC are bound to promoters to enhance the rate of future reactivation (Light et al., 2010; Light and Brickner 2013; D'Urso et al., 2016). For some genes such as *GALI*, this involves the formation of an intragenic loop between the promoter and 3' end of the loci, known as a memory gene loop. Memory gene loops are stabilized by Mlp1 and are thought to facilitate reactivation by retaining TSFs (Brickner et al., 2007, 2016; Tan-Wong, Wijayatilake, & Proudfoot, 2009). For other genes such as *INO1*, transcriptional memory requires a DNA sequence known as a memory recruitment sequence (MRS). When going from activating to repressive conditions, the MRS binds TSFs, which facilitates the incorporation of other factors required for reactivation (D'Urso et al., 2016; D'Urso and Brickner 2017).

1.5 Telomeres

As discussed above (1.3.1), interactions of chromatin with the nuclear periphery contribute to the organization of the genome. In yeast, the Rab1 conformation of chromosomes, which involves the tethering to telomeres to the NE, is an important determinant of the spatial organization of the genome. In contrast to *S. cerevisiae*, where telomeres are normally tethered to the NE throughout the cell cycle, mammals principally anchor telomeres transiently in meiosis (Scherthan et al., 1996), although interactions of telomeres with the nuclear matrix have been reported in different contexts (De Lange 1992; Dechat et al., 2004; Kaminker et al., 2009; Crabbe et al., 2012; Chojnowski et al., 2015; Noordermeer et al., 2018).

Telomeres consist of repetitive DNA sequences and nucleoprotein structures positioned at the ends of chromosomes. Telomeres protect the ends of chromosomes from degradation, recombination, and DNA repair pathways. The structure of telomeres and the functional roles of telomeres in *S. cerevisiae* will be discussed in greater detail below.

1.5.1 Telomere structure in yeast

Telomeres consist of repetitive telomeric DNA sequences and a G-rich repetitive DNA sequence, which form a 3' single-stranded overhang. Telomeres in yeast are composed of ~300 to 350 bp of TG₁₋₃ DNA repeats, followed by a 3'-orientated G-rich single-stranded overhang of approximately 10-15 nucleotides. Telomeric repeat sequences are free of nucleosomes and are bound by the DNA binding protein, Rap1 every 18 bps. Adjacent subtelomeric chromatin regions

contain subtelomeric repeat elements that are organized into nucleosomes. The amino-terminal tails of histones in subtelomeric chromatin are hypoacetylated relative to histones elsewhere in the genome (Tham and Zakian 2002). There are two classes of subtelomeric repeat elements in yeast which are called Y' and X elements. Both Y' and X elements contain autonomously replicating sequences. Y' elements are found as single or tandem repeats of 2 to 4 copies but are not found in all telomeres. X elements are variable in size but contain a "core-X" repeat and are found in all telomeres. Histone density and nucleosome distribution at X and Y' elements differ, with Y' elements being shown to be more transcriptionally active (Zhu and Gustafsson 2009; Ellahi, Thurtle, and Rine 2015).

Telomere capping involves binding proteins to telomeric DNA sequences to prevent the ends of chromosomes from being recognized as double-stranded breaks. Proteins that function in telomere capping include Rap1/Rif1 (Marcand et al., 2008; Bonetti et al., 2010; Cornacchia et al., 2012), the yKu complex (Bonetti et al., 2010; Mimitou and Symington 2010), and the Cst complex (Kupiec 2014). The Cst complex binds to the single-stranded overhang, while the yKu complex and Rap1 bind to double-stranded telomeric DNA. Telomere association of Rif1 occurs through interactions with the C-terminus of Rap1 (Mishra and Shore 1999). The uncapping of telomeres caused by the loss or mutations in these proteins results in telomere ends being inappropriately recognized as double-stranded DNA breaks (Mieczkowski et al., 2003; Pardo and Marcand 2005; Marcand et al., 2008).

Telomeres also protect the ends of chromosomes from degradation by serving as a template for the reverse transcriptase, telomerase. Telomerase contains

an enzymatically catalytic protein subunit (Est2) and an RNA molecule containing a short template sequence (transcribed from *TLC1*; Singer and Gottschling, 1994; Lin et al., 2004) that is added onto the 3' G-rich single-stranded overhang. The addition of these repeats onto telomeres prevents the continual shortening of the chromosome with each round of replication. Only short stretches of the RNA template are copied in each round (Förstemann & Lingner, 2001; Lin et al., 2004), and not all telomeres are extended by telomerase every S-phase (Teixeira et al., 2004). The recruitment of telomerase is promoted by interactions with the yKu heterodimer (Stellwagen et al., 2003; Ferreira et al., 2011) and the Cst complex (Pennock, Buckley, and Lundblad 2001; Tseng, Lin, and Teng 2006; S. Li et al., 2009). Conversely, telomerase interactions with telomeres are inhibited by Pif1 and Rif1/2. Rif1/2 is proposed to antagonize telomerase by the "Rap1-counting mechanism." This mechanism provides a method to monitor and maintain telomere structure and length. In the "Rap1-counting mechanism," the amount of Rif1/2 bound to telomeres is dependent on the amount of Rap1 bound to telomeres. Because Rap1 binds to telomeric TG repeats every 18 bps, longer telomeres will have more Rap1/Rif bound to inhibit telomerase activity, whereas shorter telomeres will have less Rap1/Rif bound to inhibit telomerase (Levy and Blackburn 2004).

In addition to the functions outlined above, the structure of telomeres also facilitates the formation of heterochromatin-like regions to promote the silencing of subtelomeric regions. The structure of telomeres also promotes the tethering of these regions to the INM, which further enhances the transcriptional regulation of

these regions and functions to establish the spatial organization of the genome. Both telomere silencing and telomere anchoring are discussed in greater detail below.

1.5.2 Telomere silencing in yeast

Telomeric DNA repeats, and adjacent subtelomeric chromatin, carries features of repressive chromatin. Vertebrate telomeres and subtelomeric chromatin are enriched with heterochromatin histone marks, including the trimethylated (me³) H3 histone at lysine 9 (H3K9me³). *S. cerevisiae* lack this major histone modification. Instead, they contain a SIR complex that represses transcription and forms heterochromatin-like regions (Kupiec 2014).

The transcriptional silencing of subtelomeric chromatin in yeast, requires the binding of the silent information regulatory (SIR) proteins (includes Sir2, Sir3, and Sir4) to the C-terminus of telomere bound Rap1 (Moretti et al., 1994). The binding of Sir4 to Rap1 allows Sir2, a NAD dependent histone deacetylase, to deacetylate H3 and H4 histones within these regions (Tanny et al., 1999; Imai et al., 2000). The deacetylation of H4 lysine 16 (H4K16) specifically promotes the binding of Sir3 (Liou et al., 2005; Buchberger et al., 2008). This, in turn, facilitates multiple rounds of SIR complex recruitment, whereby Sir2 generates additional binding sites through deacetylation, and the SIR complex can spread into subtelomeric regions (Zimmer and Fabre 2011). Boundary regions prevent silencing from spreading into sites of active transcription. The boundaries at subtelomeric regions are established through the competition between Sir2-mediated deacetylation and Sas2-mediated acetylation of the histone H4K16

(Kimura, Umehara, and Horikoshi 2002; Suka, Luo, and Grunstein 2002). The spreading of the SIR complex is also limited by the enrichment of Sir proteins into telomere-localized compartments through their interactions with the NE-associated components required for telomere anchoring (Taddei and Gasser 2004).

More recently, the idea of SIR complex binding and spreading across entire subtelomeric regions to facilitate silencing has been challenged. Rather SIR complex binding to subtelomeric regions has been shown to be “patchy,” with Sir proteins having the highest level of enrichment at core X-elements and telomeric repeats. Furthermore, the silencing of subtelomeric genes adjacent to sites enriched with the SIR complex only represents a small proportion of subtelomeric genes (Ellahi, Thurtle, and Rine 2015). As a result, SIR-mediated silencing may not be as widespread as previously thought. However, the SIR complex still appears to be required for the lower level of transcription observed at subtelomeric regions (Ellahi, Thurtle, and Rine 2015). The SIR complex may function to regulate the transcription of these subtelomeric genes in response to various agents or under different conditions (Fabre et al., 2005; Ellahi, Thurtle, and Rine 2015). The SIR complex may also contribute to silencing at subtelomeric regions in conjunction with other chromatin factors. Alternatively, the enrichment of SIR proteins at subtelomeric chromatin may function to primarily prevent recombination of telomeric repeats, similar to the function of Sir2 in repressing recombination at rDNA (Ellahi, Thurtle, and Rine 2015).

1.5.3 Telomere anchoring to the INM in yeast

The binding of specific proteins to telomeric/subtelomeric chromatin and NE-associated proteins facilitates the anchoring of telomeres to the NE throughout the cell cycle. Similar to the tethering of activated inducible genes to the NPCs, the tethering of telomeres to the NE limits the mobility of this chromatin (Hediger et al., 2002).

Telomere association with the NE is dynamically regulated throughout the cell cycle, with different NE-associated tethers being utilized during G1- and S-phase (Fig. 1-2). During late S-phase, DNA replication causes the delocalization of telomeres from the NE (Ebrahimi and Donaldson 2008). Telomeres are then proposed to reassociate with the NE during the later stages of mitosis (Laroche et al., 2000; Hediger et al., 2002; Ebrahimi and Donaldson 2008). Interestingly, the association of telomeres with the NE in mammalian cells has been shown to occur following mitosis (Crabbe et al., 2012; Noordermeer et al., 2018). These observations suggest a potentially conserved regulatory pathway facilitating telomere tethering to the NE during mitosis. However, a mitotic specific telomere tethering pathway has yet to be elucidated. The telomere anchoring pathways in G1- and S-phase in yeast have been shown to occur by two redundant pathways: the SIR-dependent telomere tethering pathway and the yKu-dependent telomere tethering pathway.

The SIR-dependent telomere tethering pathway involves the interactions of Sir4 with various NE-associated proteins. In G1-phase, the C-terminus PAD domain of Sir4 interacts with NE-associated Esc1 to facilitate telomere tethering

(Andrulis et al., 2002; Taddei et al., 2004). The interaction of Sir4 with Esc1, Nup170, and other Nups required for telomere tethering during G1-phase appears to occur at distinct Nup subcomplexes, termed the Snup complex (Lapetina et al., 2017). During S-phase, telomere tethering is promoted by Sir4 interactions with NE-associated Mps3 (Bupp et al., 2007). Nup170 (Van De Vosse et al., 2013) and the Smc5/6 complex (Moradi-Fard et al., 2016) also facilitates telomere tethering to the NE by promoting the incorporation of Sir4 into subtelomeric chromatin.

The interactions of the yKu complex (composed of yKu70 and yKu80) with various NE-associated proteins regulates the yKu-dependent telomere tethering pathway. The yKu70/80 complex facilitates telomere tethering in G1-phase through interactions with Esc1 and an unknown NE anchor (Taddei et al., 2004). While S-phase telomere tethering is facilitated by the interactions of yKu80 with the telomerase complex (Est1) and NE-associated Mps3 tether (Taddei et al., 2004; Schober et al., 2009). The SUMOylation of the yKu complex has also been shown to enhance telomere tethering in S-phase (Ferreira et al., 2011). SUMOylation and its role in various cellular processes, including telomere tethering, will be discussed in greater detail in 1.6.

Other components of the NPC, including the nuclear basket components, Mlp1/Mlp2 (Feuerbach et al., 2002; Galy et al., 2000), have also been shown to contribute to telomere association with the NE; however, these observations were controversial as they were not reproducible (Hediger et al., 2002).

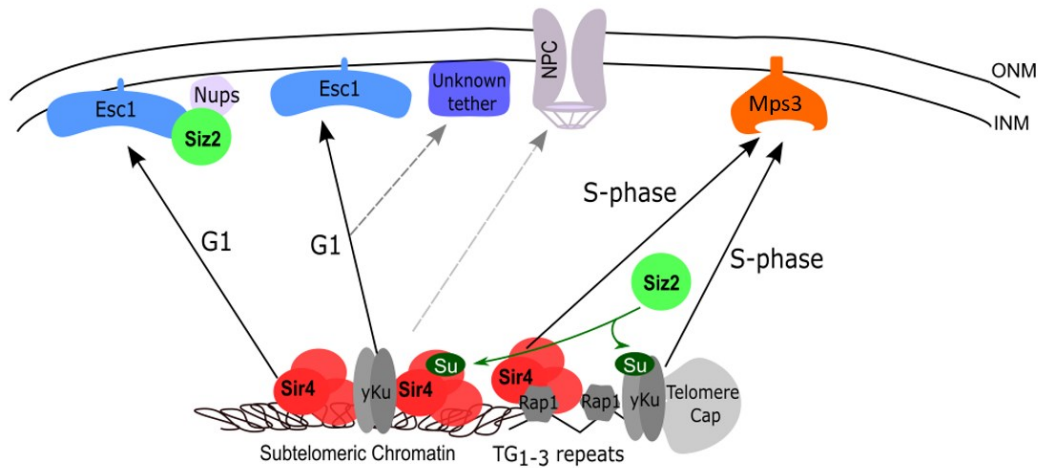


Figure 1-2. Schematic representation of telomere tethering mechanisms at the NE in *S. cerevisiae*. Telomeres are tethered to the NE through partially redundant mechanisms involving the transient interactions of chromatin-bound proteins, Sir4 and the yKu70/80 (yKu) complex, and INM tethers. During G1-phase, telomere anchoring is mediated through yKu interactions with Esc1 and an unknown NE tether. Telomere tethering in G1-phase is also mediated through the interaction of Sir4 with Esc1 and Nup170. Sir4 interactions with Esc1 and Nup170, appear to occur within the Snup complex (complex composed of Siz2, Sir4, Esc1, and various Nups). During S-phase, Sir4 tethers telomeres predominantly through interactions with the integral INM protein, Mps3. yKu80 tethers telomeres predominantly through interactions with telomerase and Mps3, during S-phase. Conjugation of SUMO (Su) to yKu enhances telomere anchoring during S-phase. Components of the NPC have also been implicated in telomere recruitment to the NE.

1.6 SUMOylation

Post-translation modifications, such as SUMOylation, are versatile mechanisms that regulate multiple biological functions, including many NE-associated processes. The Small Ubiquitin-like MOdifier, or SUMO, is a conserved ~12 kDa protein part of the ubiquitin-like family of proteins. Ubiquitin and SUMO share a similar 3D globular structure termed the ubiquitin or β -grasp fold (Bayer et al., 1998; Hochstrasser 2000; Jentsch and Pyrowolakis 2000), which facilitates their functions as small polypeptide modifiers of target proteins. Similarities between SUMO and ubiquitin also extend to the enzymatic pathway that chemically activates and conjugates these proteins to their targets. However, unlike the ubiquitin system, which contains multiple enzymes to regulate target specific conjugation, the SUMOylation system in comparison is relatively simple, containing significantly fewer enzymes involved in these processes. Instead, target specific conjugation is predicted to be derived from the subcellular localization of SUMOylation machinery components (Jentsch and Psakhye 2013).

1.6.1 SUMO and SUMOylated proteins

The gene for SUMO encodes a pro-protein, which contains a C-terminal extension that must be cleaved to produce its mature and conjugatable form (S. J. Li and Hochstrasser 2003). In *S. cerevisiae*, there is only one SUMO gene, *SMT3*, while in mammalian cells, there are five putative SUMO genes (SUMO-1-5; Liang et al., 2016). Yeast *SMT3* and mammalian SUMO-1 are highly conserved, with SUMO-1 being able to rescue the loss of *SMT3* in yeast (Yoshimitsu Takahashi et

al., 1999). Mammalian SUMO-1 only shares a ~50% sequence identity with SUMO-2 and SUMO-3, while SUMO-2 and SUMO-3 themselves have a 97% shared sequence identity and are, therefore, often referred to as SUMO-2/3. Mammalian SUMO paralogs differ in their intracellular distributions, and target protein specificity. SUMO-1 is constitutively conjugated to substrates, while SUMO-2/3 are preferentially conjugated to proteins in response to stress (Saitoh and Hinchev 2000; Ayaydin and Dasso 2004). It is unclear whether SUMO-4 and SUMO-5 are processed into conjugatable forms.

The cleavage of SUMO into its mature and conjugatable form exposes a C-terminal di-glycine motif. The C-terminal di-glycine motif of mature SUMO can then be conjugated to a lysine in a target protein. SUMOylation can occur at numerous lysine sites, including those with no apparent motif (Hoegge et al., 2002; Erica S. Johnson 2004). However, most SUMOylation sites are found within a defined motif. SUMO is often conjugated to the lysine within the SUMO consensus motif ψ -K-x-D/E, where ψ is a hydrophobic residue and x is any amino acid residue (Rodriguez, Dargemont, and Hay 2001; Sampson, Wang, and Matunis 2001). Alternative SUMO motifs expand on the specific characteristics of the SUMO consensus motif. Variants of the consensus SUMO motif include those that introduce a negative charge, which facilitates the recruitment of the E2-SUMO thioester for efficient SUMOylation (S. H. Yang et al., 2006; Mohideen et al., 2009). The negative charge can be introduced by either phosphorylation (phosphorylation-dependent SUMOylation motif; PDSM) or by acidic amino acid residues (negatively charged amino acid-dependent SUMOylation motif; NDSM).

PDSMs require a nearby phosphorylation event to increase the SUMOylation of a substrate (Grégoire et al., 2006; Hietakangas et al., 2006). Whereas NDSMs require the presence of two acidic residues downstream of the conjugated lysine for efficient SUMOylation (S. H. Yang et al., 2006). SUMOylation has also been found to occur at inverted SUMOylation motifs (E/D-x-K-ψ), and hydrophobic cluster motifs (ψψψ-K-x-D/E), although how these alternative motifs facilitate SUMOylation is not fully understood (Matic et al., 2010; Impens et al., 2014; Hendriks and Vertegaal 2016).

1.6.2 SUMO Conjugation

SUMOylation results in the formation of an isopeptide bond with the ε-amino group of the acceptor lysine in the target protein (Johnson & Blobel, 1997). SUMO can either be conjugated to a target protein (SUMOylation) or itself to result in the formation of SUMO chains (polySUMOylation; Bylebyl, Belichenko, & Johnson, 2003). SUMO conjugation (Fig. 1-3) begins with activating mature SUMO in an ATP-dependent mechanism. This is facilitated by the E1-activating enzyme, which in yeast is the Aos1/Uba2 heterodimer. The adenylation of SUMO results in the formation of a thioester bond between the catalytic cysteine of the E1 enzyme and SUMO (Desterro et al., 1999; Erica S. Johnson et al., 1997; Gong et al., 1999). The E1-SUMO thioester complex can then interact with the E2-conjugating enzyme. There is only one E2 conjugating enzyme, Ubc9, whose primary sequence is highly conserved across all eukaryotes. Activated SUMO is transferred, in a

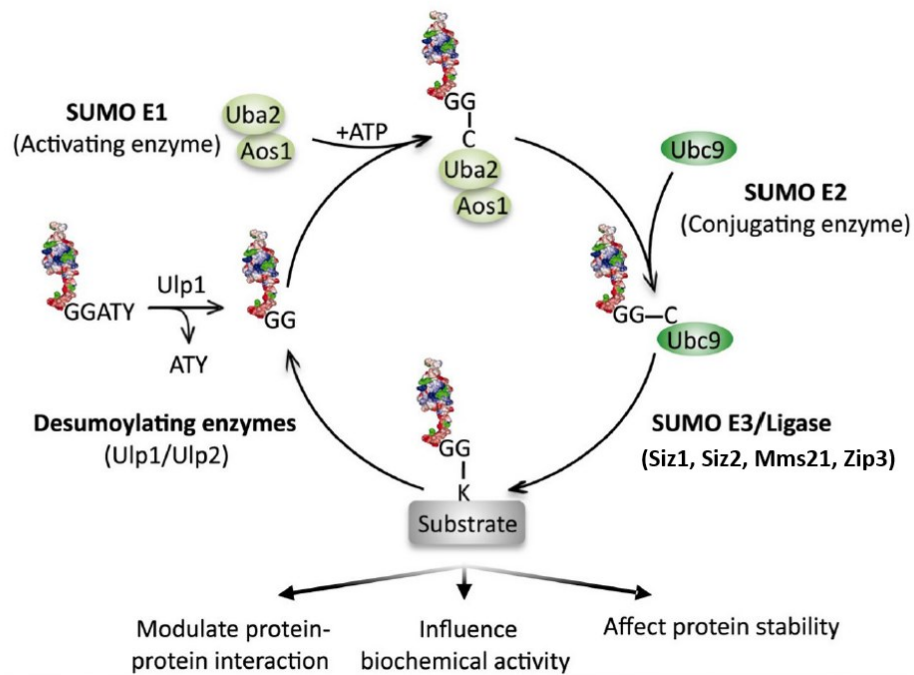


Figure 1-3. SUMO maturation and targeting in *S. cerevisiae*. SUMO is a post-translational modification that promotes various cellular functions by modulating the interactions of the SUMOylated protein, the biochemical activity of the SUMOylated protein or the localization of the SUMOylated protein. Initial maturation of SUMO occurs through the removal of the C-terminal tripeptide, by the isopeptidase, Ulp1. This exposes a di-glycine motif and produces a mature SUMO that can then be conjugated to a target protein. Mature SUMO is transferred to the E1 activating enzyme, Uba2/Aos1, in an ATP-dependent manner forming an adenylated intermediate. The E1 enzyme then transfers activated SUMO to the E2 conjugate enzyme, Ubc9. Ubc9 can then SUMOylate a target protein itself by recognizing the SUMO consensus motif. SUMOylation of target proteins can also be facilitated with the aid of E3 ligases. In yeast there are four E3 ligases; Siz1, Siz2, Mms21, and Zip3. Removal of SUMOylation occurs through the deSUMOylating enzymes, Ulp1 and Ulp2. Adapted from (Cremona, Sarangi, and Zhao 2012).

trans-esterification reaction, to the thiol group of the active site cysteine in Ubc9 (Johnson & Blobel, 1997; D. Lin et al., 2002). Ubc9 can then SUMOylate target proteins on its own, by binding directly to SUMO consensus motif (Bernier-Villamor et al., 2002), or with the assistance of SUMO E3 ligases.

1.6.3 SUMO E3 ligases

SUMO E3 ligases coordinate SUMOylation by binding the target, Ubc9, and SUMO, and positioning all components into the optimal conformation required for conjugation (Geiss-Friedlander & Melchior, 2007; Johnson, 2004; Yunus & Lima, 2009). Several proteins have been proposed to be SUMO E3 ligases in the literature. However, only three classes of SUMO E3 ligases have had comprehensive biochemical and structural analysis to confirm their status as E3 ligases (Pichler et al., 2017). The three main classes of E3 ligases are SP-RING, RanBP2, and ZNF451. RanBP2 is vertebrate-specific and does not resemble any other ubiquitin enzyme or SUMO ligase (Pichler et al., 2004). ZNF451 E3 ligases are highly specific for SUMO-2/3 conjugation (Cappadocia, Pichler, and Lima 2015; Eisenhardt et al., 2015). While SP-RING E3 ligases are the only E3 ligases conserved from yeast to humans. There are four E3 ligases in yeast: Siz1, Siz2, Mms21, and Zip3, which are all classified as SP-RING E3 ligases.

All SP-RING E3 ligases have a RING domain adjacent to a SP C-terminal domain (Johnson & Gupta, 2001). The SP-RING domain is highly similar to ubiquitin-RING domains, The SP-RING domain binds to Ubc9 and is required for SUMO ligase activity (X. Zhao and Blobel 2005). SP-RING ligases also contain a

SIM motif. The SIM motif may interact with the SUMO of the E2-thioester for optimal orientation and discharge (Song et al., 2004; 2005) or facilitate target specificity and SUMOylation enhancement (Psakhye and Jentsch 2012). The C-terminus of SP-RING ligases have minimal sequence similarity, which helps facilitate substrate specificity (Johnson & Gupta, 2001). Mms21 is part of the Smc5/6 complex, which localizes to sites of DNA damage, centromeres, telomeres, and the nucleolus (X. Zhao and Blobel 2005; Potts 2009). While the localization and target specificity of Zip3 is regulated by its incorporation into the synaptonemal complex (C. H. Cheng et al., 2006).

Siz1 and Siz2 are considered PIAS SP-RING E3 ligases due to their sequence similarity with proteins of the PIAS family (Johnson & Gupta, 2001). Mammalian PIAS SP-RING E3 ligases include PIAS 1-4 (Varejão et al., 2020). In addition to a SP-RING and SIM motif, PIAS SP-RING E3 ligases also contain a SAP and PINIT domain. The SAP domain is required for DNA association (Okubo et al., 2004; Suzuki et al., 2009), while the PINIT domain is required for substrate interactions/specificity and the subcellular localization of the E3 ligase (Yunus and Lima 2009; Mautsa et al., 2011; Duval et al., 2003; Reindle et al., 2006).

The subcellular localization of SUMO E3 ligases is an important determinant of SUMOylation target specificity. While Siz2 can SUMOylate septins *in vitro*, Siz1 is strictly required for the SUMOylation of septins *in vivo* (Takahashi & Kikuchi, 2003). This is due to the subcellular localization of Siz1. During mitosis, Siz1 is exported from the nucleus by Kap142/Msn5 and subsequently targeted to septins to facilitate SUMOylation (Makhnevych et al., 2007). Siz2 is

localized to sites of DNA damage (Psakhye and Jentsch 2012), while Mms21 and Zip3 target specificity and subcellular localization are regulated by the incorporation of these ligases into the protein complexes mentioned above.

1.6.4 SUMO Proteases

SUMOylated proteins can be deSUMOylated by SUMO proteases, which are also referred to as isopeptidases or deSUMOylases. SUMO-specific proteases function to cleave SUMO precursors into their mature form and remove SUMO from target proteins. In yeast, there are two SUMO-specific proteases (Ulp; Li & Hochstrasser, 2000; Li & Hochstrasser, 1999), and in humans, there are six sentrin/SUMO-specific proteases (SENP; Hay, 2007). Ulps and SENPs have a conserved cysteine protease domain at their C-terminus required for their catalytic activity (Li & Hochstrasser, 1999). In yeast and mammalian cells, SUMO-specific proteases differ in their subcellular distributions and target specificity.

In mammalian cells, SENP-1 and SENP-2 are responsible for removing SUMO-1-3 and are localized to the NE (Y. Wang et al., 2009). SENP-3 and SENP-5 preferentially remove SUMO-2/3 and are localized to the nucleolus. While SENP-6 and SENP-7 preferentially remove SUMO-2/3 in the nucleoplasm (Drag and Salvesen 2008). The two SUMO proteases in yeast, Ulp1, and Ulp2, also have different subcellular localizations and remove SUMO from distinct sets of substrates (Li & Hochstrasser, 2000; Li & Hochstrasser, 1999). Ulp1 is the C-terminal hydrolase responsible for cleaving the *SMT3* precursor into its mature form (S. J. Li and Hochstrasser 1999; S.-J. Li and Hochstrasser 2000; S. J. Li and

Hochstrasser 2003) and is localized to NPCs (V. G. Panse et al., 2003; Y. Zhao et al., 2004; Y. Takahashi et al., 2000). Ulp1 is essential due to its C-terminal hydrolase activity and its role in maintaining free SUMO (S. J. Li and Hochstrasser 1999; De Albuquerque et al., 2016). Ulp2 is not essential and is required for the disassembly of SUMO chains (Eckhoff and Dohmen 2015; Bylebyl, Belichenko, and Johnson 2003). Ulp2 localizes to the nucleus and nucleolus (Srikumar, Lewicki, and Raught 2013) and associates with chromatin (S.-J. Li and Hochstrasser 2000; Strunnikov, Aravind, and Koonin 2001).

The subcellular localization of Ulp1 and Ulp2 appears to facilitate the deSUMOylation of specific targets (S. J. Li and Hochstrasser 1999; S.-J. Li and Hochstrasser 2000). For example, altering the NPC association of Ulp1 results in the deSUMOylation of additional substrates by Ulp1 (Makhnevych et al., 2007; Sydorsky et al., 2010; Texari et al., 2013). The association of Ulp1 with the NPC is dependent on its interactions with karyopherins (Kap121 and Kap95-Kap60) and specific Nups (V. G. Panse et al., 2003; Y. Takahashi et al., 2000; Makhnevych et al., 2007; Srikumar, Lewicki, and Raught 2013; Y. Zhao et al., 2004; Palancade et al., 2007). These interactions are lost during mitosis or under alcohol stress, resulting in the relocalization of Ulp1 to septins (Makhnevych et al., 2007) or the nucleolus (Sydorsky et al., 2010), respectively, where Ulp1 facilitates specific deSUMOylation events.

Post-translational modifications may also regulate Ulp/SENp substrate specificity. Ulp2 phosphorylation by Cdc5 during mitosis inhibits Ulp2 activity (Baldwin et al., 2009). While alterations to SENP-3 ubiquitination in response to

reactive oxygen species stabilizes the protein to facilitate specific deSUMOylation events (Kuo et al., 2008; Huang et al., 2009).

1.6.5 Molecular Consequences of SUMOylation

The consequences of inhibiting SUMOylation can lead to both detectable and nondetectable changes in the function of the SUMOylated protein. In the latter case, this may be due to the fact that mutating the modified lysine may also block competitive modifications, such as acetylation or ubiquitination, resulting in the same effect as SUMOylation. Mutating the lysine targeted for SUMOylation may also show no observable phenotype as the SUMOylation of the target protein may still occur at an alternative lysine. Furthermore, protein group SUMOylation, which involves the SUMOylation of many proteins in one pathway or complex (Erica S. Johnson and Blobel 1999; Cremona, Sarangi, and Zhao 2012; Psakhye and Jentsch 2012), may be unaffected by the loss of a single SUMOylated protein. As SUMOylation and deSUMOylation events are highly dynamic, with less than 1% of the proteome predicted to be SUMOylated at a given time (Erica S. Johnson 2004), low SUMOylation steady states may also contribute to the difficulties in identifying the function of a SUMOylation event. However, despite these difficulties, a vast array of cellular processes and the molecular consequences of SUMOylation have been established.

SUMOylation can regulate the cellular localization, enzymatic activity, and stability of a protein (Cubebñas-Potts and Matunis 2013). Many of these consequences are the result of SUMOylation altering protein interactions. The

SUMOylation of RanGAP1, for example, facilitates its interactions with NPCs and was the first example of SUMOylation altering the localization of a protein (Matunis, Coutavas, and Blobel 1996; Mahajan, Gerace, and Melchior 1998; Mahajan et al., 1997). SUMOylation can also inhibit (Pichler et al., 2005; Ryu et al., 2010) or enhance (Kirsh et al., 2002; David, Neptune, and Depinho 2002; J. Cheng et al., 2004; Morris et al., 2009) the enzymatic activity of a protein. Because SUMOylation targets lysine residues, it can compete with other lysine-specific post-translational modifications such as acetylation or ubiquitination. For example, the SUMOylation of MEF2A prevents its acetylation, which results in the inhibition of MEF2 activity (Shalizi et al., 2006). Conversely, the SUMOylation of I κ B α prevents its ubiquitin-mediated degradation promoting its stability (Desterro, Rodriguez, and Hay 1998).

1.6.5.1 SUMO:SIM interactions

As mentioned above, SUMOylation often mediates physical interactions. SUMOylation can inhibit protein interactions by blocking the interaction sites of other substrates (Moldovan, Pfander, and Jentsch 2006). However, more common is the ability of SUMO to promote protein interactions. The most common way SUMOylation promotes protein interactions is by non-covalent interactions between SUMO and a SUMO interacting motif (SIM) in an interacting partner (Lascorz et al., 2021). SIMs are hydrophobic regions often surrounded by acidic amino acid residues that weakly bind to SUMO (Song et al., 2004; Hannich et al., 2005; Hecker et al., 2006). The SIM consensus motif is [V/I]-x-[V/I]-[V/I], where x can be any residue. Multiple SIM consensus motifs can be clustered in a protein

to facilitate the binding of SUMO chains (Sun and Hunter 2012). However, SIM motifs are not always utilized and may require additional factors to promote their utilization. For example, phospho-SIMs require a phosphorylation event near a SIM motif to introduce a negative charge which enhances binding to the positive SUMO patch (Stehmeier and Muller 2009; Anamika and Spyropoulos 2016; Naik et al., 2011).

SUMO:SIM interactions can facilitate intramolecular (Steinacher and Schär 2005) and intermolecular interactions (Papouli et al., 2005; Pfander et al., 2005; Matunis, Zhang, and Ellis 2006; Psakhye and Jentsch 2012). SUMO:SIM interactions can also facilitate and strengthen the interactions of macromolecule assemblies through protein group SUMOylation and the formation of “SUMO hubs.” Examples of protein group SUMOylation includes interactions within PML nuclear bodies (Matunis, Zhang, and Ellis 2006) and DNA-damage associated protein complexes (Psakhye and Jentsch 2012). The formation of these “SUMO hubs” is thought to be promoted by many weak SUMO:SIM interactions (Jentsch and Psakhye 2013). It is estimated that up to 90% of SUMO binding proteins with SIMs are also SUMOylation targets (González-Prieto et al., 2021). This may explain how SUMO:SIM protein networks enhance SUMOylation events and amplify weak SUMO:SIM interactions to promote various biological functions.

1.6.6 SUMOylation and the NE

The characterization of SUMO first occurred when it was discovered that there were two versions of RanGAP1; a smaller 70 kDa cytoplasmic version, consistent with the predicted size of RanGAP1, and a larger NPC-associated form,

which was identified as SUMOylated RanGAP1 (Matunis, Coutavas, and Blobel 1996; Mahajan et al., 1997; Bayer et al., 1998). As RanGAP1 is a protein involved in regulating nucleocytoplasmic transport, the requirement of SUMOylation for the association of RanGAP1 with the NPCs suggested a link between SUMOylation and nucleocytoplasmic transport. Over the years, studies have supported this conclusion and identified additional roles and targets of SUMOylation at the NE (V. G. Wilson 2017). For example, the SUMOylation of lamins is involved in preserving nuclear shape (Zhang and Sarge 2008) and regulating nucleophagy in response to DNA damage (Yunong Li et al., 2019). Various laminopathies are also associated with abnormalities in SUMOylation (Boudreau et al., 2012; Kelley et al., 2011). NPC formation is affected by SUMOylation (Lewis, Felberbaum, and Hochstrasser 2007; Rouvière et al., 2018). The targeting of eroded telomeres, and other forms of DNA damage to the nuclear periphery for repair are also regulated by SUMOylation (Palancade et al., 2007; Psakhye and Jentsch 2012; Churikov et al., 2016; Horigome et al., 2016; Seeber and Gasser 2017). SUMOylation at the NE is also crucial for the spatial organization of the genome. The role of SUMOylation in the spatial organization of the genome will be discussed in greater detail below (1.6.6.1, 1.6.6.2). In addition to those functions mentioned above, are a plethora of other NE-associated events regulated by SUMOylation. However, numerous SUMOylated INM-associated proteins identified have still not been fully characterized (Srikumar, Lewicki, and Raught 2013; Vikram Govind Panse et al., 2004; Wohlschlegel et al., 2004; Y. Zhao et al., 2004; Hannich et al., 2005; Wykoff and O'Shea 2005).

In addition to the enrichment of SUMOylated proteins at the NE is the association of various SUMOylation machinery components with the NE, including SUMO E3 ligases and SUMO proteases. In mammals, the RanBP2 E3 ligase, which binds RanGAP1-SUMO-Ubc9, is associated with the NPC (Pichler and Melchior 2002). The PIAS1 E3 ligase is also associated with the nuclear matrix in mammals (Sachdev et al., 2001; Zhou et al., 2008; Z. Chen et al., 2021). While in yeast, the SUMO E3 ligase, Siz2, is part of a physically distinct Nup complex, termed the Snup complex, at the INM (Lapetina et al., 2017). deSUMOylases are also enriched at the NE. In mammals, SENP-1 and SENP-2 are localized to the NE (Y. Wang et al., 2009). While in yeast, Ulp1 is associated with NPCs (Y. Takahashi et al., 2000; Makhnevych et al., 2007; Srikumar, Lewicki, and Raught 2013; Y. Zhao et al., 2004; Palancade et al., 2007). The localization of these SUMOylation machinery components to the NE facilitates specific SUMOylation and deSUMOylation events which regulate various NE-associated processes.

Overall, SUMOylation at the NE has emerged as an important regulator of various cellular processes. This thesis focuses on identifying biological functions of SUMOylation at the NE. Specific cellular events and their connections to SUMOylation which are relevant to the focus of this thesis, are discussed in greater detail below.

1.6.6.1 SUMOylation and transcriptional activation

As discussed above, SUMOylated proteins and SUMOylation machinery components are enriched at the INM, where they can regulate multiple NE-

associated functions. This includes the transcriptional regulation of NPC-associated genes. For example, SUMOylation is involved in the transcriptional regulation and subcellular localization of the inducible gene, *GALI*. Upon activation, there is an accumulation of SUMOylated proteins at the *GALI* locus (Rosonina, Duncan, and Manley 2010; 2012). Following activation, the deSUMOylation of the transcriptional repressors Tup1 and Ssn6 by Ulp1 facilitates the efficient activation of *GALI* (Texari et al., 2013). The deSUMOylation of these proteins at NPCs is proposed to uncover binding sites which could promote the association of various transcription activators and chromatin remodellers required for transcriptional activation (Texari et al., 2013). Consistent with deSUMOylation promoting the transcription of *GALI*, SUMOylated histones were detected at *GALI* under uninduced conditions, with transcriptional activation corresponding to a decrease in SUMOylated histones at these regions (Nathan et al., 2006). Thus, both SUMOylation and deSUMOylation events are important for the transcriptional regulation of *GALI* and potentially other loci. As multiple TSFs have been identified as SUMOylation targets (Denison et al., 2005; Hannich et al., 2005; Wohlschlegel et al., 2004; Makhnevych et al., 2009; Srikumar, Lewicki, and Raught 2013; Rosonina et al., 2017), SUMOylation is likely involved in regulating other inducible genes in yeast.

1.6.6.2 SUMOylation and telomeres

The regulation of telomeres by SUMOylation has been reported in numerous contexts. SUMOylation has been linked to the transcriptional activity of subtelomeric associated genes (Nathan et al., 2006; Hang et al., 2011). For

example, in yeast, SUMOylated histones are enriched at subtelomeric chromatin, where they are proposed to enhance the transcriptional repression of subtelomeric associated genes (Nathan et al., 2006). SUMOylation has also been shown to regulate telomere tethering (Ferreira et al., 2011; Lapetina et al., 2017) and telomere clustering (X. Zhao and Blobel 2005; Moradi-Fard et al., 2016). Furthermore, SUMOylation has been shown to regulate telomere length by two-independent mechanisms (Hang et al., 2011; Ferreira et al., 2011). The SUMOylation of Cdc13 during S-phase has been shown to inhibit telomere elongation (Hang et al., 2011). While Siz2-mediated SUMOylation of yKu70/80 enhances telomere tethering during S-phase to prevent elongation (Ferreira et al., 2011). Siz2 has also been shown to interact with a distinct Nup subcomplex, termed the Snup complex, which contains Sir4 and Esc1. The association of Sir4 and Siz2 with this complex is predicted to play a role in subtelomeric chromatin organization and the NE tethering of telomeres (Lapetina et al., 2017). As multiple telomere-associated proteins, in addition to those mentioned above, have been identified as SUMOylation targets (Denison et al., 2005; Hannich et al., 2005; Wohlschlegel et al., 2004; Makhnevych et al., 2009; Srikumar, Lewicki, and Raught 2013) SUMOylation is likely involved in additional aspects of telomere biology.

1.7 Thesis focus

The INM is endowed with a specialized proteome critical to its functions in numerous nuclear processes, including the spatial organization of the genome. A significant amount of work has linked SUMOylation to these and other biological processes at the NE. However, the spatial and temporal regulation of these

SUMOylation events, the SUMOylation machinery components, and the exact SUMOylation targets involved in the regulation of these NE-associated processes is still unclear. The broad focus of this thesis was to identify SUMOylated proteins at the NE, characterize the biological consequences of SUMOylating these proteins, and to identify the regulatory mechanisms that facilitate the SUMOylation of these proteins. The following chapters examined the regulation of Siz2 and Siz2-mediated SUMOylation at the NE in response to external stimuli and temporal cues. The molecular consequences of these NE-associated SUMOylation events were characterized to identify new ways in which SUMOylation and the SUMO pathway machinery contributes to cellular functions of the INM.

In Chapter 3, I describe data on the role of Siz2-mediated SUMOylation in facilitating the relocalization of the activated *INO1* loci to the NPC. In Chapter 4, I describe data on a specific spatial and temporal regulatory system that facilitates the enrichment of Siz2 at the INM during mitosis. While in Chapters 4 and 5, I show that the enrichment of Siz2 and Siz2-mediated SUMOylation at the INM regulates chromatin interactions with the NE and lipid metabolism during mitosis. The work in these chapters has identified novel biological functions for SUMOylation at the INM and elucidated previously unidentified systems which facilitate the re-association of chromatin with the INM and the expansion of the NE during mitosis.

The work described in this thesis provides new insights into specific INM-associated processes regulated by Siz2 and Siz2-mediated SUMOylation.

Chapter II: Experimental Procedures

2.1 Yeast strains and media

All yeast strains were grown in YPD (1% yeast extract, 2% bactopectone, and 2% glucose), or synthetic medium lacking inositol or amino acids (per l: 1.7g yeast nitrogen base, 5g ammonium acetate, 1.7 g amino acid dropout powder and 2% glucose), as required. 5-FOA containing plates were made according to (Boeke et al., 1987). Strains were grown overnight at RT temperature under agitation. The following day cells were diluted into fresh media at an OD of 0.1 and grown for at least three generations at 30°C, unless otherwise indicated. All W303 telomere tethering strains were grown in YPD medium supplemented with 120 µg/ml adenine. All yeast strains used in this thesis are listed in Table 2-1.

Transformations were performed using a lithium acetate/polyethylene glycol method (Gietz and Woods 2002). Gene deletions, protein fusions, and amino acid substitutions of genes were generated using a PCR-based one-step method for gene modifications (Longtine et al., 1998). PCR templates were either isolated from chromosomal DNA or from plasmid DNA (listed below). Deletion strains were generated by replacing the ORF of a given gene with a PCR cassette consisting of ~60 bp 5' of the ORF start codon -a MX marker gene - ~60 bp 3' of the ORF's stop codon. The genomic integration of protein fusions (protein A, V5₃, 13xMYC, eGFP, mCherry) were generated using PCR cassettes consisting of a 40 bp 5'-overhang that anneals to regions immediately upstream and downstream of the start or stop codon of the gene of interest. Confirmation of protein fusions were primarily confirmed by western blotting. Amino acid substitutions were introduced by site-directed mutagenesis of genomic loci using a PCR-based one-step integration method. Genomic DNA derived

from WT tagged genomic loci were used as DNA templates for PCR amplification and genomic integration. Sense oligonucleotides contained ~60 bp 5' upstream of the altered sequence -the mutagenic nucleotides- ~20 nucleotides downstream of the altered sequence. Antisense oligonucleotides were the same as those used for C-terminal tagging. In the case of *scs2* mutants the antisense oligonucleotides included mutagenic nucleotides within the relevant *SCS2* codon(s). The sense oligonucleotide encompassed 20 nucleotides within the 5' end of the *KAN-MX TEF1* promoter and 60 bases upstream of position 242 5' of the *SCS2* start codon. All mutations were sequence verified. Strains bearing multiple gene modifications were derived by crossing relevant strains followed by sporulation, dissection, and selection. Gene deletions assessed for Siz2-SUMOylation targeting assays (Table 4-2) were derived from the haploid Mata yeast deletion library (Invitrogen). TAP-tagged proteins were obtained from the yeast TAP tag library (Ghaemmaghami et al., 2003).

Table 2-1. Yeast strains.

Strain Name	Genotype	Base Strain	Source
YEF473A	<i>MATa ura3-52 lys2-801 leu2-Δ1 his3-Δ200 trp1-Δ63</i>	YEF473A	Bi and Pringle, 1996
NY109	<i>MATa his3-Δ200::lacI-GFP-HIS3 INO1::lacO(256)-TRP1 NUP49-mRFP-hph</i>	YEF473A	These Studies
NPY1202	<i>MATa his3-Δ200::lacI-GFP-HIS3 INO1::lacO(256)-TRP1 NUP49-mRFP-HPH siz1Δ::KAN</i>	YEF473A	These Studies
NPY1203	<i>MATa his3-Δ200::lacI-GFP-HIS3 INO1::lacO(256)-TRP1 NUP49-mRFP-HPH siz2Δ::KAN</i>	YEF473A	These Studies
NPY1010	<i>MATa SIZ2-PrA-HIS3</i>	YEF473A	These Studies
CPY4245	<i>MATa siz2Δ::KAN</i>	YEF473A	These Studies

NPY1101	<i>MATa ULP1-PrA-HIS3</i>	YEF473A	These Studies
NY259	<i>MATa ulp1Δ₁₋₁₅₀-NAT</i>	YEF473A	These Studies
CPY4198	<i>MATa ulp1Δ₁₅₀₋₃₄₀-NAT</i>	YEF473A	These Studies
CPY4182	<i>MATa ulp1Δ₁₋₃₄₀-KAN</i>	YEF473A	These Studies
CPY4201	<i>MATa ULP1-GFP-HIS</i>	YEF473A	These Studies
CPY4202	<i>MATa ulp1Δ₁₅₀₋₃₄₀-GFP-HIS</i>	YEF473A	These Studies
CPY4203	<i>MATa ulp1Δ₁₋₃₄₀-GFP-HIS</i>	YEF473A	These Studies
CPY4204	<i>MATa ulp1Δ₁₋₃₄₀-GFP-HIS</i>	YEF473A	These Studies
NY336	<i>MATa his3-Δ200::lacI-GFP-HIS3 INO1::lacO(256)-TRP1 NUP49-mRFP- HPH ulp1Δ₁₋₁₅₀-NAT</i>	YEF473A	These Studies
NY337	<i>MATa his3-Δ200::lacI-GFP-HIS3 INO1::lacO(256)-TRP1 NUP49-mRFP- HPH ulp1Δ₁₅₀₋₃₄₀-NAT</i>	YEF473A	These Studies
CPY4191	<i>MATa his3-Δ200::lacI-GFP-HIS3 INO1::lacO(256)-TRP1 NUP49-mRFP- HPH ulp1Δ₁₋₃₄₀-KAN</i>	YEF473A	These Studies
CPY200	<i>MATa his3-Δ200::lacI-GFP-HIS3 INO1::lacO(256)-TRP1 NUP49-mRFP- HPH ulp1Δ₁₋₃₄₀-KAN pRS315</i>	YEF473A	These Studies
CPY201	<i>MATa his3-Δ200::lacI-GFP-HIS3 INO1::lacO(256)-TRP1 NUP49-mRFP- HPH ulp1Δ₁₋₃₄₀-KAN pRS315.ULP1</i>	YEF473A	These Studies
CPY202	<i>MATa his3-Δ200::lacI-GFP-HIS3 INO1::lacO(256)-TRP1 NUP49-mRFP- hph pRS315</i>	YEF473A	These Studies
CPY203	<i>MATa his3-Δ200::lacI-GFP-HIS3 INO1::lacO(256)-TRP1 NUP49-mRFP- hph pRS315-ULP1</i>	YEF473A	These Studies
CPY204	<i>MATa pRS315-ULP1-GFP</i>	YEF473A	These Studies
CPY205	<i>MATa pRS315-ulp1^{CSDN}-GFP</i>	YEF473A	These Studies
CPY206	<i>MATa ULP1-mCherry-NAT pRS315- ULP1-GFP</i>	YEF473A	These Studies
CPY207	<i>MATa ULP1-mCherry-NAT pRS315- ulp1^{CSDN}-GFP</i>	YEF473A	These Studies

CPY209	<i>MATa his3-Δ200::lacI-GFP-HIS3 INO1::lacO(256)-TRP1 NUP49-mRFP- HPH pRS315</i>	YEF473A	These Studies
CPY209	<i>MATa his3-Δ200::lacI-GFP-HIS3 INO1::lacO(256)-TRP1 NUP49-mRFP- HPH pRS315.ULP1-GFP</i>	YEF473A	These Studies
CPY210	<i>MATa his3-Δ200::lacI-GFP-HIS3 INO1::lacO(256)-TRP1 NUP49-mRFP- HPH pRS315.ulp1^{CSDN}-GFP</i>	YEF473A	These Studies
CPY211	<i>MATa his3-Δ200::lacI-GFP-HIS3 INO1::lacO(256)-TRP1 NUP49-mRFP- HPH pRS315.ULP1</i>	YEF473A	These Studies
CPY212	<i>MATa his3-Δ200::lacI-GFP-HIS3 INO1::lacO(256)-TRP1 NUP49-mRFP- HPH pRS315.ulp1^{CSDN}</i>	YEF473A	These Studies
NY347	<i>MATa his3-Δ200::lacI-GFP-HIS3 INO1::lacO(256)-TRP1 NUP49-mRFP- HPH nup53Δ::KAN nup60Δ-URA3</i>	YEF473A	These Studies
NPY2076	<i>MATa his3-Δ200::lacI-GFP-HIS3 INO1::lacO(256)-TRP1 NUP49-mRFP- HPH nup53Δ::KAN nup2Δ-URA3</i>	YEF473A	These Studies
NPY2001	<i>MATa his3-Δ200::lacI-GFP-HIS3 INO1::lacO(256)-TRP1 NUP49-mRFP- hph ULP1::P_{ULP1}-NUP53-ulp1³⁴⁰⁻⁶²¹-NAT nup53Δ::KAN</i>	YEF473A	These Studies
NPY2013	<i>MATa his3-Δ200::lacI-GFP-HIS3 INO1::lacO(256)-TRP1 NUP49-mRFP- HPH nup53Δ::KAN nup60Δ-URA3 ULP1::P_{ULP1}-NUP53-ulp1³⁴⁰⁻⁶²¹-NAT</i>	YEF473A	These Studies
NPY2079	<i>MATa his3-Δ200::lacI-GFP-HIS3 INO1::lacO(256)-TRP1 NUP49-mRFP- HPH nup53Δ::KAN nup2Δ-URA3 ULP1::P_{ULP1}-NUP53-ulp1³⁴⁰⁻⁶²¹-NAT</i>	YEF473A	These Studies
CPY4183	<i>MATa nup60Δ::HPH</i>	YEF473A	These Studies
CPY4184	<i>MATa nup2Δ::HPH</i>	YEF473A	These Studies
NPY2032	<i>MATa nup53Δ::KAN ULP1::P_{ULP1}- NUP53-ulp1³⁴⁰⁻⁶²¹-GFP-HIS</i>	YEF473A	These Studies
CPY4185	<i>MATa nup60Δ::HPH nup53Δ::KAN ULP1::P_{ULP1}-NUP53-ulp1³⁴⁰⁻⁶²¹-GFP-HIS</i>	YEF473A	These Studies
CPY4186	<i>MATa nup2Δ::HPH nup53Δ::KAN ULP1::P_{ULP1}-NUP53-ulp1³⁴⁰⁻⁶²¹-GFP-HIS</i>	YEF473A	These Studies
NS3144	<i>MATa his3-Δ200::lacI-GFP-HIS3 INO1::lacO(256)-TRP1 NUP49-mRFP- HPH ulp1Δ₁₋₃₄₀-NAT pRS316</i>	YEF473A	These Studies

NS3145	<i>MATa his3-Δ200::lacI-GFP-HIS3 INO1::lacO(256)-TRP1 NUP49-mRFP- HPH ulp1Δ₁₋₃₄₀-NAT pRS316.CUPpr- SIZ2-V5₃</i>	YEF473A	These Studies
NS3146	<i>MATa his3-Δ200::lacI-GFP-HIS3 INO1::lacO(256)-TRP1 NUP49-mRFP- HPH ulp1Δ₁₋₃₄₀-NAT pRS316.NOPpr- SIZ2-V5₃</i>	YEF473A	These Studies
NS3196	<i>MATa his3-Δ200::lacI-GFP-HIS3 INO1::lacO(256)-TRP1 NUP49-mRFP- HPH siz2Δ::KAN pRS316</i>	YEF473A	These Studies
NS3197	<i>MATa his3-Δ200::lacI-GFP-HIS3 INO1::lacO(256)-TRP1 NUP49-mRFP- HPH siz2Δ::KAN pRS316.CUPpr-SIZ2- V5₃</i>	YEF473A	These Studies
NS3198	<i>MATa his3-Δ200::lacI-GFP-HIS3 INO1::lacO(256)-TRP1 NUP49-mRFP- HPH siz2Δ::KAN pRS316.NOPpr-SIZ2- V5₃</i>	YEF473A	These Studies
BY4741	<i>MATa his3Δ1 leu2Δ0 ura3Δ0 met15Δ0</i>	BY4741	Brachmann et al.,1998
NS2001	<i>MATa bar1Δ::NAT</i>	BY4741	These Studies
NS2099	<i>MATa SIZ2-V5₃-HIS scs2Δ::KAN bar1Δ::NAT</i>	BY4741	These Studies
CPY4082	<i>MATa SIZ2-V5₃-HIS KAN-scs2^{K180R} bar1Δ::NAT</i>	BY4741	These Studies
CPY4006	<i>MATa scs2Δ::NAT</i>	BY4741	These Studies
CPY3888	<i>MATa KAN-scs2^{K180R}</i>	BY4741	These Studies
CPY3908	<i>MATa ulp1^{K352E}-KAN bar1Δ::NAT</i>	BY4741	These Studies
CPY3847	<i>MATa ulp1^{K352E/Y583H}-V53-HIS bar1Δ::NAT</i>	BY4741	These Studies
CPY3864	<i>MATa HPH-SCS2pr-HA₃-SCS2 ulp1^{K352E/Y582H}-V53-HIS bar1Δ::NAT</i>	BY4741	These Studies
CPY4163	<i>MATa SCS2-V53-KAN ulp1^{K352E/Y583H}-V53- HIS bar1Δ::NAT</i>	BY4741	These Studies

CPY3821	<i>MATa HIS-SCS2pr-HA₃-SCS2 bar1Δ::NAT</i>	BY4741	These Studies
CPY4402	<i>MATa SCS2-V5₃-HPH bar1Δ::NAT</i>	BY4741	These Studies
NS2018	<i>MATa siz2Δ::KAN bar1Δ::NAT</i>	BY4741	These Studies
CPY4004	<i>MATa siz2Δ::NAT</i>	BY4741	These Studies
CPY3784	<i>MATa HIS-SIZ2pr-GFP-SIZ2 SUR4-mCherry-NAT</i>	BY4741	These Studies
CPY3909	<i>MATa SIZ2-V5₃-KAN bar1Δ::NAT</i>	BY4741	These Studies
CPY4252	<i>MATa siz2^{S522A}-V5₃-KAN bar1Δ::NAT</i>	BY4741	These Studies
CPY3867	<i>MATa HIS-SIZ2pr-GFP-siz2^{S522A}-HPH SUR4-mCherry-NAT</i>	BY4741	These Studies
CPY4325	<i>MATa siz1Δ::KAN bar1Δ::NAT</i>	BY4741	These Studies
CPY3134	<i>MATa siz1Δ::KAN</i>	BY4741	These Studies
CPY4193	<i>MATa mms21¹⁻¹⁸⁴-V5₃-KAN</i>	BY4741	These Studies
CPY3801	<i>MATa HIS- SIZ2pr-GFP-SIZ2 NOP56-mCherry-NAT</i>	BY4741	These Studies
CPY3851	<i>MATa siz2^{S527A}-V5₃-KAN bar1Δ::NAT</i>	BY4741	These Studies
CPY3869	<i>MATa HIS- SIZ2pr-GFP-siz2^{S527A}-HPH SUR4-mCherry-NAT</i>	BY4741	These Studies
CPY3641	<i>MATa siz2^{S674A}-V5₃-HIS bar1Δ::NAT</i>	BY4741	These Studies
CPY3841	<i>MATa HIS-SIZ2pr-GFP-siz2^{S674A}-HPH SUR4-mCherry-NAT</i>	BY4741	These Studies
CPY4100	<i>MATa NAT-CDC42pr-GFP₁₋₁₀-SCS2 pRS315-GFP₁₁-mCherry-Pus1</i>	BY4741	These Studies
CPY4101	<i>MATa NAT-CDC42pr-GFP₁₋₁₀-SCS2 pRS315-GFP₁₁-mCherry-Hxk1</i>	BY4741	These Studies
NS2911	<i>MATa SCS2-TAP-HIS SIZ2-V5₃-KAN</i>	BY4741	These Studies
NS2917	<i>MATa SCS2-TAP-HIS siz2^{S522A}-V5₃-KAN</i>	BY4741	These Studies
NS4024	<i>MATa KAN-scs2^{K84D/L86D}-TAP-HIS SIZ2-V5₃-HPH bar1Δ::NAT</i>	BY4741	These Studies
CPY3952	<i>MATa HIS-SIZ2pr-GFP-SIZ2 SUR4-mCherry-NAT scs2Δ::KAN</i>	BY4741	These Studies
CPY4061	<i>MATa SIZ2-V5₃-HIS KAN-scs2^{K84D/L86D} bar1Δ::NAT</i>	BY4741	These Studies

CPY4036	<i>MATa HIS-SIZ2pr-GFP-SIZ2 SUR4-mCherry-NAT KAN-scs2^{K84D/L86D}</i>	BY4741	These Studies
CPY4066	<i>MATa siz2^{A569D}-V53-KAN bar1Δ::NAT</i>	BY4741	These Studies
CPY4089	<i>MATa HIS-SIZ2pr-GFP- siz2^{A569D}-HPH SUR4-mCherry-NAT</i>	BY4741	These Studies
CPY4028	<i>MATa HIS-SIZ2pr-GFP-SIZ2 scs2^{I-225}-mCherry-NAT</i>	BY4741	These Studies
CPY4225	<i>MATa NAT-CDC42pr-GFP₁₋₁₀-scs2^{K84D/L86D} pRS315-GFP₁₁-mCherry-Pus1</i>	BY4741	These Studies
CPY3911	<i>MATa SIZ2-V53-KAN ulp1^{K352E/Y583H}-V53-HPH bar1Δ::NAT</i>	BY4741	These Studies
CPY4030	<i>MATa KAN-scs2^{K84D/L86D} ulp1^{K352E/Y583H}-V53-HIS bar1Δ::NAT</i>	BY4741	These Studies
CPY4072	<i>MATa siz2^{A569D}-V53-KAN ulp1^{K352E/Y583H}-V53-HIS bar1Δ::NAT</i>	BY4741	These Studies
CPY3894	<i>MATa HIS-SIZ2pr-GFP-SIZ2-HPH SUR4-mCherry-NAT KAN-scs2^{K180R}</i>	BY4741	These Studies
CPY3915	<i>MATa siz2^{I472/473A}-V53-KAN bar1Δ::NAT</i>	BY4741	These Studies
CPY3835	<i>MATa HIS-SIZ2pr-GFP-siz2^{I472/473A}-HPH SUR4-mCherry-NAT</i>	BY4741	These Studies
CPY4092	<i>MATa siz2^{V720/721A}-V53-KAN bar1Δ::NAT</i>	BY4741	These Studies
CPY3837	<i>MATa HIS-SIZ2pr-GFP-siz2^{V720/721A}-HPH SUR4-mCherry-NAT</i>	BY4741	These Studies
CPY3917	<i>MATa siz2^{I472/473A}-V53-KAN ulp1^{K352E/Y583H}-V53-HPH bar1Δ::NAT</i>	BY4741	These Studies
CPY3835	<i>MATa HIS-SIZ2pr-GFP-siz2^{I472/473A}-HPH SUR4-mCherry-NAT ulp1^{K352E/Y583H}-V53-KAN</i>	BY4741	These Studies
NS4019	<i>MATa SCS2-TAP-HIS siz2^{I472/473A}-V53-KAN</i>	BY4741	These Studies
NS4025	<i>MATa KAN-scs2^{K180R}-TAP-HIS SIZ2-V53-HPH bar1Δ::NAT</i>	BY4741	These Studies
CPY4221	<i>MATa NAT-CDC42pr-GFP₁₋₁₀-scs2^{K180R} pRS315-GFP₁₁-mCherry-Pus1</i>	BY4741	These Studies
DVY1534	<i>MATa TelXIV-L::256xlacOR-TRP1 HIS3::GFP-lacI-HIS3 SEC63-GFP-NAT</i>	W303	Van de Vosse et al.,2013
DL220	<i>MATa TelXIV-L::256xlacOR-TRP1 HIS3::GFP-lacI-HIS3 SEC63-GFP-NAT siz2Δ::KAN</i>	W303	Lapetina et al.,2017

NS2074	<i>MATa TelXIV-L::256xlacOR-TRP1 HIS3::GFP-lacI-HIS3 SEC63-GFP-NAT scs2Δ::KAN</i>	W303	These studies
CPY3981	<i>MATa TelXIV-L::256xlacO-TRP1 HIS3::GFP-lacI-HIS3 SEC63-GFP-NAT siz2^{S522A}-V5₃-KAN</i>	W303	These Studies
CPY4070	<i>MATa TelXIV-L::256xlacO-TRP1 HIS3::GFP-lacI-HIS3 SEC63-GFP-NAT siz2^{A569D}-V5₃-KAN</i>	W303	These Studies
CPY3776	<i>MATa TelXIV-L::256xlacO-TRP1 HIS3::GFP-lacI-HIS3 SEC63-GFP-NAT siz2^{I472/473A}-V5₃-KAN</i>	W303	These Studies
CPY3992	<i>MATa TelXIV-L::256xlacO-TRP1 HIS3::GFP-lacI-HIS3 SEC63-GFP-NAT KAN-scs2^{K84D/L86D}</i>	W303	These Studies
NS2418	<i>MATa TelXIV-L::256xlacO-TRP1 HIS3::GFP-lacI-HIS3 SEC63-GFP-NAT KAN-scs2^{K180R}</i>	W303	These Studies
CPY4049	<i>MATa SIR4-V5₃-KAN</i>	BY4741	These Studies
NS2433	<i>MATa SIR4-V5₃-KAN siz2Δ::HPH</i>	BY4741	These Studies
DVY2190	<i>MATa YKU70-MYC₁₃-KAN bar1Δ::NAT</i>	BY4741	Van de Vosse et al.,2013
NS2665	<i>MATa YKU70-MYC₁₃-KAN bar1Δ::NAT siz2Δ::HPH</i>	BY4741	These Studies
CPY4240	<i>MATa YKU80-V5₃-KAN</i>	BY4741	These Studies
CPY4249	<i>MATa YKU80-V5₃-KAN siz2Δ::NAT</i>	BY4741	These Studies
NS2500	<i>MATa SIR4-V5₃-KAN siz2^{S522A}-NAT</i>	BY4741	These Studies
NS2506	<i>MATa SIR4-V5₃-KAN NAT-scs2^{K84D/L86D}</i>	BY4741	These Studies
NS2504	<i>MATa SIR4-V5₃-KAN NAT-scs2^{K180R}</i>	BY4741	These Studies
NS3522	<i>MATa TelXIV-L::256xlacO-TRP1 HIS3::GFP-lacI-HIS3 SEC63-GFP-NAT ulp1^{K352E/Y583H}-V5₃-HPH</i>	W303	These Studies
NS3524	<i>MATa TelXIV-L::256xlacO-TRP1 HIS3::GFP-lacI-HIS3 SEC63-GFP-NAT ulp1^{K352E/Y583H}-V5₃-HPH siz2^{S522A}-V5₃- KAN</i>	W303	These Studies

NS3206	<i>MATa TelXIV-L::256xlacO-TRP1 HIS3::GFP-lacI-HIS3 SEC63-GFP-NAT yku80 Δ::KAN</i>	W303	These Studies
DVY1539.1	<i>MATa TelXIV-L::256xlacO-TRP1 HIS3::GFP-lacI-HIS3 SEC63-GFP-NAT yku70Δ::KAN</i>	W303	Van de Vosse et al.,2013
DVY1539	<i>W303 MATa TelXIV-L::256xlacO-TRP1 HIS3::GFP-lacI-HIS3 SEC63-GFP-NAT sir4Δ::KAN</i>	W303	Van de Vosse et al.,2013
NS2078	<i>MATa SIR4-eGFP-HIS SUR4-mCherry-NAT</i>	BY4741	These Studies
NS2144	<i>MATa SIR4-eGFP-HIS SUR4-mCherry-NAT siz2Δ::KAN</i>	BY4741	These Studies
DVY2055	<i>MATa TelVI-R::256xlacO-TRP1 HIS3::GFP-lacI-HIS3 SEC63-GFP-NAT</i>	W303	Van de Vosse et al.,2013
CPY3988	<i>MATa TelVI-R::256xlacO-TRP1 HIS3::GFP-lacI-HIS3 SEC63-GFP-NAT siz2^{S522A}-V5₃-KAN</i>	W303	These Studies
NS2111	<i>MATa SIR4-PrA-HIS</i>	BY4741	These Studies
NS3447	<i>MATa SIR4-PrA-HIS ulp1^{K352E/Y583H}-V5₃-KAN</i>	BY4741	These Studies
NS3513	<i>MATa SIR4-PrA-HIS siz2^{S522A}-NAT</i>	BY4741	These Studies
NS3511	<i>MATa SIR4-PrA-HIS ulp1^{K352E/Y583H}-V5₃-KAN siz2^{S522A}-NAT</i>	BY4741	These Studies
NS2515	<i>MATa SIR3-V5₃-KAN</i>	BY4741	These Studies
NS2516	<i>MATa SIR3-V5₃-KAN siz2Δ::NAT</i>	BY4741	These Studies
NS2519	<i>MATa SIR3-V5₃-KAN scs2Δ::NAT</i>	BY4741	These Studies
NS2523	<i>MATa SIR3-V5₃-KAN siz2^{S522A}-NAT</i>	BY4741	These Studies
NS2527	<i>MATa SIR3-V5³-KAN NAT-scs2^{K180R}</i>	BY4741	These Studies
NS2529	<i>MATa SIR3-V5₃-KAN NAT-scs2^{K84D/L86D}</i>	BY4741	These Studies
NS2533	<i>MATa SIR3-V5₃-KAN sir4^{K1037R}-eGFP-HIS</i>	BY4741	These Studies
CPY4050	<i>MATa SIR4-V5₃-KAN SMT3pr-HIS₈-SMT3-HPH</i>	BY4741	These Studies
CPY4053	<i>MATa SIR4-V5₃-KAN SMT3pr-HIS₈-SMT3-HPH siz2^{S522A}-NAT</i>	BY4741	These Studies

CPY4056	<i>MATa SIR4-V5₃-KAN SMT3pr-HIS₈-SMT3-HPH NAT-scs2^{K180R}</i>	BY4741	These Studies
CPY4057	<i>MATa SIR4-V5₃-KAN SMT3pr-HIS₈-SMT3-HPH NAT-scs2^{K84D/L86D}</i>	BY4741	These Studies
NS3501	<i>MATa SIR4-V5₃-KAN SMT3pr-HIS₈-SMT3-HPH ulp1^{K352E/Y583H}-V5₃-HIS</i>	BY4741	These Studies
NS3503	<i>MATa SIR4-V5₃-KAN SMT3pr-HIS₈-SMT3-HPH ulp1^{K352E/Y583H}-V5₃-HIS siz2^{S522A}-NAT</i>	BY4741	These Studies
CPY4051	<i>MATa sir4^{K1037R}-V5₃-KAN SMT3pr-HIS₈-SMT3-HPH</i>	BY4741	These Studies
CPY4008	<i>MATa TelXIV-L::256lacO-TRP1 HIS3::GFP-lacI-HIS3 SEC63-GFP-NAT sir4^{K1037R}-V5₃-KAN</i>	W303	These Studies
CPY4014	<i>MATa sir4^{K1037R}-V5₃-KAN</i>	BY4741	These Studies
NS2705	<i>MATa SIR4-V5₃-KAN bar1Δ::NAT</i>	BY4741	These Studies
NS2705	<i>MATa SIR4-V5₃-KAN siz2^{S522A}-NAT bar1Δ::NAT</i>	BY4741	These Studies
CPY4244	<i>MATa TelVI-R::256lacO-TRP1 HIS3::GFP-lacI-HIS3 SEC63-GFP-NAT sir4^{K1037R}-V5₃-KAN</i>	W303	These Studies
NS2633	<i>MATa sir4^{K1037R}-eGFP-HIS SUR4-mCherry-NAT</i>	BY4741	These Studies
NS2709	<i>MATa sir4^{K1037R}-V5₃-KAN bar1Δ::NAT</i>	BY4741	These Studies
NS2433	<i>MATa SIR4-V5₃-KAN siz2Δ::HPH</i>	BY4741	These Studies
NS2496	<i>MATa SIR4-V5₃-KAN scs2Δ::NAT</i>	BY4741	These Studies
NS2693	<i>MATa his3-Δ200::lacI-GFP-HIS3 INO1::lacO(256)-TRP1 NUP49-mRFP-HPH siz2^{S522A}-V5₃-KAN</i>	YEF473A	These Studies
NS2614	<i>MATa his3-Δ200::lacI-GFP-HIS3 INO1::lacO(256)-TRP1 NUP49-mRFP-HPH KAN-scs2^{K180R}</i>	YEF473A	These Studies
NS2692	<i>MATa his3-Δ200::lacI-GFP-HIS3 INO1::lacO(256)-TRP1 NUP49-mRFP-HPH sir4^{K1037R}-V5₃-KAN</i>	YEF473A	These Studies
DL175	<i>MATa his3Δ200 leu2Δ1 ura3-52 lys2-801 trp1Δ63 ade2-101 ppr1::HIS3 adh4::URA3-TEL-VIII ADE2-TEL-VR</i>	UCC3505	Van de Vosse et al.,2013
DL180	<i>MATa his3Δ200 leu2Δ1 ura3-52 lys2-801 trp1Δ63 ade2-101 ppr1::HIS3</i>	UCC3505	Van de Vosse et al.,2013

	<i>adh4::URA3-TEL-VIIL ADE2-TEL-VR sir3Δ::KAN</i>		
DL197	<i>MATa his3Δ200 leu2Δ1 ura3-52 lys2-801 trp1Δ63 ade2-101 ppr1::HIS3 adh4::URA3-TEL-VIIL ADE2-TEL-VR siz2Δ::KAN</i>	UCC3505	These Studies
NS3420	<i>MATa his3Δ200 leu2Δ1 ura3-52 lys2-801 trp1Δ63 ade2-101 ppr1::HIS3 adh4::URA3-TEL-VIIL ADE2-TEL-VR scs2Δ::KAN</i>	UCC3505	These Studies
NS3421	<i>MATa his3Δ200 leu2Δ1 ura3-52 lys2-801 trp1Δ63 ade2-101 ppr1::HIS3 adh4::URA3-TEL-VIIL ADE2-TEL-VR siz2^{SS22A}-V53-KAN</i>	UCC3505	These Studies
NS3422	<i>MATa his3Δ200 leu2Δ1 ura3-52 lys2-801 trp1Δ63 ade2-101 ppr1::HIS3 adh4::URA3-TEL-VIIL ADE2-TEL-VR KAN-scs2^{K180R}</i>	UCC3505	These Studies
NS3423	<i>MATa his3Δ200 leu2Δ1 ura3-52 lys2-801 trp1Δ63 ade2-101 ppr1::HIS3 adh4::URA3-TEL-VIIL ADE2-TEL-VR ulp1^{K352E/Y583H}-V53-HPH</i>	UCC3505	These Studies
NS4044	<i>MATa PUS1-GFP-HIS bar1Δ::NAT</i>	BY4741	These Studies
NS4046	<i>MATa PUS1-GFP-HIS bar1Δ::NAT siz2^{SS22A}-V53-KAN</i>	BY4741	These Studies
CPY4317	<i>MATa KAN-MET3pr-HA3-CDC20 SUR4-mCherry-NAT HIS-GFP-SIZ2pr-SIZ2</i>	BY4741	These Studies
NS3811	<i>MATa KAN-MET3pr-HA3-CDC20, SUR4-mCherry-NAT HIS-GFP-SIZ2pr-SIZ2^{SS22A}-HPH</i>	BY4741	These Studies
NS3786	<i>MATa HPH-MET3pr-HA3-CDC20 SUR4-mCherry-NAT</i>	BY4741	These Studies
NS3805	<i>MATa HPH-MET3pr-HA3-CDC20, SUR4-mCherry-NAT siz2^{SS22A}-V53-KAN</i>	BY4741	These Studies
NS4067	<i>MATa PUS1-GFP-HIS HPH-MET3pr-HA3-CDC20</i>	BY4741	These Studies
NS4065	<i>MATa PUS1-GFP-HIS HPH-MET3pr-HA3-CDC20siz2^{SS22A}-V53-KAN</i>	BY4741	These Studies
CPY4113	<i>MATa SIZ2-GFP₁₋₁₀-URA pRS315-NOPpr-GFP₁₁-mCherry-SCSTM</i>	BY4741	These Studies

CPY4114	<i>MATa SIZ2-GFP₁₋₁₀-URA pRS315-NOPpr-mCherry-SCSTM-GFP₁₁</i>	BY4741	These Studies
NS4079	<i>MATa SIZ2-GFP₁₋₁₀-URA PUS1-GFP-HIS pRS315-NOPpr-GFP₁₁-mCherry-SCSTM</i>	BY4741	These Studies
NS4080	<i>MATa SIZ2-GFP₁₋₁₀-URA PUS1-GFP-HIS pRS315-NOPpr-mCherry-SCSTM-GFP₁₁</i>	BY4741	These Studies
NS4077	<i>MATa SIZ2-GFP₁₋₁₀-URA bar1Δ::NAT</i>	BY4741	These Studies
NS4229	<i>MATa SIZ2-GFP₁₋₁₀-URA PUS1-GFP-HIS KAN-scs2^{K180R} pRS315-NOPpr-GFP₁₁-mCherry-SCSTM</i>	BY4741	These Studies
NS4230	<i>MATa SIZ2-GFP₁₋₁₀-URA PUS1-GFP-HIS KAN-scs2^{K180R} pRS315-NOPpr-mCherry-SCSTM-GFP₁₁</i>	BY4741	These Studies
NS2181	<i>MATa SUR4-mCherry-NAT</i>	BY4741	These Studies
NS2485	<i>MATa SUR4-mCherry-NAT ulp1^{K352E/Y583H}-V5₃-HIS</i>	BY4741	These Studies
NS4048	<i>MATa PUS1-GFP-HIS bar1Δ::NAT ulp1^{K352E/Y583H}-V5₃-HPH</i>	BY4741	These Studies
NS4056	<i>MATa PUS1-GFP-HIS siz2^{S522A}-V5₃-KAN ulp1^{K352E/Y583H}-V5₃-HPH bar1Δ::NAT</i>	BY4741	These Studies
CPY3959	<i>MATa HIS-GFP-SIZ2 ulp1^{K352E}-KAN SUR4-mCherry-NAT</i>	BY4741	These Studies
CPY3962	<i>MATa HIS-GFP-siz2^{S522A}-HPH ulp1^{K352E}-KAN SUR4-mCherry-NAT</i>	BY4741	These Studies
NS4084	<i>MATa PUS1-GFP-HIS HPH-MET3pr-HA₃-CDC20 pRS316-CYC1pr-NUP60¹⁻²⁴-OPII^{Q2}-mCherry</i>	BY4741	These Studies
NS4085	<i>MATa PUS1-GFP-HIS HPH-MET3pr-HA₃-CDC20 siz2^{S522A}-V5₃-KAN pRS316-CYC1pr-NUP60¹⁻²⁴-OPII^{Q2}-mCherry</i>	BY4741	These Studies
NS4231	<i>MATa PUS1-GFP-HIS bar1Δ::NAT ulp1^{K352E/Y583H}-V5₃-HPH pRS316-CYC1pr-NUP60¹⁻²⁴-OPII^{Q2}-mCherry</i>	BY4741	These Studies

NS4232	<i>MATa PUS1-GFP-HIS bar1Δ::NAT ulp1^{K352E/Y583H}-V53-HPH siz2^{S522A}-V53-KAN pRS316-CYC1pr-NUP60¹⁻²⁴-OPI1^{Q2}-mCherry</i>	BY4741	These Studies
NS4105	<i>MATa SIZ2-GFP₁₋₁₀-KAN PUS1-GFP-HIS bar1Δ::HPH pRS316-CYC1pr-NUP60¹⁻²⁴-OPI1^{Q2}-mCherry pRS315-NOPpr-GFP₁₁-SCSTM</i>	BY4741	These Studies
NS4108	<i>MATa SIZ2-GFP₁₋₁₀-KAN PUS1-GFP-HIS bar1Δ::HPH pRS316-CYC1pr-NUP60¹⁻²⁴-OPI1^{Q2}-mCherry pRS315-NOPpr-SCSTM-GFP₁₁</i>	BY4741	These Studies
NS4237	<i>MATa HPH-MET3pr-HA3-CDC20 PUS1-GFP-HIS YCplac111-PAH1-PtA pRS316-CYC1pr-NUP60¹⁻²⁴-OPI1^{Q2}-mCherry</i>	BY4741	These Studies
NS4238	<i>MATa HPH-MET3pr-HA3-CDC20 PUS1-GFP-HIS YCplac111-pah1^{S110/S114/S168/S602/T723/S744/S7484}-PtA pRS316-CYC1pr-NUP60¹⁻²⁴-OPI1^{Q2}-mCherry</i>	BY4741	These Studies
NS4127	<i>MATa HPH-MET3pr-HA3-CDC20 PUS1-GFP-HIS YCplac111-PAH1-PtA</i>	BY4741	These Studies
NS4128	<i>MATa HPH-MET3pr-HA3-CDC20PUS1-GFP-HIS YCplac111-pah1^{S110/S114/S168/S602/T723/S744/S7484}-PtA</i>	BY4741	These Studies
NS4119	<i>MATa PUS1-GFP-HIS bar1Δ::NAT YCplac111-PAH1-PtA</i>	BY4741	These Studies
NS4121	<i>MATa PUS1-GFP-HIS bar1Δ::NAT ulp1^{K352E/Y583H}-V53-HPH YCplac111-PAH1-PtA</i>	BY4741	These Studies
NS4123	<i>MATa PUS1-GFP-HIS bar1Δ::NAT YCplac111-pah1^{S110/S114/S168/S602/T723/S744/S7484}-PtA</i>	BY4741	These Studies
NS4124	<i>MATa PUS1-GFP-HIS bar1Δ::NAT ulp1^{K352E/Y583H}-V53-HPH YCplac111-pah1^{S110/S114/S168/S602/T723/S744/S7484}-PtA</i>	BY4741	These Studies

NS4111	<i>MATa PUS1-GFP-HIS bar1Δ::NAT YCplac111-PAH1-PtApRS316-CYC1pr-NUP60¹⁻²⁴-OPI1^{Q2}-mCherry</i>	BY4741	These Studies
NS4112	<i>MATa PUS1-GFP-HIS bar1Δ::NAT YCplac111-pah1^{S110/S114/S168/S602/T723/S744/S7484}-PtA pRS316-CYC1pr-NUP60¹⁻²⁴-OPI1^{Q2}-mCherry</i>	BY4741	These Studies
NS4113	<i>MATa PUS1-GFP-HIS bar1Δ::NAT ulp1^{K352E/Y583H}-V5₃-HPH YCplac111-PAH1-PtA pRS316-CYC1pr-NUP60¹⁻²⁴-OPI1^{Q2}-mCherry</i>	BY4741	These Studies
NS4114	<i>MATa PUS1-GFP-HIS bar1Δ::NAT ulp1^{K352E/Y583H}-V5₃-HPH YCplac111-pah1^{S110/S114/S168/S602/T723/S744/S7484}-PtA pRS316-CYC1pr-NUP60¹⁻²⁴-OPI1^{Q2}-mCherry</i>	BY4741	These Studies
NS2784	<i>MATa PAH1-GFP₁₋₁₀-URA pRS315-NOPpr-GFP₁₁-mCherry-SCSTM</i>	BY4741	These Studies
NS2786	<i>MATa PAH1-GFP₁₋₁₀-URA pRS315-NOPpr-mCherry-SCSTM-GFP₁₁</i>	BY4741	These Studies
NS2788	<i>MATa PAH1-GFP₁₋₁₀-URA pRS315-NOPpr-GFP₁₁-mCherry-SCSTM ulp1^{K352E/Y583H}-V5₃-HIS</i>	BY4741	These Studies
NS2790	<i>MATa PAH1-GFP₁₋₁₀-URA pRS315-NOPpr-mCherry-SCSTM-GFP₁₁ ulp1^{K352E/Y583H}-V5₃-HIS</i>	BY4741	These Studies
NS4115	<i>MATa PUS1-GFP-HIS PAH1-GFP₁₋₁₀-URA pRS315-NOPpr-GFP₁₁-mCherry-SCSTM</i>	BY4741	These Studies
NS4116	<i>MATa PUS1-GFP-HIS PAH1-GFP₁₋₁₀-URA pRS315-NOPpr-mCherry-SCSTM-GFP₁₁</i>	BY4741	These Studies
NS4117	<i>MATa PUS1-GFP-HIS PAH1-GFP₁₋₁₀-URA ulp1^{K352E/Y583H}-V5₃-HPH pRS315-NOPpr-GFP₁₁-mCherry-SCSTM</i>	BY4741	These Studies
NS4118	<i>MATa PUS1-GFP-HIS PAH1-GFP₁₋₁₀-URA ulp1^{K352E/Y583H}-V5₃-HPH pRS315-NOPpr-mCherry-SCSTM-GFP₁₁</i>	BY4741	These Studies

NS3826	<i>MATa HPH-MET3pr-HA₃-CDC20 PAH1-GFP₁₋₁₀-URA pRS315-NOPpr-mCherry-SCSTM-GFP₁₁</i>	BY4741	These Studies
NS3827	<i>MATa HPH-MET3pr-HA₃-CDC20 PAH1-GFP₁₋₁₀-URA pRS315-NOPpr-GFP₁₁-mCherry-SCSTM</i>	BY4741	These Studies
NS4125	<i>MATa HPH-MET3pr-HA₃-CDC20 PUS1-GFP-HIS PAH1-GFP₁₋₁₀-URA pRS315-NOPpr-GFP₁₁-mCherry-SCSTM</i>	BY4741	These Studies
NS4126	<i>MATa HPH-MET3pr-HA₃-CDC20PUS1-GFP-HIS PAH1-GFP₁₋₁₀-URA pRS315-NOPpr-mCherry-SCSTM-GFP₁₁</i>	BY4741	These Studies
NS4106	<i>MATa PAH1-GFP₁₋₁₀-KAN PUS1-GFP-HIS pRS316-CYC1pr-NUP60¹⁻²⁴-OPI1^{Q2}-mCherry pRS315-NOPpr-GFP₁₁-SCSTM</i>	BY4741	These Studies
NS4107	<i>MATa PAH1-GFP₁₋₁₀-KAN PUS1-GFP-HIS ulp1^{K352E/Y583H}-V5₃-HPH pRS316-CYC1pr-NUP60¹⁻²⁴-OPI1^{Q2}-mCherry pRS315-NOPpr-GFP₁₁-SCSTM</i>	BY4741	These Studies
NS4225	<i>MATa HPH-MET3pr-HA₃-CDC20 PUS1-GFP-HIS PAH1-GFP₁₋₁₀-URA pRS316-CYC1pr-NUP60¹⁻²⁴-OPI1^{Q2}-mCherry pRS315-NOPpr-GFP₁₁-SCSTM</i>	BY4741	These Studies
NS4109	<i>MATa PAH1-GFP₁₋₁₀-KAN PUS1-GFP-HIS pRS316-CYC1pr-NUP60¹⁻²⁴-OPI1^{Q2}-mCherry pRS315-NOPpr-SCSTM-GFP₁₁</i>	BY4741	These Studies
NS4110	<i>MATa PAH1-GFP₁₋₁₀-KAN PUS1-GFP-HIS ulp1^{K352E/Y583H}-V5₃-HPH pRS316-CYC1pr-NUP60¹⁻²⁴-OPI1^{Q2}-mCherry pRS315-NOPpr-SCSTM-GFP₁₁</i>	BY4741	These Studies
NS4226	<i>MATa HPH-MET3pr-HA₃-CDC20PUS1-GFP-HIS PAH1-GFP₁₋₁₀-URA pRS316-CYC1pr-NUP60¹⁻²⁴-OPI1^{Q2}-mCherry pRS315-NOPpr-SCSTM-GFP₁₁</i>	BY4741	These Studies
NS3701	<i>MATa SPO7-TAP-HIS NEM1-V5₃-KAN bar1Δ::NAT</i>	BY4741	These Studies

NS4205	<i>MATa SPO7-TAP-HIS NEM1-V5₃-KAN ulp1^{K352E/Y583H}-GFP-HPH</i>	BY4741	These Studies
NS4204	<i>MATa SPO7-TAP-HIS NEM1-V5₃-KAN siz2^{S522A}-NAT ulp1^{K352E/Y583H}-GFP-HPH</i>	BY4741	These Studies
NS2836	<i>MATa PAH1-MYC₁₃-KAN bar1Δ::NAT SPO7-TAP-HIS</i>	BY4741	These Studies
NS4203	<i>MATa SPO7-TAP-HIS PAH1-MYC₁₃-KAN ulp1^{K352E/Y583H}-GFP-HPH</i>	BY4741	These Studies
NS4202	<i>MATa SPO7-TAP-HIS PAH1-MYC₁₃-KAN siz2^{S522A}-NAT ulp1^{K352E/Y583H}-GFP-HPH</i>	BY4741	These Studies
NS4197	<i>MATa SPO7-TAP-HIS NEM1-V5₃-KAN bar1Δ::URA HPH-MET3pr-HA₃-CDC20</i>	BY4741	These Studies
NS4198	<i>MATa SPO7-TAP-HIS NEM1-V5₃-KAN bar1Δ::URA HPH-MET3pr-HA₃-CDC20 siz2^{S522A}-NAT</i>	BY4741	These Studies
NS4199	<i>MATa bar1Δ::URA HPH-MET3pr-HA₃-CDC20 SPO7-TAP-HIS PAH1-V5₃-KAN</i>	BY4741	These Studies
NS4200	<i>MATa bar1Δ::URA HPH-MET3pr-HA₃-CDC20 SPO7-TAP-HIS PAH1-V5₃-KAN siz2^{S522A}-NAT</i>	BY4741	These Studies
NS4165	<i>MATa SPO7-TAP-HIS bar1Δ::HPH PAH1-MYC₁₃-KAN siz2^{S522A}-NAT</i>	BY4741	These Studies
NS4167	<i>MATa SPO7-TAP-HIS bar1Δ::HPH NEM1-V5₃-KAN siz2^{S522A}-NAT</i>	BY4741	These Studies
NS2569	<i>MATa spo7Δ::KAN</i>	BY4741	These Studies
NS2574	<i>MATa nem1Δ::KAN</i>	BY4741	These Studies
NS3782	<i>MATa PAH1-GFP₁₋₁₀-URA nem1Δ::KAN pRS315-NOPpr-GFP₁₁-mCherry-SCSTM</i>	BY4741	These Studies
NS3783	<i>MATa PAH1-GFP₁₋₁₀-URA spo7Δ::KAN pRS315-NOPpr-mCherry-SCSTM-GFP₁₁</i>	BY4741	These Studies
NS3784	<i>MATa PAH1-GFP₁₋₁₀-URA spo7Δ::KAN pRS315-NOPpr-GFP₁₁-mCherry-SCSTM</i>	BY4741	These Studies

NS3785	<i>MATa PAH1-GFP₁₋₁₀-URA nem1Δ::KAN pRS315-NOPpr-mCherry-SCSTM-GFP₁₁</i>	BY4741	These Studies
NS3207	<i>MATa TelXIV-L::256xlacO-TRP1 HIS3::GFP-lacI-HIS3 SEC63-GFP-NAT nem1Δ-KAN</i>	W303	These Studies
NS3208	<i>MATa TelXIV-L::256xlacO-TRP1 HIS3::GFP-lacI-HIS3 SEC63-GFP-NAT spo7Δ-KAN</i>	W303	These Studies
NS3114	<i>MATa NEM1-TAP-His, ulp1^{K352E/Y583H}- V5₃-HPH, bar1Δ::NAT</i>	BY4741	These Studies
NS3116	<i>MATa NEM1-TAP-His bar1Δ::NAT</i>	BY4741	These Studies

*strains in BY4741 background with multiple gene modifications were derived from dissections and therefore not genotypes for met15Δ0 or lys2Δ0.

2.2 Plasmids

All plasmids used in this thesis are listed in Table 2-2, with sources which provided plasmids indicated. Plasmids generated for these works, were made by the restriction digestion of PCR products and ligation into the indicated plasmid backbone.

pRS315-SMT3pr-His₈-SMT3-HPH was constructed by cloning three PCR products into pRS315 (Sikorski and Hieter 1989), including: 1) 350 bp of the *SMT3* 5' UTR bounded by SacI/NotI restriction enzyme sites; 2) the coding region for His₈-Smt3 plus 324 bp of the *SMT3* 3' UTR bounded by NotI/SalI restriction enzyme sites; 3) the *HPH-MX* sequence bounded by SalI/ApaI restriction sites (New England Biolabs).

pFA6a-kanMX6-SCS2pr-3HA was generated by replacing the *GAL1* promoter, bounded by BglII/PacI restriction enzyme sites in *pFA6a-kanMX6-*

PGAL1-3HA (Longtine et al., 1998), with a PCR cassette bounded by BglII/PacI restriction enzyme sites and containing 372 bp of the *SCS2* 5'UTR.

pRS315-NOP1pr-GFP₁₁-SCS2TM was generated by replacing the *NOP1pr-GFP₁₁-mcherry-SCS2TM* insert bounded by EagI/NheI restriction enzymes sites in the *pRS315-NOP1pr-GFP₁₁-mCherry-SCS2TM* (Smoyer et al., 2016) with a PCR cassette bounded by EagI/NheI restriction sites and containing the *NOP1pr-GFP₁₁-SCS2TM* insert.

pRS315-NOP1pr-mCherry-SCS2TM-GFP₁₁ was generated by replacing the *NOP1pr-mCherry* insert bounded by EagI/NheI restriction enzyme sites in the *pRS315-NOP1pr-mCherry-SCS2TM-GFP₁₁* (Smoyer et al., 2016) with a PCR cassette bounded by EagI/NheI restriction sites and containing the *NOP1pr* insert.

Table 2-2. Plasmids.

Plasmids	Utilization	Reference
<i>pRS315</i>	-empty plasmid control -backbone for integration of <i>SMT3pr-His₈-SMT3-HPH</i> insert	Sikorski and Hieter, 1989
<i>pRS315-Ulp1-GFP</i>	-used to visualize the localization of exogenously expressed Ulp1 relative to endogenous Ulp1; control for <i>pRS315-ulp1^{CSDN}-GFP</i>	Elmore et al.,2011
<i>pRS315-ulp1^{CSDN}-GFP</i>	-used to visualize the localization of catalytically dead <i>ulp1</i>	Elmore et al.,2011
<i>pRS315-Ulp1</i>	-control for <i>pRS315-ulp1^{CSDN}</i>	Gift from Dr. Chris Ptak University of Alberta
<i>pRS315-ulp1^{CSDN}</i>	- catalytically dead <i>ulp1</i> used in <i>INO1</i> localization assays	Gift from Dr. Christ Ptak

		University of Alberta
<i>pRS315-CUPpr-Siz2-V5₃</i>	-used to exogenously express Siz2 at levels similar to endogenous Siz2 levels.	Gift from Dr. Christ Ptak University of Alberta
<i>pRS315-NOPpr-Siz2-V5₃</i>	-used to exogenously express Siz2 at higher levels than endogenous Siz2 levels.	Gift from Dr. Christ Ptak University of Alberta
<i>pTM1198</i>	-used for integrating the coding sequence for the V5 ₃ tag at the 3' end of relevant genes	Lapetina et al.,2017
<i>pFA6a-kanMX6-PGAL1-3HA</i>	-backbone for integration of <i>SCS2pr-3HA</i> insert	Longtine et al.,1998
<i>pFA6a-kanMX6-SCS2pr-3HA</i>	- used for genomic integration of N-terminally tagged <i>SCS2</i>	These studies
<i>pGEM-4Z-mCherry-NAT</i>	-used to integrate the coding sequence for mCherry at the 3' end of relevant genes	Cairo et al.,2013
<i>pRS315-SMT3pr-His₈-SMT3-HPH</i>	-used for genomic integration of N-terminally tagged <i>SMT3</i>	These studies
<i>pFA6-NAT-CDC42pr-GFP₁₋₁₀</i>	-used to integrate the coding sequence for GFP ₁₋₁₀ at the 5' end of <i>SCS2</i>	Smoyer et al.,2016
<i>pRS315-GFP₁₁-mCherry-Hxk1</i>	-used to visualize cytoplasmic localization of GFP ₁₋₁₀	Smoyer et al.,2016
<i>pRS315-GFP₁₁-mCherry-Pus1</i>	-used to visualize nuclear localization of GFP ₁₋₁₀	Smoyer et al.,2016
<i>pFA6-NAT-CDC42pr-GFP₁₋₁₀</i>	-used to integrate the coding sequence for GFP ₁₋₁₀ at the 3' end of relevant genes	Smoyer et al.,2016
<i>pRS315-NOPpr-GFP₁₁-mCherry-SCSTM</i>	-used to visualize nucleoplasmic/cytosol membrane localization of GFP ₁₋₁₀	Smoyer et al.,2016
<i>pRS315-NOPpr-mCherry-SCSTM-GFP₁₁</i>	-used to visualize ER/nuclear luminal localization of GFP ₁₋₁₀	Smoyer et al.,2016
<i>pRS315-NOPpr-GFP₁₁-SCSTM</i>	-used to visualize nucleoplasmic/cytosol membrane localization of GFP ₁₋₁₀ in conjunction with <i>pRS316-CYC1pr-NUP60^{l-24}-OPII^{Q2}-mCherry</i>	These studies

<i>pRS315-NOPpr-SCSTM-GFP₁₁</i>	-used to visualize ER/nuclear luminal localization of GFP ₁₋₁₀ in conjunction with <i>pRS316-CYC1pr-NUP60^{l-24}-OPI1^{Q2}-mCherry</i>	These studies
<i>pRS316-CYC1pr-NUP60^{l-24}-OPI1^{Q2}-mCherry</i>	-used to visualize INM PA	Romanausk a and Kohler, 2018
<i>YCplac111-PAH1-PtA</i>	-control for <i>YCplac111-pah1^{S110/S114/S168/S602/T723/S744/S748}-⁴-PtA</i>	Santos-Rosa et al.,2005
<i>YCplac111-pah1^{S110/S114/S168/S602/T723/S744/S748}-⁴-PtA</i>	-constitutively active Pah1	O'Hara et al.,2006

2.3 Antibodies

Primary antibodies used include rabbit polyclonal anti-Smt3 (Wozniak Lab), mouse monoclonal anti-V5 (AbCam ab27671), mouse monoclonal anti-HA (Santa Cruz sc-7392), rabbit polyclonal anti-Clb2 (Santa Cruz sc-9071), rabbit polyclonal anti-PrA (used to probe Scs2-TAP; Sigma P3775), rabbit polyclonal anti-GFP (Wozniak Lab), and rabbit polyclonal anti-Gsp1 (Wozniak Lab). Secondary antibodies used: goat anti-rabbit IgG (H+L)-HRP conjugate (BioRad 170-6515) and goat anti-mouse IgG (H+L)-HRP conjugate (BioRad 170-6516). Antibodies were all used at a 1:10 000 dilution for western blot analysis.

2.4 Affinity purification of TAP fusion proteins

Affinity purification of TAP-tagged proteins was performed as described in (Van De Vosse et al., 2013). Wherein a starter culture for each strain used for TAP-tagged affinity purification was grown overnight at RT. In the case of asynchronous co-immunoprecipitations cells were diluted in 1L of fresh YPD to an OD₆₀₀ of 0.1.

In the case of cell cycle arrest/release co-immunoprecipitations cells from the starter culture were diluted in 2L of fresh YPD (α -arrest release) or 2L of fresh SC-Met (Cdc20 degradation) to an OD₆₀₀ of 0.1. Cultures were then incubated at 30°C to an OD₆₀₀ ~ 1.0. Cells were pelleted, washed once with 25 ml cold ddH₂O and the pellet was transferred to a syringe. Cells were then flash frozen by pushing the cells through the syringe directly into a 50 ml falcon tube containing liquid nitrogen. The liquid nitrogen was removed, and the noodles were stored at -80°C. In the case of cell cycle arrest/release co-immunoprecipitations an OD equivalent of 1000 was pelleted and used to produce noodles. Remaining cells were washed and diluted into fresh medium for arrest experiments, as described below. Frozen cells were then lysed using 8 rounds of ball mill grinding (Reitch PM100; 1 min 30s, 450 rpm per round with intermittent cooling in liquid N₂). The resulting powder was stored at -80°C.

1 g of lysed cell powder was resuspended in 2ml of cold IP buffer (2mM MgCl₂, 20mM HEPES-KOH (pH 7.4), 0.1% Tween-20, 110mM KOAc, antifoam-B emulsion at 1:5000 dilution, and protease inhibitors (1 complete EDTA-free pellets (Roche 05056489001)/50 ml buffer). The suspension was incubated on ice for 30 min, with vortexing every 5 min. The resulting lysate was cleared by centrifugation at 1 500 g for 10 min at 4°C. 25 μ l of the clarified lysate, representing the load, was added to 1 ml of ddH₂O, followed by TCA precipitation. The resulting pellet was resuspended in 75 μ l of 2X SDS-PAGE sample buffer. 3 mg of IgG-conjugated magnetic beads (Dynabeads; Invitrogen 143.01, Rabbit IgG; Sigma I5006-10MG) in 100 μ l of IP buffer were added to the remaining 2 ml of clarified

cell lysate, and the mixture was incubated for 1 h at 4°C with rotation. Beads were collected using a magnet and washed 10x with 1ml of IP buffer at 4°C. Proteins bound to beads were eluted at 4°C using 0.5 ml IP buffer containing incrementally increasing concentrations of MgCl₂ (0.05, 0.5, and 2 M) followed by a final elution using 0.5 ml of 0.5 M acetic acid to release the TAP fusion protein from the beads (Bound). To the 500 µl eluate fractions 500 µl of ddH₂O was added followed by TCA precipitation as described above. All samples collected were analyzed by western blotting. In the case of Spo7-TAP affinity purification proteins an equal proportion of each eluate fraction was combined and loaded for western blot analysis.

The conjugation of IgG to magnetic beads was performed as previously described (Alber et al.,2007; Van de Vosse et al.,2013). 10 mg of rabbit IgG (Sigma-Aldrich, St. Louis, MO, USA) was dissolved in 2 mL Na-phosphate buffer (0.1 M NaPO₄ pH 7.4) for 10 minutes under rotation at RT. The solution was clarified by centrifugation at 14,000 rpm for 10 minutes at 4°C. 2 mL Na-phosphate buffer, followed by 1.33 mL of 3M ammonium sulfate pH 7.5 was added to the cleared IgG. The IgG solution was then used to resuspend 60 mg of Epoxy M-270 Dynabeads which had been washed and equilibrated with the Na-phosphate buffer. Conjugation of IgG to magnetic beads was facilitated by incubation 30°C for 20 hours under rotation. Following incubation IgG-conjugated beads were washed once with 1 mL 100 mM glycine pH 2.5, once with 1 mL 10 mM Tris pH 8.8, once with 1 mL 100 mM triethylamine pH 6.0, four times with 1 mL PBS for 5 min per wash, once with 1 mL PBS + 0.5% triton X-100 for 5 min, once with 1 mL PBS +

0.5% triton X-100 for 15 min, followed by three consecutive washes with 1 mL PBS for 5 min for each wash. Washed beads were then resuspended in 2 mL PBS + 0.02% sodium azide and stored at 4°C.

2.5 Affinity purification of His8 SUMO fusion proteins

Frozen lysed cell powder was produced as described in 2.4. 1 g of lysed cell powder was resuspended in 10 mL of resuspension buffer (8 M Urea, 50 mM NaPO₄ (pH 8.0), 500 mM NaCl, 1% NP40-Igepal) and the mixture was resuspended by vortexing at RT. The lysate was cleared by centrifugation at 15 000 rpm for 20 min. 25 µl of the clarified lysate, was added to 1 ml ddH₂O, followed by TCA precipitation and resuspension in 100 ml of 2X SDS-PAGE sample buffer (Load sample). The remaining lysate was transferred to a 15 ml falcon tube and 1 ml of a 50% slurry consisting of NiNTA agarose beads (Qiagen 30210) in resuspension buffer was added, and incubated at RT with rotation for 2 h. The beads were then washed 3X with 5 mL of wash buffer (8 M Urea, 50 mM NaPO₄ (pH 6.3), 500 mM NaCl, 1% NP40-Igepal). The supernatant was removed by pipetting, following the pelleting of the agarose beads by centrifugation (1000 rpm for 1 min). After the last wash, 2 ml of elution buffer (8 M Urea, 50 mM NaPO₄, 500 mM NaCl, 1% NP40-Igepal adjusted to pH 4.5) was added to the beads and the slurry was incubated under rotation at RT for 1 h. The eluant was then collected and subjected to TCA precipitation. Following TCA precipitation samples were resuspended in a final volume of 100 ml 2X SDS-PAGE sample buffer. Load and eluate samples were then analyzed by western blotting. Note that all 8M urea/phosphate buffers were made fresh just prior to use.

2.5 Western Blotting

An OD equivalent of 1 for whole cell lysates were pelleted by centrifugation, resuspended in 50 μ l 2X SDS-PAGE sample buffer, heated at 70°C for 15 minutes, sonicated (Branson Sonifier 250) and pelleted by centrifugation to remove debris prior to being loaded onto SDS-PAGE gels for analysis. In the case of Pah1-PrA, whole cell lysates were subjected to 0.1N NaOH extraction for 5 minutes at RT, before resuspension in 50 μ l 2X SDS-PAGE sample buffer.

Protein samples were resolved by SDS-PAGE gels containing 8% acrylamide, and were transferred to nitrocellulose membranes. Following transfer membranes were blocked with 5% skim milk powder resuspended in PBS-T (PBS containing 0.1% Tween-20) for at least 1 h at RT. Fresh blocking buffer supplemented with primary antibody was added and the membrane was incubated overnight at 4°C. Primary antibodies are listed 2.3. Membranes were then washed with PBST for 15 minutes three times, followed by incubation in fresh blocking buffer supplemented with a secondary antibody-HRP conjugate (2.3) for at least 1 h at RT. Membranes were then washed three times with PBST and proteins were visualized by chemiluminescence (Amersham RPN2106) using an ImageQuant LAS 4000 (GE) imaging system, with exposure times taken in 10 second increments. All western blot images were rendered using Image J software (National Institute of Health).

2.6 Phosphatase treatment

Whole cell lysates in 2x SDS-PAGE sample buffer were methanol-chloroform extracted. 50 μ l of chloroform, and 150 μ l of ddH₂O were added

sequentially to a 50 μ l lysate sample. The mixture was centrifuged for 2 min at 15000 rpm. The resulting top layer was removed and 300 μ l of methanol was added to the remaining sample. The mixture was vortexed and centrifuged for 2 min at 15000 rpm. Residual liquid was removed, and the resulting pellet air dried. The dried pellet was resuspended in 50 μ l of 0.5% w/v SDS. 10 μ l of this sample was added to 10 μ l of lambda phosphatase buffer (New England Biolabs B0761S), 10 μ l of 10 mM MnCl₂, 1 μ l lambda phosphatase (New England Biolabs P0753S) and 69 μ l ddH₂O. For the -PPase sample 1 μ l lambda phosphatase was replaced with 1 μ l of ddH₂O. Reactions were incubated at 30°C for 1 h, followed by TCA precipitation, and resuspension of the resulting pellet in 25 ml of 2X SDS-PAGE sample buffer. Samples were heated at 80°C for ~15 min prior to western blot analysis.

2.7. Alpha-factor arrest release

All strains used in α -factor arrest release assays were *MATa bar1 Δ* . Starter cultures were incubated overnight at RT and diluted to an OD₆₀₀=0.1 in fresh media the following day. Cultures were grown for ~2 ½ hours at 30°C before the addition of α -factor (Sigma T6901). α -factor was added at 10ng/ml in YPD medium and 20ng/ml in SC medium. Cultures were incubated at 30°C for ~2 h 15 min to induce G1-phase arrest. G1 arrest was monitored microscopically for the accumulation of cells with a shmoo phenotype. Collected arrested cells represent the 0 min time point. The remaining cells were pelleted, washed extensively with water, and resuspended in fresh media to a final OD₆₀₀=0.6. Cultures were grown at 30°C and

collected at indicated time points for analysis by western blotting, Co-IP, ChIP or epifluorescence imaging.

2.8 Cdc20 shutoff

All strains used for metaphase arrest were *p_{MET3}-HA₃-CDC20*. Starter cultures were incubated overnight at RT in SC -Met. Cultures were diluted to an $OD_{600}=0.1$ in fresh SC -Met media the following day and grown for two generations at 30°C before the addition of methionine. Cultures were incubated at 30°C for 2 h to induce metaphase-phase arrest. Arrest was monitored microscopically for the accumulation of large-budded cells. Cells were collected for analysis by western blotting, Co-IP, or epifluorescence imaging.

2.9 INO1 induction

Overnight cultures grown in SC +inositol media at RT were diluted to an $OD_{600}=0.1$ in fresh SC +inositol then incubated at 30°C to an $OD_{600} = \sim 0.8$. Cells were then pelleted, washed once with water, and then resuspended in synthetic media lacking inositol to an $OD_{600} = 0.5$ to induce *INO1* activation. Cultures were incubated at 30°C for the indicated times followed by analysis by epifluorescence imaging, RT-qPCR, or ChIP.

2.10 FACs analysis

An equivalent to $OD_{600} = 1$ of cells were pelleted, resuspended in 1 ml of 70% ethanol and incubated overnight at 4°C. Cells were washed twice with 1 ml 50 mM Tris-HCl (pH 8.0). Cells were then resuspended in 0.5 ml of 50 mM Tris-HCl (pH 8.0) containing RNase A (0.4 mg/ml) and incubated at 37°C for 2 h.

Following incubation cells were washed twice with 1 ml 50 mM Tris-HCl (pH 8.0) and the final pellet was resuspended in 200 μ l of a 5 mg/ml pepsin solution (5 mg pepsin, 5 μ l conc. HCl, per ml ddH₂O), and incubated at 37°C for 1 h. Cells were washed with 1 ml of 50 mM Tris-HCl (pH 8.0). Cells were resuspended in 250 μ l propidium iodide solution (50 mM Tris-HCl (pH 8.0), 50 μ g/ml propidium iodide) and incubated overnight at 4°C. 50 μ l of this cell suspension was added to 2 ml of 50 mM Tris-HCl (pH 8.0) in a round bottom tube and the sample was briefly sonicated at low power to resuspend cells. DNA content was then determined using a BD LSRFortessa cell analyzer (Software Version 2.0).

2.11 RT-qPCR

RNA preparation from an OD₆₀₀=10 equivalent of cells was analyzed by RT-qPCR as previously described in Wan et al.,2009. Cell pellets were immediately frozen in liquid nitrogen. Total RNA was isolated from cell pellets using hot acidic phenol. Cell pellets were resuspended in 1 ml of RNase free TES buffer (10 mM Tris-HCl, 10 mM EDTA, pH 7.5, 0.5% SDS) and 1 ml unbuffered acidic phenol. Samples were vortexed and incubated in a 65°C water bath for 30 min. Samples were then vortexed and incubated in the 65°C water bath for another 30 min. Following incubation, cell lysates were centrifuged at 4000 rpm for five minutes. The aqueous layer was then re-extracted with an equal volume of acidic phenol and briefly vortexed prior to centrifugation at 4000rpm for 5 min. Residual phenol was removed from the newly isolated aqueous layer by adding an equal volume of a 24:1 chloroform to the iso-amyl alcohol solution. Samples were briefly vortexed and centrifuged for 5 min at 4000 rpm. From the resulting aqueous phase total RNA was precipitated with 95% EtOH and 3M

NaOAc (made with DEPC treated dH₂O) at -20°C overnight. The following day samples were centrifuged at 4000rpm for 10 min at 4°C. The pellet was washed once with 70% EtOH and following centrifugation at 4000rpm for 10 min at 4°C the pellet was air dried for 3 h. The air-dried pellets were resuspended in 100µl of DEPC water and concentration of RNA was measured using spectrophotometry.

2 µg of total RNA was treated with DNaseI (Invitrogen, Carlsbad, CA, USA) and incubated for 15 min at RT. The DNaseI digestion was quenched by the addition of 1 µL of 25 mM EDTA and incubation at 65°C for 10 min. cDNA was then amplified from DNase treated RNA using random primers and 200 units of Superscript II reverse transcriptase (Invitrogen) according to the manufacturer's directions. The resulting cDNAs were diluted 100-fold. Reactions were assembled using PerfeCTa SYBR green PCR mix (Quanta Biosciences 95056-500), as per the manufacturer's protocol including oligonucleotides listed in Table 2-3. Primers for RT-qPCR were designed within the 5'-end of their coding regions of their target cDNAs to generate PCR products ~120 bp in length. Reactions were carried out on an Mx3000P QPCR System (Agilent Technologies). The relative fold enrichment of indicated mRNA was evaluated by the $\Delta\Delta C_t$ method (Livak and Schmittgen 2001). The expression levels of each gene was normalized against expression levels of a load control to generate a ΔC_t value. The expression of each gene was then normalized to the corresponding WT sample to generate $\Delta\Delta C_t$ values. The relative fold enrichment of mRNA for indicated strains relative to WT was given as $2^{-\Delta\Delta C_t}$, based on the assumption that the PCR reaction was 100% efficient. Expression levels of the *ACT1* and/or *TUB2* genes were determined as load controls, as indicated.

Table 2-3. Oligonucleotides used in RT-qPCR

Target cDNA	Oligonucleotide sequence
<i>ACT1</i>	S-GGATTCCGGTGATG GTGTTA AS-TCAAATCTCTACCGGCCAAA
<i>INO1</i>	S-CACCATGGAAAACCTCTTGC AS-GGGGACACCTTCCAAGATAGA
<i>TUB2</i>	S-TACTAGTGAAGGTATGGACGAATTG AS-TTCTTCATCATCTTCTACAGTAGCC
<i>YFR057W</i>	S-TCTTTGCGTGGCAATATACCTCATA AS-TCTGAGACGAAGTCGTTGCTAAAAT
<i>YKR105C</i>	S-ATGGAGGAAACTAAGTACTCTTCGC AS-GGAAAGTCCCATTGGAGAATCATTG
<i>YPR201W</i>	S-CTGCAAAGTTTCCTGGGAGT AS-CAAAGGACCGATGACCCAAT
<i>YGL263W</i>	S-GAGGACGAATACTTACATGTTTGAG AS-AGATACAGGGGTACTGAAATACCAT
<i>YEL073C</i>	S-GCATGGTCTAATACAGTTCCGTTAG AS-AAGGGTTTCATTCATCCAGATTACG
<i>YKR106W</i>	S-CGACCCGTCTCACCATGTAT AS-CATTTCAAGGAGGAGAAATCTGAG

2.12 RNA Seq

Wild type, *siz2Δ* and *siz2^{S522/527A}* cells were grown in YPD medium to mid-log phase. Total RNA was isolated from cell pellets using hot acidic phenol (2.11). The quality and quantity of RNA was then measured using spectrophotometry and sent for RNA Seq analysis.

The transcriptome analysis pipeline as performed by the Aitchison lab included- RNA-Seq paired-end reads of ~50 bp were mapped to genomic sequence of *S. cerevisiae* strain using BWA (Burrows-Wheeler Aligner). The mapped reads were extracted in proper pairs with a minimum MAPQ (MAPing Quality) score of 20 by SAMtools and then were aligned to annotated transcripts by BEDtools. Paired-end reads were then visualized by ChromoZoom. The transcript abundances were calculated based on FPKM (Fragments Per Kilobase of transcript per Million mapped reads). All FPKMs of annotated transcripts were normalized by an upper bound quantile normalization. The statistical significance for transcript level changes was calculated using t-test based on $(\text{FPKM}_{\text{mut}}/\text{FPKM}_{\text{wt}})$ values against an empirical null distribution. The empirical null distribution was computed from all possible permutations of the samples. pFDR values were calculated using the *mafdr* MATLAB function. Transcriptional differences in expression profiles were represented as log₂ fold changes.

2.13 Subtelomeric gene-silencing assay

Yeast strains used for the assessment of subtelomeric gene silencing are derivatives of UCC3505, in which the reporter genes *URA3* and *ADE2* are integrated adjacent to Tel7L and Tel5R, respectively (Singer and Gottschling 1994). Integration of reporter genes was an adjacent 81 bp sequence of telomere repeats (TG₁₋₃) that were integrated into *ADH4* (Tel7L) and a Y' element (Tel5R) resulting in the truncation of the endogenous chromosomes, and the generation of new telomeres to which telomerase adds telomeric repeats to.

Cells cultures with indicated gene alterations were generated by transformation as described in (2.1). 10-fold serial dilutions of cell cultures were spotted onto SC, SC -Ura -Ade and SC + 1mg/ml 5-FOA plates. Plates were then incubated for 3 days at 30°C.

2.14 Chromatin Immunoprecipitation

Chromatin immunoprecipitation experiments were performed as previously described in (Wan et al., 2009). An OD₆₀₀ = 50 equivalent of cultures in mid-log phase that had been grown at 30°C were pelleted and resuspended in 50ml of fresh YPD with 1% formaldehyde. Cultures were incubated for 20 min at 30°C to induce crosslinking. Glycine was added to a concentration of 125mM followed by a 5 min incubation at RT to quench crosslinking. Cells were pelleted, washed with TBS and the resulting pellet was flash frozen using liquid nitrogen and stored at -80°C.

Cells were resuspended in 500 ml FA lysis buffer (50mM HEPES-KOH pH 7.5, 150mM NaCl, 1mM EDTA, 1% Triton X-100, 0.1% Na deoxycholate) and lysed by glass bead beating at 4°C for half an hour. Glass beads were then removed from the lysate. Lysates were then sonicated (Branson Sonifier 250) on ice to shear chromosomal DNA to an average size of ~ 400 bp. Sonicated lysates were clarified by centrifugation at 14000 rpm for 10 min at 4°C. 50 ml of clarified lysate was removed for reverse crosslinking and isolation of DNA which was assessed by electrophoresis for appropriate sheared size of DNA. Reverse crosslinking and DNA isolation is described below. The remaining lysate was flash frozen with liquid nitrogen and stored at -80°C to be used for ChIP analysis.

Frozen lysates were then thawed on ice and diluted with FA lysis buffer; 1.5 ml for 1 IP and 2.5 ml for 2 IPs. 500 ml, representing the Input, was then diluted 100X into a TE 1% SDS solution, and subsequently reverse crosslinked as described below. 1 ml of the remaining lysate was then incubated with 5 ml of ssDNA (10mg/ml) and 2 μ l of mouse monoclonal anti-V5 antibody (Abcam ab27671), 4 μ l of rabbit polyclonal anti-PrA (Sigma P3775) antibody or 4 μ l of rabbit polyclonal anti-Smt3 (SUMO) antibody (Wozniak lab) for 2 hours at 4°C. 30 μ l of Protein G Dynabeads (Invitrogen 10004D) per IP were resuspended in PBS + 1% BSA. 10 μ l of heat-denatured ssDNA was added to the resuspended beads and incubated under rotation at RT for 30 min. The beads were then washed three times with PBS, three times with FA lysis buffer and resuspended in 50 μ l of FA lysis buffer. Following antibody/lysate incubation washed Protein G Dynabeads were added to each lysate and incubated for 1 h at 4°C under rotation. Beads were collected by magnet and sequentially washed 2x with FA lysis buffer, 1x with FA lysis buffer including 500mM NaCl, 1x with wash buffer (10mM Tris-HCl pH 8, 0.25M LiCl, 1mM EDTA, 0.5% NP-40, 0.5% sodium deoxycholate), and 1X with TE buffer. After the final wash, chromatin was eluted from the beads using 2 rounds of incubation at 65°C for 10 minutes with 200 μ l of TE 1% SDS. Input and ChIP samples were then reverse cross-linked by overnight incubation at 65°C. The following day 5 μ l of Proteinase K (20mg/ml) and 1 μ l of glycogen (20mg/ml) were added to the samples and incubated at 37°C for 2 h. 40 μ l of 5M LiCl was then added to each sample, followed by phenol/chloroform extraction, and ethanol precipitation. The resulting DNA pellets were resuspended in 50 μ l TE and 5 μ l of

RNase A (5mg/ml) and incubated at 37°C for 1 h followed by purification using Qiagen PCR Purification Kit (28106). Samples were eluted from PCR kit columns using 100ul of 10mM Tris-HCl pH8 and stored at -20°C.

DNA samples were analyzed by qPCR as described in (Makio and Wozniak 2020). ChIP and Input DNA were used to amplify the target sequences of interest using PerfeCTa SYBR green PCR mix (Quanta Biosciences 95056-500) and a MX3000 (Agilent) instrument. The relative fold enrichment of chromatin immunoprecipitated with the protein of interest was evaluated by the $\Delta\Delta C_t$ method (Livak and Schmittgen 2001). PCR amplification of each region was first normalized against the amplification of the corresponding Input DNA to generate a ΔC_t value. Each region was then normalized to the amplification of a non-specific binding control region including either 17.1 kb from Tel6R (subtelomeric Chip for Sir4) or an intergenic region in Chromosome V (subtelomeric ChIP for SUMO & *INO1* ChIP), to generate $\Delta\Delta C_t$ values. The relative fold change of chromatin over background was given as $2^{-\Delta\Delta C_t}$, based on the assumption that the PCR reaction was 100% efficient. Oligonucleotides used for qPCR are listed in Table 2-4.

Table 2-4. Oligonucleotides used in qPCR

Target DNA	Oligonucleotide Sequence
Chromosome V intergenic region	S-ACATTCTTGGAAA CCCATCG AS-TCGTATCATGATTTAGCGTCGT
<i>INO1 GRS1</i>	S-TCGTTCCTTTTGTTC TTCACG AS-GCCTCCGCATATTTACATT
<i>INO1 A</i>	S-AAATGCGGCATGTGAAAAGT AS-AGAG GTGCGCTTTCTCTGC

<i>INOI B</i>	S-AGAGAAAGCGCACCTCTGC AS-AGGAACCCGACAACAGAACA
<i>INOI C</i>	S-CGACAAGTGCACGTACAAGG AS-CAGTGGGCGTTACATCGAA
<i>INOI D</i>	S-CTTCGGCTCC ATGACTCAAT AS-GCTAACCATGGGCAACAGAG
<i>INOI E</i>	S-GGACTCAAAAGTGGCAATGG AS-TCAAGGGCGTAGCCAGTAAA
<i>INOI F</i>	S-CGTCTTAAAAGGGGCGTTTT AS-TTTACTGAGG TGGCCCTTGA
Chr. VI 0.5kb	S-GATAACTCTGAACTGTGCATCCAC AS-ACTGTC GGAGAGTTAACAAGCGGC
Chr. VI 2.5kb	S-GAGCAATGAATCTTCGGTGCTTGG AS-CGCAGTACCTTGGA AAAATCTAGGC
Chr. VI 4.1kb	S-CGTTCTTCTTGGCCCTTATC AS-CATCATCGGTGGTTTTGTCGTG
Chr. VI 7.7kb	S-AAGTCACTATGGGTTGCCGGTATC AS-AACT ACCTCTATAGGACCTGTCTC
Chr. VI 17.1kb	S-GAAAGTTTGGATGCTAGCAAGGGC ASGCATAGCCTTTGAAAACGGCG

2.14 Immunofluorescence

To each 5 ml culture of log-phase cells 0.6 ml of 10X phosphate buffer (1M KH_2PO_4 , 370 mM KOH, 0.5 mM MgCl_2) and 0.8 ml of 37% formaldehyde was added, followed by incubation at 30°C for 30 min. Cells were then pelleted and washed 2x with 1X phosphate buffer. The final pellets were resuspended in 100 ml

of sorbitol-citrate buffer (100 mM K₂PO₄, 3.6 mM citric acid, 1.2 M sorbitol, 0.5 mM MgCl₂) and DTT was added to final concentration of 1 mM. Cells were pelleted and incubated at 30°C for 20 min in 100 ml of sorbitol-citrate buffer supplemented with 2 mg/ml 20T zymolyase. Following incubation cells were pelleted and washed 2x with 1 ml sorbitol-citrate buffer. The final pellet was resuspended in 50 ml of sorbitol-citrate buffer. 20 ml of the cell suspension was pipetted onto a multi-well slide coated with 0.1 % poly-L-lysine and the slide was incubated at RT in a covered box lined with damp paper towels for 30 min. All subsequent incubations and washes were carried out at RT in the same box with ~ 20 ml each solution. Steps included 1) 1x PBST wash, 2) 1x addition of PBS 0.1% Triton X-100 with a 10 min incubation, 3) 2x wash with PBST, 4) 1x addition of PBST, 1% BSA with a 10 min incubation, 4) 1x addition of PBST, 1% BSA supplemented with a rabbit polyclonal anti-SUMO antibody (Wozniak Lab) at a 1:500 dilution with a 1 h incubation, 5) 10x wash with PBST, 0.1% BSA, 6) 1x addition of PBST, 1% BSA supplemented with Alexa Fluor 488 donkey anti-rabbit IgG antibody (Life technologies A11055) at a 1:200 dilution with a 1 h incubation 6) 10x wash with PBST, 0.1% BSA. After the final wash, 7) ~ 3 ul of DAPI-Fluoromount-G (SouthernBiotech 0100-20) was added to each well and a coverslip was placed over the slide. Cells were then analyzed by epifluorescence imaging.

2.15 Epifluorescence microscopy

Epifluorescence images of were acquired on a DeltaVision Elite imaging system (GE Healthcare Life Sciences) with a 60x/1.42 NA oil, Plan Apo N

objective (Olympus). Images were collected as 15 x 0.2 μm z-stacks, except for images used for calculating nuclear surface area which involved 40 x 0.2 μm z-stacks, using the SoftWoRx software, (version 6.5.2, GE Healthcare Life Sciences). All cells used for live cell imaging were grown to mid-log phase at 30°C, except for GFP-Siz2 strains which were incubated at RT. 1 ml of cultures were pelleted, washed once with dH₂O, and resuspended in SC. 1.5 ml of this cell suspension was then spotted onto a microscope slide and imaged at RT.

2.15.1 Image analysis

Images were rendered and analyzed using Image J (NIH). Representative images used in figures and for quantification were filtered with the unsharp mask filter (Radius (Sigma): 2.0 pixels; Mask Weight: 0.8).

Cell cycle stage of cells was assessed based on bud size and/or nuclear morphology. Specifically, G1 phase - unbudded cells, round nucleus; S phase - small-budded cells, round nucleus away from budneck; anaphase/telophase - large-budded cells, barbell shaped nuclei.

For line scan quantifications images from each channel were rendered in Image J as described above and converted to an 8-bit image. A line of a specific length, was drawn through individual cell nuclei and the fluorescence intensity along the line was quantified for each channel using Image J. Each line segment was drawn to be an equatorial optical section, such that the line drawn was centered upon the DAPI or Pus1-GFP signal or that the line passed through two points of the Sur4-mCherry signal along the NE, avoiding the nucleolus. However, as the weak

NE GFP-Siz2 signal in *scs2^{K180R}* and *siz2^{I472/473A}* backgrounds was most apparent in the regions adjacent to the nucleolus, lines drawn through the nuclei of these cells were initiated at the NE region adjacent to the nucleolus.

The NE localization of Sir4-GFP foci was determined as previously described (Lapetina et al., 2017). Cells producing Sir4-GFP and the nuclear/ER marker Sur4-mCherry were acquired 15 x 0.2 μm z-stacks. Images were deconvolved using the iterative 15 cycle conservative ratio in the softWoRx program (version 6.5.2, GE Healthcare Life Sciences) and rendered using ImageJ (National Institute of Health). Distinct Sir4-eGFP foci were counted, and grouped as either: colocalizing, where complete or partial signal overlap was observed between Sir4-eGFP and Sur4-mCherry, or not colocalizing with the NE signal. Colocalization was then expressed as a percentage of the total number of Sir4-eGFP foci.

The subnuclear position of the *INO1* locus was assessed relative to the nuclear periphery (Nup49-mRFP signal) and was considered to colocalize with NPCs when the GFP-lacI focus fully or partially overlapped with Nup49-mRFP, similar to the previously described method (J. H. Brickner and Walter 2004; Donna Garvey Brickner and Brickner 2010).

Tel14-L position inside the nucleus was determined relative to the NE marker Sec63-eGFP (Van De Vosse et al., 2013; Lapetina et al., 2017). Images were acquired as 15 x 0.2 μm z-stacks, and only the telomere present in the stack containing the brightest foci was counted. The distance of the telomere from the NE was measured (TD) and divided by the radius of the nuclei (r). The TD/ r ratio

(R) was used to group telomeres into three concentric zones of equal volume. Zone 1 represents foci with ratios $\leq 0.184 \times R$ (telomere at the NE); zone 2 foci with ratios $> 0.184 \times R$ and $< 0.422 \times R$; and zone 3 represents foci with ratios $\geq 0.422 \times R$. This method was only used in cells, and at cell cycle stages, where the nuclei remained spherical. In M-phase or mutant cells where nuclear flares were observed the localization of the GFP-tagged telomeres was determined to colocalize with the NE when the foci fully or partially overlapped with the NE localized marker, Sec63-GFP.

The surface area of the nucleus was determined using Imaris surface analysis (Surface detail $0.2 \mu\text{m}$, Thresholding: Background Subtraction $0.81299 \mu\text{m}$). Images processed in Imaris were acquired as $40 \times 0.2 \mu\text{m}$ z-stacks, and images were deconvolved using the iterative 15 cycle conservative ratio in the softWoRx program (version 6.5.2, GE Healthcare Life Sciences). In the case of M-phase cells where the surface area of the membrane bridge between the mother and daughter nucleus was not calculated by the Imaris software, the distance of the bridge was measured and used to calculate the cylindrical surface area of the bridge assuming a radius of 58 nm (Yamaguchi et al., 2011). The surface area of the mother nucleus, daughter nucleus and membrane bridge were then added to derive the total nuclear surface area of mitotic cells.

Chapter III: Recruitment of an activated gene to the yeast nuclear pore complex requires SUMOylation*

* A version of this chapter has been published and was co-authored in conjunction with N. Park and C. Ptak: Saik, N.O., Park, N., Ptak, C., Adames, N., Aitchison, J.D., and R.W. Wozniak. (2020) Recruitment of an Activated Gene to the Yeast Nuclear Pore Complex Requires Sumoylation. *Front Genet.* 2020 11:174.

3.1 Overview

Nuclear pore complexes (NPCs) can influence the spatial organization and transcriptional activity of genes by mediating protein interactions with chromatin. The NPC association and transcriptional activation of specific genes, such as *INO1*, is facilitated by various components of the NPC which are referred to as Nups. Several Nups, which play a role in the NPC association of *INO1*, also functionally and physically interact with the SUMO isopeptidase Ulp1. These observations led us to investigate the role of SUMOylation and deSUMOylation in the localization and expression of activated *INO1*. Our analysis shows that activation of *INO1* is accompanied by changes in the SUMOylation of proteins associated with the *INO1* locus. These changes are dependent on the binding of the SUMO E3 ligase, Siz2, and the SUMO isopeptidases, Ulp1, to specific regions of the *INO1* locus. Our results indicate that Siz2-mediated SUMOylation is a crucial regulator of *INO1* targeting to the NPC and a cycle of SUMOylation and deSUMOylation events at the NPC contributes to the activation of *INO1*.

3.2 Results

3.2.1 Ulp1 interacts with activated *INO1*.

Numerous yeast genes are repositioned from the nucleoplasm to NPCs upon activation, including the *INO1* gene (J. H. Brickner and Walter 2004; Texari et al., 2013; Donna Garvey Brickner et al., 2019). When cells are switched from medium containing inositol to medium depleted of this carbon source, the *INO1* gene is targeted to NPCs and transcriptionally activated. The association of activated *INO1* with the NPCs is dependent on Nup60 and the related Mlp1/Mlp2 proteins (Donna Garvey Brickner et al., 2007; Ahmed et al., 2010; Light et al., 2010; Donna Garvey Brickner et al., 2019). Both Nup60 and the Mlps are also required for the association of the deSUMOylase Ulp1 with the NPCs (Y. Zhao et al., 2004; Palancade et al., 2007; Srikumar, Lewicki, and Raught 2013). This could represent a system that would facilitate an interaction of Ulp1 with the *INO1* locus at the NPCs. Therefore, we tested whether the *INO1* gene physically interacts with Ulp1 upon induction. Prior to induction, no significant enrichment of Ulp1-PrA was detected along the *INO1* locus, as determined by ChIP analysis. However, following activation, a significant increase in Ulp1 occupancy was observed within the *INO1* ORF (Fig. 3-1). These results show that Ulp1 associates with specific regions of the *INO1* gene upon its induction and relocalization to the NPCs.

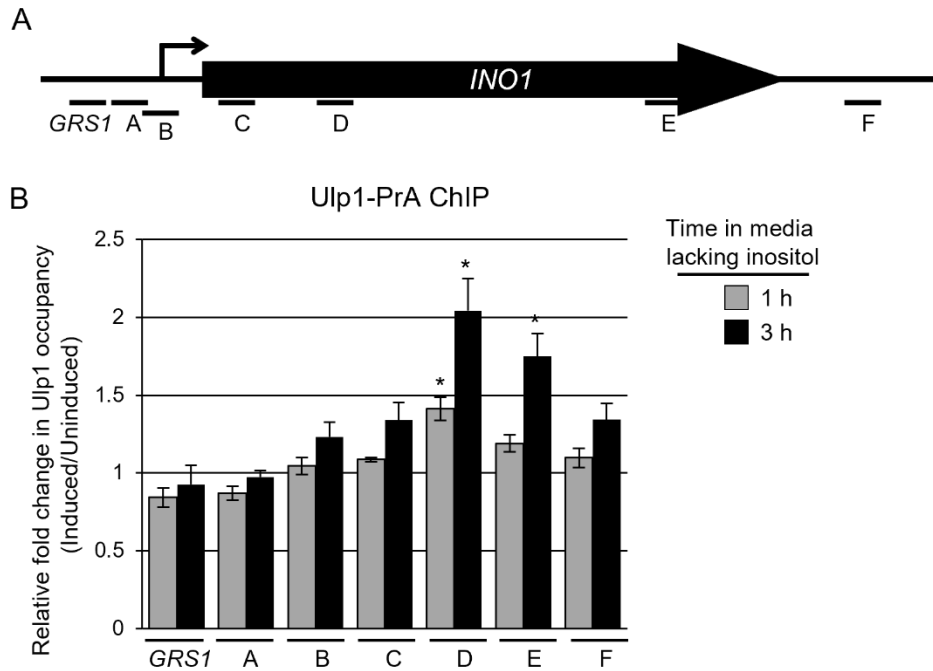


Figure 3-1. Ulp1 interacts with the induced *INO1* gene. **A)** Diagram of the *INO1* locus with regions investigated by ChIP analysis relative to the transcriptional start site (arrow), *GRS1* sequence, and open reading frame indicated below. **B)** Ulp1-PrA producing cells were first grown in medium containing inositol (repressing conditions) and then transferred to medium lacking inositol (inducing conditions). Cells were collected 0, 1, and 3h after *INO1* induction and subjected to ChIP analysis using antibodies directed against PrA. Occupancy of Ulp1-PrA at the *INO1* locus relative to an intergenic control was examined by qPCR using primer pairs that amplify regions of *INO1* indicated in panel A. Shown is the relative fold change in Ulp1-PrA association with the various regions of *INO1* for the indicated times after induction relative to uninduced samples. Graphs represent 3 biological replicates. Error bars- SEM. Asterisks- significant change in Ulp1-PrA association with *INO1* relative to uninduced counterpart using a paired two-tailed student's t-test. * $p < 0.05$. Experiments performed by N. Park. Figures constructed by N.O. Saik.

3.2.2 NPC recruitment and expression of *INO1* requires Ulp1 isopeptidase activity at the NPC.

To evaluate whether the interaction of Ulp1 with *INO1* at the NPC was necessary for *INO1* relocalization and activation upon induction, we examined how alterations to Ulp1 localization affected the activation of *INO1*. NPC binding domains of Ulp1 include residues 1-150 (*ulp1Δ₁₋₁₅₀*) and 150-340 (*ulp1Δ₁₅₀₋₃₄₀*). Mutants lacking either domain still bind to NPCs; however, mutants lacking both domains (*ulp1Δ₁₋₃₄₀*) show reduced levels of NPC association (S. J. Li and Hochstrasser 2003; V. G. Panse et al., 2003). We assessed the subnuclear localization of the *INO1* locus prior to and following induction in various *ulp1* mutants lacking domains required for NPC association. The position of *INO1* was visualized by tagging the gene with a *lacO₂₅₆* cassette in cells also producing the GFP-lacI protein (Brickner and Walter, 2004; Ahmed *et al.*, 2010; Fig. 3-2A). Induction of *INO1* led to a rapid accumulation of *INO1::lacO₂₅₆*/GFP-lacI foci at the nuclear periphery in WT cells and cells producing the *ulp1Δ₁₋₁₅₀* or *ulp1Δ₁₅₀₋₃₄₀* truncations (Fig. 3.2-B). In contrast, cells producing the *ulp1Δ₁₋₃₄₀* truncation (mutant ulp1 which fails to associate with the NPC) did not significantly change *INO1* localization following induction (Fig. 3.2B) or *INO1* transcript levels at various times following induction (Fig. 3-2C). In contrast, cells producing *ulp1Δ₁₋₁₅₀* or *ulp1Δ₁₅₀₋₃₄₀* truncations had WT levels of *INO1* gene expression (Fig. 3-2C). To test whether the phenotypes associated with the *ulp1Δ₁₋₃₄₀* mutant were due to a loss of ulp1₃₄₀₋₆₂₁ at the NPCs or inappropriate ulp1₃₄₀₋₆₂₁ localization and activity within the nucleus, we exogenously expressed

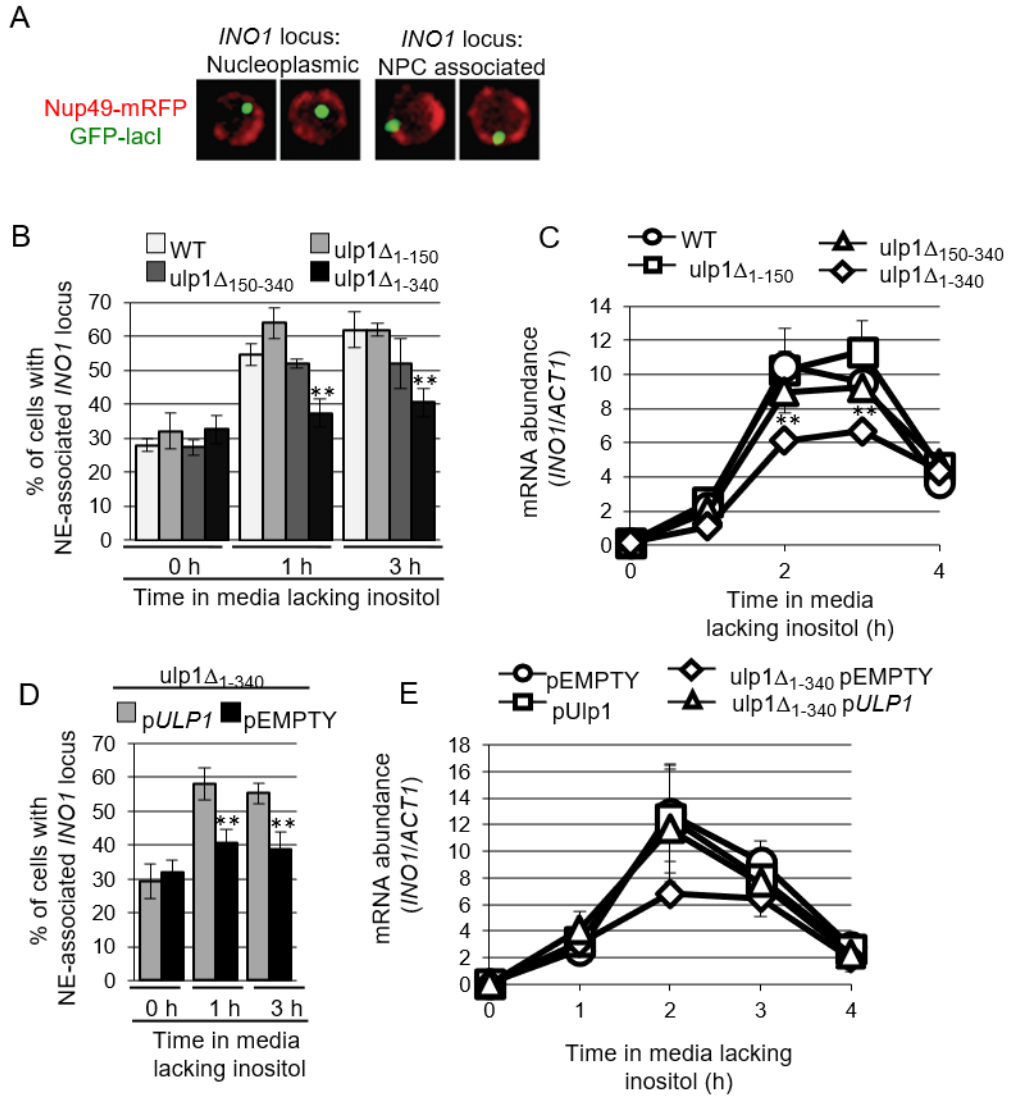


Figure 3-2. Ulp1 association with NPCs is required for NE-association and expression of *INO1* following induction. **A)** *INO1* localization relative to the nuclear envelope prior to and following induction was examined in cells containing an *INO1-lacO₂₅₆* construct and producing a GFP-lacI (green). Cells also produced Nup49-mRFP (red) to allow visualization of the nuclear envelope. Epifluorescence images of nuclei showing the subnuclear position of the GFP foci are shown. The *INO1* loci was determined to be associated with the NE when the GFP-lacI signal fully or partially overlapped with Nup49-mRFP. Bar – 2 μ m. **B and D)** The percentage of cells showing NE-association of *INO1-lacO₂₅₆* was determined prior to (0h), 1h and 3h post induction in WT and the indicated *ulp1* mutant strain backgrounds. The *ulp1* Δ_{1-340} strains were transformed with either an empty plasmid (pEMPTY) or a plasmid containing a version of WT *ULP1* (p*ULP1*). Graphs show data from 3 biological replicates where n=50 cells per replicate. Error bars-SD. Asterisks- significant change in *INO1* NE-association in *ulp1* mutant strain backgrounds relative to WT cells at corresponding time points using a two-tailed student's t-test. **p<0.01. **C and E)** Levels of *INO1* encoded mRNA following induction (0, 1, 2, 3, 4h) for the indicated strains as determined by RT-qPCR. *INO1* mRNA levels were normalized to *ACT1* mRNA. Graphs show data from 3 biological replicates. Error bars- SEM. Asterisks- significant change in *INO1* mRNA levels in *ulp1* mutant strain backgrounds relative to WT cells at corresponding time points using a two-tailed student's t-test. **p<0.01.

Ulp1 in *ulp1Δ₁₋₃₄₀* mutant cells; this restored *INO1* localization (Fig. 3-2D) and transcription to WT levels (Fig. 3-2E). Together these results suggest that the NPC localization of Ulp1 is necessary for the proper regulation of *INO1* upon induction.

The effects of the *ulp1Δ₁₋₃₄₀* mutant on *INO1* localization and expression could be the consequence of losing the N-terminal domain of Ulp1 (residues 1-340) or losing the isopeptidases activity of Ulp1 at the NPC. To distinguish between these possibilities, we examined whether tethering the *ulp1Δ₁₋₃₄₀* truncation to NPCs could rescue *ulp1Δ₁₋₃₄₀* associated *INO1* phenotypes. We tethered the *ulp1Δ₁₋₃₄₀* truncation to the NPCs by constructing a chimeric gene where the catalytic domain of Ulp1 (residues 340-621) was fused to the C-terminus of Nup53 (Fig. 3-3A). This fusion protein restored NPC association of *ulp1* (Fig. 3-3B) and resulted in WT levels of *INO1* mRNA (Fig. 3-3C) and NPC localization following induction (Fig. 3-3D). These results are consistent with a requirement for Ulp1 isopeptidase activity at the NPC in regulating *INO1* localization and gene expression.

We also examined whether altering Ulp1 isopeptidase activity at the NPC could inhibit *INO1* localization and transcription upon induction. We utilized a catalytically dead *ULP1* mutant (*ulp1^{CSDN}*) which inhibits the isopeptidases activity of Ulp1 independently of the targeting of Ulp1 to the NPC (Mossessova and Lima, 2000; Elmore et al., 2011; Fig. 3-4A). Because the *ulp1^{CSDN}* mutant does not support cell viability in the absence of WT Ulp1 (Elmore et al., 2011), we expressed the *ulp1^{CSDN}* mutant in WT cells and assessed for a dominant-negative phenotype for *INO1* localization and transcriptional activation. *ulp1^{CSDN}*-GFP localization to the NPCs was inversely proportional to WT Ulp1-mCherry (Fig. 3-4B), suggesting the

mutant protein could compete with WT Ulp1 for NPC binding sites. Consistent with the requirement for Ulp1 isopeptidase activity at NPCs to facilitate *INO1* relocation upon induction, cells expressing the *ulp1^{CSDN}* mutant prevented NPC association of the *INO1* locus upon induction (Fig. 3-4C). Cells expressing the *ulp1^{CSDN}* mutant did not reduce *INO1* expression following induction (Fig. 3-4A), suggesting the mutant may not exhibit a dominant-negative phenotype for *INO1* expression. Together these data suggest that Ulp1 isopeptidase activity at the NPC facilitates relocation of the *INO1* locus upon induction.

Several Nups regulate *INO1* localization and expression following induction, including Nup60 and Nup2 (Donna Garvey Brickner et al., 2007; Ahmed et al., 2010; Light et al., 2010; Donna Garvey Brickner et al., 2019), which have also been shown to physically and functionally interact with Ulp1. Nup60 is required for the NPC association of Ulp1 and for maintaining cellular levels of Ulp1 (Palancade et al., 2007). Nup2 interacts with Ulp1 and has been reported as a SUMO target (Folz et al., 2019; Hannich et al., 2005; Srikumar, Lewicki, and Raught 2013). We tested whether defects in *INO1* localization and expression in *nup60Δ* and *nup2Δ* cells were depended on Ulp1 catalytic activity at NPCs by using the Nup53-ulp1³⁴⁰⁻⁶²¹ protein in *nup60Δ* and *nup2Δ* mutants. The Nup53-ulp1³⁴⁰⁻⁶²¹-GFP fusion showed an NPC localization pattern in both *nup60Δ* and *nup2Δ* mutant cells (Fig. 3-5A), and rescued *INO1* recruitment to the NPCs (Fig. 3-5B) and restored *INO1* mRNA to WT levels (Fig. 3-5C) following induction. Based on these data, we conclude that the defects in *INO1*

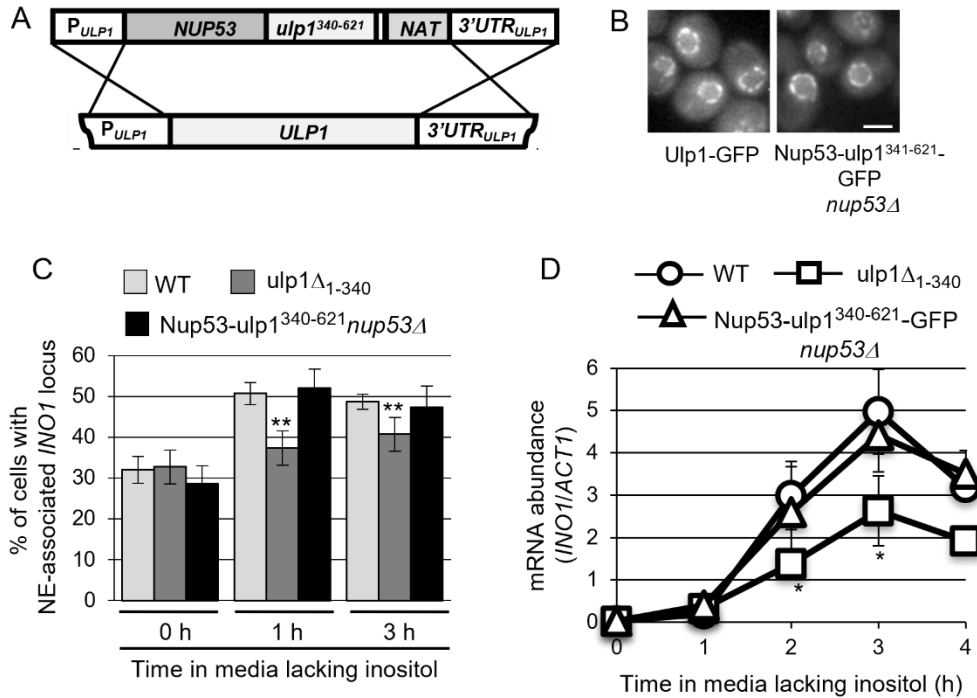


Figure 3-3. Tethering of the C-terminal domain of Ulp1 to the NPC supports NE-association and expression of *INO1* following induction. **A)** Diagram of the *NUP53-ulp1³⁴⁰⁻⁶²¹* chimera used to replace endogenous *ULP1*. **B)** Localization of GFP tagged *NUP53-ulp1³⁴⁰⁻⁶²¹* chimera. Bar-2 μ m. **C)** The percentage of cells showing NE-association of *INO1-lacO₂₅₆* in indicated strains following induction (0,1,3h). Localization of *INO1-lacO₂₅₆* locus was determined as described in Fig. 3-2. Graph shows data from at least 3 biological replicates where n=100 cells per replicate. Error bars-SD. Asterisks- significant change in *INO1* NE-association of various strains relative to WT cells at corresponding time points using a two-tailed student's t-test. **p<0.01. **D)** Levels of *INO1* encoded mRNA following induction (0, 1, 2, 3, 4h) for the indicated strains as described in Fig. 3-2. Graph shows data from 3 biological replicates. Error bars- SEM. Asterisks- significant change in *INO1* mRNA levels in various strains relative to WT cells at corresponding time points using a two-tailed student's t-test. *p<0.05. Strains were constructed by C. Ptak. Images in panel B were obtained by C. Ptak. Experiments in panel C and D were performed by N.O. Saik.

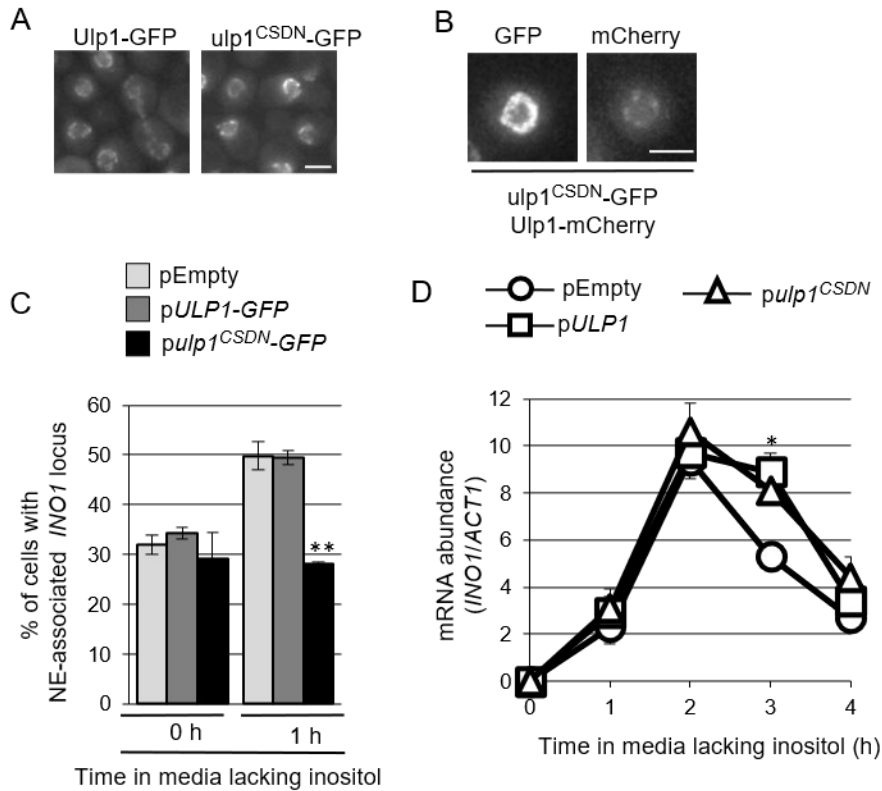


Figure 3-4. Ulp1 catalytic activity is required at the nuclear periphery to facilitate the NE-association of *INO1* upon induction. **A)** Epifluorescence images of WT cells producing plasmid-encoded Ulp1-GFP or Ulp1^{CSDN}-GFP. Bar-2 μ m. **B)** Representative epifluorescence images of cells producing endogenous Ulp1 tagged with mCherry and plasmid encoded Ulp1^{CSDN}-GFP. Bar-2 μ m. **C)** NE-association of the *INO1-lacO*₂₅₆ locus in strains containing the indicated plasmid as described in Fig. 3-2. Graph shows data from at least 3 biological replicates where n=50 cells per replicate. Error bars-SD. Asterisks- significant change in *INO1* NE-association of various strains relative to WT (pEMPTY) cells at corresponding time points using a two-tailed student's t-test. **p<0.01. **D)** Levels of *INO1* encoded mRNA following induction (0, 1, 2, 3, 4h) for strains containing the indicated plasmid as described in Fig. 3-2. Graph shows data from 3 biological replicates. Error bars- SEM. Asterisks- significant change in *INO1* mRNA levels of various strains relative to WT (pEMPTY) cells at corresponding time points using a two-tailed student's t-test. *p<0.05. Experiments in panel A and B were performed by C. Ptak. Experiments in panel C were performed by N. Park. Experiments in panel D were performed by N.O. Saik.

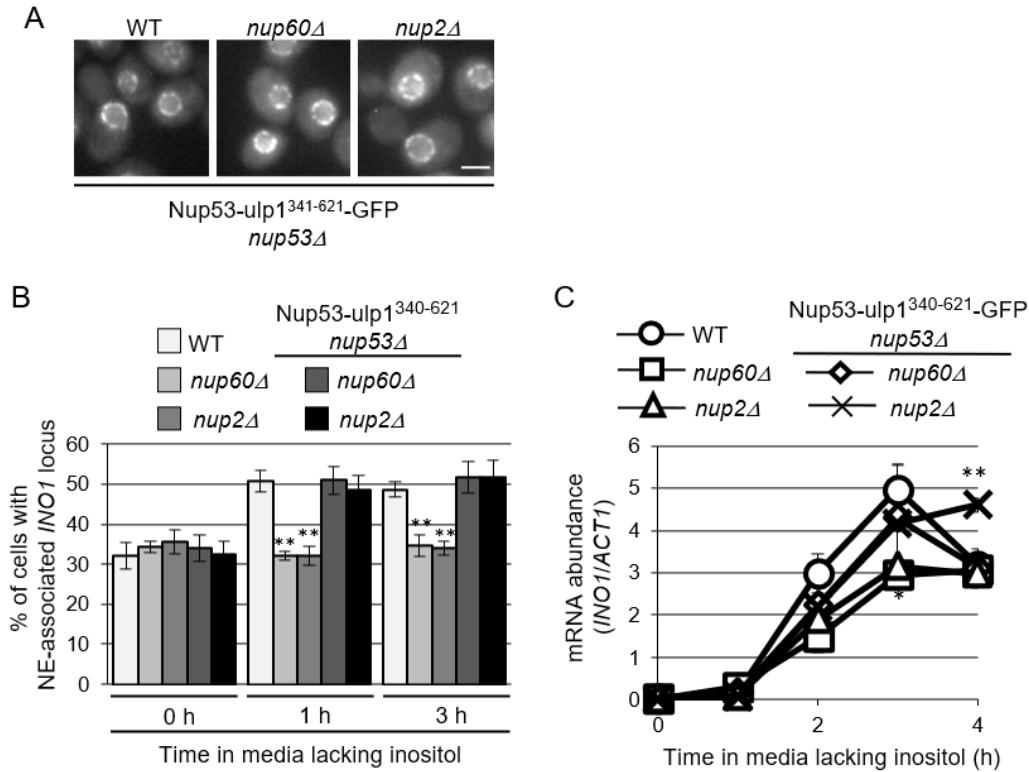


Figure 3-5. Artificially tethering the C-terminal domain of Ulp1 to the NPC rescues the *INO1* NE-association and transcriptional defects of *nup2* Δ and *nup60* Δ cells. **A)** Localization of the GFP-tagged *NUP53-ulp1*³⁴⁰⁻⁶²¹ chimera in strains lacking *NUP2* or *NUP60*. Bar- 2 μ m. **B)** Percentage of cells showing NE-association of *INO1-lacO*₂₅₆ in the indicated strains following induction (0, 1, 3h). Localization of *INO1-lacO*₂₅₆ locus was determined as described in Fig. 3-2. Graph shows data from at least 3 biological replicates where n=100 cells per replicate. Error bars-SD. Asterisks- significant change in *INO1* NE-association of various strains relative to WT cells at corresponding time points using a two-tailed student's t-test. **p<0.01. **C)** Levels of *INO1* encoded mRNA following induction (0, 1, 2, 3, 4h) for the indicated strains as described in Fig. 3-2. Graph shows data from 3 biological replicates. Error bars- SEM. Asterisks- significant change in *INO1* mRNA levels of various strains relative to WT cells at corresponding time points using a two-tailed student's t-test. *p<0.05, **p<0.01. Experiments in panel A were performed by C. Ptak. Experiments in panel B and C were performed by N.O. Saik.

regulation previously observed in the *nup60Δ* and *nup2Δ* mutants are functionally linked to Ulp1.

3.2.3 Repression of *INO1* is maintained by SUMOylation.

The requirement of Ulp1 to activate the *INO1* locus led us to investigate whether the induction of *INO1* altered the SUMOylation state of associated proteins. Antibodies directed against SUMO were used for ChIP analysis for specific regions within and near the *INO1* gene prior to and following induction. Upon induction, the gene recruitment sequence 1 (GRS1) showed a significant decrease in the SUMOylation of associated proteins, while regions containing the transcriptional start site showed a significant increase in SUMOylation. At the same time, proteins associated with the ORF and 3' UTR showed little or no changes in SUMOylation (Fig. 3-6A, B). While in *ulp1Δ₁₋₃₄₀* mutant cells, proteins associated with the ORF showed a significant increase in SUMOylation following induction (Fig. 3-6C). These results suggest that specific SUMOylation events within the *INO1* ORF may maintain the repression of *INO1*, and that specific deSUMOylation and SUMOylation events may regulate *INO1* localization and expression upon induction.

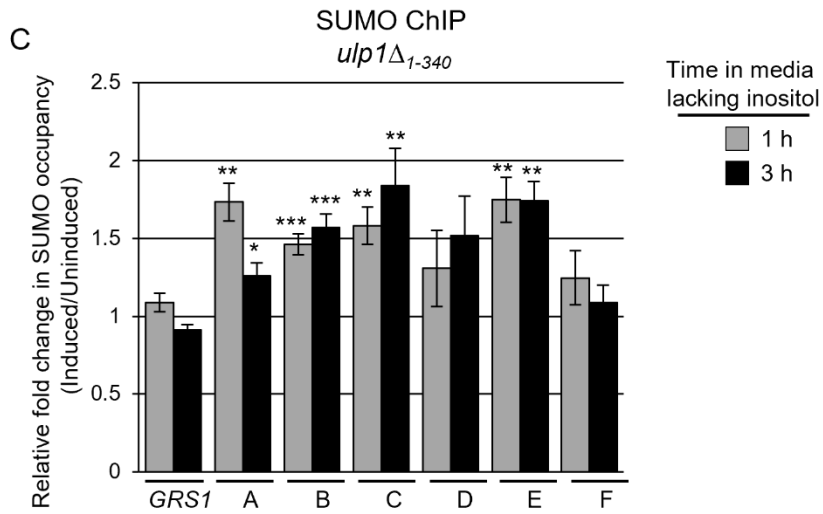
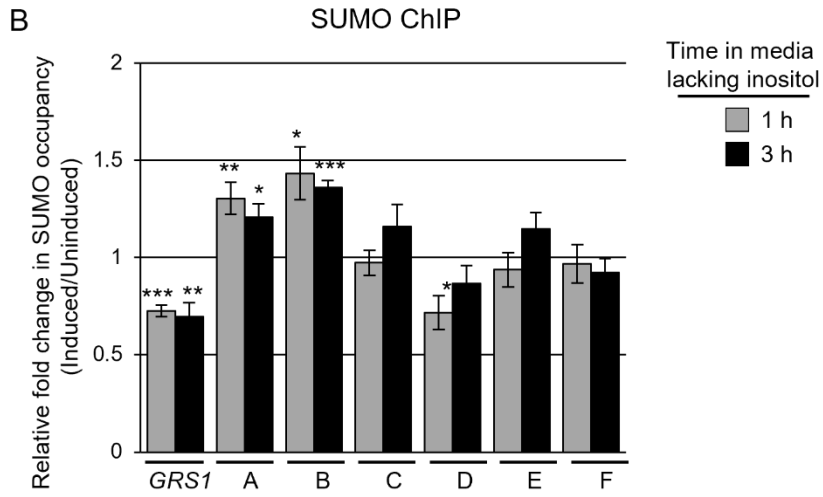


Figure 3-6. SUMOylation of *INO1*-associated proteins is altered upon *INO1* induction. **A)** Diagram of the *INO1* locus with regions investigated by ChIP analysis relative to the transcriptional start site (arrow), GRS1 sequence, and open reading frame indicated below. **B and C)** Indicated cells were grown and analyzed by ChIP analysis as described in Fig. 3-1, using antibodies directed against the SUMO polypeptide. Shown is the relative fold change of SUMOylated proteins associated with the various regions of *INO1* for the indicated times after induction relative to uninduced samples. Graphs represent at least 5 biological replicates. Error bars- SEM. Asterisks- significant change in association of SUMOylated proteins associated with *INO1* relative to uninduced counterpart using a paired two-tailed student's t-test. * $p < 0.05$, ** $p < 0.01$, *** $p < 0.001$.

3.2.4 The SUMO ligase Siz2 is required for the recruitment of *INO1* to NPCs.

Siz2 has been previously shown to play a role in the nuclear envelope association of chromatin (Ferreira et al., 2011; Lapetina et al., 2017; Churikov et al., 2016). Therefore, to further investigate the role of SUMOylation events in *INO1* regulation, we examined the role of Siz2, and the related SUMO ligase Siz1, in *INO1* localization and gene activation following induction. *INO1* recruitment to the NPCs was indistinguishable from WT cells in *siz1Δ* cells. Cells lacking Siz2 (*siz2Δ*), however, showed a significant decrease in association (Fig. 3-7A). Following induction, relative to WT cells, no differences in *INO1* mRNA were observed in cells lacking Siz1 or Siz2 (Fig. 3-7B). These results suggest that Siz2 is required for *INO1* binding to the nuclear periphery but not for *INO1* expression upon induction. Unobservable changes to *INO1* mRNA in *siz2Δ* cells support our observations that SUMOylation events within the ORF of *INO1* are required for repression, as these are absent in *siz2Δ* cells (Fig. 3-8).

The requirement of Siz2-mediated SUMOylation events for the NPC association of *INO1* led us to investigate whether Siz2 physically interacted with the *INO1* locus. We examined the binding of Siz2-PrA along the *INO1* locus prior to and following induction by ChIP analysis. Uninduced cells showed significantly higher levels of Siz2-PrA bound to the *GRS1* region relative to the intergenic control, and upon induction, a significant increase in Siz2 occupancy within the *INO1* ORF occurred (Fig. 3-9). These results are consistent with Siz2 functioning

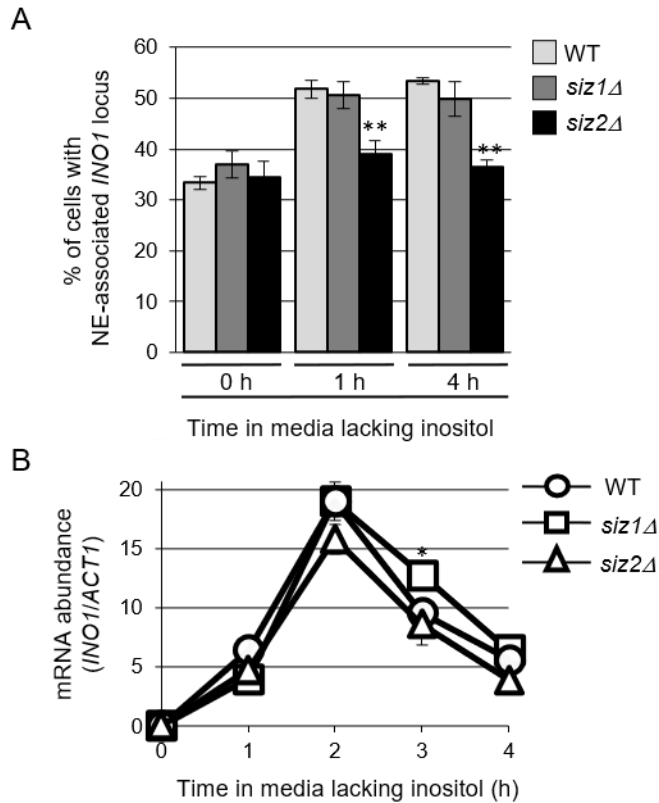


Figure 3-7. The SUMO E3 ligase Siz2 is required for NE-association of *INO1* following induction. **A)** Percentage of cells showing NE-association of *INO1-lacO₂₅₆* in indicated strains following induction (0, 1, 4h). Localization of *INO1-lacO₂₅₆* locus was determined as described in Fig. 3-2. Graph shows data from at least 3 biological replicates where n=100 cells per replicate. Error bars-SD. Asterisks- significant change in *INO1* NE-association of various strains relative to WT cells at corresponding time points using a two-tailed student's t-test. **p<0.01. **B)** Levels of *INO1* encoded mRNA following induction (0, 1, 2, 3, 4h) for the indicated strains as described in Fig. 3-2. Graph shows data from 3 biological replicates. Error bars- SEM. Asterisks- significant change in *INO1* mRNA levels for various strains relative to WT cells at corresponding time points using a two-tailed student's t-test. *p<0.05. Experiments were performed by N. Park. Figures were constructed by N.O. Saik.

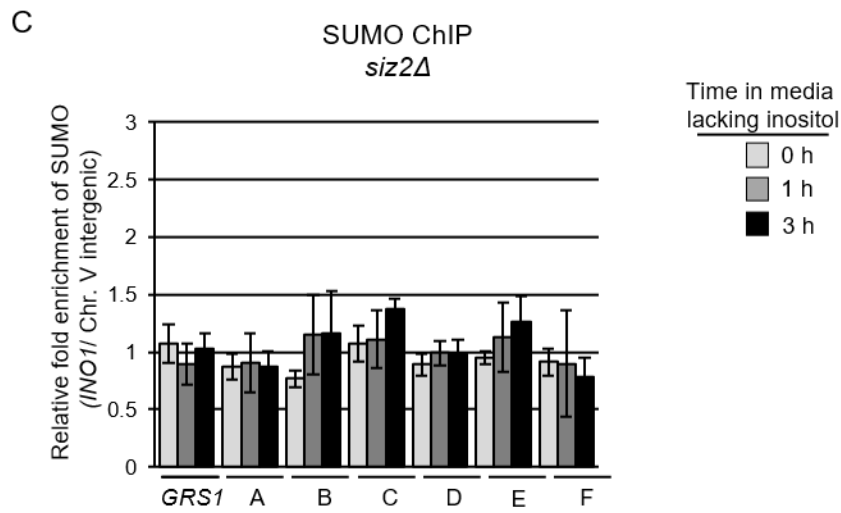
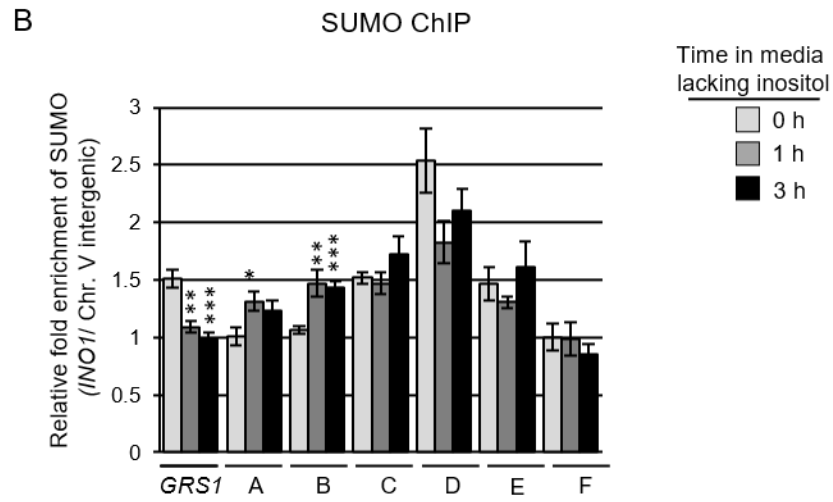


Figure 3-8. SUMOylation of *INO1*-associated proteins is dependent on Siz2. **A)** Diagram of the *INO1* locus with regions investigated by ChIP analysis relative to the transcriptional start site (arrow), GRS1 sequence, and open reading frame indicated below. **B** and **C)** Indicated cells were grown as described in Fig. 3-1, and collected 0, 1, and 3h after *INO1* induction for ChIP analysis using antibodies directed against the SUMO polypeptide. Changes of SUMO occupancy through the *INO1* locus upon induction were examined by qPCR to regions of *INO1* indicated in panel A. Shown is the relative fold enrichment of associated SUMOylated proteins at the various regions of *INO1* for the indicated times relative to an intergenic control. Graphs represent at least 3 biological replicates. Error bars-SEM. Asterisks- significant change in association of SUMOylated proteins associated with *INO1* relative to uninduced (0h) counterpart using a two-tailed student's t-test. * $p < 0.05$, ** $p < 0.01$, *** $p < 0.001$.

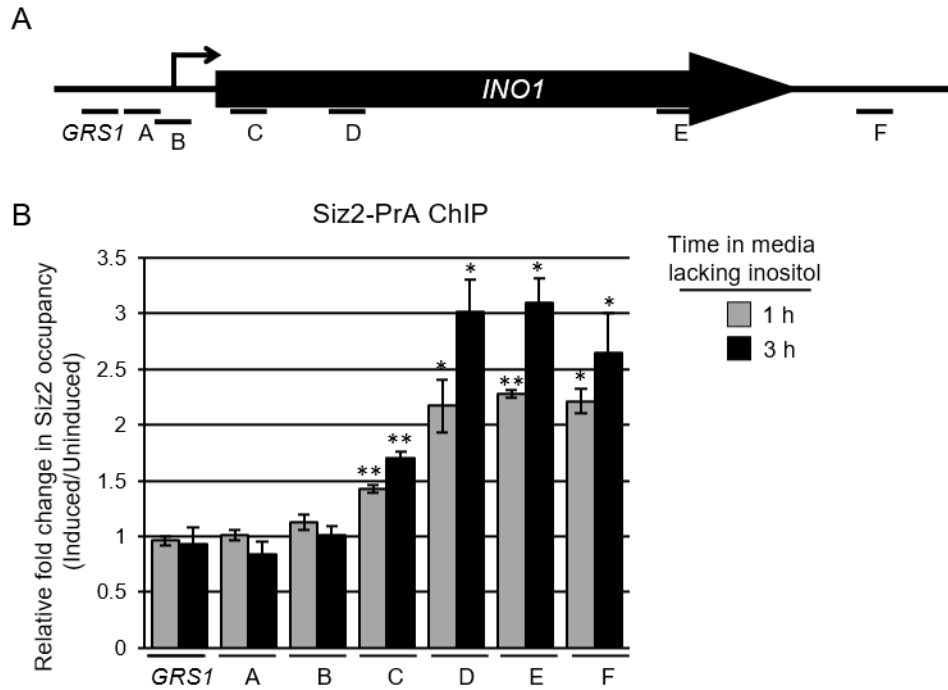


Figure 3-9. Siz2 interacts with the induced *INO1* locus. **A)** Diagram of the *INO1* locus with regions investigated by ChIP analysis relative to the transcriptional start site (arrow), GRS1 sequence, and open reading frame indicated below. **B)** Siz2-PrA producing cells were grown and analyzed by ChIP as described in Fig. 3-1. Shown is the relative fold change in Siz2-PrA association with the various regions of *INO1* for the indicated times after induction relative to uninduced samples. Graphs represent 3 biological replicates. Error bars- SEM. Asterisks- significant change in Siz2-PrA association with *INO1* relative to uninduced counterpart using a paired two-tailed student's t-test. * $p < 0.05$, ** $p < 0.01$, *** $p < 0.001$. Experiments were performed by N. Park. Figures were constructed by N.O. Saik.

in the SUMOylation of proteins associated with the *INO1* locus prior to (GRS1) and in response to *INO1* activation (upstream and within the ORF).

3.2.5 Siz2 protein levels regulate the recruitment of the *INO1* locus to NPCs.

When we investigated the SUMOylation profiles of *ulp1Δ₁₋₃₄₀* and *siz2Δ* mutant cells, we observed a similar SUMOylation pattern between the mutants, including the loss of at least four SUMOylated species within the 40-55kDa range (Fig. 3-10 A). Interestingly, in *S. pombe*, the NPC association of Ulp1 maintains SUMOylation events by preventing the degradation of a SUMO E3 ligase (Nie and Boddy 2015). Therefore, we investigated Siz2 protein levels in *ulp1Δ₁₋₃₄₀* mutant cells to determine whether the NPC association of Ulp1 was required for Siz2 stability. Siz2 protein levels were decreased in *ulp1Δ₁₋₃₄₀* mutant cells (Fig. 3-10 B), while *ulp1* protein levels were unaltered (Fig. 3-10 C). Together these results suggest that NPC-association of Ulp1 in *S. cerevisiae* stabilizes Siz2.

We reasoned that the loss of *INO1* localization to NPCs in the *ulp1Δ₁₋₃₄₀* mutant (Fig. 3-2B) might result from reduced Siz2 and Siz2-mediated SUMOylation events. To test this, we restored Siz2 protein levels in *ulp1Δ₁₋₃₄₀* mutant cells and investigated the subcellular localization of activated *INO1*. We exogenously expressed Siz2 using two different promoters in *ulp1Δ₁₋₃₄₀* and *siz2Δ* mutant cells. Exogenous expression of Siz2 from both promoters allowed Siz2 and Siz2-dependent SUMOylation events to accumulate in *ulp1Δ₁₋₃₄₀* and *siz2Δ* mutant cells (Fig. 3-11 C). NPC localization of induced *INO1* was comparable to WT cells when Siz2 levels were highly expressed (Nop promoter) in *ulp1Δ₁₋₃₄₀* and *siz2Δ* mutant cells. Upon induction, *INO1* localization to NPCs in *ulp1Δ₁₋₃₄₀* mutant cells

expressing *Siz2* with a Cup promoter was comparable to WT cells. In comparison, *INO1* localization to NPCs in *siz2Δ* mutant cells expressing *Siz2* using a Cup promoter was increased from uninduced (Fig. 3-11 A). This discrepancy may be due to residual endogenous *Siz2* present in the *ulp1Δ₁₋₃₄₀* mutant. Interestingly, when *Siz2* was highly expressed in either mutant background, increased levels of *INO1* association with NPCs were observed in uninduced cells (Fig. 3-11A). Together these data indicate that *Siz2* is a vital regulator of *INO1* localization to the NPCs. The loss of *INO1* localization to the NPCs in *ulp1Δ₁₋₃₄₀* mutant cells is due to a decrease in *Siz2* and *Siz2*-mediated SUMOylation. Importantly, despite restoring *INO1* localization to the NPCs in *ulp1Δ₁₋₃₄₀* mutant cells, exogenously expressing *Siz2* did not restore *INO1* mRNA to WT levels upon induction (Fig. 3-11B). These results further support our observations that SUMOylation mediates repression of the *INO1* loci, and transcriptional activation requires deSUMOylation by Ulp1 at the NPCs.

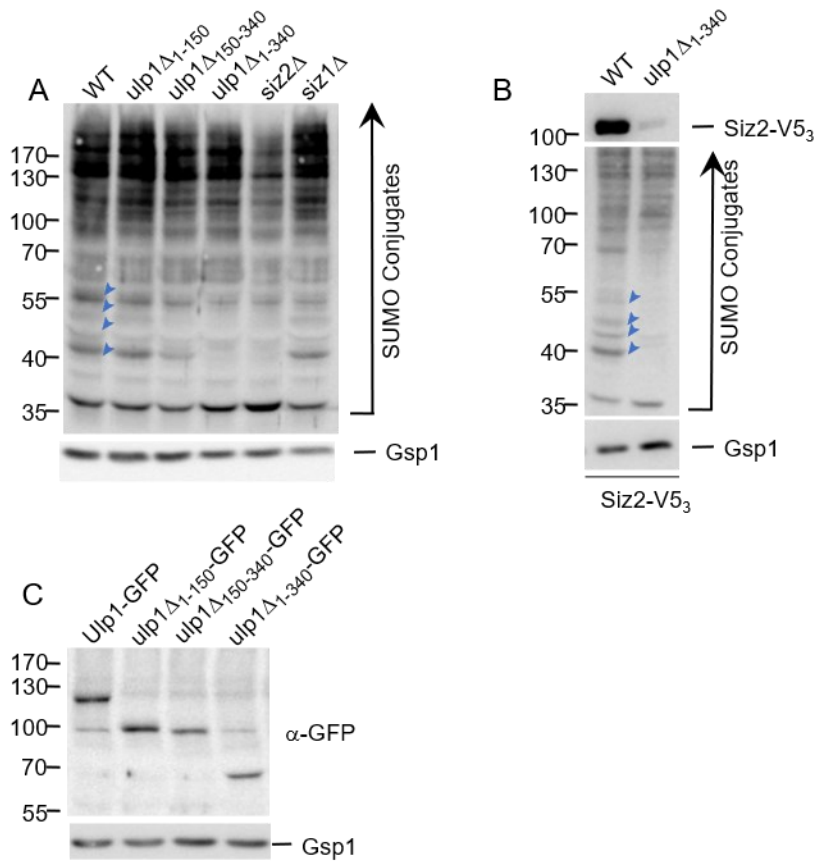
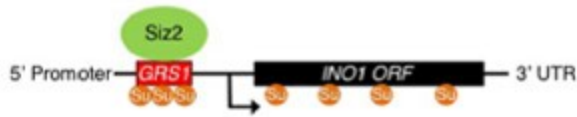


Figure 3-10. Loss of Ulp1 association with NPCs reduces Siz2 and Siz2-mediated SUMOylation events. **A)** Whole-cell lysates of the indicated strains were examined by western blotting to detect SUMO conjugates using an anti-SUMO antibody. Gsp1 is used as a loading control. Blue arrowheads point to four SUMO conjugates absent in *ulp1*Δ₁₋₃₄₀ and *siz2*Δ mutant cells. **B)** Whole-cell lysates of the indicated strains were examined by western blotting to detect Siz2-V5₃ and SUMO conjugate profiles using an anti-V5 antibody and anti-SUMO antibody. Gsp1 is used as a loading control. Blue arrowheads point to four SUMO conjugates absent in *ulp1*Δ₁₋₃₄₀ mutant cells. **C)** Whole-cell lysates of the indicated strains were examined by western blotting to detect *ulp1* derivatives using an anti-GFP antibody. Gsp1 is used as a loading control. Molecular mass markers for Western blot analysis are shown in kDa. Experiments in panel A and C were performed by C. Ptak. Experiments in panel B were performed by N.O. Saik. Figures were constructed by N.O. Saik.

Figure 3-11. Exogenously expressing Siz2 rescues the *INO1* NE-association defects of *ulp1* Δ_{1-340} cells. **A)** Percentage of cells showing NE-association of *INO1-lacO₂₅₆* in indicated strains following induction (0 and 3h). Localization of *INO1-lacO₂₅₆* locus was determined as described in Fig. 3-2. Graph shows data from at least 3 biological replicates where n=100 cells per replicate. Error bars- SD. Asterisks- significant change in *INO1* NE-association of various strain backgrounds relative to WT cells at the corresponding time point using a two-tailed student's t-test. **p<0.01, ***<0.001. **B)** Levels of *INO1* encoded mRNA following induction (3h) for the indicated strains as described in Fig. 3-2. Graph shows data from 3 biological replicates. Error bars- SEM. Asterisks- significant change in *INO1* mRNA levels in various strains relative to WT cells using a two-tailed student's t-test. *p<0.05, **p<0.01. **C)** Whole-cell lysates of the indicated strains 0 and 3h following induction were examined by western blotting to detect Siz2-V5₃ and SUMO-conjugate profiles using anti-V5 and anti-SUMO antibody. Gsp1 is used as a loading control. Molecular mass markers for western blot analysis are shown in kDa.

Uninduced nucleoplasmic *INO1*



Induced NPC associated *INO1*

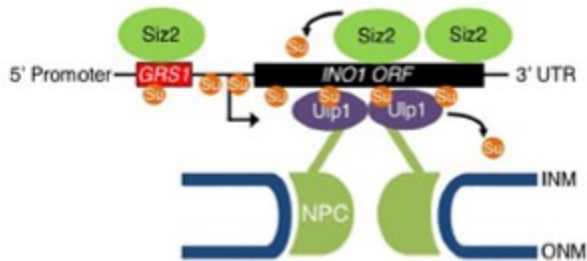


Figure 3-12. Model for the role of SUMOylation and deSUMOylation in *INO1* NE-association and expression following induction. Shown is the proposed model for the role of SUMOylation in NPC targeting and transcriptional activation of the *INO1* gene. In a repressed state *INO1* is positioned away from the nuclear periphery and bound by SUMOylated proteins. Following induction, Siz2 is recruited to the ORF of the *INO1* locus where Siz2 facilitates the SUMOylation of *INO1* associated proteins. These events facilitate the targeting of the *INO1* locus to the NPC where it interacts with NPC-associated Ulp1. Ulp1 then deSUMOylates *INO1* bound proteins to promote *INO1* transcription.

3.3 Discussion

Numerous observations have established the importance of the spatial organization of the genome in regulating chromatin transcription (Mekhail et al., 2008; Van de Vosse et al., 2011; Ptak and Wozniak 2016). In yeast, inducible genes, such as *INO1*, are relocalized from the nucleoplasm to the nuclear periphery upon their induction (J. H. Brickner and Walter 2004; Texari et al., 2013; Donna Garvey Brickner et al., 2019). Relocalization is associated with the loss of transcriptional repressors from chromatin and interactions of the locus with transcriptional machinery (Donna Garvey Brickner et al., 2019; Randise-Hinchliff et al., 2016). Here we show that specific SUMOylation and deSUMOylation events along the *INO1* locus are associated with the activation and relocalization of the gene to the NPCs (Fig. 3-6). We show that SUMOylation at the *INO1* loci is facilitated by the SUMO E3 ligase Siz2 (Fig. 3-8, 3-9) and that Siz2 is essential for the relocalization of activated *INO1* from the nucleoplasm to NPCs (Fig. 3-7), where it interacts with NPC-associated Ulp1 (Fig. 3-1). Our data suggest that this interaction facilitates the deSUMOylation of proteins within the *INO1* ORF to facilitate *INO1* expression. These results imply that a cycle of SUMOylation and NPC-associated deSUMOylation contributes to *INO1* regulation (Fig. 3-12).

Siz2-mediated SUMOylation events facilitate *INO1* localization to the NPCs.

Several proteins which associate with *INO1* to mediate the relocalization of the locus to the NPCs are SUMOylated or predicted to be SUMOylated. For example, Put3 and Cbf1 bind to GRSI and GRSII, respectively, to facilitate targeting to the NPC upon induction (Shetty and Lopes 2010; Donna G. Brickner

and Brickner 2012; Randise-Hinchliff et al., 2016; Donna Garvey Brickner et al., 2019). Put3 contains a consensus SUMOylation site (Q. Zhao et al., 2014), and the SUMOylation of Cbf1 has been reported (Wohlschlegel et al., 2004; Denison et al., 2005). Likewise, Nup2 and Nup60 which interact with and are required for the relocalization of *INO1* to the NPC upon induction (Dilworth et al., 2005; Donna Garvey Brickner et al., 2007; Ahmed et al., 2010; Light et al., 2010; Donna Garvey Brickner et al., 2019) have been identified as SUMOylation targets (Folz et al., 2019). Therefore, the binding of Siz2 (Fig. 3-9) and subsequent Siz2-mediated SUMOylation events within *INO1* (Fig. 3-8) following induction likely represents the SUMOylation of these or other TSF and INM proteins required for the relocalization of *INO1* to NPCs. The SUMOylation of these proteins may enhance interactions with other proteins involved in *INO1* regulation. Consistent with this idea are our observations that increasing Siz2 and Siz2-mediated SUMOylation events (p_{Nop}-Siz2-V5₃) causes aberrant localization of *INO1* to NPCs under uninduced conditions (Fig. 3-11 A).

Siz2 and Siz2-mediated SUMOylation of *INO1* associated proteins are required for NPC localization but not for the transcription of *INO1* (Fig. 3-7). This is consistent with observations that show gene positioning and transcription can be mediated by distinct elements. Put3 and Cbf1, for example, are required for recruiting *INO1* to the nuclear periphery but not for transcription (Donna G. Brickner and Brickner 2012). Our observations that Siz2 and Siz2-mediated SUMOylation is required for NPC localization but not for the transcription of *INO1* is also consistent with previous observations that NPC association of *INO1* with the

NPC is not required for RNA polymerase II-mediated transcription (Schmid et al., 2006; Donna Garvey Brickner et al., 2007).

We cannot rule out the possibility that Siz2 and Siz2-mediated SUMOylation may be involved in facilitating transcriptional memory. Transcriptional memory is established under specific stimuli to allow for a more efficient response to the stimuli in the future (D'Urso and Brickner 2017). During transcriptional memory, poised RNA Pol II PIC is bound to promoters to enhance the rate of future reactivation. *INO1* transcriptional memory requires a DNA sequence known as a memory recruitment sequence (MRS), which will be bound by specific TSFs when going from activating to repressive conditions. This facilitates the incorporation of other factors required for future reactivation (Light et al., 2010; D'Urso et al., 2016; D'Urso and Brickner 2017). We show an increase in SUMOylation of the MRS region (region A) following induction (Fig. 3-6). SUMOylation at the MRS during initial activation may “prime” these regions and facilitate the incorporation of TSFs and other factors required for transcriptional memory following repression. Whether Siz2-mediated SUMOylation at *INO1* is required for transcriptional memory would be of interest to further distinguish the role of Siz2 in *INO1* localization and transcriptional regulation.

Ulp1-mediated deSUMOylation events facilitate transcriptional activation of *INO1*.

We propose that the SUMOylation events which arise from Siz2 binding to *INO1* upon induction facilitate the binding of the locus to NPCs where interactions with Ulp1 can then direct deSUMOylation events necessary for transcription. We

show that the loss of Ulp1 isopeptidase activity at the NPC prevents the deSUMOylation of the *INO1* locus, which is necessary for transcriptional activation (Fig. 3-6). Because restoring the isopeptidase activity of Ulp1 at the NPCs, restores *INO1* mRNA to WT levels (Fig. 3-3C), this suggests that the ability of Ulp1 to bind the *INO1* ORF is dependent on NPC interactions. Nup2 and Nup60 may function to facilitate Ulp1 interactions with the *INO1* ORF at NPCs. Consistent with this idea, we show that positioning the Ulp1 C-terminal catalytic domain at the NPC restores *INO1* regulation in *nup60Δ* and *nup2Δ* cells (Fig.3-5). Our observations that re-establishing *INO1* localization to the NPCs independently of Ulp1 isopeptidase activity (*ulp1Δ₁₋₃₄₀ p_{Nop/Cup}-Siz2-V5₃*) does not restore *INO1* mRNA to WT levels upon induction (Fig. 3-11) also supports the idea that the interaction of Ulp1 with the NPCs is required for the deSUMOylation and transcriptional activation of *INO1*. Overall, we propose that Siz2 and Ulp1 support a cycle of SUMOylation and deSUMOylation events required for the expression and localization of *INO1* to the NPCs upon induction (Fig. 3-12).

INO1 induction requires the dynamic regulation of SUMOylation and deSUMOylation events.

The requirement for SUMOylation and deSUMOylation events in regulating *INO1* is similar to those reported for *GALI* (Rosonina, Duncan, and Manley 2010; 2012; Texari et al., 2013). This suggests that the dynamic regulation of SUMOylation and deSUMOylation events may be a general regulatory mechanism required for the cell to respond to various stimuli. The localization of Ulp1 to the NPC situates deSUMOylation events at an essential point for receiving

regulatory signals required for transcriptional regulation. As global changes to SUMOylation under numerous stress conditions have been reported (Enserink 2015), testing a broader role for SUMOylation and NPC-mediated deSUMOylation on transcriptional response pathways under different stress conditions will be of interest.

Consistent with previous reports (Nie and Boddy 2015), we show that the NPC association of Ulp1 is required for E3 ligases stability (Fig. 3-10). We have identified *INO1* regulation as a biological function maintained by this stability pathway. In the case of *INO1* regulation, the degradation of Siz2 upon Ulp1 mislocalization ensures Siz2-mediated SUMOylation does not accumulate within *INO1* and cause aberrant localization to NPCs under uninduced conditions, as seen when Siz2 levels are stabilized in the *ulp1Δ₁₋₃₄₀* (Fig. 3-11A). Although this may not necessarily affect the transcriptional regulation of *INO1* (Fig. 3-11B), the inappropriate tethering of the *INO1* locus to the NPC may disrupt other NPC transcriptional regulation pathways. Furthermore, without the isopeptidase activity of Ulp1 at the NPCs to facilitate deSUMOylation, the increased SUMOylation of *INO1* associated proteins could prevent the SUMOylation of other targets required for other biological processes.

Overall, the requirement of Siz2-mediated SUMOylation and Ulp1 facilitated deSUMOylation events in regulating induced *INO1* highlights the dynamic regulatory mechanisms required for gene regulation.

Chapter IV: Phosphorylation-dependent mitotic SUMOylation drives nuclear envelope-chromatin interactions*

* A version of this chapter has been published and was co-first authored in conjunction with C. Ptak: Ptak, C., Saik, N.O., Premashankar, A., Lapetina, D.L., Aitchison, J.D., Montpetit, B., and R.W. Wozniak. (2021) Phosphorylation-dependent mitotic SUMOylation drives nuclear envelope-chromatin interactions. *J Cell Biol.* 2021 6;220(12):e202103036.

4.1 Overview

SUMOylation is a post-translational modification that targets a diverse set of proteins to regulate various biological functions. The SUMOylation of specific targets can be facilitated by regulating the spatial and temporal localization of SUMO machinery components. SUMOylation events can then facilitate protein-protein interactions by generating a new contact site for an interacting partner containing a SUMO-Interacting (SIM) motif. The formation of SUMO:SIM protein networks within a subcellular compartment can regulate a specific biological function by enhancing complex formation and activity required for these processes. We have identified a novel regulatory system that facilitates the spatiotemporal relocalization of Siz2 and its subsequent SUMOylation events to the INM. We show that Siz2 undergoes phosphorylation-dependent relocalization to the INM during mitosis. The compartmentalization of Siz2 to the INM depends on both FFAT:MSP interactions and SUMO:SIM interactions between Siz2 and its receptor, Scs2. We show that the Siz2-Scs2 protein complex facilitates the enrichment of SUMOylation at the INM generating SUMO:SIM protein interaction networks required for the re-association of chromatin with the INM during mitosis.

4.2 Results

4.2.1 NE associated SUMOylation events occur during mitosis.

Various biological functions, including the spatial orientation of chromatin relative to the nuclear periphery, are regulated by SUMOylation (Ferreira et al., 2011; Lapetina et al., 2017; Psakhye and Jentsch 2012; Moradi-Fard et al., 2016; Texari et al., 2013; Saik et al., 2020). The biological functions of SUMOylation at the NE led us to investigate whether we could visualize an enrichment of SUMOylated species at the INM. The spatial localization of SUMOylation species in asynchronously grown cells was assessed by immunofluorescence microscopy (IF) using a SUMO-specific antibody. Consistent with the majority of previously identified SUMOylated proteins being nuclear (Srikumar, Lewicki, and Raught 2013; Vikram Govind Panse et al., 2004; Wohlschlegel et al., 2004; Y. Zhao et al., 2004; Hannich et al., 2005; Wykoff and O'Shea 2005) interphase cells (unbudded and small-budded) cells showed a predominantly nuclear SUMO signal. As previously reported, mitotic cells (large budded) had a SUMO signal at septins (Erica S. Johnson and Gupta 2001); however, they also showed an enriched SUMO signal at the NE (Fig. 4-1).

4.2.2 Mitotic SUMOylation events at the NE are dependent on Siz2.

Three SUMO E3 ligases in *S. cerevisiae*, Siz1, Siz2/Nfi1, and Mms21 facilitate the SUMOylation of specific targets in actively growing cells (Jentsch and Psakhye 2013). We examined the spatial localization of SUMOylation species in mutant strains lacking specific E3 ligase activity to determine whether the mitotic enrichment of SUMO conjugates was dependent on a specific SUMO E3 ligase.

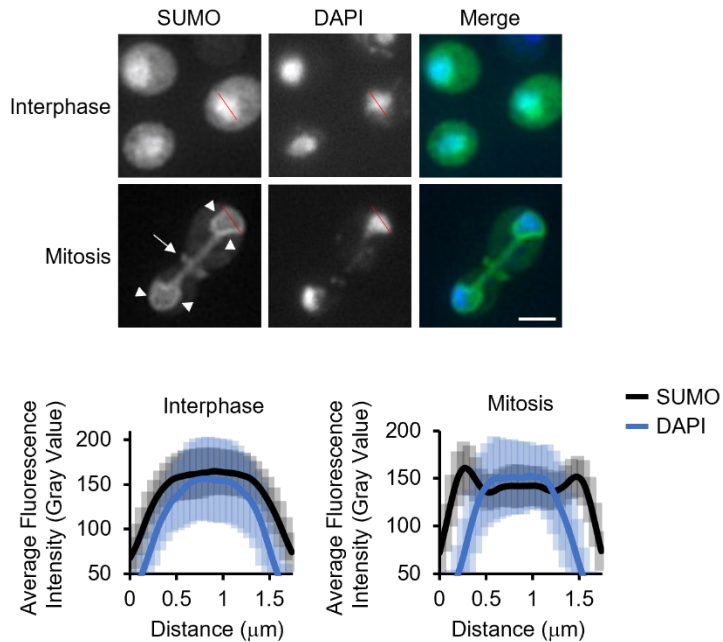


Figure 4-1. SUMOylation events are enriched at the NE during mitosis. Anti-SUMO immunofluorescence analysis of asynchronously grown cells. Arrowheads highlight SUMO along the NE, with nuclear position determined by DAPI staining. A SUMOylated septin ring is indicated by an arrow. Nuclear fluorescence levels were quantified using line scan intensities of equatorial optical sections through the nuclei (see red lines) of interphase (unbudded or small-budded) and mitotic (large budded) cells. Plots show average fluorescence intensity for SUMO-IF and DAPI at multiple points along a 1.75 μm line for $n=25$ nuclei. Bar- 2 μm . Error bars- SD. Experiments were performed by C. Ptak. Figures were constructed by C. Ptak and N.O. Saik.

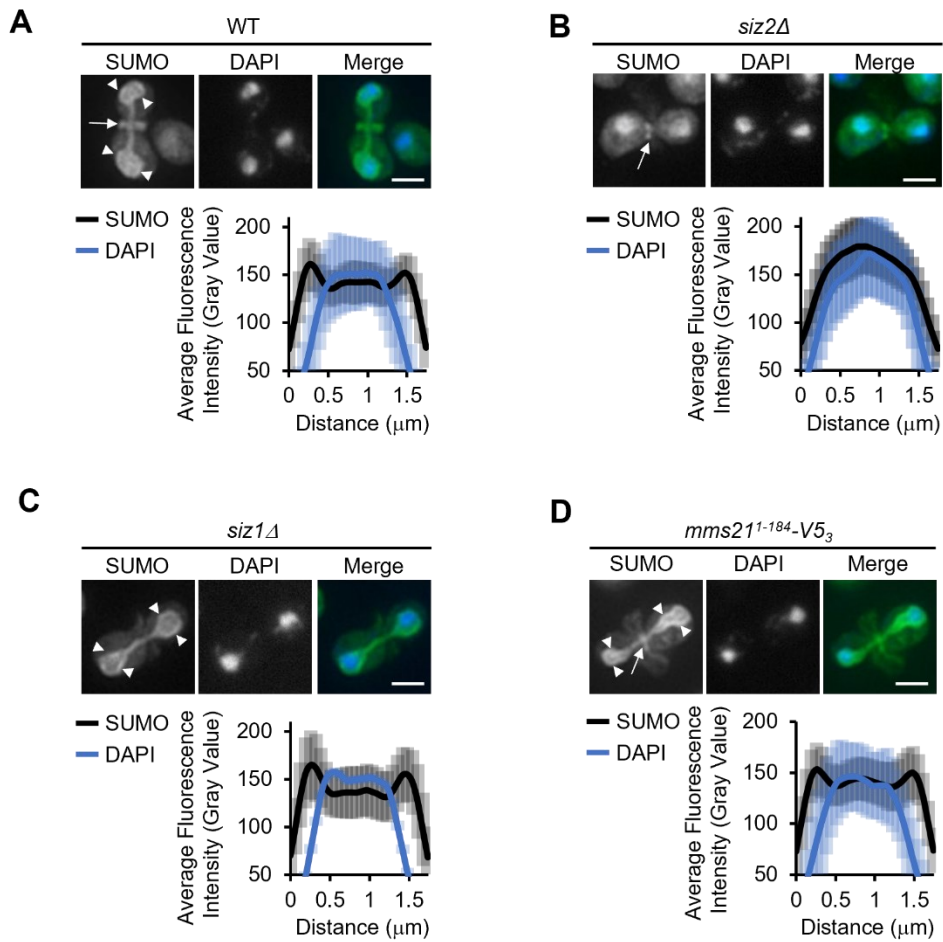


Figure 4-2. The mitotic enrichment of SUMO conjugates at the NE is dependent on Siz2. Anti-SUMO immunofluorescence analysis of indicated strains. Imaging and quantification of the nuclear distribution of SUMO in mitotic cells ($n = 25$) was performed as in Fig. 4-1. Arrowheads highlight SUMO along the NE, with nuclear position determined by DAPI staining. A SUMOylated septin ring is indicated by an arrow. Bar- $2 \mu\text{m}$. Error bars- SD. Experiments were performed by C. Ptak. Figures were constructed by C. Ptak and N.O. Saik.

The loss of Siz2 activity, but not Siz1 or Mms21, prevented the mitotic accumulation of SUMO conjugates at the NE (Fig. 4-2). These observations indicate Siz2 is required for the mitotic accumulation of SUMO conjugates at the NE.

Coinciding with the mitotic enrichment of SUMO at the NE, western blotting analysis in synchronized cells revealed an increase in the mitotic levels of various SUMOylated species, including four SUMOylated species in the 40-55 kDa size range (Fig. 4-3A). Clb2 protein levels were used to determine the onset of mitosis, as degradation of Clb2 occurs upon anaphase onset (Irniger, 2002). The four mitotic SUMOylation species in the 40-55 kDa range could also be visualized by western blotting analysis of asynchronous cells (Fig. 4-3B). We investigated whether the cell cycle specific changes in SUMOylation proteins detected by western blot analysis were the Siz2-dependent mitotic SUMOylated proteins observed at the NE. Anti-SUMO western blotting of synchronized or asynchronous cell cultures showed that cells lacking Siz2, but not Siz1 or Mms21, failed to accumulate the prominent SUMOylated species during mitosis (Fig. 4-3B-D). Together, these observations indicate that Siz2 is required to direct specific mitotic SUMOylation events at the NE.

Enrichment of SUMOylation events to specific regions can be achieved by targeting SUMO regulatory components to these regions (Jentsch and Psakhye 2013). Therefore, we examined GFP-Siz2 localization in asynchronously grown cells. GFP-Siz2 showed a primarily diffuse localization throughout the nucleoplasm in interphase cells, with dynamic GFP-Siz2 puncta also visible along

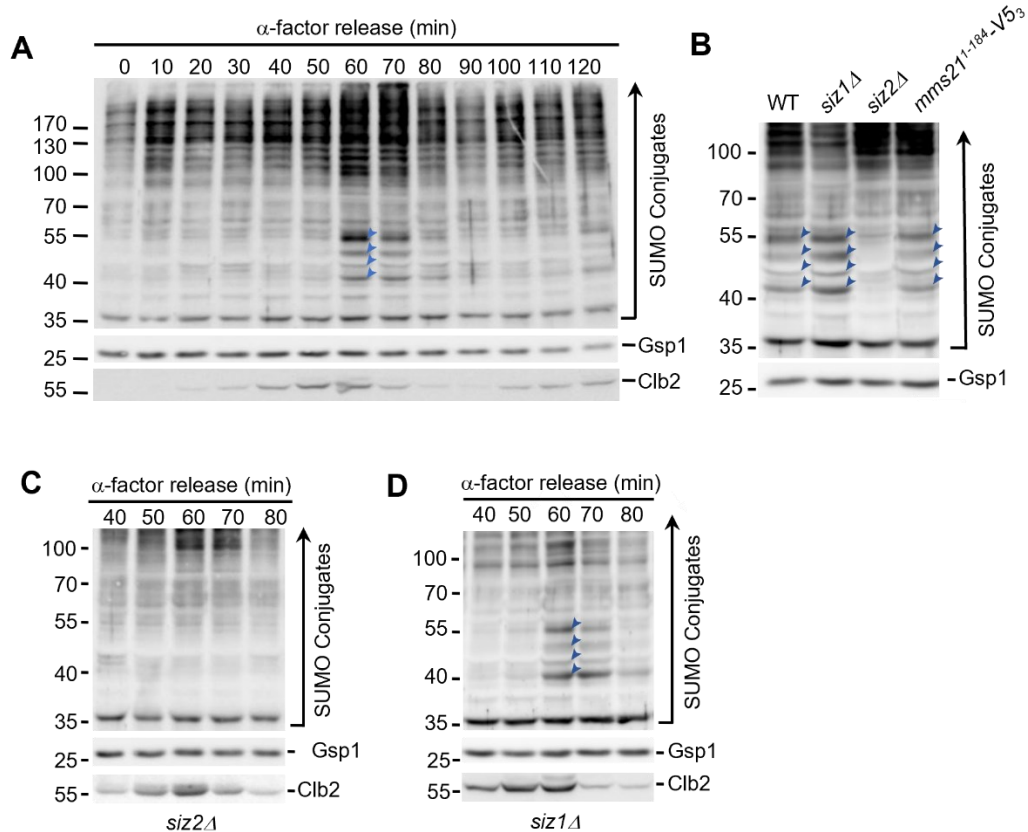


Figure 4-3. The enrichment of specific mitotic SUMOylation events is dependent on Siz2. **A, C, D)** Indicated strains were arrested in G1-phase using α -factor. Following α -factor removal, cultures were sampled every 10 min and analyzed by western blotting using antibodies directed against the proteins indicated on the right. Gsp1 is a loading control. Blue arrowheads highlight four prominent SUMOylated species in the 40-55 kDa range that arise in mitosis and decay as cell enter G1-phase. Molecular mass markers are shown in kDa. **B)** Cell lysates derived from asynchronous cultures of WT, *siz1* Δ , *siz2* Δ , and *mms21*^{1-184-V53} (Mms21 derivative deficient in SUMO E3 ligase activity) cells were assessed by western blotting using an anti-SUMO antibody to assess SUMO conjugate profiles. Gsp1 is a loading control. Blue arrowheads highlight prominent mitotic SUMO conjugates in the 40-55 kDa range. Molecular mass markers are shown in kDa. Experiments were performed by C. Ptak. Figures were constructed by C. Ptak and N.O. Saik.

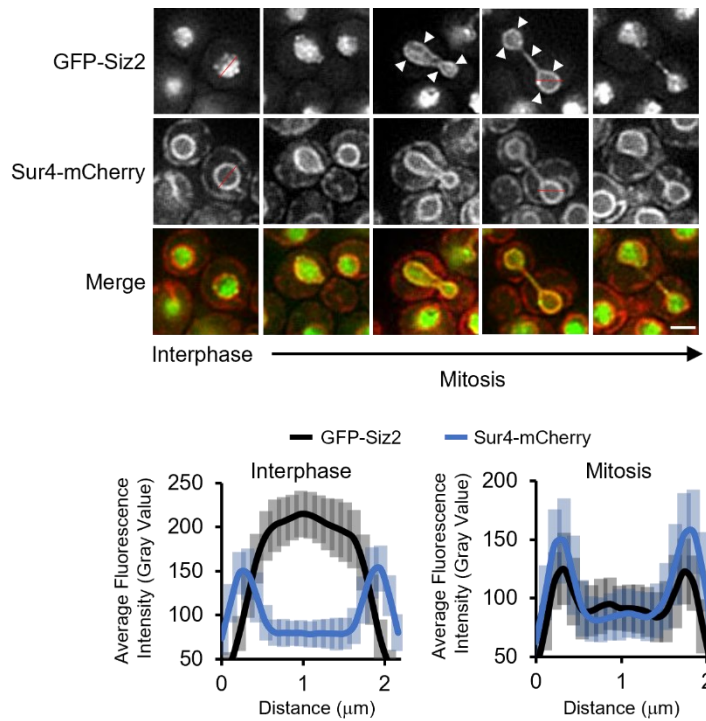


Figure 4-4. Siz2 is enriched at the NE during mitosis. Representative epifluorescence images of cells producing GFP-Siz2 at the indicated cell cycle stage. Sur4-mCherry is a NE/ER marker. The cell cycle stage was determined by bud size and nuclear morphology. Arrowheads highlight GFP-Siz2 at the NE. Nuclear distribution of GFP-Siz2 relative to Sur4-mCherry was determined using line scan intensities of equatorial optical sections through the nuclei (see red lines) of interphase (unbudded or small-budded) and mitotic (large budded) cells. Plots show average fluorescence intensity for GFP-Siz2 and Sur4-mCherry at multiple points along a 2.1 μm line for $n=25$ nuclei. Bar- 2 μm . Error bars- SD. Experiments were performed by C. Ptak. Figures were constructed by C. Ptak and N.O. Saik.

the NE. In these cells, GFP-Siz2 was partially excluded from the nucleolus. However, as the NE elongated and cells progressed into anaphase, a uniform localization of GFP-Siz2 at the NE accumulated. GFP-Siz2 enrichment at the NE was retained until the dissolution of the NE membrane bridge that links the mother and daughter nuclei during cytokinesis (Fig. 4-4). Together these results suggest that the mitotic relocalization of Siz2 to the INM facilitates the enrichment of SUMOylated proteins.

4.2.3 Mitotic phosphorylation facilitates Siz2 enrichment at the NE.

Post-translational modifications, such as phosphorylation, drive critical transitions through mitosis (Cuijpers and Vertegaal 2018). Therefore, we examined whether the relocalization of Siz2 during mitosis was the result of a post-translational modification. Western blot analysis of synchronized cells showed alterations in the electrophoretic mobility of Siz2, consistent with Siz2 being post-translationally modified during mitosis (Fig. 4-5A). Phosphatase treatment of mitotic cell lysates removed the slower migrating species of Siz2, indicating that Siz2 undergoes mitotic phosphorylation (Fig. 4-5B). Putative Siz2 phosphorylation sites at serine residues 522, 527, and 674 were previously identified by phosphoproteome analyses (De Albuquerque et al., 2016; Holt et al., 2009). We generated phosphomutants for each of these residues to determine the mitotic phosphorylation site of Siz2. The mitotic phosphorylation of Siz2 was unaltered in *siz2^{S527A}* (Fig. 4-6A) and *siz2^{S674A}* mutants (Fig. 4-6B). In addition, *siz2^{S527A}*-GFP and *siz2^{S674A}*-GFP were still localized to the NE during mitosis (Fig. 4-6C, D), and Siz2-dependent mitotic SUMOylation events still accumulated in these mutants

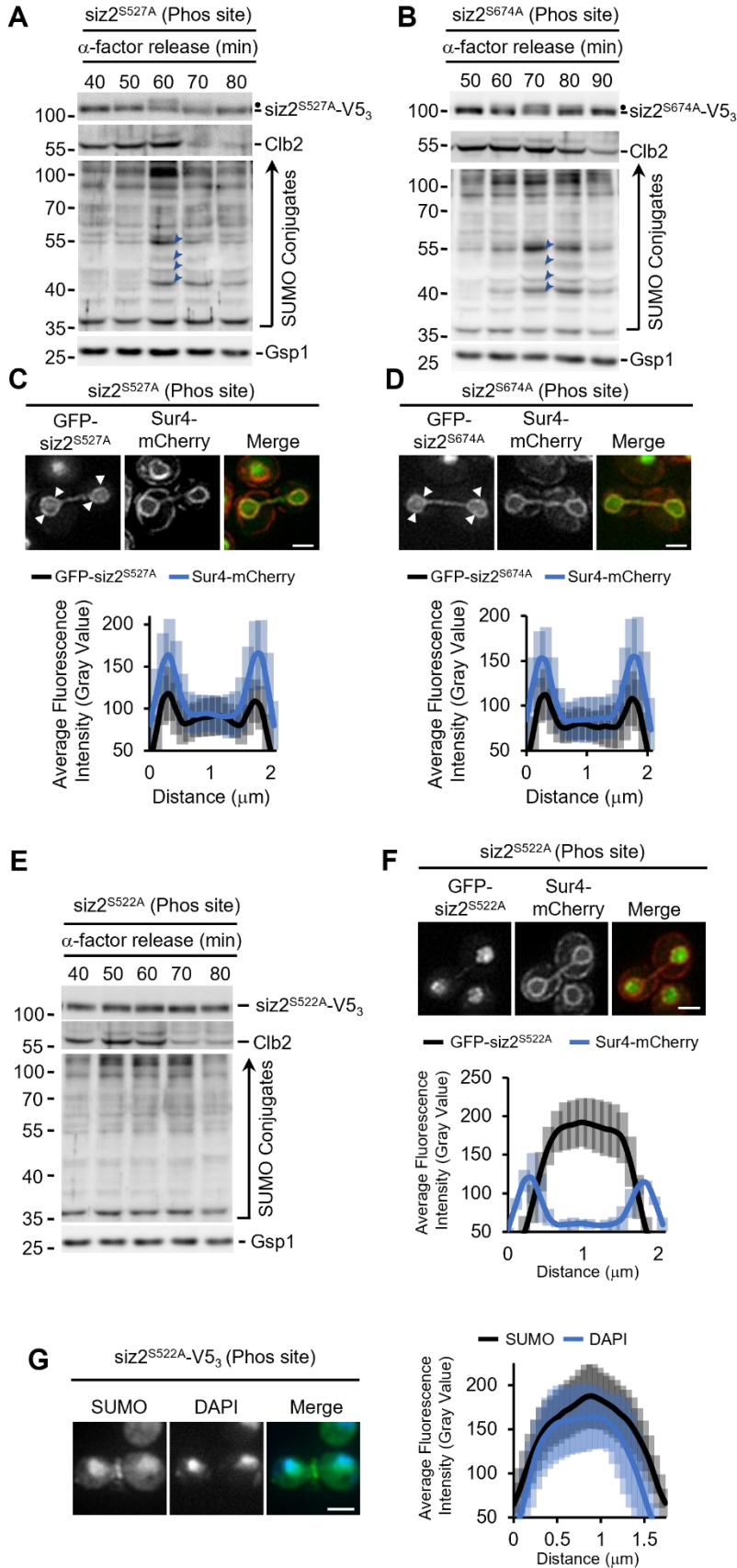


Figure 4-6. The mitotic phosphorylation of Siz2 at residue 522, is required for mitotic SUMOylation events at the NE. A, B, E) α -factor arrest-release assays on the indicated strains were carried out as described in Fig. 4-3. Cell lysates were analyzed by western blotting to detect SUMO conjugates, *siz2*-V5₃ derivatives, Clb2, and the Gsp1 load control. Dots highlight mitotically phosphorylated *siz2*-V5₃. Blue arrowheads highlight four prominent SUMOylated species in the 40-55 kDa range that arise in mitosis. Molecular mass markers are shown in kDa. **C, D, F)** Epifluorescence images of mitotic cells producing GFP-Siz2 or GFP-*siz2*^{Phos site} mutants. Sur4-mCherry is a NE/ER marker. Arrowheads highlight GFP-Siz2 or GFP-*siz2*^{Phos site} mutants at the NE. Imaging and quantification of the nuclear distribution of GFP-Siz2 or GFP-*siz2*^{Phos site} mutants in mitotic cells (n = 25) was performed as described in Fig. 4-4. Quantification of line scans were obtained at the same time as data shown in Fig. 4-4. Error bars - SD. Bar – 2 μ m. **G)** Anti-SUMO immunofluorescence analysis of *siz2*^{S522A}-V5₃ cells. Imaging and quantification of the nuclear distribution of SUMO in mitotic cells (n = 25) was performed as in Fig. 4-1. Error bars - SD. Bar – 2 μ m. Experiments were performed by C. Ptak. Figures were constructed by C. Ptak and N.O. Saik.

(Fig. 4-6A,B). Mitotic phosphorylation of Siz2, however, was absent in *siz2^{S522A}* mutants (Fig. 4-6E). Preventing phosphorylation at residue 522 also prevented *siz2* localization to the NE during mitosis (Fig. 4-6F) and prevented the mitotic accumulation of SUMO at the NE (Fig. 4-6F,G). Therefore, the phosphorylation-dependent recruitment of Siz2 to the NE regulates the SUMOylation of NE-associated proteins during mitosis.

4.2.4 Scs2 is an INM-associated receptor of Siz2 during mitosis.

We created a list of previously identified SUMOylated proteins that were 40-55 kDa in size (Table 4-1) and investigated whether the loss of any of these nonessential genes altered Siz2-dependent mitotic SUMOylation. We reasoned that if any of these previously reported SUMOylated proteins were mitotic SUMOylation targets of Siz2 western blot analysis of the null mutants would cause one or more of the four mitotic SUMOylated species to be absent. Western blot analysis revealed that all four Siz2-dependent mitotic SUMOylation species were absent in cells lacking the gene encoding Scs2 (Fig. 4-7). Scs2 is an ER/NE localized membrane protein of the VAP (Vesicle-associated membrane protein (VAMP)-Associated Protein) family (Christopher J.R. Loewen and Levine 2005). Scs2 has been previously identified as a ~55 kDa SUMOylation species (Felberbaum et al., 2011). Therefore, SUMOylated Scs2 would be consistent with the size of at least one of the Siz2-dependent SUMO modifications observed during mitosis.

Table 4-1. Genes representing SUMOylated proteins 40-55kDa in size that were deleted to investigate alterations to SUMOylation profiles.

<u>Gene</u>	<u>Gene Name</u>	<u>Size (Da)</u>	<u>Reference Reporting SUMOylation</u>
<i>YAL027W</i>	<i>SAW1</i>	29778	Dension et al.,2004; Wohlschlegel et al.,2004; Makhnevych et al.,2009
<i>YAL060W</i>	<i>BDH1</i>	41574	Wohlschlegel et al.,2004; Makhnevych et al.,2009
<i>YBL002W</i>	<i>HTB2</i>	14251	Wohlschlegel et al.,2004; Makhnevych et al.,2009
<i>YBL003C</i>	<i>HTA2</i>	14002	Wohlschlegel et al.,2004; Makhnevych et al.,2009
<i>YBL006C</i>	<i>LDB7</i>	19797	Dension et al.,2004; Wohlschlegel et al.,2004; Makhnevych et al.,2009
<i>YBL027W</i>	<i>RPL19B</i>	21736	Hannich et al.,2005; Makhnevych et al.,2009
<i>YBL072C</i>	<i>RPS8A</i>	22517	Dension et al.,2004; Zhou et al.,2004; Makhnevych et al.,2009
<i>YBR009C</i>	<i>HHF1</i>	11386	Wohlschlegel et al.,2004; Makhnevych et al.,2009
<i>YBR018C</i>	<i>GAL7</i>	42385	Dension et al.,2004; Makhnevych et al.,2009
<i>YBR031W</i>	<i>RPL4A</i>	39126	Dension et al.,2004; Makhnevych et al.,2009
<i>YBR048W</i>	<i>RPS11B</i>	17775	Hannich et al.,2005; Makhnevych et al.,2009
<i>YBR072W</i>	<i>HSP26</i>	23874	Zhou et al.,2004; Makhnevych et al.,2009
<i>YBR106W</i>	<i>SND3</i>	21142	Makhnevych et al.,2009
<i>YBR129C</i>	<i>OPY1</i>	37742	Makhnevych et al.,2009
<i>YBR149W</i>	<i>ARA1</i>	38874	Wohlschlegel et al.,2004; Makhnevych et al.,2009
<i>YBR189W</i>	<i>RPS9B</i>	22313	Hannich et al.,2005; Makhnevych et al.,2009

<i>YBR191W</i>	<i>RPL21A</i>	18262	Hannich et al.,2005; Makhnevych et al.,2009
<i>YBR221C</i>	<i>PDB1</i>	40044	Wohlschlegel et al.,2004; Makhnevych et al.,2009
<i>YBR249C</i>	<i>ARO4</i>	39747	Panse et al.,2004; Makhnevych et al.,2009
<i>YCL050C</i>	<i>APA1</i>	36475	Wohlschlegel et al.,2004; Panse et al.,2004; Makhnevych et al.,2009
<i>YCR002C</i>	<i>CDC10</i>	37016	Panse et al.,2004; Makhnevych et al.,2009
<i>YCR016W</i>	<i>YCR016W</i>	33594	Hannich et al.,2005; Makhnevych et al.,2009
<i>YDL002C</i>	<i>NHP10</i>	23858	Wohlschlegel et al.,2004; Makhnevych et al.,2009
<i>YDL022W</i>	<i>GPD1</i>	42854	Panse et al.,2004; Makhnevych et al.,2009
<i>YDL051W</i>	<i>LHP1</i>	32107	Makhnevych et al.,2009
<i>YDL075W</i>	<i>RPL31A</i>	12962	Wohlschlegel et al.,2004; Makhnevych et al.,2009
<i>YDL082W</i>	<i>RPL13A</i>	22580	Dension et al.,2004; Makhnevych et al.,2009
<i>YDL191W</i>	<i>RPL35A</i>	13932	Makhnevych et al.,2009
<i>YDL213C</i>	<i>NOP6</i>	25238	Wohlschlegel et al.,2004; Makhnevych et al.,2009
<i>YDL226C</i>	<i>GCS1</i>	39289	Panse et al.,2004; Makhnevych et al.,2009
<i>YDR071C</i>	<i>PAA1</i>	21941	Hannich et al.,2005; Makhnevych et al.,2009
<i>YDR130C</i>	<i>FIN1</i>	33202	Dension et al.,2004; Wohlschlegel et al.,2004; Makhnevych et al.,2009
<i>YDR155C</i>	<i>CPR1</i>	17390	Dension et al.,2004; Hannich et al.,2005; Makhnevych et al.,2009

<i>YDR158W</i>	<i>HOM2</i>	39541	Panse et al.,2004; Makhnevych et al.,2009
<i>YDR171W</i>	<i>HSP42</i>	42794	Hannich et al.,2005; Makhnevych et al.,2009
<i>YDR174W</i>	<i>HMO1</i>	27546	Dension et al.,2004; Zhou et al.,2004; Hannich et al.,2005; Makhnevych et al.,2009
<i>YDR225W</i>	<i>HTA1</i>	14002	Dension et al.,2004; Wohlschlegel et al.,2004; Makhnevych et al.,2009
<i>YDR226W</i>	<i>ADK1</i>	24252	Wohlschlegel et al.,2004; Makhnevych et al.,2009
<i>YDR233C</i>	<i>RTN1</i>	32923	Hannich et al.,2005; Makhnevych et al.,2009
<i>YDR318W</i>	<i>MCM21</i>	42950	Wohlschlegel et al.,2004; Makhnevych et al.,2009
<i>YDR336W</i>	<i>MRX8</i>	35635	Zhou et al.,2004; Makhnevych et al.,2009
<i>YDR382W</i>	<i>RPP2B</i>	11035	Dension et al.,2004; Makhnevych et al.,2009
<i>YDR447C</i>	<i>RPS17B</i>	15820	Zhou et al.,2004; Makhnevych et al.,2009
<i>YDR450W</i>	<i>RPS18A</i>	17049	Dension et al.,2004; Makhnevych et al.,2009
<i>YDR469W</i>	<i>SDC1</i>	19434	Dension et al.,2004; Wohlschlegel et al.,2004; Hannich et al.,2005; Makhnevych et al.,2009
<i>YDR471W</i>	<i>RPL27B</i>	15525	Hannich et al.,2005; Makhnevych et al.,2009
<i>YEL009C</i>	<i>GCN4</i>	31300	Dension et al.,2004; Wohlschlegel et al.,2004; Makhnevych et al.,2009
<i>YER039C</i>	<i>HVG1</i>	27691	Panse et al.,2004; Makhnevych et al.,2009
<i>YER074W</i>	<i>RPS24A</i>	15348	Makhnevych et al.,2009

<i>YER120W</i>	<i>SCS2</i>	26915	Panse et al.,2004; Zhou et al.,2004; Makhnevych et al.,2009
<i>YER177W</i>	<i>BMH1</i>	30074	Dension et al.,2004; Makhnevych et al.,2009
<i>YFR001W</i>	<i>LOC1</i>	23622	Wohlschlegel et al.,2004; Makhnevych et al.,2009
<i>YGL076C</i>	<i>RPL7A</i>	27662	Dension et al.,2004; Makhnevych et al.,2009
<i>YGL148W</i>	<i>ARO2</i>	40839	Panse et al.,2004; Makhnevych et al.,2009
<i>YGL157W</i>	<i>ARI1</i>	38076	Wohlschlegel et al.,2004; Panse et al.,2004; Makhnevych et al.,2009
<i>YGR135W</i>	<i>PRE9</i>	28706	Panse et al.,2004; Makhnevych et al.,2009
<i>YGR192C</i>	<i>TDH3</i>	35745	Panse et al.,2004; Zhou et al.,2004; Makhnevych et al.,2009
<i>YGR214W</i>	<i>RPS0A</i>	28006	Zhou et al.,2004; Makhnevych et al.,2009
<i>YHL031C</i>	<i>GOS1</i>	25401	Wohlschlegel et al.,2004; Makhnevych et al.,2009
<i>YHL033C</i>	<i>RPL8A</i>	28150	Dension et al.,2004; Makhnevych et al.,2009
<i>YHR134W</i>	<i>WSS1</i>	30631	Hannich et al.,2005; Makhnevych et al.,2009
<i>YHR193C</i>	<i>EGD2</i>	18702	Makhnevych et al.,2009
<i>YHR203C</i>	<i>RPS4B</i>	29432	Hannich et al.,2005; Makhnevych et al.,2009
<i>YIL053W</i>	<i>GPP1</i>	27939	Dension et al.,2004; Panse et al.,2004; Zhou et al.,2004; Makhnevych et al.,2009
<i>YIL110W</i>	<i>HPM1</i>	42489	Dension et al.,2004; Makhnevych et al.,2009

<i>YIL148W</i>	<i>RPL40A</i>	14568	Zhou et al.,2004; Makhnevych et al.,2009
<i>YIR038C</i>	<i>GTT1</i>	26792	Wohlschlegel et al.,2004; Makhnevych et al.,2009
<i>YJL052W</i>	<i>TDH1</i>	35752	Dension et al.,2004; Makhnevych et al.,2009
<i>YJL092W</i>	<i>SRS2</i>	134321	Hannich et al.,2005; Makhnevych et al.,2009
<i>YJL140W</i>	<i>RPB4</i>	25397	Dension et al.,2004; Wohlschlegel et al.,2004; Makhnevych et al.,2009
<i>YJL148W</i>	<i>RPA34</i>	26879	Dension et al.,2004; Wohlschlegel et al.,2004; Makhnevych et al.,2009
<i>YJR009C</i>	<i>TDH2</i>	35845	Dension et al.,2004; Makhnevych et al.,2009
<i>YJR024C</i>	<i>MDE1</i>	27423	Panse et al.,2004; Makhnevych et al.,2009
<i>YJR048W</i>	<i>CYCI</i>	12190	Dension et al.,2004; Makhnevych et al.,2009
<i>YJR060W</i>	<i>CBF1</i>	39366	Dension et al.,2004; Wohlschlegel et al.,2004; Makhnevych et al.,2009
<i>YJR063W</i>	<i>RPA12</i>	13662	Wohlschlegel et al.,2004; Makhnevych et al.,2009
<i>YJR104C</i>	<i>SOD1</i>	15849	Dension et al.,2004; Zhou et al.,2004; Hannich et al.,2005; Wykoff et al.,2005; Makhnevych et al.,2009
<i>YJR145C</i>	<i>RPS4A</i>	29432	Dension et al.,2004; Makhnevych et al.,2009
<i>YJR153W</i>	<i>PGUI</i>	37291	Hannich et al.,2005; Makhnevych et al.,2009
<i>YKL094W</i>	<i>YJU3</i>	35566	Wohlschlegel et al.,2004; Makhnevych et al.,2009
<i>YKL096W</i>	<i>CWPI</i>	24256	Wohlschlegel et al.,2004; Makhnevych et al.,2009

<i>YKL142W</i>	<i>MRP8</i>	25081	Dension et al.,2004; Wohlschlegel et al.,2004; Zhou et al.,2004; Makhnevych et al.,2009
<i>YKL216W</i>	<i>URA1</i>	34798	Wohlschlegel et al.,2004; Makhnevych et al.,2009
<i>YKR092C</i>	<i>SRP40</i>	40971	Dension et al.,2004; Makhnevych et al.,2009
<i>YLL039C</i>	<i>UBI4</i>	42826	Dension et al.,2004; Makhnevych et al.,2009
<i>YLR048W</i>	<i>RPS0B</i>	27945	Panse et al.,2004; Makhnevych et al.,2009
<i>YLR150W</i>	<i>STMI</i>	30007	Wohlschlegel et al.,2004; Zhou et al.,2004; Hannich et al.,2005; Makhnevych et al.,2009
<i>YLR180W</i>	<i>SAM1</i>	41803	Panse et al.,2004; Makhnevych et al.,2009
<i>YLR192C</i>	<i>HCR1</i>	29554	Zhou et al.,2004; Makhnevych et al.,2009
<i>YLR221C</i>	<i>RSA3</i>	24642	Dension et al.,2004; Wohlschlegel et al.,2004; Makhnevych et al.,2009
<i>YLR350W</i>	<i>ORM2</i>	24855	Hannich et al.,2005; Makhnevych et al.,2009
<i>YLR354C</i>	<i>TAL1</i>	37034	Dension et al.,2004; Makhnevych et al.,2009
<i>YLR406C</i>	<i>RPL31B</i>	12976	Wohlschlegel et al.,2004; Makhnevych et al.,2009
<i>YLR420W</i>	<i>URA4</i>	40307	Wohlschlegel et al.,2004; Makhnevych et al.,2009
<i>YLR441C</i>	<i>RPS1A</i>	28763	Dension et al.,2004; Zhou et al.,2004; Makhnevych et al.,2009
<i>YLR448W</i>	<i>RPL6B</i>	20004	Wohlschlegel et al.,2004; Makhnevych et al.,2009
<i>YLR455W</i>	<i>PDP3</i>	35521	Dension et al.,2004; Wohlschlegel et al.,2004; Makhnevych et al.,2009

<i>YML028W</i>	<i>TSAI</i>	21583	Dension et al.,2004; Zhou et al.,2004; Makhnevych et al.,2009
<i>YML041C</i>	<i>VPS71</i>	32039	Dension et al.,2004; Wohlschlegel et al.,2004; Makhnevych et al.,2009
<i>YML073C</i>	<i>RPL6A</i>	19980	Dension et al.,2004; Wohlschlegel et al.,2004; Makhnevych et al.,2009
<i>YMR083W</i>	<i>ADH3</i>	40375	Panse et al.,2004; Makhnevych et al.,2009
<i>YMR230W</i>	<i>RPS10B</i>	12741	Dension et al.,2004; Wohlschlegel et al.,2004; Makhnevych et al.,2009
<i>YMR233W</i>	<i>TRII</i>	26480	Hannich et al.,2005; Makhnevych et al.,2009
<i>YMR241W</i>	<i>YHM2</i>	34203	Panse et al.,2004; Makhnevych et al.,2009
<i>YMR269W</i>	<i>TMA23</i>	23981	Wohlschlegel et al.,2004; Makhnevych et al.,2009
<i>YMR303C</i>	<i>ADH2</i>	36728	Zhou et al.,2004; Makhnevych et al.,2009
<i>YMR318C</i>	<i>ADH6</i>	39613	Dension et al.,2004; Makhnevych et al.,2009
<i>YNL030W</i>	<i>HHF2</i>	11386	Wohlschlegel et al.,2004; Makhnevych et al.,2009
<i>YNL055C</i>	<i>POR1</i>	30429	Panse et al.,2004; Makhnevych et al.,2009
<i>YNL067W</i>	<i>RPL9B</i>	21667	Wohlschlegel et al.,2004; Makhnevych et al.,2009
<i>YNL069C</i>	<i>RPL16B</i>	22277	Dension et al.,2004; Makhnevych et al.,2009
<i>YNL096C</i>	<i>RPS7B</i>	21646	Dension et al.,2004; Makhnevych et al.,2009
<i>YNL097C</i>	<i>PHO23</i>	37026	Dension et al.,2004; Wohlschlegel et al.,2004; Makhnevych et al.,2009

<i>YNL134C</i>	<i>YNL134C</i>	41158	Wohlschlegel et al.,2004; Makhnevych et al.,2009
<i>YNL301C</i>	<i>RPL18B</i>	20593	Hannich et al.,2005; Makhnevych et al.,2009
<i>YNL333W</i>	<i>SNZ2</i>	32025	Panse et al.,2004; Makhnevych et al.,2009
<i>YOL086C</i>	<i>ADH1</i>	36845	Dension et al.,2004; Panse et al.,2004; Zhou et al.,2004; Makhnevych et al.,2009
<i>YOL109W</i>	<i>ZEO1</i>	12587	Hannich et al.,2005; Makhnevych et al.,2009
<i>YOR028C</i>	<i>CIN5</i>	32987	Dension et al.,2004; Wohlschlegel et al.,2004; Makhnevych et al.,2009
<i>YOR120W</i>	<i>GCY1</i>	35080	Dension et al.,2004; Makhnevych et al.,2009
<i>YOR185C</i>	<i>GSP2</i>	24988	Wohlschlegel et al.,2004; Makhnevych et al.,2009
<i>YOR189W</i>	<i>IES4</i>	13086	Dension et al.,2004; Wohlschlegel et al.,2004; Makhnevych et al.,2009
<i>YOR251C</i>	<i>TUM1</i>	34213	Hannich et al.,2005; Makhnevych et al.,2009
<i>YOR293W</i>	<i>RPS10A</i>	12741	Wohlschlegel et al.,2004; Makhnevych et al.,2009
<i>YOR295W</i>	<i>UAF30</i>	25971	Dension et al.,2004; Wohlschlegel et al.,2004; Makhnevych et al.,2009
<i>YOR312C</i>	<i>RPL20B</i>	20457	Dension et al.,2004; Makhnevych et al.,2009
<i>YOR344C</i>	<i>TYE7</i>	32674	Dension et al.,2004; Wohlschlegel et al.,2004; Makhnevych et al.,2009
<i>YPL129W</i>	<i>TAF14</i>	27431	Dension et al.,2004; Wohlschlegel et al.,2004; Panse et al.,2004; Makhnevych et al.,2009
<i>YPL273W</i>	<i>SAM4</i>	36658	Wohlschlegel et al.,2004; Makhnevych et al.,2009

<i>YER062C</i>	<i>GPP2</i>	27809	Makhnevych et al.,2009; Srikumar et al.,2013
<i>YDL059C</i>	<i>RAD59</i>	26634	Srikumar et al.,2013
<i>YER142C</i>	<i>MAG1</i>	34335	Srikumar et al.,2013
<i>YGL175C</i>	<i>SAE2</i>	40094	Srikumar et al.,2013
<i>YJR043C</i>	<i>POL32</i>	40314	Srikumar et al.,2013
<i>YKL114C</i>	<i>APN1</i>	41442	Srikumar et al.,2013
<i>YML060W</i>	<i>OGG1</i>	42789	Srikumar et al.,2013
<i>YBR010W</i>	<i>HHT1</i>	15378	Srikumar et al.,2013
<i>YML095C</i>	<i>RAD10</i>	24314	Srikumar et al.,2013
<i>YNL031C</i>	<i>HHT2</i>	15378	Srikumar et al.,2013
<i>YFR031C-A</i>	<i>RPL2A</i>	27437	Srikumar et al.,2013
<i>YIR034C</i>	<i>LYS1</i>	41473	Srikumar et al.,2013

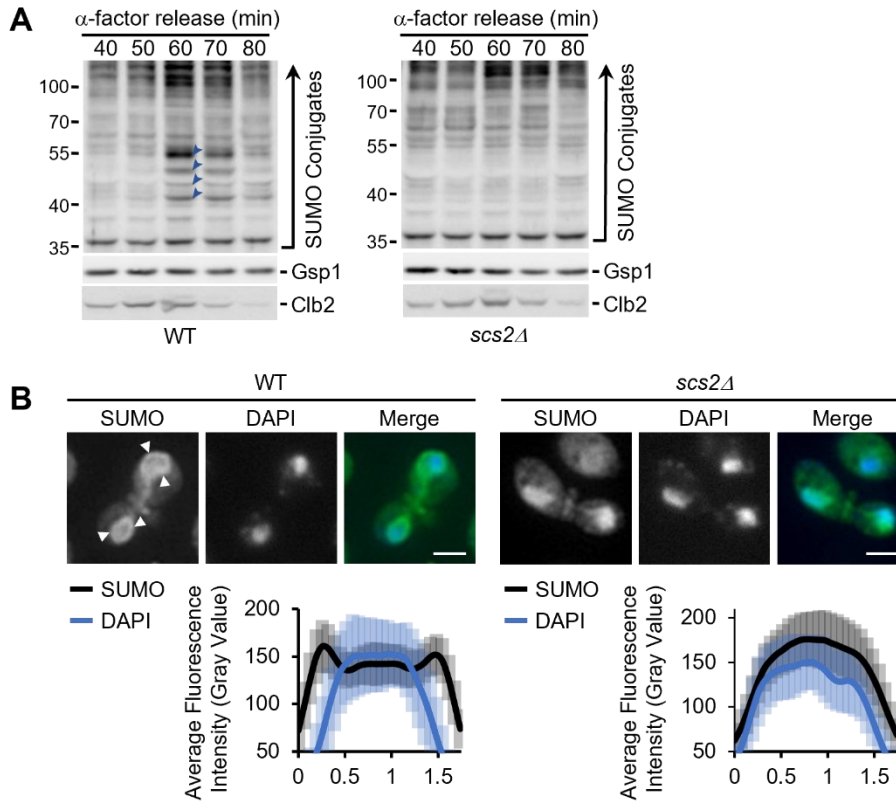


Figure 4-7. Scs2 is required for mitotic SUMOylation events at the NE. **A)** α -factor arrest-release assays were carried out as described in Fig. 4-3 on WT and *scs2 Δ* cells. Cell lysates were analyzed by western blotting to detect SUMO conjugate profiles, Clb2, and the Gsp1 load control. Molecular mass markers are shown in kDa. Blue arrowheads highlight four prominent SUMOylated species in the 40-55 kDa range that arise in mitosis. **B)** Anti-SUMO immunofluorescence analysis of WT and *scs2 Δ* mitotic cells. Imaging and quantification of the nuclear distribution of SUMO in mitotic cells (n = 25) was performed as in Fig. 4-1. Arrowheads highlight SUMO along the NE. Quantification of lines scans were obtained at the same time as data shown in Fig. 4-1, with the WT data shown here for comparison. Error bars - SD. Bar - 2 μ m. Experiments were performed by C. Ptak and N.O. Saik. Figures were constructed by C. Ptak and N.O. Saik.

The loss of Scs2 (*scs2Δ*), however, prevented the accumulation of all four Siz2-dependent mitotic SUMOylation species (Fig. 4-7). This suggested that Scs2 may function to direct Siz2-dependent mitotic SUMOylation events. Because Scs2 functions as a receptor at the ER for multiple cytoplasmic proteins (Stefan et al., 2011; Christopher J.R. Loewen et al., 2014; Manford et al., 2012; Encinar del Dedo et al., 2017; Ng, Ng, and Zhang 2020), we postulated that Scs2 could function as a receptor for Siz2 at the NE during mitosis. Consistent with Scs2 functioning as a receptor for Siz2, Siz2 no longer localized to the NE during mitosis in cells lacking Scs2 (Fig.4-8A), despite being phosphorylated (Fig. 4-8B). Removing the transmembrane domain of Scs2 (*scs2¹⁻²²⁵*) results in the nuclear accumulation of Scs2 (Christopher J.R. Loewen et al., 2007; J. H. Brickner and Walter 2004), and also prevents Siz2 accumulation at the NE during mitosis (Fig. 4-8C). Furthermore, physical interactions between Scs2 and Siz2 were detected by immunoprecipitation. These interactions were dependent on Siz2 localization to the NE, as *siz2^{S522A}* interactions with Scs2 were significantly reduced (Fig. 4-8D).

VAP family proteins, such as Scs2, bind to FFAT (two phenylalanines in an acidic tract) motifs in interacting partners through their N-terminal MSP (major sperm protein) domain (Christopher J.R. Loewen, Roy, and Levine 2003; Christopher J.R. Loewen and Levine 2005; Kaiser et al., 2005). To investigate whether Scs2 interactions with Siz2 were dependent on a MSP:FFAT interaction, we disrupted the MSP domain of Scs2 (previously identified *scs2^{K84D/L86D}* mutant; Kaiser *et al.*,2005)) and a predicted FFAT motif (Fig. 4-9A) in Siz2 (*siz2^{A569D}* mutant) and investigated the consequences on Siz2 mitotic NE-localization and

SUMOylation. Both the *scs2*^{K84D/L86D} and *siz2*^{A569D} mutations inhibited mitosis-specific localization of Siz2 to the NE (Fig. 4-9D,E), independently of the mitotic phosphorylation of Siz2. Consistent with the loss of Siz2 NE-localization, *scs2*^{K84D/L86D} and *siz2*^{A569D} mutations also prevented the accumulation of Siz2-directed SUMOylation events during mitosis (Fig. 4-9B,C). Furthermore, interactions between Siz2 and *scs2*^{K84D/L86D} were reduced as determined by immunoprecipitation analysis (Fig. 4-9F). Collectively, these data support the conclusion that Scs2 functions as a receptor for Siz2, through its MSP domain, to facilitate Siz2-directed mitotic SUMOylation events.

To function as a receptor for Siz2 during mitosis, Scs2 would presumably need access to the INM. The INM localization of Scs2, however, has not been described. To assess whether Scs2 can access the INM, we utilized a split superfolder GFP assay previously used to characterize the INM proteome (Smoyer et al., 2016). In this assay, a target protein is fused to GFP₁₋₁₀. If the target and a GFP₁₁-reporter reside in the same subcellular compartment, the two GFP fragments can assemble and fluoresce. GFP₁₋₁₀-Scs2 associated with the cytoplasmic GFP₁₁-Hxk1 reporter, allowing the visualization of Scs2 at the ER/ONM (Fig. 4-10A). At the same time, GFP₁₋₁₀-Scs2, also associated with the nuclear GFP₁₁-Pus1 reporter, allows the visualization of Scs2 at the INM (Fig. 4-10A). Using this assay, we could also detect *scs2*^{K84D/L86D}-GFP₁₋₁₀ at the INM (Fig. 4-10B). These data indicate Scs2 could function as a receptor for Siz2 at the INM.

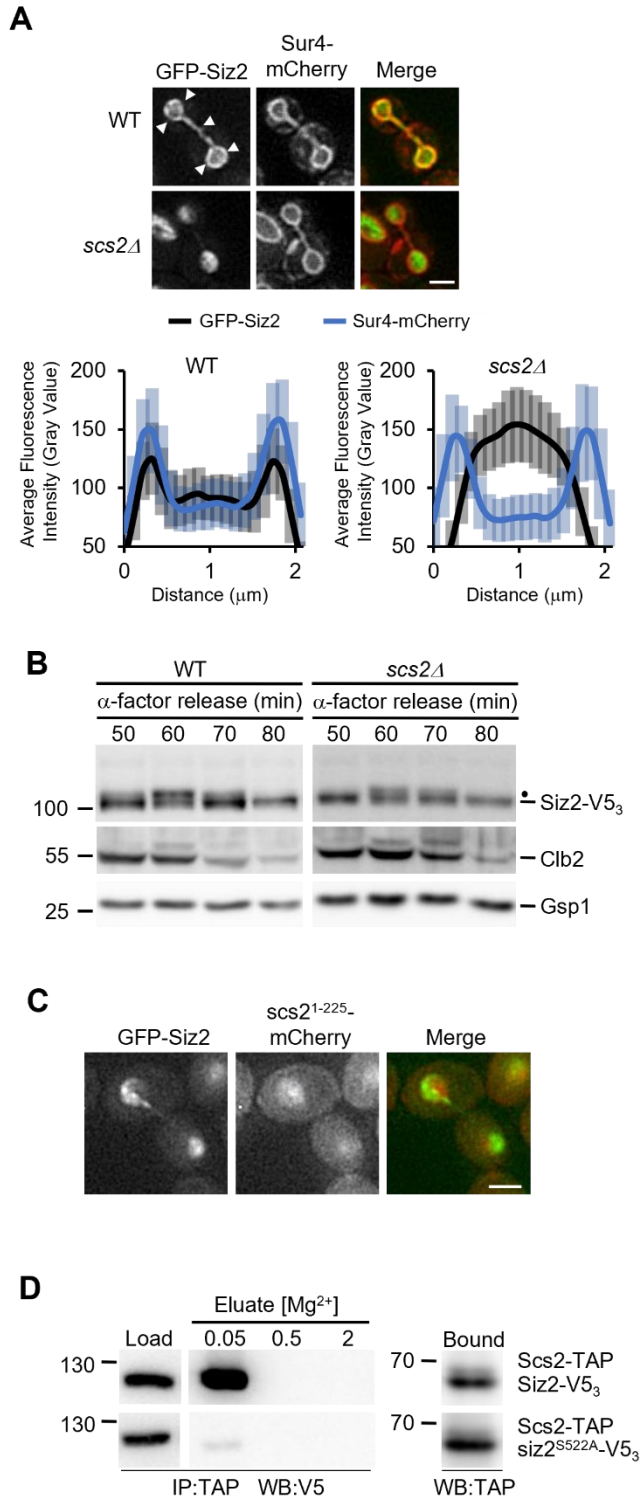


Figure 4-8. Scs2 is required for the mitotic enrichment of Siz2 at the NE. A) Representative epifluorescence images of mitotic WT and *scs2Δ* cells producing GFP-Siz2. Sur4-mCherry is a NE/ER marker. Arrowheads highlight GFP-Siz2 at the NE. Imaging and quantification of the nuclear distribution of GFP-Siz2 in mitotic cells (n = 25) was performed as described in Fig. 4-4. Quantification of lines scans were obtained at the same time as data shown in Fig. 4-4, with the WT data shown here for comparison. Error bars - SD. Bar – 2 μm. **B)** α-factor arrest-release assays were carried out as in Fig. 4-3 on WT and *scs2Δ* cells producing Siz2-V5₃. Cell lysates were analyzed by western blotting to detect Siz2-V5₃, Clb2, and the Gsp1 load control. Molecular mass markers are shown in kDa. Dots highlight mitotically phosphorylated Siz2-V5₃. **C)** Epifluorescence images of a mitotic cell producing GFP-Siz2 and *scs2*¹⁻²²⁵-mCherry. Bar – 2 μm. **D)** Scs2-TAP was affinity-purified from strains (IP) producing either Siz2-V5₃ or *siz2*^{S522A}-V5₃. Bound proteins were eluted using a Mg²⁺ step gradient. Equivalent portions of the indicated fractions were analyzed by western blotting (WB) to assess levels of V5- and TAP-tagged fusions. Load, Elution, or Bound fractions were derived from the same western blot. Experiments in panel A and B were performed by C. Ptak. Experiments in panel C were performed by A. Premashankar and C. Ptak. Experiments in panel D were performed by N.O. Saik. Figures were constructed by C. Ptak and N.O. Saik.

A

Position:	1	2	3	4	5	6	7	FFAT Score
Optimal FFAT:	E	F	F	D	A	X	E	0
Siz2 FFAT-like:	N	Y	Q	D	A	F	Q ⁵³⁴⁻⁵⁴⁰	4.5
	S	F	V	T	A	T	N ⁵⁶⁵⁻⁵⁷¹	4.5
	D	F	N	T	S	A	Q ⁷⁰⁹⁻⁷¹⁵	4.5

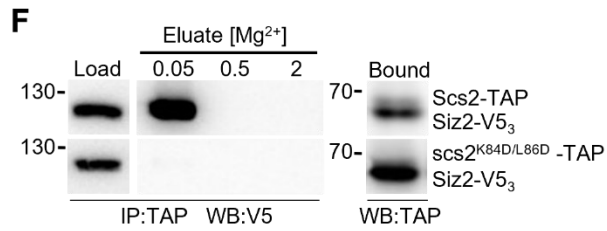
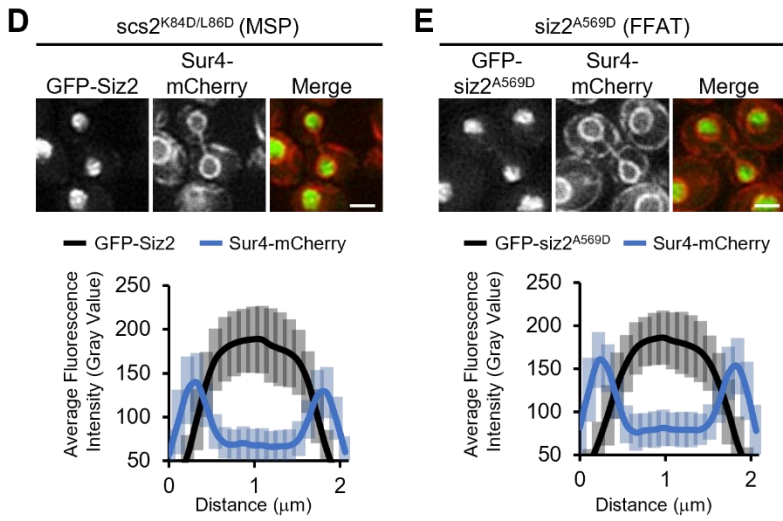
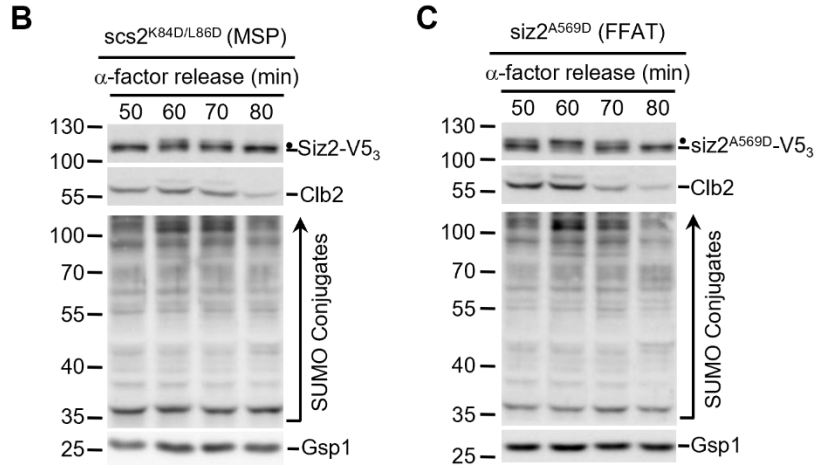


Figure 4-9. Interactions between Scs2 and Siz2 are regulated through MSP:FFAT interactions. **A)** The position, sequence, and score (Murphy and Levine 2016) of putative Siz2 FFAT-like motifs are shown. An optimal FFAT sequence is shown for comparison. **B, C)** α -factor arrest-release assays on the indicated strains were carried out as described in Fig. 4-3. Cell lysates were analyzed by western blotting to detect SUMO conjugates, siz2-V5₃ derivatives, Clb2, and the Gsp1 load control. Dots highlight mitotically phosphorylated siz2-V5₃. Blue arrowheads highlight four prominent SUMOylated species in the 40-55 kDa range that arise in mitosis. Molecular mass markers are shown in kDa. **D, E)** Nuclear distribution of GFP-Siz2 or GFP-siz2^{A569D} relative to the NE/ER marker Sur-mCherry was performed on mitotic cells (n=25) of indicated strains as described in Fig. 4-4. Quantification of line scans were obtained at the same time as data shown in Fig. 4-4. Bar – 2 μ m. **F)** Scs2-TAP or scs2^{K84D/L86D}-TAP were affinity-purified from cells (IP) producing Siz2-V5₃. Bound proteins were eluted using a Mg²⁺ step gradient. Equivalent portions of the indicated fractions were analyzed by western blotting (WB) to assess levels of the V5- and TAP-tagged fusions. Load, Elution, or Bound fractions shown were derived from the same western blot. Experiments were performed at the same time as data shown in Fig. 4-8, with WT data shown here for comparison. Experiments in panel A - E were performed by C. Ptak. Experiments in panel F were performed by N.O. Saik. Figures were constructed by C. Ptak and N.O. Saik.

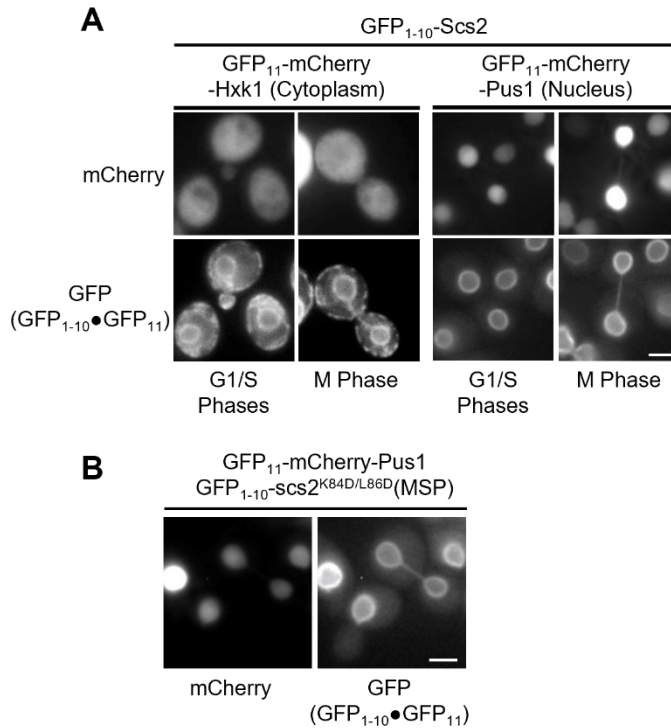


Figure 4-10. Scs2 is localized to the INM. A) A split-superfolder GFP system was used to assess Scs2 localization. Epifluorescence images of WT cells containing GFP₁₋₁₀-Scs2 and plasmid-encoded GFP₁₁-mCherry-Hxk1(cytoplasmic) or GFP₁₁-mCherry-Pus1 (nuclear) are shown. Localization of the reporter (mCherry) and assembled GFP₁₋₁₀•GFP₁₁ (GFP) in representative G1-, S-, and M-phase cells are shown. **B)** The INM association of the *scs2* MSP domain mutant (*scs2*^{K84D/L86D}) was assessed using the split-superfolder GFP system in cells producing GFP₁₋₁₀-scs2^{K84D/L86D} and the plasmid-encoded GFP₁₁-mCherry-Pus1 reporter. Bar – 2 μm. Experiments were performed by A. Premashankar and C. Ptak. Figures were constructed by C. Ptak and N.O. Saik.

4.2.5 Scs2 is a mitotic SUMOylation target of Siz2.

Scs2 was previously identified as a ~55 kDa SUMOylation species (Felberbaum et al., 2011), which is consistent with the size of the most prominent Siz2-dependent mitotic SUMOylation species. Eliminating the previously identified Scs2 SUMO acceptor site, K180 (Felberbaum et al., 2011) abolished the accumulation of the Siz2-dependent 55 kDa mitotic SUMO-conjugate (Fig. 4-11A,B). Western blot analysis in synchronized *ulp1^{K352E}* mutant cells, which was previously shown to increase the cellular levels of SUMOylated Scs2 (Felberbaum et al., 2011), revealed increased levels of the mitotic 55kDa SUMOylation species (Fig. 4-11C). A *ULP1* allele bearing an additional mutation (*ulp1^{K352E/Y583H-V53}*) showed further elevated levels of the 55 kDa SUMO species (Fig. 4-11C). These results are consistent with SUMOylated Scs2 being the 55kDa mitotic SUMOylation species. Furthermore, the 55kDa mitotic SUMO species was absent in cells producing an endogenously tagged Scs2 (HA₃-Scs2 or Scs2-V5₃) in the *ulp1^{K352E/Y583H}* mutant, with a SUMOylation species of higher molecular weight, consistent with the predicted size of tagged Scs2, appearing in these cells. Eliminating the Scs2 SUMO acceptor site in these backgrounds eliminated these SUMOylated Scs2 species. As only the ~55 kDa SUMOylation species was altered by tagging Scs2, it is unlikely that the other mitotic SUMOylation species within the 40-55 kDa range were proteolytic fragments of Scs2-SUMO (Fig. 4-11D), and these mitotic SUMOylation events thus represent distinct mitotic SUMOylation targets.

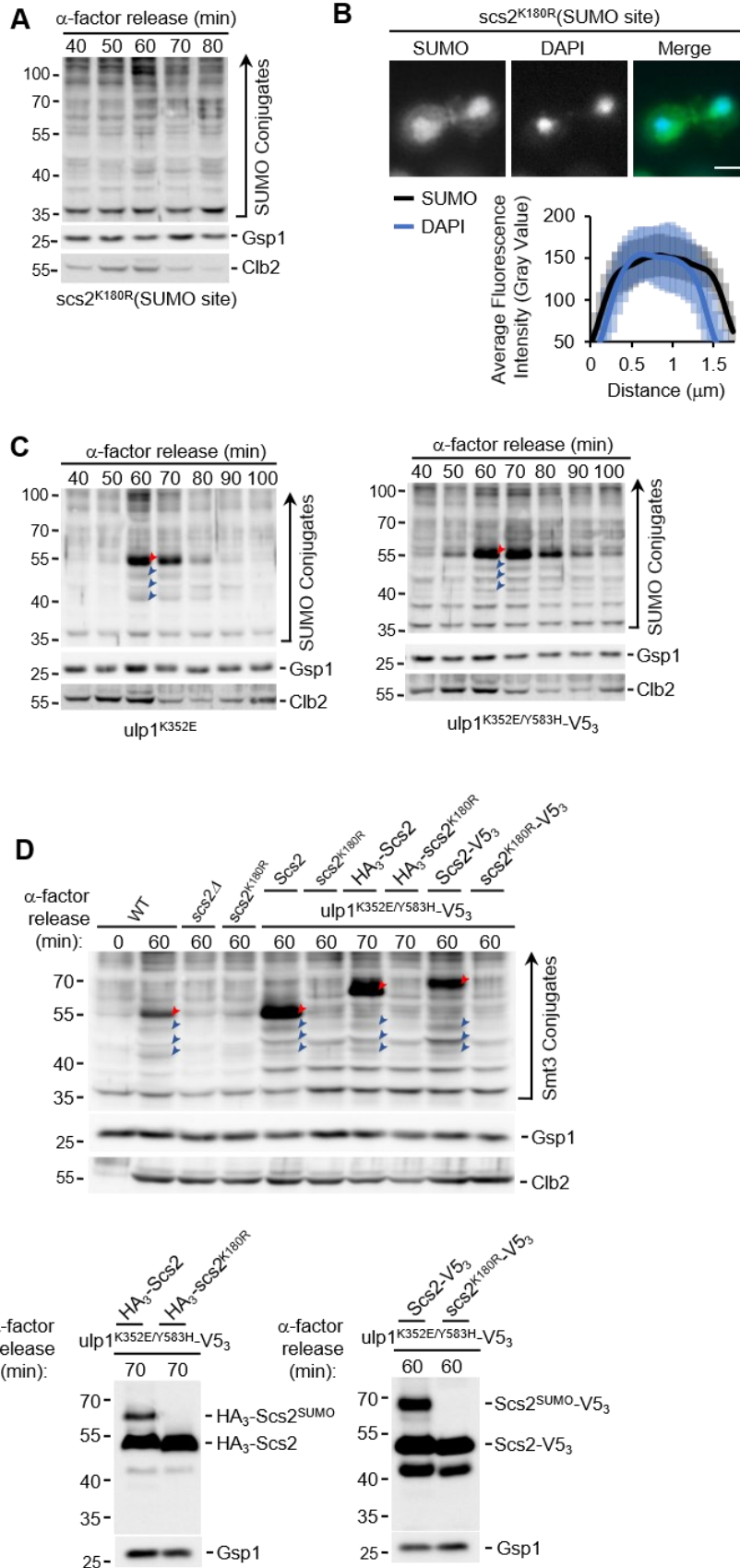


Figure 4-11. Scs2 is a mitotic SUMOylation target of Siz2. A, C, D) α -factor arrest-release assays were carried out as described in Fig. 4-3. Cell lysates from the indicated strains, at the times shown after release, were analyzed by western blotting to detect SUMO conjugates, Clb2, and the Gsp1 load control (A, C, D), as well as the V5₃ and HA₃ tags (D) as specified to the right of the blot. The form of Scs2 produced in the cells is indicated above the lane, in panel D. Red arrowheads point to SUMOylated Scs2 or SUMOylated tagged Scs2. Blue arrowheads highlight the other three prominent SUMOylated species in the 40-55 kDa range that arise in mitosis. Molecular mass markers are shown in kDa. **B)** Anti-SUMO immunofluorescence analysis of mitotic cells in the indicated strain. Imaging and quantification of the nuclear distribution of SUMO in mitotic cells (n = 25) was performed as described in Fig. 4-1. Quantification of line scans were obtained at the same time as data shown in Fig. 4-1. Error bars-SD. Bar- 2 μ m. Experiments were performed by C. Ptak and N.O. Saik. Figures were constructed by C. Ptak and N.O. Saik.

4.2.6 SUMO:SIM interactions enhance the mitotic enrichment of Siz2 at the NE.

SUMO:SIM interactions facilitate physical interactions between proteins (Jentsch and Psakhye 2013). Because Scs2 is SUMOylated and Siz2 contains two SIM motifs (Psakhye and Jentsch 2012), we investigated whether a SUMO:SIM interaction may stabilize Siz2 and Scs2 interactions. In support of this, we observed a reduction in Siz2 recruitment to the NE when the SUMOylation of Scs2 was prevented (*scs2^{K180R}*), despite Siz2 still being mitotically phosphorylated (Fig. 4-12A, B). Consistent with loss of Siz2 enrichment at the NE was a decrease in Siz2-dependent mitotic SUMOylation events in *scs2^{K180R}* mutant cells (Fig. 4-11A). Preventing the SUMOylation of Scs2 (*scs2^{K180R}*) did not alter the INM localization of Scs2 (Fig. 4-12C). Furthermore, Siz2 and *scs2^{K180R}* interactions were reduced as determined by immunoprecipitation analysis (Fig. 4-12D).

To investigate whether the SUMOylation of Scs2 contributed to the localization of Siz2 to the NE through a SUMO:SIM interaction, we next examined whether the SIM motifs of Siz2 functioned in Siz2 localization. Mutations in neither the SIM1 (*siz2^{I472/473A}*) or SIM2 (*siz2^{V720/721A}*) motifs of Siz2 altered Siz2 mitotic phosphorylation. The SIM1 mutant, but not the SIM2 mutant, however, caused a visible reduction in NE-association of Siz2 and the SUMOylation of Scs2 and other mitotic targets (Fig. 4-13A,-D). The mitotic SUMOylation defect of the SIM1 mutant, but not *siz2* localization, was restored when *ulp1* was mutated to increase Scs2 SUMOylation (*ulp1^{K352E/Y583H-V53}*; Fig. 4-13E,F), consistent with a

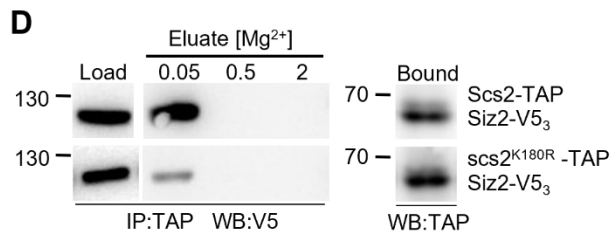
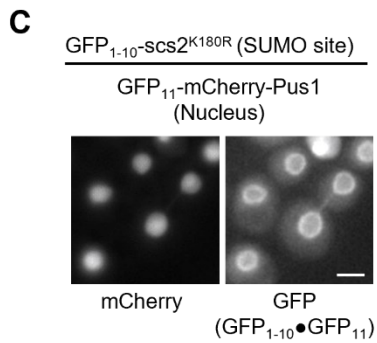
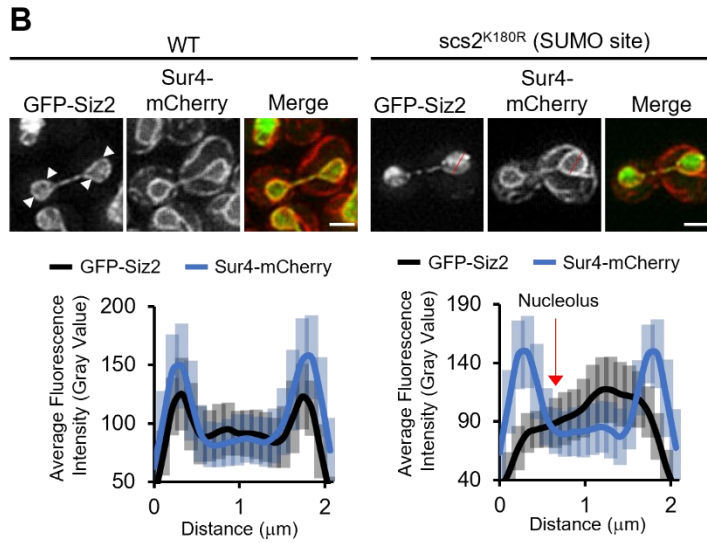
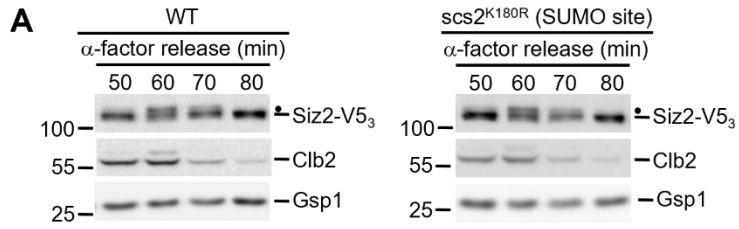


Figure 4-12. SUMOylation of Scs2 is required for the mitotic enrichment of Siz2 to the INM. **A)** α -factor arrest-release assays were carried out as described in Fig. 4-3 on indicated strains producing Siz2-V5₃. Cell lysates were analyzed by western blotting to detect Siz2-V5₃, Clb2, and the Gsp1 load control. Molecular mass markers are shown in kDa. Dot highlights mitotically phosphorylated Siz2-V5₃. **B)** Epifluorescence images of mitotic cells producing GFP-Siz2 in the indicated strains. Sur4-mCherry is a NE/ER marker. For quantification of the GFP-Siz2 nuclear distribution in mitotic *scs2*^{K180R} cells (n=25) a line was drawn starting at a point along the NE adjacent to the nucleolus as exemplified by the red arrow. Quantification of line scans were obtained at the same time as data shown in Fig. 4-4, with WT data shown here for comparison. Error bars - SD. Bar - 2 μ m. **C)** The INM association of the *scs2* SUMO site mutation (*scs2*^{K180R}) was assessed using the split-superfolder GFP system in cells producing GFP₁₋₁₀-*scs2*^{K180R} and the plasmid-encoded GFP₁₁-mCherry-Pus1 reporter, as described in Fig. 4-10. Bar- 2 μ m. **D)** Scs2-TAP or *scs2*^{K180R}-TAP were affinity-purified from cells (IP) producing Siz2-V5₃. Bound proteins were eluted using a Mg²⁺ step gradient. Equivalent portions of the indicated fractions were analyzed by western blotting (WB) to assess levels of the V5- and TAP-tagged fusions. Load, Elution, or Bound fractions shown were derived from the same western blot. Experiments were performed in parallel with those shown in Fig. 4-8 and 4-9. Experiments in panel A and B were performed by C. Ptak. Experiments in panel C were performed by A. Premashankar and C. Ptak. Experiments in panel D were performed by N.O. Saik. Figures were constructed by C. Ptak and N.O. Saik.

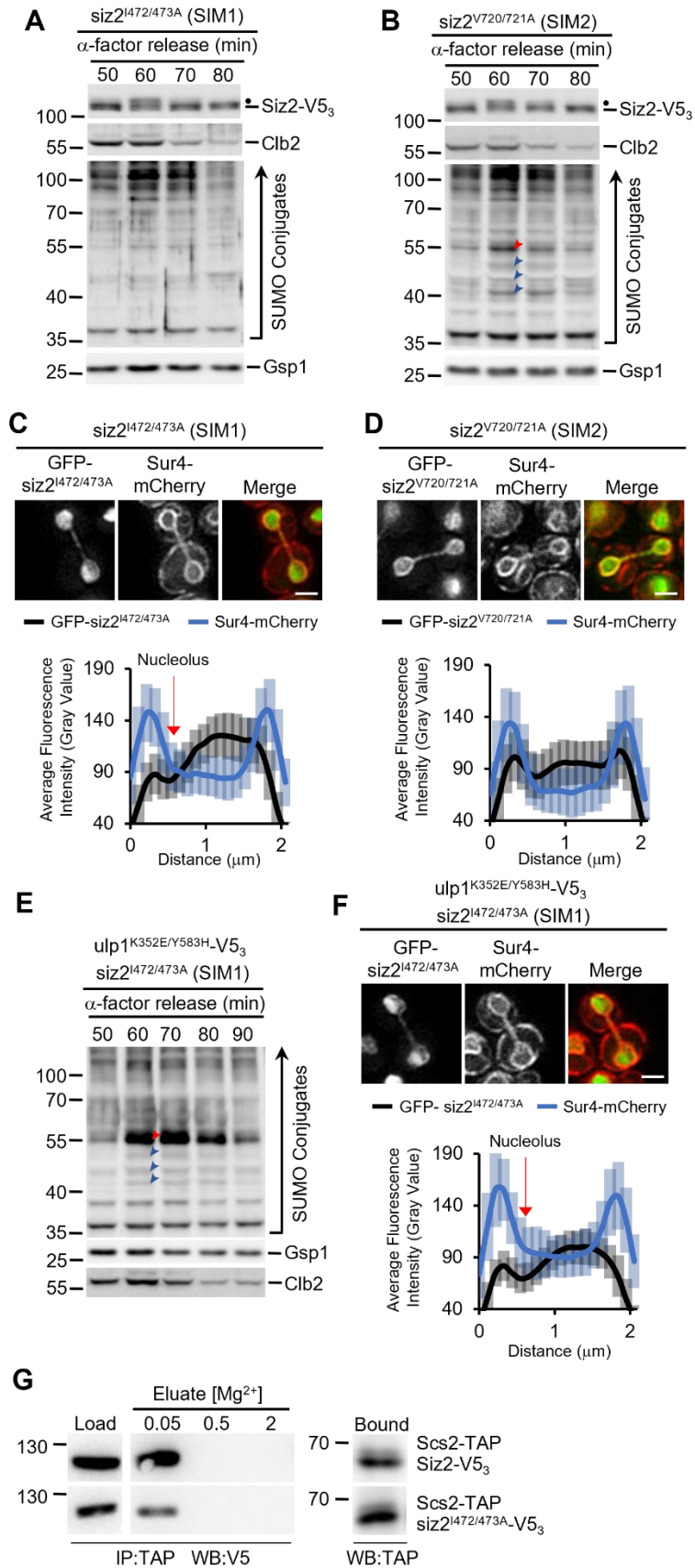


Figure 4-13. Interactions with SUMOylated targets at the INM enhances the mitotic enrichment of Siz2 to the INM. **A, B, E)** α -factor arrest-release assays on the indicated strains were carried out as described in Fig. 4-3. Cell lysates were analyzed by western blotting to detect SUMO conjugates, siz2-V5₃ derivatives, Clb2, and the Gsp1 load control. Dot highlights mitotically phosphorylated siz2-V5₃. Red arrowhead highlights SUMOylated Scs2. Blue arrowheads highlight the other three prominent SUMOylated species in the 40-55 kDa range that arise in mitosis. Molecular mass markers are shown in kDa. **C, D, F)** Epifluorescence images of mitotic cells producing GFP-siz2^{I472/473A} or GFP-siz2^{V720/721A} in the indicated strains are shown. Sur4-mCherry is a NE/ER marker. Imaging and quantification of the nuclear distribution of GFP-siz2 derivatives in mitotic cells (n = 25) was performed as in Fig. 4-4. For quantification of GFP-siz2^{I472/473A} the nuclear distribution line was drawn starting at a point along the NE adjacent to the nucleolus as, exemplified by the red arrow. Error bars - SD. Bar – 2 μ m. **G)** Scs2-TAP was affinity-purified from cells (IP) producing Siz2-V5₃ or siz2^{I472/473A}-V5₃. Bound proteins were eluted using a Mg²⁺ step gradient. Equivalent portions of the indicated fractions were analyzed by western blotting (WB) to assess levels of the V5- and TAP-tagged fusions. Load, Elution, or Bound fractions shown were derived from the same western blot. Experiments were performed at the same time as data shown in Fig. 4-12, with the WT data shown here for comparison. Experiments were performed in parallel with those shown in Fig. 4-8 and 4-9. Experiments in panel A -F were performed by C. Ptak. Experiments in panel G were performed by N.O. Saik. Figures were constructed by C. Ptak and N.O. Saik.

weak NE-association of Siz2 and not the loss of Siz2 SUMO ligase activity. Furthermore, decreased interactions were observed between Scs2 and Siz2 when the Siz2 SIM1 motif (*siz2*^{1472/473A}) was abrogated (Fig. 4-13G). These results demonstrate that the SIM1 motif of Siz2 contributes to Siz2 NE localization and Siz2-mediated SUMOylation during mitosis. Cumulatively these data suggest interactions between Scs2 and Siz2 established by phosphorylation and FFAT:MSP motifs are enhanced by SUMO:SIM interactions between Scs2 and Siz2.

4.2.7 Siz2-dependent SUMOylation events at the NE during mitosis re-establish chromatin-NE interactions.

Siz2 enrichment at the INM is initiated during the transition from metaphase to anaphase. During this time, sister chromosomes are segregated to daughter nuclei, and specific chromatin-NE interactions are proposed to be re-established in these nuclei (Hediger et al., 2002; Ebrahimi and Donaldson 2008; Donna Garvey Brickner and Brickner 2010). Therefore, we investigated whether Scs2-Siz2 mediated SUMOylation at the INM facilitates the re-establishment of NE-chromatin interactions during mitosis.

We have previously shown that Siz2 and Siz2-mediated SUMOylation events are necessary for NPC localization of the induced *INO1* locus (Saik et al., 2020; Chapter 3). Additionally, relocalization of the active *INO1* locus to the NPCs occurs during M-phase (Donna Garvey Brickner and Brickner 2010). Therefore, we postulated that Siz2 mitotic enrichment at the NE and corresponding mitotic SUMOylation

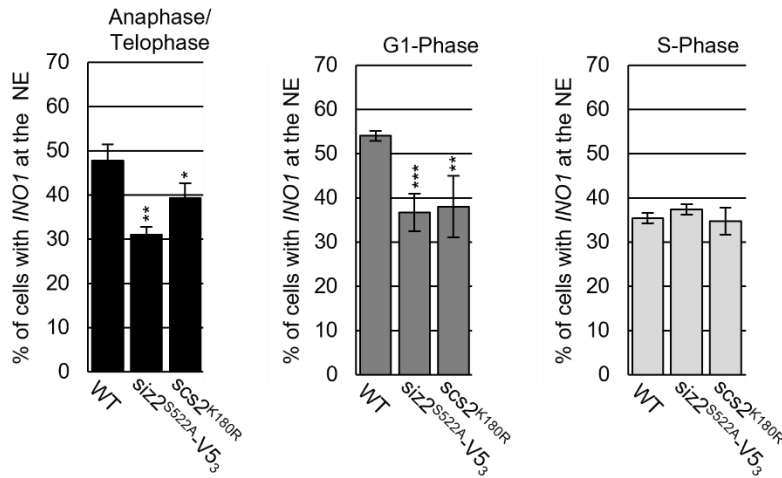


Figure 4-14. Siz2-mediated mitotic SUMOylation events are required for the NPC association of *INO1* following induction. NE localization of the activated *INO1* locus was examined using epifluorescence imaging. The graphs show the percentage of total GFP-lacI/*INO1-LacO₂₅₆* foci that colocalize with NE localized Nup49-mRFP. For each indicated strain, three biological replicates were assessed. Cell cycle stage was determined using bud size, and nuclear morphology. n = 50 cells per replicate/cell cycle stage. Error bars - SD. Asterisks - significant change relative to WT using a two-tailed student's t-test. *p ≤ 0.05, **p ≤ 0.01, ***p ≤ 0.001.

events might facilitate these interactions. Examination of the subcellular localization of activated *INO1* throughout the cell cycle revealed an enrichment of the *INO1* locus to NPCs during M- and G1-phase (~50-55% of cells), but not S-phase. In *siz2^{2S522A}* and *scs2^{K180R}* mutant cells, the activated *INO1* locus did not show increased localization to the NPCs during M- and G1-phase (Fig. 4-14). These observations suggest that the Scs2-Siz2 complex promotes SUMOylation events at the NE, which directs the establishment of *INO1*-NPC interactions during mitosis.

To expand our analysis, we investigated whether Scs2-Siz2 mediated SUMOylation at the INM functioned in establishing the association of other forms of chromatin with the NE during mitosis. Because Siz2 and Siz2-mediated SUMOylation events have been shown to regulate telomere interactions with the NE (Ferreira et al., 2011), we examined the consequences of altering Siz2-mediated mitotic SUMOylation events on the nuclear position of telomeres. We examined the association of telomeres with the INM using a GFP-labeled telomere localization assay (Hediger et al., 2002). In WT cells, telomeres were detected at the NE in ~65-75% of cells in each of the three cell cycle stages examined: anaphase/telophase, G1-phase, and S-phase. A loss of Siz2 (*siz2Δ*) or Scs2 (*scs2Δ*) reduced telomere tethering to the NE at all cell cycle stages (Fig. 4-15). *siz2* and *scs2* point mutants that inhibited Siz2 NE-association and the mitotic SUMOylation of NE targets showed decreased telomere tethering to the NE during anaphase/telophase. Reduced telomere tethering persisted into G1-phase, except for the *siz2^{A569D}* (FFAT motif) mutation, which showed minor defects. By contrast, in the *ulp1^{K352E/Y583H}-V5₃* mutant, where Scs2-SUMO levels are elevated in mitosis

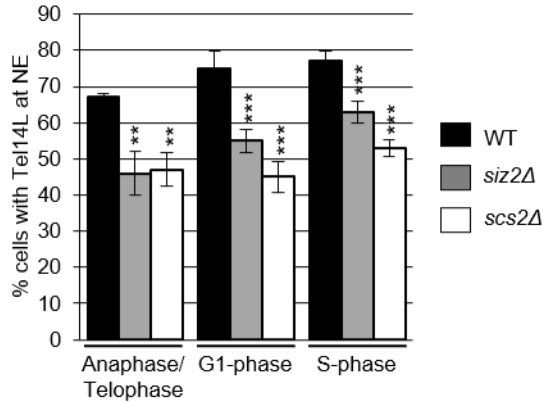


Figure 4-15. Siz2 and Scs2 are required for NE-association of telomeres during M- and G1-phase. Tethering of Tel14L to the NE was examined using epifluorescence imaging for the indicated strains. The percentage of the total number of GFP-lacI/*Tel14L-LacO₂₅₆* foci examined that overlapped with NE-associated Sec63-GFP signal was determined for at least three biological replicates for the indicated cell cycle stage. Telomere localization for G1 and S-phase nuclei was assessed by measuring the distance between the GFP loci to the NE marker and assigning the foci to one of three concentric nucleoplasmic zones of equal volume. Telomere loci were determined to be associated with the NE when the GFP-lacI signal fully or partially overlapped with Sec63-GFP for mitotic nuclei. n = 50 cells per replicate/cell cycle stage. Error bars - SD. Asterisks - significant change relative to WT using a two-tailed student's t-test. *p ≤ 0.05, **p ≤ 0.01, ***p ≤ 0.001.

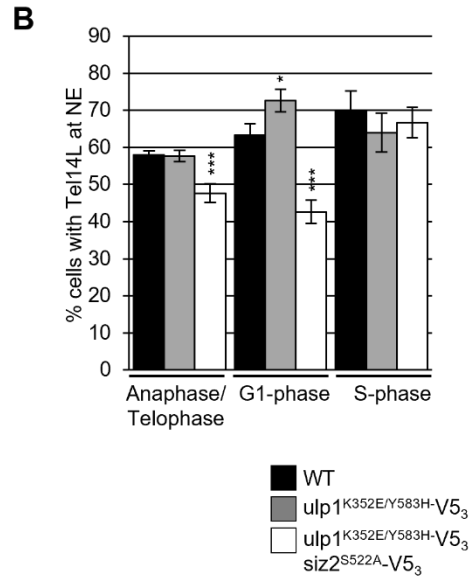
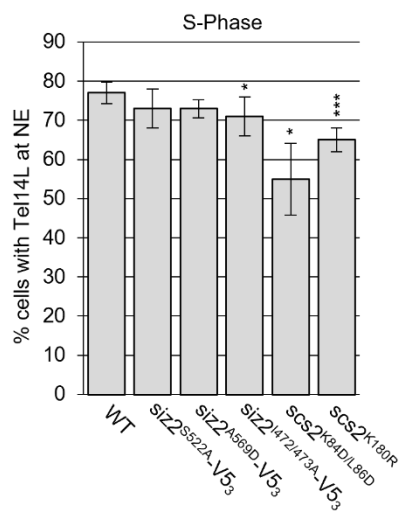
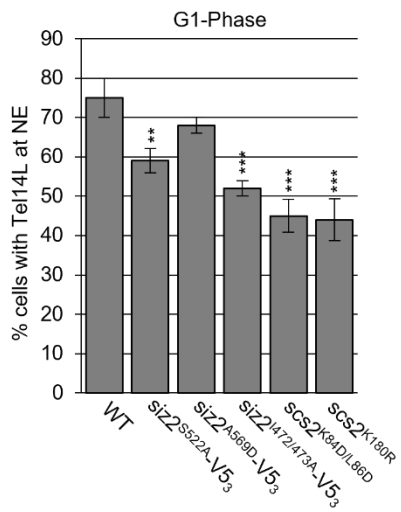
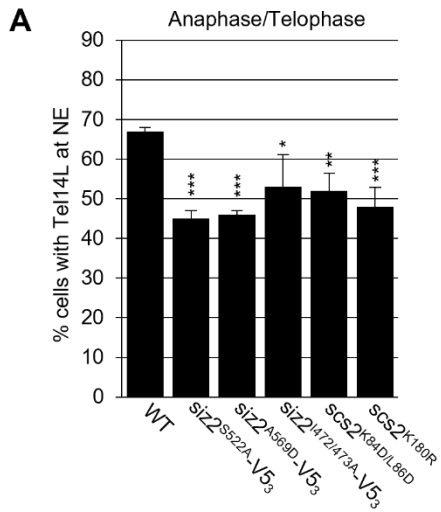


Figure 4-16. Siz2-mediated mitotic SUMOylation events are required for NE-association of telomeres during M- and G1-phase. **A)** Tethering of Tel14L to the NE was examined using epifluorescence imaging for the indicated strains. The percentage of the total number of GFP-lacI/*Tel14L-LacO₂₅₆* foci examined that overlapped with NE-associated Sec63-GFP signal was determined for at least three biological replicates for the indicated cell cycle stage as described in Fig. 4-15. n = 50 cells per replicate/cell cycle stage. Error bars - SD. Asterisks - significant change relative to WT using a two-tailed student's t-test. *p ≤ 0.05, **p ≤ 0.01, ***p ≤ 0.001. Quantification of telomere localization was performed at the same time as data shown in Fig. 4-15, with WT data shown here for comparison. **B)** Tethering of Tel14L to the NE was examined using epifluorescence imaging for the indicated strains. The percentage of the total number of GFP-lacI/*Tel14L-LacO₂₅₆* foci examined that overlapped with NE-associated Sec63-GFP signal was determined for at least three biological replicates for the indicated cell cycle stage. Telomere loci were determined to be associated with the NE when the GFP-lacI signal fully or partially overlapped with Sec63-GFP. Cell cycle stage was assessed by bud size and nuclear morphology. n = 50 cells per replicate/cell cycle stage. Error bars - SD. Asterisks - significant change relative to WT using a two-tailed student's t-test. *p ≤ 0.05, **p ≤ 0.01, ***p ≤ 0.001.

and into G1-phase, telomere tethering to the NE was normal in M-phase and increased in G1-phase cells. By S-phase, the NE association of telomeres in the *siz2*, *scs2*, and *ulp1* point mutants were largely normal. In the case of *scs2*^{K180R} (SUMO site mutation), telomere tethering in S-phase was increased compared to tethering in the G1-phase (Fig. 4-16A,B). These data show that the Scs2-Siz2 complex re-establishes numerous chromatin-NE interactions during mitosis.

4.2.8 Siz2-mediated SUMOylation of Sir4 regulates mitotic tethering of telomeres to the NE.

We have previously shown that Siz2 binds to the *INO1* locus to facilitate relocalization to the nuclear periphery (Saik et al.,2020; Chapter 3). Therefore, we investigated whether telomere tethering to the INM was facilitated by the binding of Siz2 to these regions. Siz2-V5₃ and *siz2*^{S522A}-V5₃ association with subtelomeric chromatin was investigated using ChIP analysis. We did not observe an enrichment of Siz2-V5₃ or *siz2*^{S522A}-V5₃ at subtelomeric chromatin (Fig. 4-17), suggesting Siz2-mediated SUMOylation events were facilitating telomere tethering to the INM during mitosis.

Factors contributing to telomere association with the INM during mitosis are unknown. Various mechanisms, however, have been described for telomere and subtelomeric chromatin tethering to the INM during other cell cycle stages. Sir4 and the yKu70/80 complex, for example, functions to tether telomeres to the NE in G1- and S-phase (Taddei and Gasser 2012; Kupiec 2014). Sir4 and yKu80 are

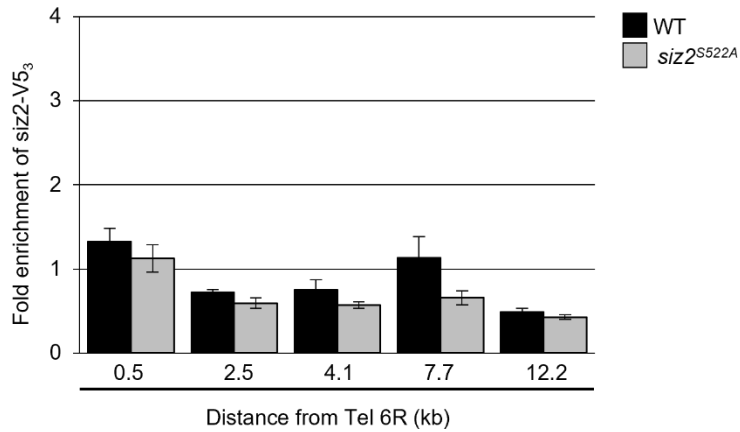


Figure 4-17. *Siz2* does not interact with subtelomeric chromatin. Cells producing *Siz2*-V5₃ or *siz2*^{S522A}-V5₃ were collected and subjected to ChIP analysis using antibodies directed against V5. Occupancy of *Siz2*-V5₃ and *siz2*^{S522A}-V5₃ at subtelomeric chromatin relative to a non-subtelomeric region was examined by qPCR using primer pairs that amplify regions for the distances indicated from Tel6R. Data represents 3 biological replicates. Error bars- SEM.

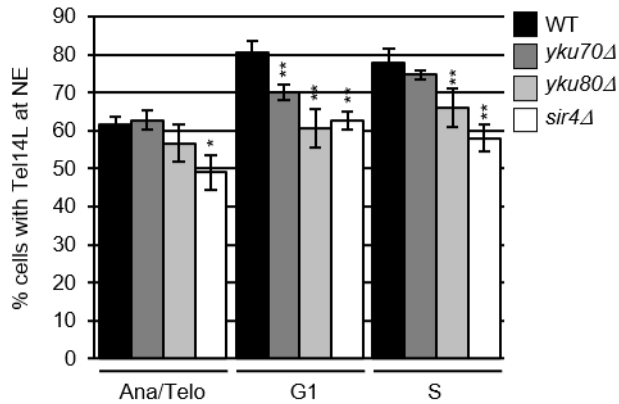


Figure 4-18. Sir4 is required for telomere tethering during M-phase. Tethering of Tel14L to the NE was examined using epifluorescence imaging for the indicated strains. The percentage of the total number of GFP-lacI/*Tel14L-LacO₂₅₆* foci examined that overlapped with NE-associated Sec63-GFP signal was determined for at least three biological replicates for the indicated cell cycle stage as described in Fig. 4-15. n = 50 cells per replicate/cell cycle stage. Error bars - SD. Asterisks - significant change relative to WT using a two-tailed student's t-test. *p ≤ 0.05, **p ≤ 0.01, ***p ≤ 0.001.

SUMOylated by Siz2, with previous studies suggesting that Siz2-mediated SUMOylation directs Sir4, but not yKu80, dependent telomere tethering during G1 (Ferreira et al., 2011). Similarly, we find that Sir4, but not yKu70/80, plays a significant role in M-phase telomere tethering (Fig. 4-18).

To investigate whether Sir4 SUMOylation was dependent on the enrichment of Siz2 at the NE during mitosis, we examined purified His8-SUMO conjugates isolated from strains producing Sir4-V5₃. We found that when Scs2-Siz2 dependent mitotic SUMOylation was inhibited (*siz2*^{S522A}, *scs2*^{K180R}, or *scs2*^{K84D/L86D} mutants), Sir4 SUMOylation was reduced in comparison to WT cells (Fig. 4-19A). By contrast, when Scs2-Siz2 dependent mitotic SUMOylation was enhanced (*ulp1*^{K352E/Y583H}-V5₃), cells showed increased Sir4 SUMOylation (Fig. 4-19B). A mutant that eliminated a SUMO acceptor site within the PAD domain of Sir4 (*sir4*^{K1037R}), a region necessary for Sir4 G1-phase telomere tethering activity (Andrulis et al., 2002; Taddei et al., 2004; Fig. 4-19C), caused a decrease in Sir4 SUMOylation. The SUMOylation of the *sir4*^{K1037R} mutant was comparable to mutants that inhibit Scs2-Siz2 dependent mitotic SUMOylation (Fig. 4-19). NE tethering of telomeres in *sir4*^{K1037R} mutant cells also showed telomere tethering defects specific to M- and G1-phases (Fig. 4-20A), similar to those observed when Siz2 mitotic enrichment at the NE was inhibited. These results suggest that the Scs2-Siz2 complex directs the SUMOylation of Sir4 to facilitate telomere tethering to the NE in mitosis and into the subsequent G1-phase. NPC localization of activated *INO1* was unaltered in *sir4*^{K1037R} mutant cells (Fig. 4-20B), indicating that

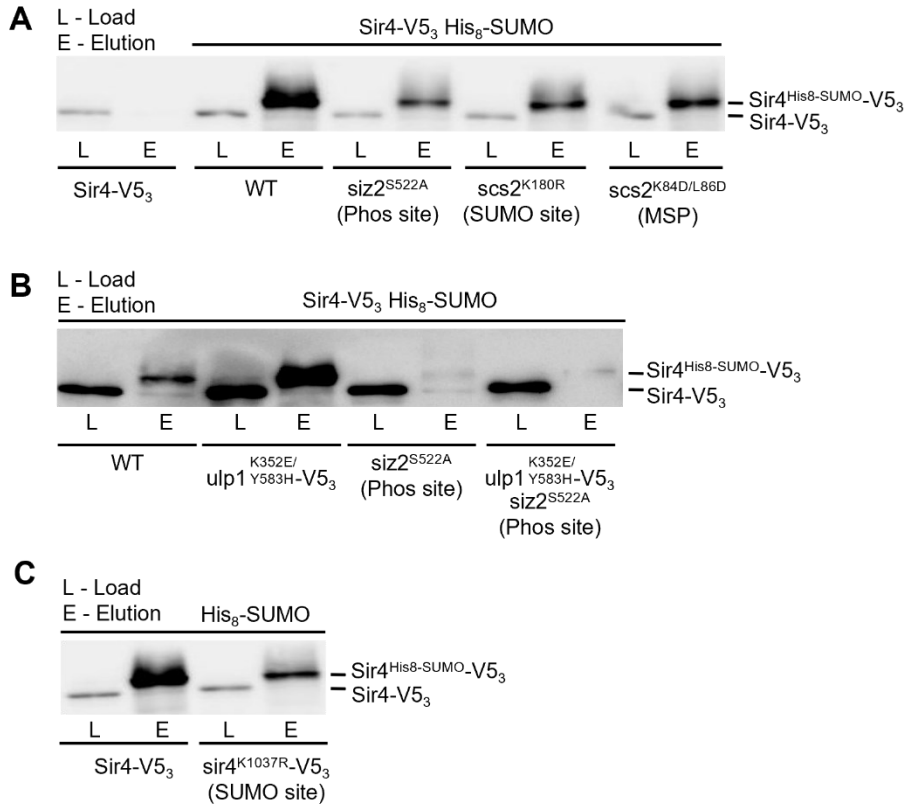


Figure 4-19. Mitotic enrichment of Siz2 to the NE facilitates the SUMOylation of Sir4. His₈-SUMO-conjugates were affinity-purified from the indicated strains containing Sir4-V5₃ (A, B) or the sir4^{K1037R}-V5₃ SUMO site mutant (C). Levels of Sir4 and sir4^{K1037R} in the cell lysates (L), and Sir4-V5₃-SUMO and sir4^{K1037R}-V5₃-SUMO in eluates (E) were examined by anti-V5 western blotting.

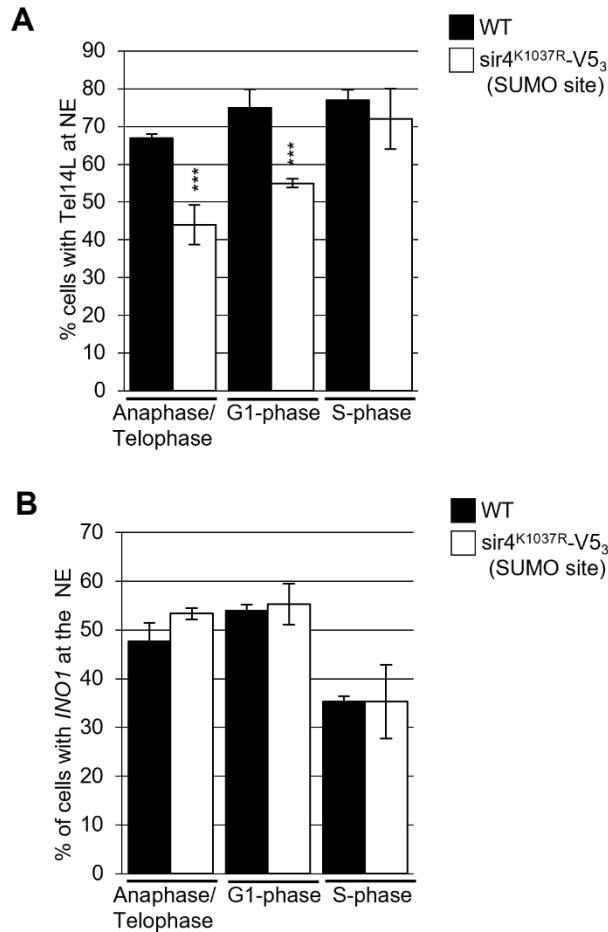


Figure 4-20. Siz2-mediated SUMOylation of Sir4 regulates telomere tethering to the NE. **A)** Tethering of Tel14L to the NE was examined using epifluorescence imaging for the indicated strains. The percentage of the total number of GFP-lacI/*Tel14L-LacO₂₅₆* foci examined that overlapped with NE-associated Sec63-GFP signal was determined for at least three biological replicates for the indicated cell cycle stage as described in Fig. 4-15. $n = 50$ cells per replicate/cell cycle stage. Error bars - SD. Asterisks - significant change relative to WT using a two-tailed student's t-test. *** $p \leq 0.001$. Quantification of telomere localization was performed at the same time as data shown in Fig. 4-15, with WT data shown here for comparison. **B)** Tethering of the *INO1* locus to the NE was examined using epifluorescence imaging for the indicated strains. The percentage of the total number of lacI/*INO1-lacO₂₅₆* foci that overlapped with the NE-associated Nup49-mRFP was determined for at least three biological replicates for the indicated cell cycle stage as described in Fig. 4-14. Quantification of *INO1* localization was performed at the same time as data shown in Fig. 4-14, with the WT data shown here for comparison. $n = 50$ cells per replicate/cell cycle stage. Error bars - SD.

the Scs2-Siz2 complex regulates different types of NE-chromatin interactions in mitosis by independent mechanisms.

4.2.9 Siz2-mediated SUMOylation of Sir4 stabilizes Sir4 association with subtelomeric chromatin during mitosis.

Cells lacking *Siz2* showed no defect in the INM association or the number of Sir4-GFP foci. Similarly, the *sir4^{K1037R}* mutant did not show any distinguishable differences in NE-association (Fig. 4-21). These data indicate that the telomere tethering defects associated with the *Siz2*-directed SUMOylation of Sir4 were not due to a mislocalization of Sir4 to the NE. Therefore, we postulated that the SUMOylation of Sir4 facilitated telomere tethering by mediating Sir4 association with subtelomeric chromatin. We investigated Sir4 association with subtelomeric chromatin using ChIP analysis. Similar to previous studies (Van De Vosse et al., 2013; Moradi-Fard et al., 2016), WT cells showed the highest enrichment of Sir4-V5₃ bound near Tel6R (0.5 kb), followed by a progressive decrease in association with increasing distance from the telomere. Cells lacking *Siz2* showed a significant reduction in Sir4 enrichment in regions adjacent to Tel6R (Fig. 4-22A). Consistent with *Siz2*-dependent mitotic telomere tethering requiring Sir4, but not yKu70/80, a loss of *Siz2* did not alter enrichment of yKu70 or yKu80 at regions adjacent to Tel6R (Fig. 4-22B, C). In *siz2* and *scs2* mutant cells defective in mitotic SUMOylation, Sir4 enrichment was significantly reduced in all regions adjacent to Tel6R (Fig. 4-23A). The *sir4^{K1037R}* mutant protein also showed a significantly reduced enrichment in all regions adjacent to Tel6R (Fig. 4-23B). These observations are consistent with the SUMOylation of Sir4 facilitating its integration

into subtelomeric chromatin. No significant difference in Sir4 enrichment at telomeres relative to WT cells was observed in *ulp1^{K352E/Y583H}-V5₃* mutant cells (Fig. 4-23C); however, these cells showed increased levels of SUMOylated proteins at subtelomeric chromatin (Fig. 4-23D). Sir3, an interacting partner of Sir4 (Moretti et al., 1994; Kupiec 2014), also showed reduced association with subtelomeric chromatin in cells defective in Siz2-dependent mitotic SUMOylation (Fig. 4-24). These observations suggest that Siz2-directed SUMOylation of Sir4 facilitates Sir4 integration into subtelomeric chromatin to establish telomere-NE interactions in mitosis.

To investigate whether Siz2-mediated SUMOylation of Sir4 facilitates the mitotic association of Sir4 with subtelomeric chromatin, we examined levels of Sir4-V5₃ bound to subtelomeric chromatin in synchronized cell cultures. In WT cells, Sir4 association with subtelomeric chromatin 0.5 kb from Tel6R was ~2-fold higher in M- and G1-phase cells compared to S-phase cells. In cells where Sir4 SUMOylation is reduced (*siz2^{S522A}* or *sir4^{K1037R}* mutant), S-phase levels of Sir4 bound to Tel6R subtelomeric chromatin were similar to WT. Sir4 bound to subtelomeric chromatin in these mutant cells; however, showed a significant reduction in M- and G1-phase relative to WT cells (Fig. 4-25). These observations are consistent with the Scs2-Siz2 complex facilitating telomere tethering by directing the assembly of SUMOylated Sir4 into subtelomeric chromatin during mitosis.

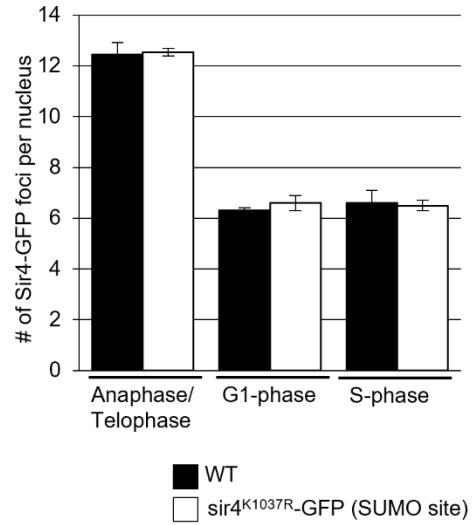
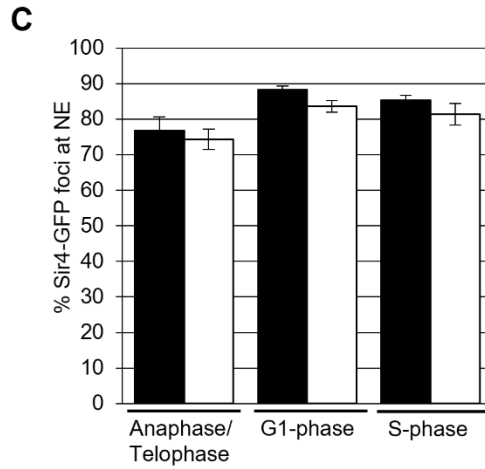
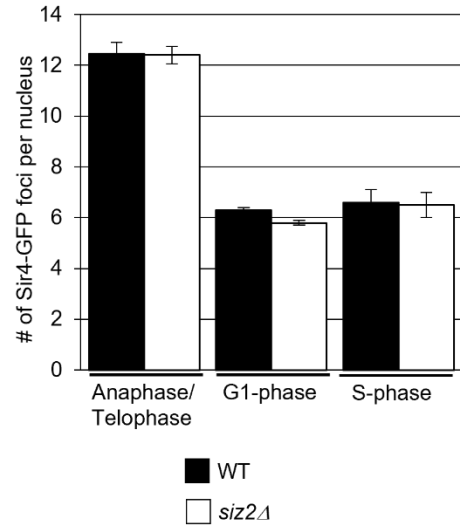
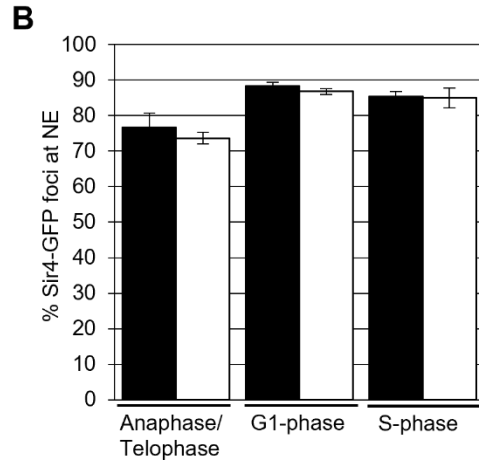
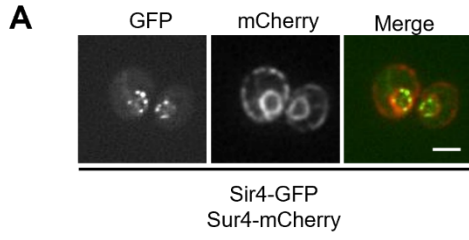


Figure 4-21. NE-association of Sir4 is unaltered by Siz2-mediated SUMOylation. **A)** Epifluorescence images of cells producing Sir4-GFP and the NE/ER localized Sur4-mCherry. Bar - 2 μm . **B, C)** Graphs showing the percentage of total Sir4-GFP or sir4^{K1037R}-GFP foci at the NE (left panel) and the average number of Sir4-GFP or sir4^{K1037R}-GFP foci per nucleus (right panel) for indicated strains at each cell cycle stage. Graphs represent data from at least three biological replicates. n=50 cells per replicate/cell cycle stage. Error bars - SD.

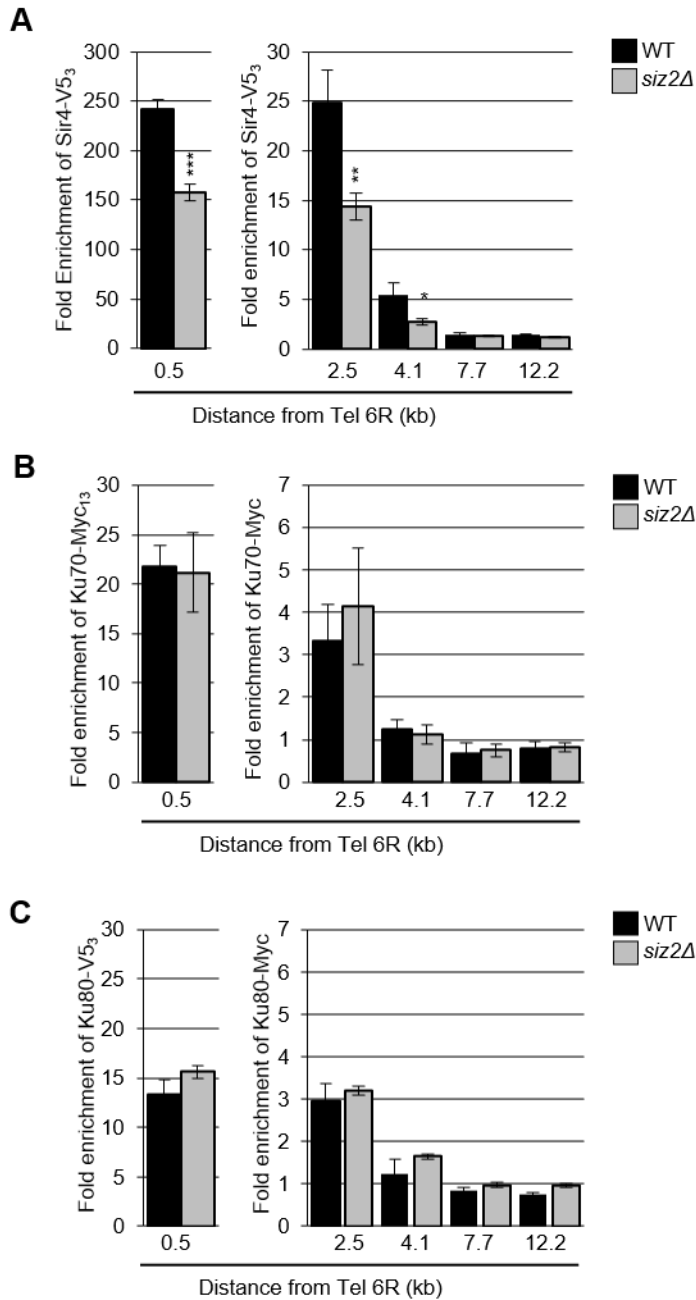


Figure 4-22. Sir4 association with subtelomeric chromatin requires Siz2. Cells producing Sir4-V5₃ (A) Ku70-Myc₁₃ (B) or Ku80-V5₃ (C) in the indicated strains were collected and subjected to ChIP analysis using antibodies directed against V5 or Myc. Occupancy of Sir4-V5₃, Ku70-Myc₁₃, or Ku80-V5₃ at subtelomeric chromatin relative to a non-subtelomeric region was examined by qPCR using primer pairs that amplify regions for the indicated distances from Tel6R. Data represents 3 biological replicates. Error bars- SEM. Asterisks - significant change relative to WT using a two-tailed student's t-test. * $p \leq 0.05$, ** $p \leq 0.01$.

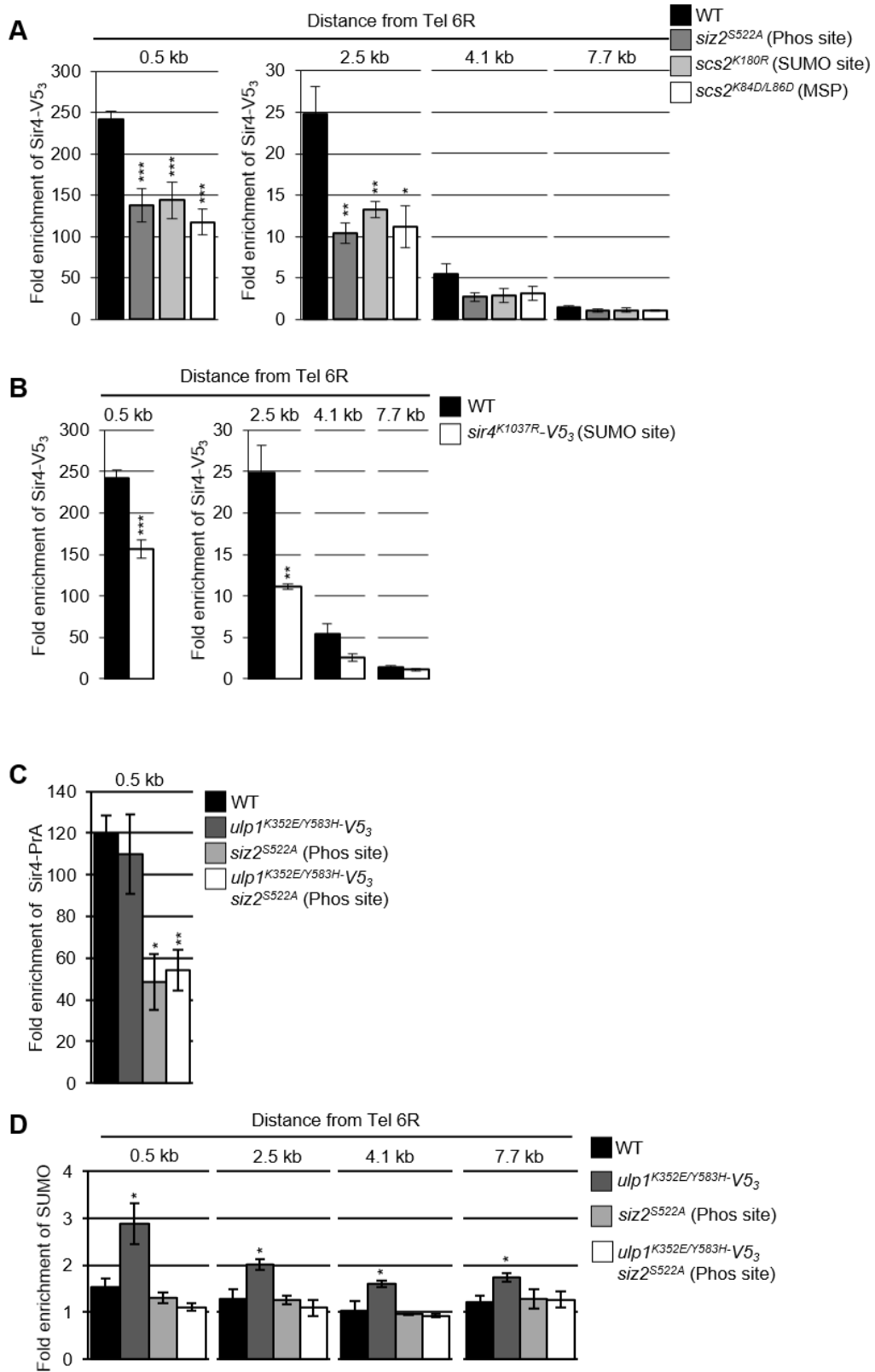


Figure 4-23. Siz2-mediated mitotic SUMOylation facilitates Sir4 association with subtelomeric chromatin. A, B) Cells producing Sir4-V5₃ or sir4^{K1037R}-V5₃ were collected and subjected to ChIP analysis using antibodies directed against V5. Occupancy of Sir4-V5₃ or sir4^{K1037R}-V5₃ at subtelomeric chromatin was examined as described in Fig. 4-22. Data represents 3 biological replicates. Error bars- SEM. Asterisks - significant change relative to WT using a two-tailed student's t-test. *p ≤ 0.05, **p ≤ 0.01, ***p ≤ 0.001. ChIP analysis in panels A and B were performed in parallel, with WT data shown for comparison in both panels. **C)** Cells producing Sir4-PrA were collected and subjected to ChIP analysis using antibodies directed against PrA in the indicated strains as described above. **D)** ChIP analysis using antibodies directed against SUMO was performed on indicated strains as described above. Error bars- SEM. Asterisks - significant change relative to WT using a two-tailed student's t-test. *p ≤ 0.05.

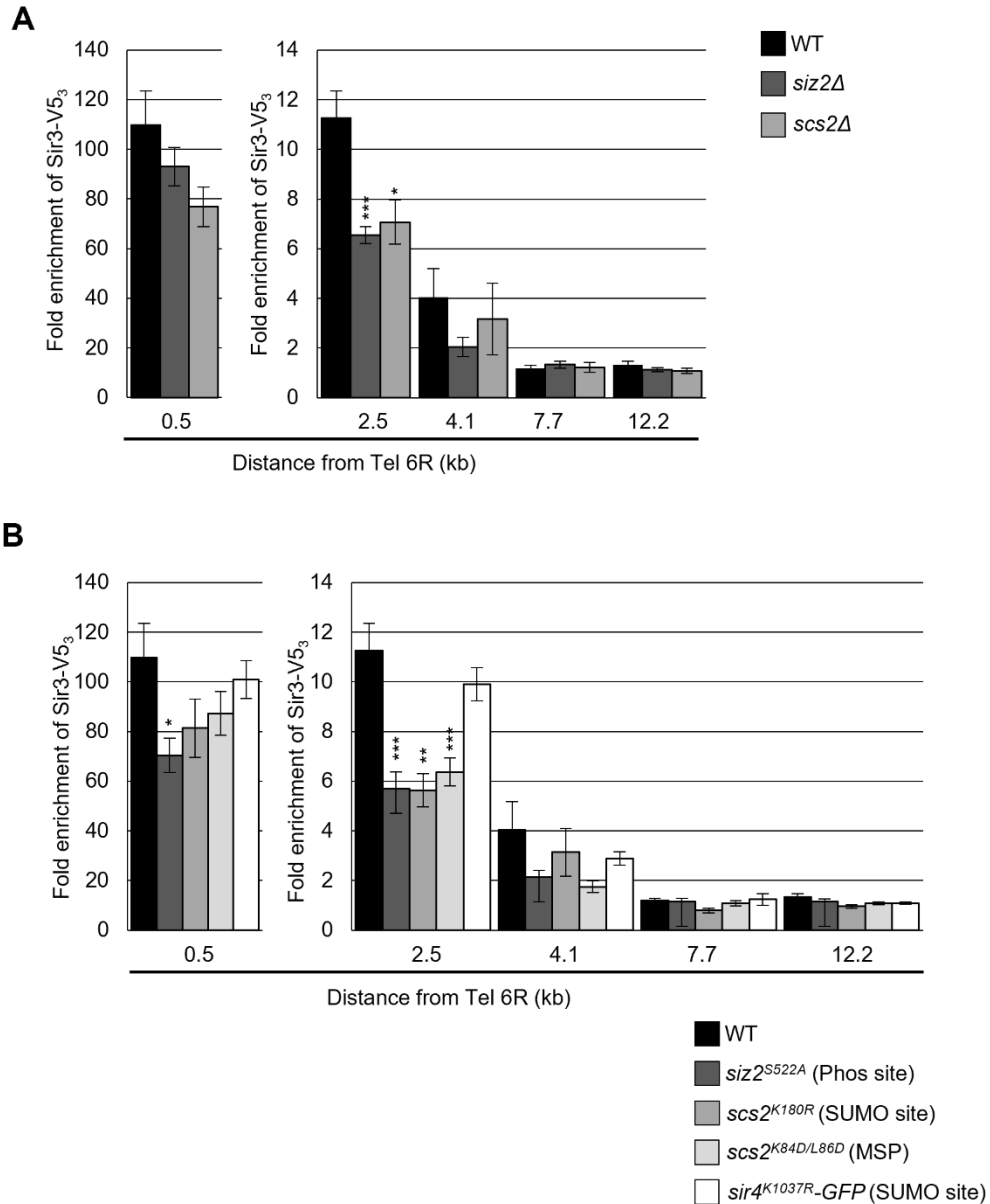


Figure 4-24. Siz2-mediated mitotic SUMOylation facilitates Sir3 association with subtelomeric chromatin. Cells producing Sir3-V5₃ were collected and subjected to ChIP analysis using antibodies directed against V5 as described in Fig. 4-22. Error bars- SEM. Data represents at least 3 biological replicates. Asterisks - significant change relative to WT using a two-tailed student's t-test. * $p \leq 0.05$, ** $p \leq 0.01$, *** $p \leq 0.001$. ChIP analysis in panels A and B were performed in parallel, with WT data shown in both panels for comparison.

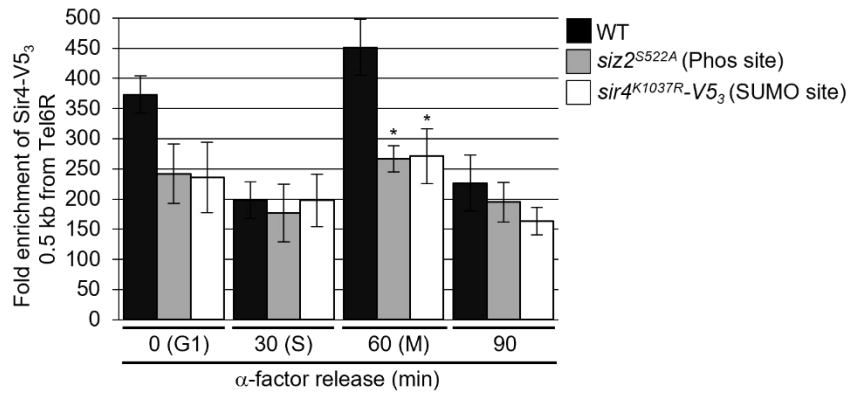
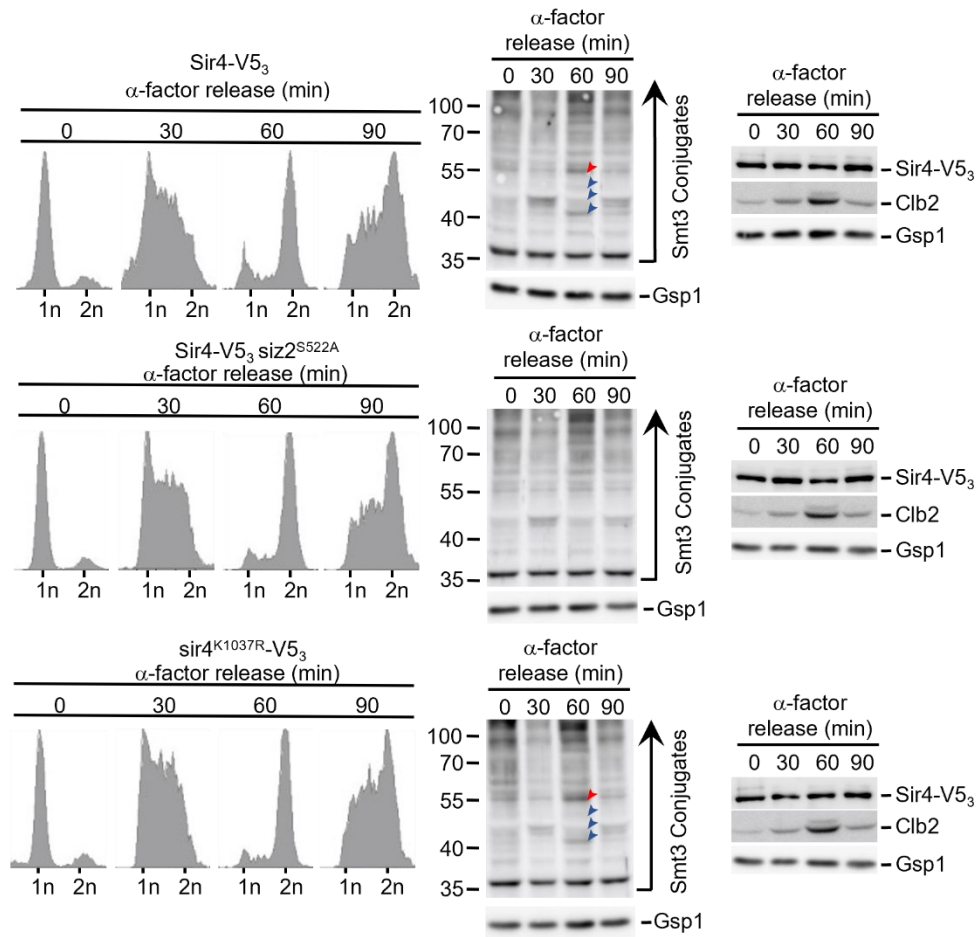
A**B**

Figure 4-25 Siz2-mediated mitotic SUMOylation re-establishes Sir4 association with subtelomeric chromatin following S-phase. A) ChIP analysis using antibodies directed against V5 was performed using synchronized cultures of the indicated strains producing Sir4-V5₃ or sir4^{K1037R}-V5₃. Strains were collected at various cell cycle stages, including G1-phase (α -factor arrested cells), S-phase (30 min post α -factor release), and M-phase (60 min post α -factor release). ChIP analysis was performed on a region 0.5 kb from Tel6R. Graphs represent at least three biological replicates. Error bars - SEM. Asterisks - significant change relative to WT using a two-tailed student's t-test. * $p \leq 0.05$. **B)** Confirmation of the cell cycle stage of cultures used in panel A. Samples at each time point were analyzed by FACS to determine DNA content of cells in the population (left). The positions of 1n and 2n DNA peaks are shown. Cell lysates harvested at the various time points in panel A were also analyzed by western blotting using anti-V5, SUMO, Clb2, and Gsp1 (load control) antibodies (right). Red arrowheads point to SUMOylated Scs2. Blue arrowheads point to other prominent mitotic SUMO conjugates. Molecular mass markers are shown in kDa.

4.2.10 The Scs2-Siz2 complex facilitates the association of subtelomeric chromatin to the NE independently of silencing.

The localization of subtelomeric chromatin to the NE is associated with the repression of genes in these regions (Taddei, Schober, and Gasser 2010). We examined mutants that altered mitotic Siz2-dependent SUMOylation events and telomere tethering for alterations in subtelomeric gene expression. Derepression of subtelomeric genes can be evaluated using a cell growth assay. In this assay, reporter genes *URA3* and *ADE2* are inserted in subtelomeric regions adjacent to telomeres VII-L (Tel7L) and V-R (Tel5R), respectively (Singer and Gottschling 1994). Under normal conditions, these genes are suppressed, preventing growth in the absence of uracil and adenine. The derepression of these reporter genes in subtelomeric chromatin allows growth in the absence of adenine and uracil. The derepression of these genes will also prevent growth in the presence of 5-FOA, as the production of uracil renders the cells sensitive to 5-FOA (Aparicio, Billington, and Gottschling 1991). Consistent with the repression of subtelomeric genes, WT cells grew in the presence of 5-FOA and showed minimal growth on medium lacking uracil or adenine. We observed growth of *sir3Δ* mutant cells on medium lacking uracil and adenine and observed a loss of growth in the presence of 5-FOA, consistent with the derepression of subtelomeric genes in cells lacking Sir3. Examination of mutants which decreased (*siz2Δ*, *scs2Δ*, *siz2^{S522A}*, *scs2^{K180R}*) Siz2-dependent mitotic SUMOylation and M-/G1-phase telomere tethering did not show an obvious difference in growth relative to WT cells (Fig. 4-26A). *ulp1^{K352E/Y583H}*-*V5₃* cells, which have increase Siz2-dependen mitotic SUMOylation slight

differences in growth relative to WT (Fig. 4-26A). To quantify differences in subtelomeric gene expression we analyzed a subset of subtelomeric genes by RT-qPCR. Analysis of a subset of subtelomeric genes by RT-qPCR also allowed us to investigate changes in subtelomeric gene expression that the growth assay may not have been sensitive enough to detect. Differences in gene expression could be detected for the subset of subtelomeric genes investigated in the various mutant backgrounds (Fig. 4-26B), however gene expression of subtelomeric genes assayed were largely unchanged relative to WT cells. Together these data suggest that the Scs2-Siz2 complex regulates telomere association with the NE independently of regulating subtelomeric gene expression.

4.2.11 Siz2-dependent SUMOylation events regulate the transcription of transposons.

To investigate whether Siz2-dependent SUMOylation events at the INM during mitosis functioned to regulate chromatin beyond facilitating NE-chromatin interactions, we performed RNA Seq on *siz2^{S522A/S527A}-V5₃* mutant cells. Consistent with our previous observations, a loss of Siz2-dependent SUMOylation events at the INM did not derepress subtelomeric genes (Fig. 4-26). Instead, a significant proportion of derepressed genes (~1/3) in *siz2^{S522A/S527A}-V5₃* mutant cells were genes involved in Ty1 (*) and Ty2 (***) retrotransposition (Table 4-2). Increased Ty1 and Ty2 transcription suggests a role for Siz2 and Siz2-mediated SUMOylation in regulating retrotransposition. This may reflect an additional role for Siz2 and Siz2-mediated SUMOylation events in regulating chromatin structure.

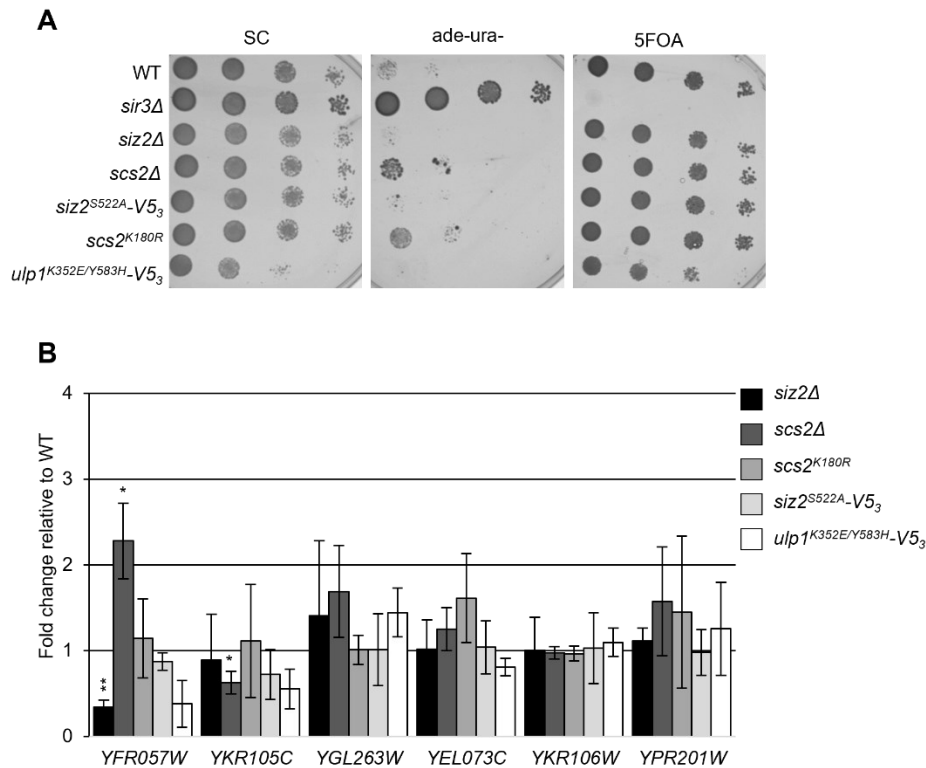


Figure 4-26. Siz2-dependent SUMOylation events do not regulate subtelomeric gene expression. **A)** The indicated mutations were introduced into the yeast strain UCC3505, which contains the *URA3* and *ADE2* genes integrated into Tel7L and Tel5R regions respectively. Log-phase cells were grown in non-selective liquid medium, and an equal number of cells from each culture were serially diluted and plated onto SC medium (non-selective), SC medium lacking adenine and uracil (selective), and SC medium containing 1mg/mL 5-FOA (selective) and incubated for 3 days at 30°C. **B)** Fold change of mRNA for various subtelomeric genes for the indicated mutant cells relative to WT cells as determined by RT-qPCR. mRNA levels were normalized to *ACT1* and *TUB2* mRNA. Graphs show data from 3 biological replicates. Error bars- SEM. Asterisks- significant change of mRNA levels in mutant cells relative to WT cells for the corresponding genes using a paired two-tailed student's t-test. * $p \leq 0.05$, ** $p \leq 0.01$.

Table 4-2. Up-regulated ORFs in asynchronously grown *siz2^{S522/527A}* cells.

<u>Gene</u>	<u>Gene Name</u>	<u>Fold Change</u>	<u>pFDR</u>
<i>YLR303W</i>	<i>MET17</i>	10.08	0.001
<i>YJL052W</i>	<i>TDH1</i>	3.343	0.025
<i>YPR160C-A</i>		2.217	0.047
<i>YBR072W</i>	<i>HSP26</i>	2.078	0.047
<i>YOR383C</i>	<i>FIT3</i>	1.834	0.044
<i>YJL144W</i>	<i>ROQ1</i>	1.746	0.048
<i>YKR093W</i>	<i>PTR2</i>	1.626	0.039
<i>YGR254W</i>	<i>ENO1</i>	1.544	0.046
<i>YOR382W</i>	<i>FIT2</i>	1.536	0.047
<i>YDR261W-A**</i>		1.369	0.025
<i>YNL284C-B*</i>		1.211	0.025
<i>YDR261W-B**</i>		1.171	0.004
<i>YPR158W-B*</i>		1.161	0.023
<i>YNL284C-A*</i>		1.159	0.025
<i>YBR157C</i>	<i>ICS2</i>	1.071	0.03
<i>YER037W</i>	<i>PHM8</i>	1.023	0.049
<i>YFR035C</i>		0.964	0.04
<i>YKL030W</i>		0.922	0.047
<i>YGL263W</i>	<i>COS12</i>	0.908	0.026
<i>YJL045W</i>		0.889	0.032
<i>YOR192C-A**</i>		0.844	0.048
<i>YKL029C</i>	<i>MAE1</i>	0.837	0.045
<i>YOR192C-B**</i>		0.829	0.048
<i>YHR214C-C*</i>		0.811	0.038
<i>YHR214C-B*</i>		0.786	0.048

<i>YAR028W</i>		0.745	0.049
<i>YGR021W</i>	<i>DPC29</i>	0.738	0.047
<i>YHR136C</i>	<i>SPL2</i>	0.662	0.047
<i>YNL054W-A*</i>		0.659	0.048
<i>YNL054W-B*</i>		0.602	0.048

* Indicates Ty1 genes, ** indicates Ty2 genes

Table 4-3. Down-regulated ORFs in asynchronously grown *siz2^{SS522/527A}* cells.

<u>Gene</u>	<u>Gene Name</u>	<u>Fold Change</u>	<u>pFDR</u>
<i>YLR367W</i>	<i>RPS22B</i>	-0.63	0.027
<i>YIL011W</i>	<i>TIR3</i>	-0.64	0.037
<i>YOL058W</i>	<i>ARG1</i>	-0.65	0.037
<i>YGL142C</i>	<i>GPI10</i>	-0.68	0.029
<i>YLR038C</i>	<i>COX12</i>	-0.7	0.051
<i>YMR062C</i>	<i>ARG7</i>	-0.7	0.037
<i>YBR045C</i>	<i>GIP1</i>	-0.78	0.047
<i>YJR109C</i>	<i>CPA2</i>	-0.79	0.007
<i>YNR050C</i>	<i>LYS9</i>	-0.82	0.023
<i>snR80</i>	<i>SNR80</i>	-0.86	0.029
<i>YOL126C</i>	<i>MDH2</i>	-0.87	0.046
<i>YLR134W</i>	<i>PDC5</i>	-0.9	0.041
<i>YHR018C</i>	<i>ARG4</i>	-0.93	0.029
<i>YLR264C-A</i>	<i>YLR264 C-A</i>	-1.03	0.047
<i>YGR286C</i>	<i>BIO2</i>	-1.08	0.047
<i>YFR023W</i>	<i>PES4</i>	-1.19	0.045
<i>YIL102C</i>	<i>YIL102C</i>	-1.58	0.047
<i>YBR115C</i>	<i>LYS2</i>	-9.89	0.001

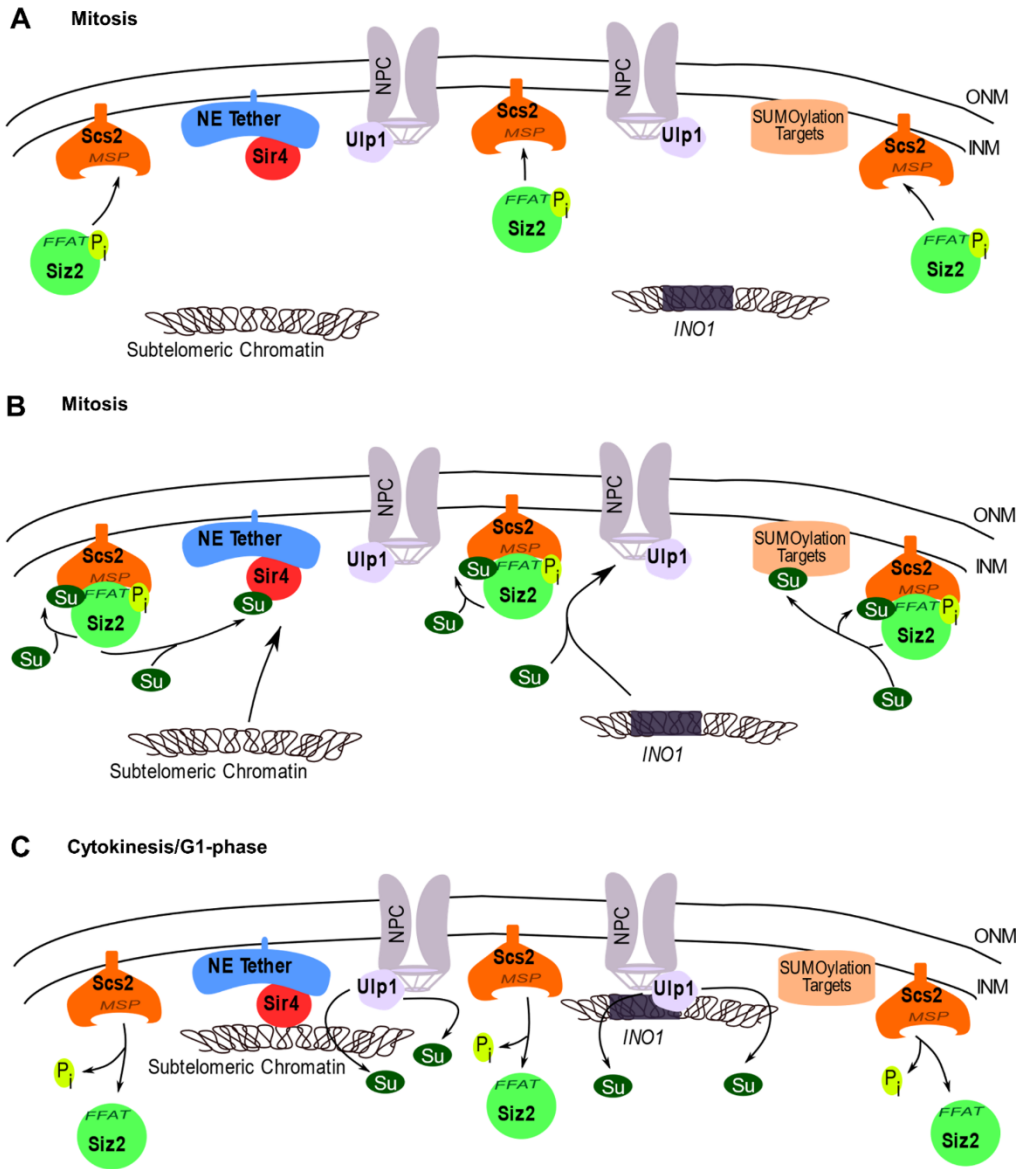


Figure 4-27. A model for Scs2-Siz2 dependent mitotic SUMOylation at the INM and its role in chromatin recruitment. **A)** Early in mitosis, Siz2, telomeres and activated *INO1* are found within the nucleoplasm. Progression into anaphase is accompanied by the phosphorylation of Siz2. Phosphorylation of Siz2 directs the enrichment of Siz2 at the INM where it interacts with the integral protein Scs2. **B)** Siz2 phosphorylation facilitates Scs2-Siz2 association through the Scs2 MSP domain and an FFAT-like motif in Siz2. These interactions lead to Scs2 SUMOylation which further stabilizes the Scs2-Siz2 complex through the association of Scs2-SUMO and Siz2-SIM interactions. The Scs2-Siz2 SUMO ligase complex then directs the SUMOylation of INM-associated proteins, including Sir4 and proteins associated with the activated *INO1* locus. These SUMOylation events facilitate Sir4 association with subtelomeric chromatin and activated *INO1* with NPCs, re-establishing NE-chromatin interactions at the end of mitosis. **C)** As cells exit mitosis and undergo cytokinesis, dephosphorylation of Siz2 and Ulp1-dependent deSUMOylation of Scs2 and other proteins along the INM occurs. These events lead to the dissolution of the Scs2-Siz2 complex, while telomeres and activated *INO1* remain associated with the nuclear periphery.

4.3 Discussion

Post-translation modifications provide rapid and reversible changes to proteins allowing them to participate in different functional circuits and regulate multiple biological functions in response to specific temporal or environmental cues. In this work, we have identified SUMOylation as a spatiotemporal regulatory mechanism at the INM that re-establishes NE chromatin interactions in newly formed nuclei following mitosis (Fig. 4-14, 4-16, 4-20). We show that these SUMOylation events are dependent on the relocalization of the SUMO E3 ligase, Siz2, to the INM (Fig. 4-6), where it binds to Scs2 to initiate a mitotic SUMOylation wave along the INM (Fig. 4-27).

Siz2-Scs2 interactions at the INM are mediated through FFAT:MSP domain and SIM:SUMO motif interactions.

We have identified a unique regulatory mechanism that facilitates the enrichment of Siz2 at the INM during mitosis. This mechanism involves Scs2 functioning as a receptor for Siz2 at the INM during mitosis (Fig. 4-8). Scs2 facilitates various cytoplasmic functions by binding to FFAT-containing proteins through its MSP domain (J. H. Brickner and Walter 2004; Manford et al., 2012; Freyre et al., 2019). We have identified a previously unreported INM localization of Scs2 (Fig. 4-10), where the MSP domain of Scs2 can interact with nuclear FFAT motif-containing proteins. We have identified Siz2 as a protein containing an FFAT-like motif that interacts with the MSP domain of Scs2 at the INM during mitosis (Fig. 4-9). Consistent with previous findings, we show that phosphorylation near the FFAT-like motif in Siz2 enhances its binding to the MSP domain of Scs2

(Goto et al., 2012; Kumagai, Kawano-Kawada, and Hanada 2014; Weber-Boyvat et al., 2015; Kirmiz et al., 2018; Di Mattia et al., 2020). As a result, the mitotic phosphorylation of Siz2 regulates a cell cycle specific interaction with the MSP domain of Scs2. These observations suggest that Scs2 could interact with other nuclear FFAT-containing proteins to facilitate additional nucleoplasmic functions during interphase. For example, Scs2 interactions with other FFAT-motif containing proteins may facilitate S-phase telomere tethering (Fig. 4-16).

We also show that Scs2-Siz2 interactions are enhanced by SUMO:SIM interactions. To our knowledge, this is the first instance where a SUMO:SIM interaction has been shown to reinforce interactions between an FFAT-like motif and an MSP-containing binding partner. Interestingly, phosphorylation events near a SIM motif generates a PhosphoSIM module which enhances binding to a SUMOylated target (Stehmeier and Muller 2009). Therefore, the mitotic phosphorylation of Siz2 may enhance the FFAT and SIM motif of Siz2 to facilitate the rapid and robust accumulation of Siz2 at the INM during mitosis. Whether SUMOylation contributes to the interactions of other VAP family members with other FFAT-containing proteins will be of future interest.

Ulp1 facilitates deSUMOylation of Siz2-Scs2 SUMOylation events following mitotic exit.

Coinciding with a loss of Siz2 at the NE following mitotic exit is the loss of SUMOylation conjugates (Fig. 4-3). We show that Ulp1 is responsible for the deSUMOylation of the Siz2-mediated SUMOylation events that accumulate at the

INM during mitosis (Fig. 4-11). The NPC association of Ulp1 (V. G. Panse et al., 2003; Y. Zhao et al., 2004; Makhnevych et al., 2007) would position the isopeptidase near these SUMOylation targets to facilitate their deSUMOylation following mitotic exit. We predict that the enrichment of Siz2 at the NE during mitosis allows SUMOylation events to outcompete mitotic deSUMOylation events. Following mitotic exit, when Siz2 accumulation at the INM is lost, Ulp1 can deSUMOylate the SUMOylation conjugates that accumulated during mitosis. The Siz2-dependent SUMOylation wave at the INM during mitosis may also promote the assembly of multi-protein complexes (including the Scs2-Siz2 receptor complex) that make these targets inaccessible to Ulp1. Furthermore, the ability of SUMOylation events to accumulate at the NE during mitosis may also be facilitated by the relocalization of Ulp1 to the septin ring during mitosis (Makhnevych et al., 2007; Elmore et al., 2011). The localization of Ulp1 to septins and Siz2 to the INM during mitosis suggests a potentially connected regulatory system that coordinates Siz2-SUMOylation events to other mitotic regulatory systems.

We have shown that a *ulp1*^{K352E} point mutation dramatically increases Scs2 SUMOylation during mitosis and sustains the SUMOylation of Scs2 into subsequent G1-phases (Fig. 4-11). This phenotype is not due to alterations in the steady-state or the localization of Ulp1 (Felberbaum et al., 2011). Furthermore, the 352 residue is within the coil:coil domain of Ulp1, a region not associated with the isopeptidase activity or SUMO binding capabilities of Ulp1 (Mossessova and Lima 2000; S. J. Li and Hochstrasser 2003; Elmore et al., 2011). Therefore, we envisage that the K352E mutation may alter the ability for Ulp1 to recognize SUMOylated

Scs2. This suggests a potentially novel function for the coil:coil domain of Ulp1 in target recognition and specificity.

The compartmentalization of mitotic SUMOylation events at the INM re-establishes NE-chromatin interactions during mitosis.

SUMO can function as a scaffold for the binding of proteins containing SIM motifs. The high concentration of SUMO-modified proteins at the INM during mitosis could establish a two-dimensional binding surface for SIM motif-containing proteins to promote the formation of various macromolecular complexes. The potential for SUMOylation to compartmentalize SIM-containing proteins near the INM parallels properties described in mammals for phase-separated PML bodies and DNA damage in yeast (van Damme et al., 2010; Psakhye and Jentsch 2012; Banani et al., 2016; Min, Wright, and Shay 2019).

We have shown that Siz2-directed SUMOylation at the INM during mitosis, including the SUMOylation of Sir4 (Fig. 4-19, 4-23, 4-25) functions to re-establish NE-chromatin interactions through what we predict is the formation of SUMO:SIM protein networks (Fig. 4-14, 4-16). Factors required for Sir4 interactions with subtelomeric chromatin such as Nup170 (Van De Vosse et al., 2013) and Rap1 (Moretti et al., 1994; Cockell et al., 1995; Luo, Vega-Palas, and Grunstein 2002) have predicted SIM motifs (Q. Zhao et al., 2014). Rap1 and Nup170 are also part of other macromolecule complexes (Rout et al., 2000; Azad and Tomar 2016; Lapetina et al., 2017), which may mask or prevent their ability to facilitate Sir4 binding to subtelomeric DNA. SUMO:SIM interactions established during mitosis

may ensure that interactions required for re-establishing NE-chromatin interactions, can outcompete other interactions at the NE. For example, during mitosis SUMOylation may ensure Nup170 and Sir4 interactions are favored over the incorporation of Nup170 into NPCs. Once integrated into subtelomeric chromatin, SUMOylated Sir4 may then facilitate other SUMO:SIM interactions required for telomere tethering. Numerous proteins involved in chromatin-NE interactions are SUMOylated or contain SIM motifs (Wohlschlegel et al., 2004; Nathan et al., 2006; Hang et al., 2011; Ferreira et al., 2011; Pasupala et al., 2012; Q. Zhao et al., 2014; Chymkowitch et al., 2017; Texari et al., 2013). Sir3, for example, is an interacting partner of Sir4 at subtelomeric chromatin, and contains multiple SIM motifs (Zhao et al., 2014). Furthermore, the association of Sir3 with subtelomeric chromatin is also regulated by Siz2-mediated SUMOylation at the NE (Fig. 4-24). The generation of a SUMO:SIM protein interaction network to re-establish chromatin interactions during mitosis may represent a conserved regulatory system, as it is similar to SUMO:SIM interactions in mammals which are required for the recruitment of lamin A to telophase chromosomes (Moriuchi et al., 2016; Moriuchi and Hirose 2021). A similar enrichment of telomeres to the nuclear periphery in human cells following mitosis has also been observed (Crabbe et al., 2012), suggesting another potentially conserved regulatory system.

The NE recruitment of Siz2 and Siz2-mediated SUMOylation events are reversed by G1-phase. However, mutants that disrupt Siz2 NE-localization and Siz2-mediated SUMOylation NE during mitosis show defects in NE-chromatin interactions in both mitosis and G1-phase (Fig. 4-14, 4-16, 4-20). We interpret this

to suggest that SUMO:SIM interactions formed in mitosis enhance protein-protein interactions that are maintained into interphase, where these complexes continue to support chromatin-NE association. The removal of SUMO modifications may also play an important role in regulating NE-chromatin interactions in G1-phase. Conditions that delay deSUMOylation of Scs2 (Fig. 4-11) and other chromatin associated proteins (Fig. 4-23D) led to increased INM retention of telomeres in G1-phase (Fig. 4-16). These results suggest that post-mitotic deSUMOylation may relax interactions and promote the periodic switching of telomeres between NE-bound and unbound states observed in interphase cells (Hediger et al., 2002). There are also multiple telomere tethering pathways utilized in G1-phase, including the SIR-dependent telomere tethering pathway and the yKu-dependent telomere tethering pathway (Taddei et al., 2004; Taddei and Gasser 2012; Kupiec 2014). During mitosis, SUMOylation may establish Sir4-mediated telomere tethering, while deSUMOylation of Siz2-mitotic specific targets in G1-phase may relax these interactions to allow alternative telomere tethering pathways to be utilized in G1-phase.

The Siz2-Scs2 complex is a regulator of chromatin.

We have shown that SUMOylation events facilitated by the Scs2-Siz2 complex at the NE during mitosis are essential for re-establishing different NE-chromatin interactions (Fig. 4-14, 4-15, 4-16). Although Siz2 has been shown to bind to chromatin and chromatin-associated proteins (Psakhye and Jentsch 2012; Saik et al., 2020; Cappadocia, Kochańczyk, and Lima 2021), we could not detect an enrichment of Siz2 at subtelomeric chromatin (Fig. 4-17). Instead, our data

suggests that specific SUMOylation conjugates regulate the re-association of chromatin with the NE during mitosis. For telomeres, we have identified Sir4 as a target of Siz2-mediated SUMOylation which supports the NE association of telomeres (Fig. 4-19, 4-20). Importantly, we show that the SUMOylation of Sir4 does not facilitate the re-association of the induced *INO1* locus to the nuclear periphery during mitosis (Fig. 4-20). As such, we envisage that Scs2-Siz2 directs the SUMOylation of multiple chromatin-associated proteins to support the binding of chromatin to the NE during mitosis. This raises the possibility that Siz2-mediated SUMOylation may alter the association of other NE-chromatin interactions, beyond those investigated here, during mitosis.

Despite the loss of telomere tethering association with the NE, mutants which alter Siz2-mediated SUMOylation events at the INM during mitosis did not show many significant changes to subtelomeric gene expression (Fig. 4-26). These results are consistent with previous observations, which show telomere anchoring can occur independently of transcriptional repression (Taddei et al., 2004; Ferreira et al., 2011). Our results are also consistent with observations which show that despite the strong enrichment of Sir proteins at telomeric regions, only a small subset of subtelomeric genes are repressed by the SIR complex (Ellahi, Thurtle, and Rine 2015) and that under normal growth conditions, many subtelomeric genes are transcriptionally silenced independently of Sir binding (Fabre et al., 2005). Because specific stress conditions mediate the transcriptional regulation of various subtelomeric genes (Ai et al., 2002; Mak, Pillus, and Ideker 2009), Siz2 enrichment at the INM during mitosis may regulate gene expression in response to specific

stress conditions. The role of Siz2-mediated SUMOylation events in regulating subtelomeric chromatin independent of transcriptional regulation is also consistent with our previous observations, which show Siz2 regulates *INO1* localization independently of expression (Saik et al., 2020; Chapter 3). Consistently, the SUMOylation of Scs2 is also not required for *INO1* expression (Felberbaum et al., 2011). Cumulatively, these data suggest a role for Siz2 in regulating the spatial organization of chromatin, independent of gene expression at the NE.

A potential additional role for Siz2 in regulating chromatin structure comes from the observations that the transcripts of Ty1 and Ty2 retrotransposons are elevated in cells lacking Siz2-mediated SUMOylation events at the NE (Table 4-2). These observations suggest that Siz2-mediated SUMOylation may function in the regulation of retrotransposition. This is consistent with previous reports implicating Siz2 in regulating retrotransposition (Manhas, Ma, and Measday 2018; Bonnet et al., 2021). The loss of Siz2 in conjunction with a loss of Siz1 causes an increase in Ty1 RNA levels (Bonnet et al., 2021). The loss of Siz2 has also been shown to impair Ty1 targeting to regions upstream of tRNA genes (Manhas, Ma, and Measday 2018) and instead retarget Ty1 retrotransposons to subtelomeric regions (Manhas, Ma, and Measday 2018). Siz2-mediated mitotic SUMOylation events at the NE may regulate interactions with retrotransposition host factors or regulate the organization of subtelomeric chromatin to prevent aberrant transposon insertions into these regions.

Overall, we have identified a novel regulatory mechanism that facilitates the accumulation of SUMOylation events at the NE. We have identified a role for

these SUMOylation events in re-establishing NE-chromatin interactions during mitosis. We have identified Sir4 and Scs2 as SUMOylation targets of Siz2 at the INM and have shown that the SUMOylation of these targets is necessary to regulate NE-chromatin interactions (Fig. 4-27). Identifying other mitosis specific SUMOylation targets at the INM is predicted to provide insights into other biological functions regulated by Siz2 at the INM during mitosis.

**Chapter V: Nuclear envelope associated
SUMOylation events regulate nuclear membrane
expansion during mitosis**

5.1 Overview

Phosphatidic acid (PA) is a key intermediate of lipid metabolism. Depending on the needs of the cell, PA is either channeled towards the synthesis of membrane phospholipids (PLs) which is required for cell proliferation or channeled towards lipid storage. The enzymatic activity of Pah1 antagonizes the channeling of PA towards PL synthesis. The activity of Pah1 is regulated by the integral Nem1/Spo7 complex, which regulates the interaction of Pah1 with membranes. During mitosis, PL synthesis increases to allow the formation of membranes that will become part of the mother and daughter cells, including the nuclear membrane. In yeast, the expansion of the nuclear membrane occurs at regions that are adjacent to the nucleolus. The expansion of the nuclear membrane at these regions is proposed to be facilitated through the mitotic inhibition of Pah1. Recently, PA metabolism at the INM has been established. However, it is still unclear whether the INM contributes to specific regulatory systems involved in facilitating the mitotic expansion of the NE. Here we have identified a spatiotemporal regulatory system at the INM that supports the mitotic expansion of the NE. We show that the enrichment of Siz2 and Siz2-mediated SUMOylation events at the INM, as identified and characterized in Chapter 4, supports the enrichment of PA at the INM and the expansion of the NE during mitosis. During mitosis Siz2-mediated SUMOylation events reduce protein interactions between Pah1, Spo7, and Nem1. Based on this we propose that Siz2-mediated SUMOylation is a unique spatiotemporal regulatory mechanism that inhibits Pah1 activity to facilitate the mitotic expansion of the NE.

5.2 Results

5.2.1 NE association of Siz2 during mitosis supports NE expansion.

As cells progress through mitosis, *de novo* lipid biogenesis contributes to producing the nuclear envelope (NE) membrane (Campbell et al., 2006; Witkin et al., 2012). Coincident with NE expansion, the SUMO E3 ligase Siz2 binds the inner nuclear membrane (INM) and mediates SUMOylation of various membrane-associated targets (Ptak et al., 2021; Chapter 4). To determine whether these spatially and temporally regulated SUMOylation events play a role in mitotic NE expansion, we investigated the consequences of inhibiting Siz2-mediated NE SUMOylation on the surface area of the NE membrane. We examined the nuclear surface area at different cell cycle stages in asynchronously grown WT and *siz2* mutant cells (*siz2^{S522A}*). This point mutant fails to bind the INM during mitosis and SUMOylate NE-associated proteins (Ptak et al., 2021; Chapter 4). Cell morphology was used to determine the cell cycle stage of individual cells. The contours of nuclear surfaces were determined by 3-dimensional reconstruction of nuclei containing a diffuse nucleoplasmic protein Pus1-GFP. These data were then used to calculate nuclear surface area using Imaris surface analysis. The nuclear surface area values of WT cells at various cell cycle stages were similar to previously reported values and increased as cells progressed from G1- to M-phase (Webster, McCaffery, and Cohen-Fix 2010; R. Wang et al., 2016). A comparison of WT and *siz2^{S522A}* mutant cells revealed similar nuclear surface areas for G1- and S-phase cells. However, the *siz2^{S522A}* mutant cells had significantly reduced nuclear surface area values in M-phase (Fig. 5-1A).

We also examined the nuclear surface area of WT and *siz2^{S522A}* cells as they progressed through the cell cycle following release from an α -factor induced G1-phase arrest. Every 20 minutes after α -factor release, the nuclear surface area of sampled cells was determined using the Imaris surface analysis. Similar to cells in the asynchronous culture (Fig.5-1A), the synchronized population of WT and *siz2^{S522A}* cells exhibited similar nuclear surface areas and rates of increase as they progressed through G1- and S-phase (0-60 mins; Fig. 5-1B). However, as cells progressed through mitosis (60 to 80 min.), the surface area of WT cells continued to increase (coincident with Siz2-dependent SUMOylation conjugates at the INM; Fig. 5-2A,B; Ptak et al.,2021), while in *siz2^{S522A}* cells, it remained largely unchanged. Following mitotic exit and formation of G1-phase progeny nuclei, the nuclear surface areas of WT and *siz2^{S522A}* cells were again similar (Fig. 5-1B) and decreased, consistent with previous observations (Webster, McCaffery, and Cohen-Fix 2010; R. Wang et al., 2016).

To further investigate NE expansion during mitosis we investigated the changes in nuclear surface area during mitotic delay. Cells arrested in mitosis, have continued phospholipid biogenesis resulting in an increase in NE membrane and distorted nuclear shape (Campbell et al., 2006; Witkin et al., 2012). These phenotypes are prevented by inhibiting phospholipid biogenesis (Walters et al., 2014). Thus, we tested the effect of the *siz2^{S522A}* mutant on membrane production during mitosis using M-phase arrested cells. Cells were arrested in metaphase by the depletion of the anaphase-promoting protein Cdc20. As shown in Fig.5-1C, depletion of Cdc20 (see Fig. 5-2D) for 2 h in an otherwise WT

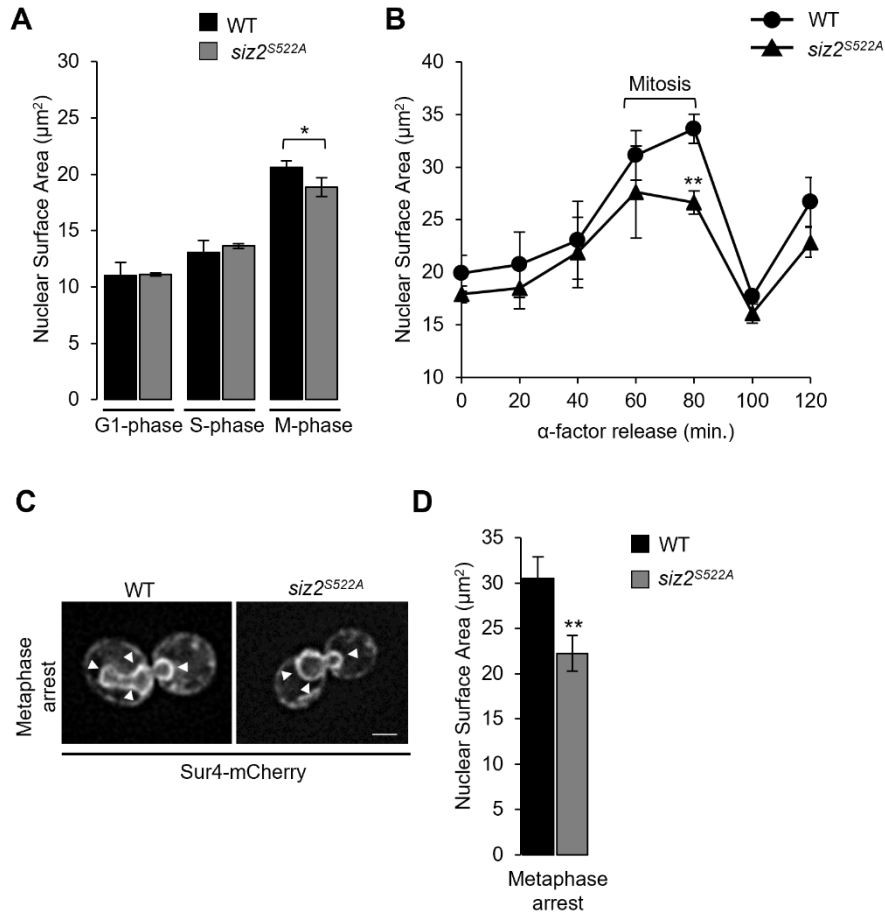


Figure 5-1. NE association of Siz2 during mitosis supports NE expansion. **A)** Epifluorescence images of asynchronously grown WT and *siz2^{S522A}* cells expressing the nucleoplasm marker Pus1-GFP were used to reconstruct nuclei from a series of z-stacks. The nuclear surface area from reconstructed nuclei was then calculated using Imaris surface analysis for the indicated cell cycle stage. The cell cycle stage was determined by bud size and nuclear morphology. **B)** WT and *siz2^{S522A}* cells expressing the nucleoplasm marker Pus1-GFP were arrested in G1-phase (0 min) using α -factor. Following release from arrest, cells were collected and imaged at the indicated times. Epifluorescence images were analyzed by Imaris surface analysis to calculate nuclear surface area (μm^2). **C)** Representative epifluorescence images of metaphase arrested *MET3pr-HA₃-CDC20* and *MET3pr-HA₃-CDC20 siz2^{S522A}* cells producing the NE/ER marker Sur4-mCherry. Arrowheads highlight the NE. Cells were arrested in metaphase 2h post methionine addition. Bar – 2 μm . **D)** Nuclear surface area of metaphase arrested *MET3pr-HA₃-CDC20* and *MET3pr-HA₃-CDC20 siz2^{S522A}* cells producing the nucleoplasm marker Pus1-GFP. Epifluorescence images were analyzed by Imaris surface analysis to calculate nuclear surface area (μm^2). All graphs (A, B, D) show data from 3 biological replicates where n=50 cells per replicate/cell cycle stage. Error bars- SD. Asterisks- significant change in the *siz2^{S522A}* containing cells relative to the WT counterpart using a two-tailed student's t-test. *p \leq 0.05 **p \leq 0.01.

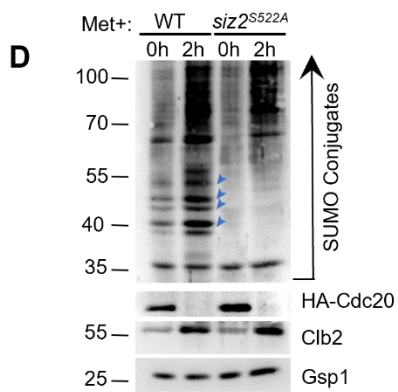
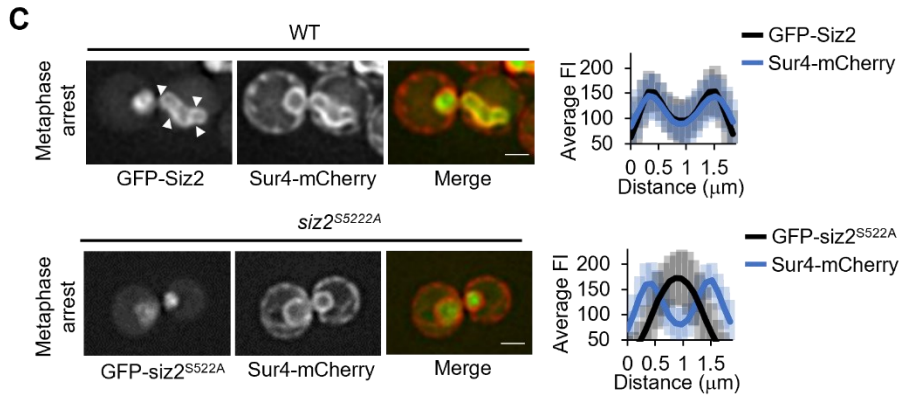
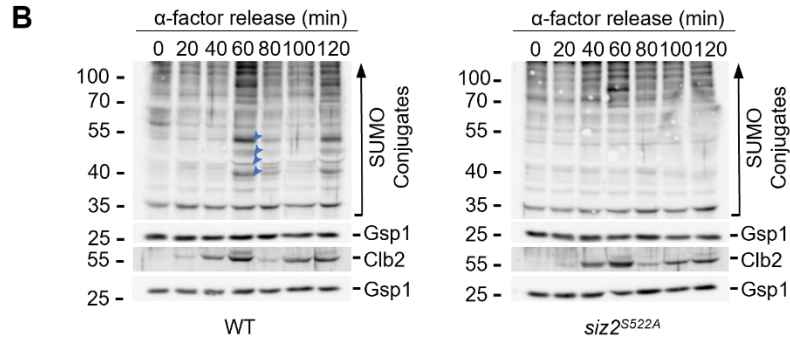
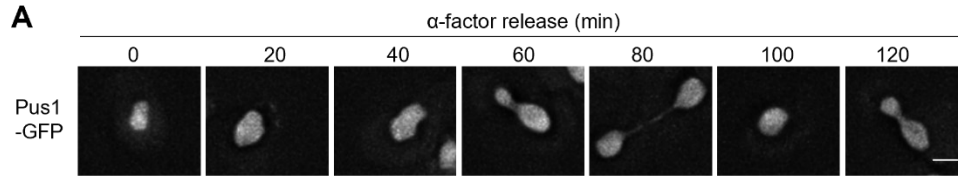


Figure 5-2. Siz2 localization and Siz2-mediated SUMOylation events at the NE during mitosis. **A)** Epifluorescence images of cells expressing the nucleoplasm marker Pus1-GFP, following arrest in G1-phase (0 min) using α factor, and release from arrest at indicated time points. **B)** WT and *siz2*^{S522A} cells were arrested in G1-phase (0min) using α -factor. Following release, cultures were sampled every 20 min and analyzed by western blotting to detect SUMO conjugates, Clb2, and the Gsp1 load control, as specified on the right of the blot. Arrowheads highlight prominent SUMOylated species in the 40-55kDa that arise in mitosis and decay as cells enter G1-phase. Molecular mass markers are shown in kDa. **C)** Representative epifluorescence images of metaphase arrested *MET3pr-HA3-CDC20* cells producing either GFP-Siz2 or GFP-*siz2*^{S522A}. Sur4-mCherry is a NE/ER marker. Cells were arrested in metaphase 2h post methionine addition. Arrowheads highlight GFP-Siz2 at the NE. The nuclear distribution of GFP-Siz2 or GFP-*siz2*^{S522A} relative to Sur4-mCherry was determined using line scan intensities of equatorial optical sections through the nuclei. Plots show average fluorescence intensity (FI) for GFP-*siz2* and Sur4-mCherry at multiple points along a 1.85 μ m line for n=25 nuclei. Bar- 2 μ m. Error bars- SD. **D)** Cell lysates derived from asynchronous (0) or metaphase arrested (2h) cultures of indicated strains were assessed by western blotting using an anti-SUMO antibody to assess SUMO conjugate profiles. Gsp1 is a loading control. Molecular mass markers are shown in kDa.

cell background results in large-budded M-phase arrested cells with nuclear extensions. The accumulation of nuclear extension is accompanied by the NE accumulation of Siz2 (Fig. 5-2C) and an increase in Siz2-dependent SUMOylation targets (Fig. 5-2D). Strikingly, the *siz2^{S522A}* mutant, which fails to interact with the NE during mitosis, prevents the formation of nuclear extensions in M-phase arrested cells; instead, these nuclei appear largely spherical (Fig. 5-1C). Consistent with these observations, the *siz2^{S522A}* mutation significantly reduced the surface area of the mitotic nuclei relative to their WT counterparts (Fig. 5-1D). Together these data suggest that the association of Siz2 with the INM during mitosis supports NE expansion.

5.2.2 Directing Siz2 to the INM is sufficient to induce NE expansion.

Phosphorylation of Siz2 during mitosis directs its binding to the INM until it is dephosphorylated and released from the membrane at cytokinesis (Ptak et al., 2021; Chapter 4). We examined whether the ability of Siz2 to support NE expansion was restricted to mitosis or whether the constitutive association of Siz2 with the NE was sufficient to induce an increase in nuclear surface area throughout the cell cycle. To position Siz2 at the INM, we utilized the two fragments of the superfolder GFP, GFP₁₋₁₀ and GFP₁₁, which bind *in vivo* when the two fragments are in the same subcellular compartment. The binding of these fragments can be detected by the formation of fluorescence (Smoyer et al., 2016). Siz2-GFP₁₋₁₀ and an ER/INM anchored GFP₁₁ fusion protein (GFP₁₁- mCherry-transmembrane (TM) domain of Scs2) with the GFP₁₁ fragment extending into the nucleoplasm/cytoplasm were expressed in cells. The GFP₁₋₁₀ moiety on

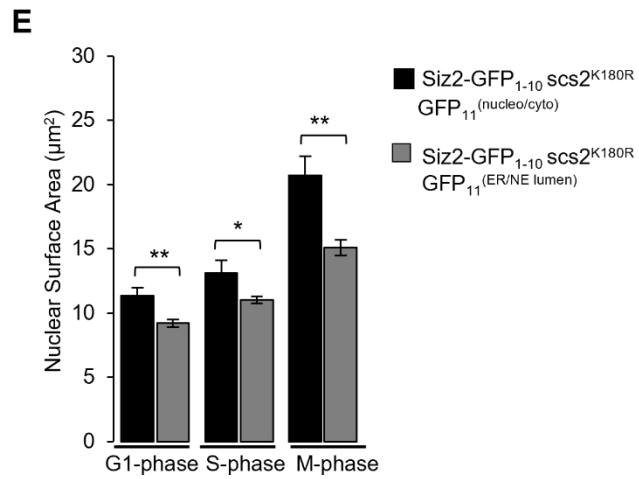
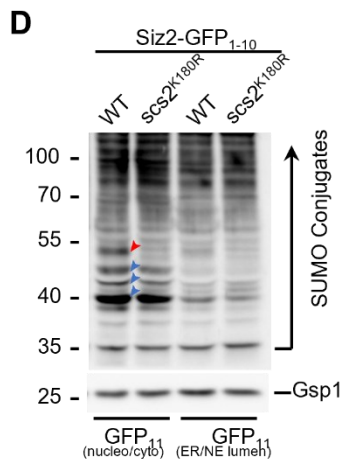
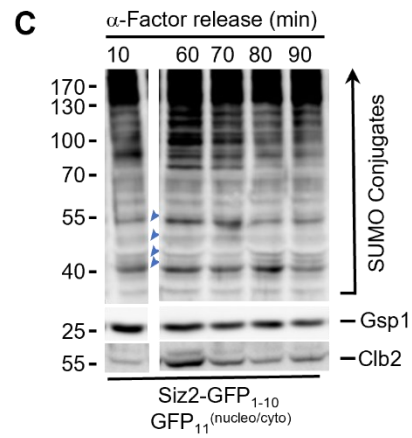
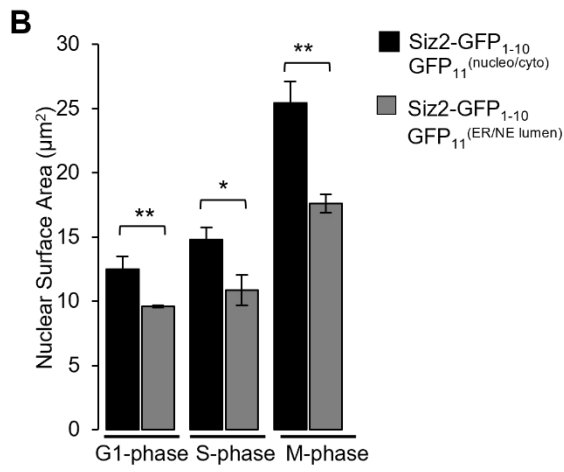
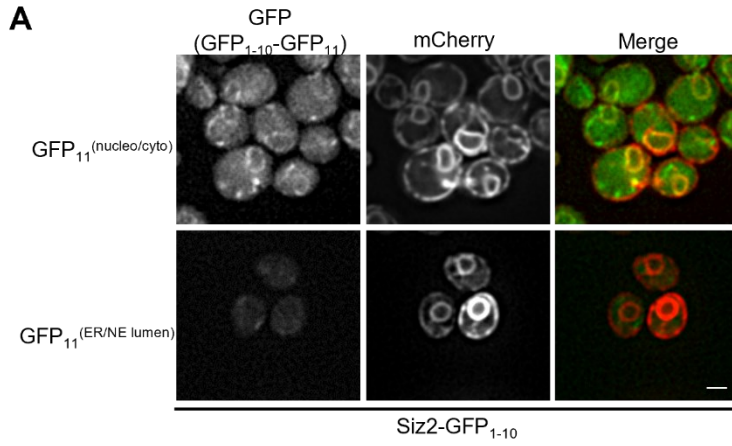


Figure 5-3. Constitutive targeting of Siz2 to the NE induces SUMOylation and increases nuclear surface area. **A)** Epifluorescence images of asynchronously grown cells producing Siz2-GFP₁₋₁₀ and a plasmid-encoded GFP₁₁-mCherry-scs2TM (GFP₁₁^(nucleo/cyto)) or mCherry-scs2TM-GFP₁₁ (GFP₁₁^(NE/ER lumen)) reporter, which positions GFP₁₁ on the nucleoplasm/cytosol or luminal face of the NE/ER membrane, respectively. Membrane integration of the GFP₁₁ reporters allows visualization of NE morphology by mCherry fluorescence. Assembled GFP₁₋₁₀-GFP₁₁ dimers are visualized by GFP fluorescence when the GFP₁₁ reporter resides in the same subcellular compartment as Siz2-GFP₁₋₁₀. Bar- 2 μ m. **B and E)** The nuclear fluorescence signal of Pus1-GFP in the indicated strains was used to calculate nuclear surface area (μ m²) for the indicated cell cycle stage as described in Fig. 5-1. Graphs show data from 3 biological replicates where n=50 cells per replicate/cell cycle stage. Error bars- SD. Asterisks- significant change in GFP₁₁-mCherry-scs2TM (GFP₁₁^(nucleo/cyto)) containing cells relative to mCherry-scs2TM-GFP₁₁ (GFP₁₁^(NE/ER lumen)) counterpart using a two-tailed student's t-test. *p \leq 0.05 **p \leq 0.01. **C)** Cells were arrested in G1-phase using α -factor. Following release, cultures were sampled every 10 min and analyzed by western blotting to detect SUMO conjugates, Clb2, and the Gsp1 load control, as specified on the right of the blot. Clb2 levels peak in metaphase. Arrowheads highlight prominent SUMOylated species in the 40-55kDa range that are dependent on Siz2 localization to the INM. Note that time points shown were derived from the same western blot. Molecular mass markers are shown in kDa. **D)** Cell lysates derived from asynchronous cultures of indicated strains were assessed by western blotting to assess SUMO conjugate profiles. Gsp1 is a loading control. The red arrowhead points to SUMOylated Scs2. Blue arrowheads point to other prominent SUMO conjugates dependent on Siz2 localization to the INM. Molecular mass markers are shown in kDa. Experiments in panels C and D were performed by C. Ptak. Experiments in panels A, B and E were performed by N.O. Saik. Figures were constructed by N.O. Saik.

Siz2-GFP₁₋₁₀ is positioned to bind the GFP₁₁ domain of GFP₁₁-mCherry-TM on the nucleoplasmic face of the INM (Smoyer et al., 2016; Ptak et al., 2021). Formation of the Siz2-GFP₁₋₁₀-GFP₁₁-mCherry-TM dimer was detected by GFP fluorescence along the INM and was not detected in the cortical ER (Fig.5-3A). This signal was seen in all stages of the cell cycle, resulting in Siz2 constitutively associated with the INM. By contrast, a fusion protein that positions the GFP₁₁ fragment on the luminal side of NE/ER membrane (mCherry-TM-GFP₁₁; Smoyer et al.,2016) did not, as predicted, produce GFP fluorescence at the NE and therefore alter endogenous Siz2 localization (Fig. 5-3A).

In cells containing Siz2 constitutively associated with the INM (Siz2-GFP₁₋₁₀ - GFP₁₁-mCherry-TM), we observed that nuclei generally appeared misshapen (Fig. 5-3A). Moreover, we detected a significant increase in nuclear surface area in these cells at all cell cycle stages (Fig. 5-3B) relative to Siz2-GFP₁₋₁₀ whose endogenous localization is unaltered by interactions between the two fragments of the superfolder GFP. Consistent with the constitutive INM association of Siz2, higher levels of SUMOylated species normally restricted to mitosis were detected throughout the cell cycle (Fig. 5-3C).

The artificially tethering Siz2 to the INM (using the Siz2- GFP₁₋₁₀ and INM anchored GFP₁₁ fusion protein dimer) is predicted to bypass the requirement for its mitosis-specific receptor, Scs2 (Ptak et al.,2021; Chapter 4). Consistent with this idea, a *scs2*^{K180R} mutant, which blocks Scs2 SUMOylation and reduces NE-association of endogenous Siz2 (Ptak et al.,2021; Chapter 4), does not inhibit the SUMOylation of NE targets and the increase in nuclear surface area caused by the

GFP₁₋₁₀-Siz2 and INM-anchored GFP₁₁ dimer complex (Fig. 5-3D and 5-3E). These results suggest that the SUMOylation of Scs2 is not required for NE expansion.

The mitotic increase in SUMOylation, mediated by Siz2, decays as cells enter into G1-phase. This occurs due to the dissociation of Siz2 from the NE at cytokinesis and the deSUMOylation of NE targets by the isopeptidase, Ulp1 (Ptak et al.,2021; Chapter 4). Cells harboring a *ulp1* mutation (*ulp1*^{K352E/Y583H}) accumulate higher levels of Siz2 mitotic NE SUMOylation targets that persist into the interphase of the next cell cycle (Ptak et al.,2021; Chapter 4; Fig.5-5), despite the similar timing of Siz2 association and dissociation with NE that occurs in these cells (Fig. 5-4). Therefore, using a strain producing *ulp1*^{K352E/Y583H} tagged with V5₃, we examined the effects of elevated SUMOylation on NE membrane morphology and nuclear surface area. As we observed in cells where Siz2 is constitutively tethered to the INM, the nuclei of *ulp1*^{K352E/Y583H}-V5₃ mutant cells were misshapen and exhibited NE extensions (Fig.5-4. 5-5, 5-6). *ulp1*^{K352E/Y583H}-V5₃ mutant cells also showed an increased nuclear surface area relative to WT cells at all cell cycle stages (Fig.5-6). Preventing SUMOylation at the INM in the *ulp1* mutant background (*ulp1*^{K352E/Y583H}-V5₃*siz2*^{S522A}) restored the spherical appearance of nuclei and the nuclear surface area to WT levels in G1- and S-phase cells (Fig. 5-6). The nuclear surface area of M-phase *ulp1*^{K352E/Y583H}-V5₃*siz2*^{S522A} mutant cells was similar to values observed in the *siz2*^{S522A} mutant (Fig.5-1A). Together these data support a role for Siz2-mediated SUMOylation in supporting NE expansion.

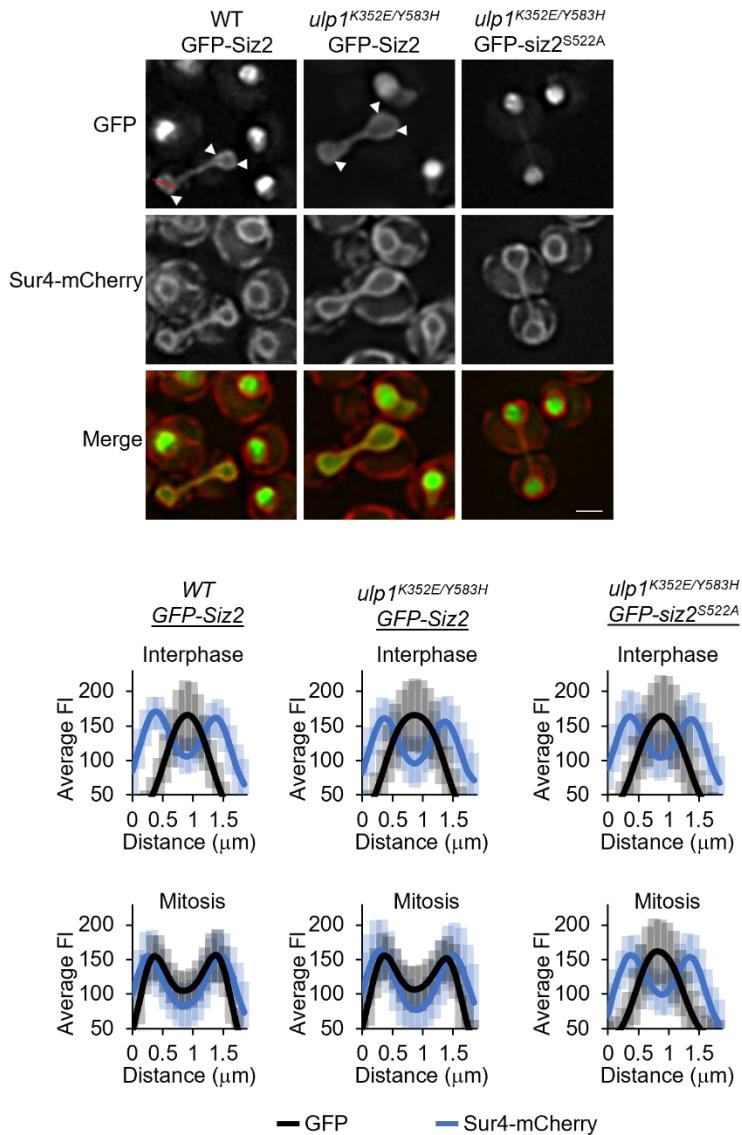


Figure 5-4. Siz2 enrichment at the INM is restricted to mitosis in *ulp1*^{K352E/Y583H} mutant cells. Representative epifluorescence images of indicated cells producing either GFP-Siz2 or GFP-siz2^{S522A}. Sur4-mCherry is a NE/ER marker. Arrowheads highlight GFP-Siz2 at the NE. Nuclear distribution of GFP-Siz2 or GFP-siz2^{S522A} relative to Sur4-mCherry was determined using line scan intensities of equatorial optical sections through the nuclei (see red lines) of interphase (unbudded or small-budded) and mitotic (large budded) cells. Plots show average fluorescence intensity (FI) for GFP-siz2 and Sur4-mCherry at multiple points along a 1.85 μm line for n=25 nuclei. Bar- 2 μm. Error bars- SD.

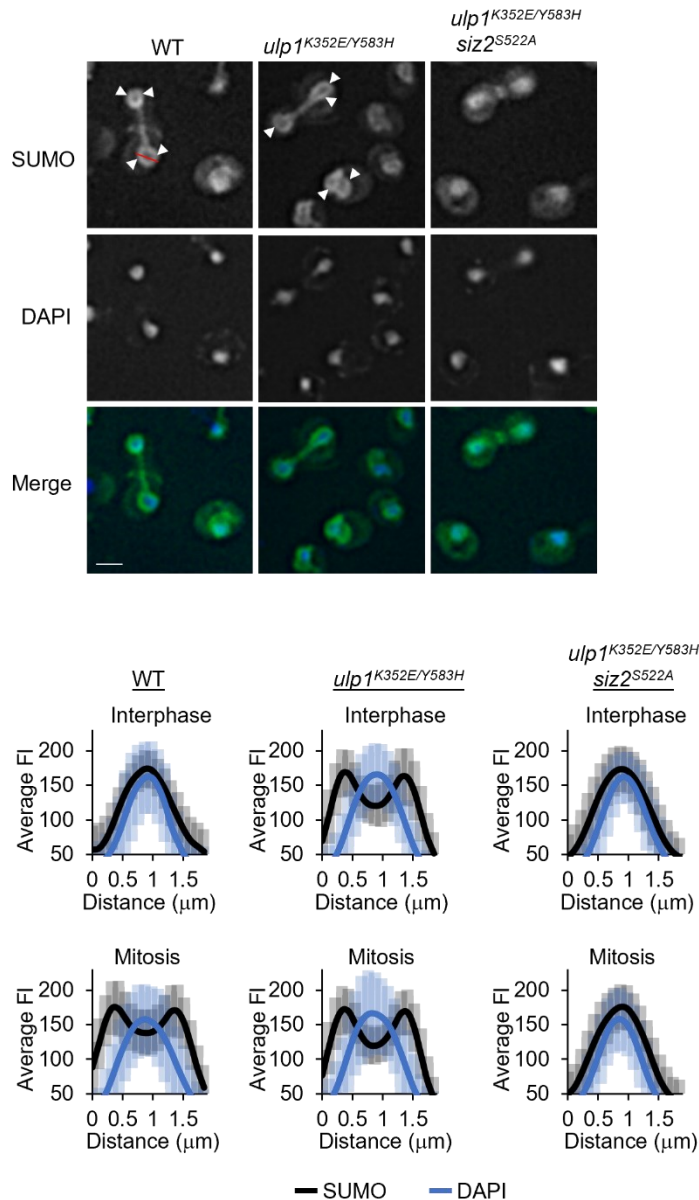


Figure 5-5. Siz2-mediated SUMOylation events are enrichment at the INM at all cell cycle stages in *ulp1*^{K352E/Y583H} mutant cells. Anti-SUMO immunofluorescence analysis of indicated strains. Arrowheads highlight SUMO along the NE, with nuclear position determined by DAPI staining. Nuclear fluorescence levels were quantified using line scan intensities of equatorial optical sections through the nuclei (see red lines) of interphase (unbudded or small-budded) and mitotic (large budded) cells. Plots show average fluorescence intensity (FI) for SUMO-IF and DAPI at multiple points along a 1.85 μm line for $n=25$ nuclei. Bar- 2 μm . Error bars- SD.

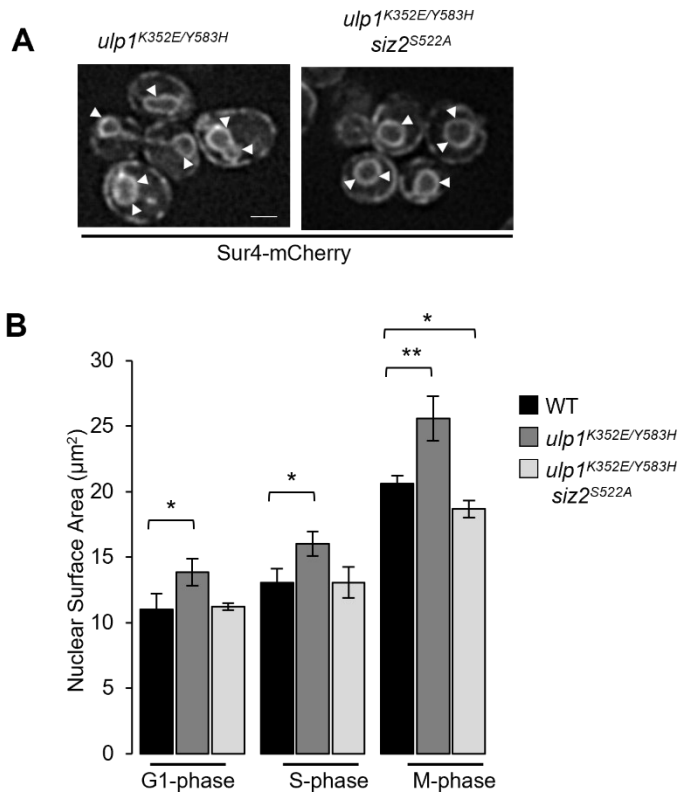


Figure 5-6. Ulp1-dependent deSUMOylation at the INM restricts nuclear membrane expansion. **A)** Representative epifluorescence images of *ulp1^{K352E/Y583H}* and *ulp1^{K352E/Y583H} siz2^{S522A}* mutant cells producing the NE/ER marker Sur4-mCherry. Bar- 2 µm. Arrowheads highlight the NE. **B)** The nuclear fluorescence signal of Pus1-GFP in the indicated strains was used to calculate nuclear surface area (µm²) for the indicated cell cycle stages as described in Fig. 5-1. The data represents 3 biological replicates of n=50 cells per replicate/cell cycle stage. Error bars- SD. Asterisks- significant change relative to WT cells of the corresponding cell cycle stage using a two-tailed student's t-test. *p≤0.05 **p≤0.01. Note all *ulp1^{K352E/Y583H}* mutations contain a C-terminal V₅₃ tag.

5.2.3 Siz2-mediated SUMOylation increases INM levels of phosphatidic acid during mitosis.

Phosphatidic acid (PA) is a key precursor for phospholipids. Increased cellular levels of PA have been linked to the expansion of the NE membrane during mitosis (Santos-Rosa et al., 2005). Moreover, mutations in genes encoding proteins that regulate PA and lead to increased cellular levels of PA also exhibit NE abnormalities (Santos-Rosa et al., 2005) similar to those observed when Siz2-mediated SUMOylation accumulates at the INM (Fig. 5-3, 5-6). With this in mind, we investigated the spatial and temporal changes to PA levels at the NE during the cell cycle. To do this, we used a nuclear-localized PA sensor (NLS-PA sensor-mCherry) which was previously used to detect PA associated with the INM by fluorescence microscopy (Romanauska and Köhler 2018). In asynchronous cultures of WT cells, the NLS-PA sensor was predominantly nuclear in interphase cells (Fig. 5-7A). However, in mitotic cells, both those in asynchronous cultures (Fig.5-7B) and metaphase arrested cells (Fig.5-7C), the NLS-PA sensor was enriched at the INM. The enrichment of the NLS-PA sensory at the INM during mitosis is consistent with increased PA levels (Romanauska and Köhler 2018). Importantly, this mitotic increase in PA at the INM was dependent on the INM association of Siz2, as it was not detected in *siz2*^{S522A} mutant cells (Fig.5-7B and 5-7C).

Because Siz2 association with the INM was necessary for the mitotic accumulation of PA at the INM, we tested whether constitutive tethering of Siz2 to

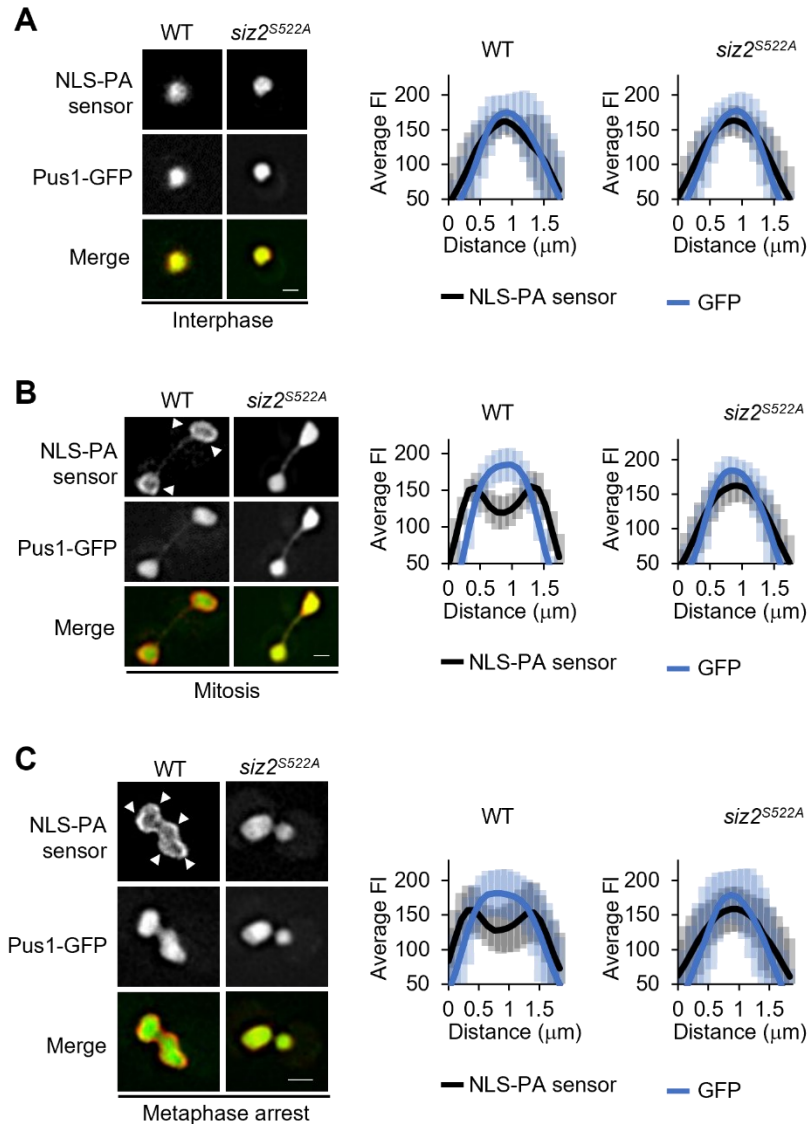


Figure 5-7. The NE association of Siz2 during mitosis supports the enrichment of PA at the INM. The indicated strains producing the nucleoplasmic marker Pus1-GFP and a plasmid-encoded PA sensor (Opi1 Q2-mCherry) with an N-terminal nuclear localization sequence (NLS) were examined by epifluorescence. Representative images of interphase (**A**) and mitotic (**B**) asynchronously grown cells and metaphase arrested *MET3pr-HA₃-CDC20* producing cells (**C**) are shown on the left. *MET3pr-HA₃-CDC20* producing cells were arrested in metaphase 2h post methionine addition. Arrowheads highlight the NLS-PA sensor at the INM as visualized by mCherry fluorescence. Nuclear fluorescence levels were quantified using line scan intensities of equatorial optical sections through the nuclei. Plots show average fluorescence intensity (FI) for the NLS-PA sensor and Pus1-GFP at multiple points along a 1.85 μm line for n=25 nuclei. Bar- 2 μm. Error bars- SD.

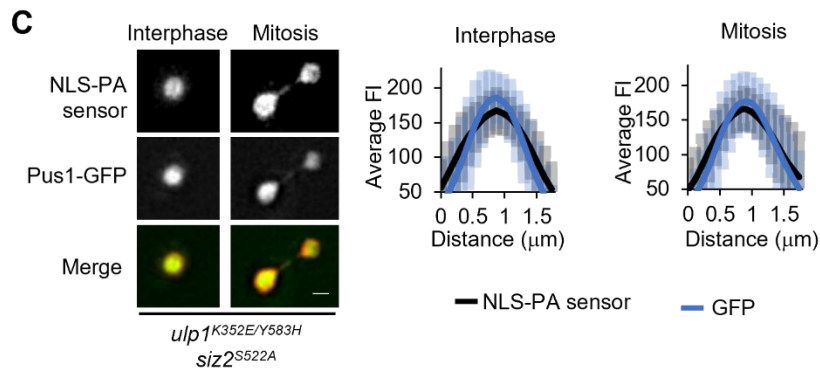
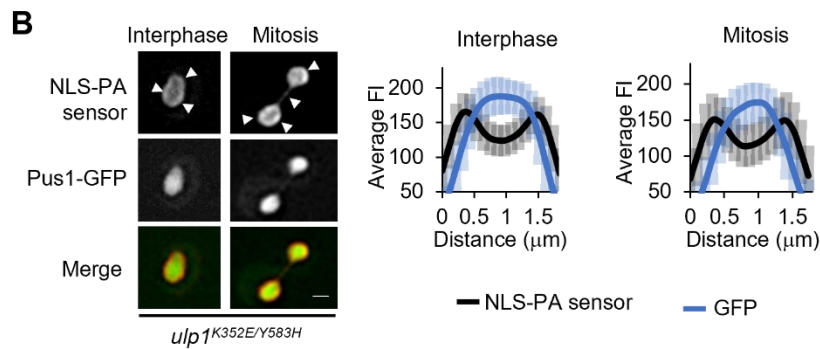
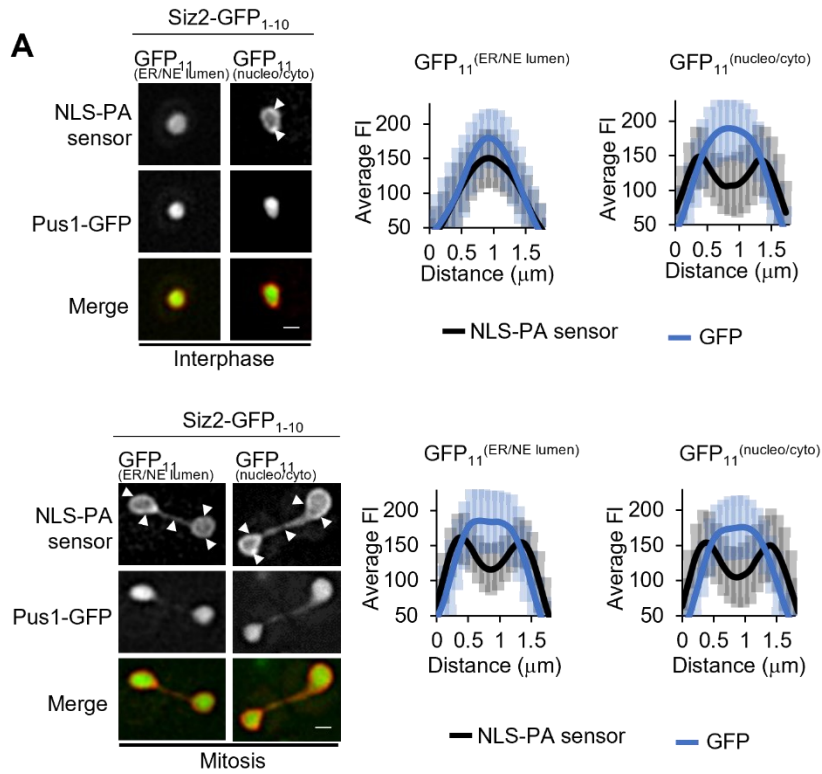


Figure 5-8. PA enrichment at the INM is dependent on Siz2-mediated SUMOylation events. The nucleoplasm marker Pus1-GFP and a plasmid-encoded PA sensor (Opi1 Q2-mCherry) with an N-terminal nuclear localization sequence (NLS) were introduced into the indicated strains and examined by epifluorescence. **A)** The nuclear distribution of the NLS-PA sensor was examined for interphase and mitotic nuclei of cells producing Siz2-GFP₁₋₁₀ and the plasmid-encoded GFP₁₁-scs2TM (GFP₁₁^(nucleo/cyto)) or scs2TM-GFP₁₁ (GFP₁₁^(NE/ER lumen)) reporter. **B,C)** The nuclear distribution of the PA sensor was also examined for interphase and mitotic nuclei of the indicated *ulp1* mutant strains. Representative epifluorescence images are shown on the left, and plots showing the average fluorescence intensity (FI) for the NLS-PA mCherry sensor and Pus1-GFP are shown on the right. Arrowheads highlight the NLS-PA sensor at the INM as visualized by mCherry. Nuclear levels of fluorescence were quantified as described in Fig. 5-7. n=25 nuclei. Bar- 2 μ m. Error bars- SD. FI= fluorescence intensity. Note all *ulp1*^{K352E/Y583H} mutations contain a C-terminal V5₃ tag.

the INM using the Siz2- GFP₁₋₁₀ and INM-anchored GFP₁₁ dimer complex was sufficient to induce increased PA levels. As shown in Fig.5-8A, INM tethering of Siz2-GFP₁₋₁₀ enriches PA in interphase cells, similar to the increases seen in mitotic cells. The increase in PA at the INM coincides with the increased nuclear surface area detected throughout the cell cycle in these cells (Fig.5-3B). Similarly, the increase in the nuclear surface area seen in the *ulp1*^{K352E/Y583H} mutant (Fig. 5-6B) was also accompanied by an increase in INM levels of PA throughout the cell cycle (Fig.5-8B). By contrast, *ulp1*^{K352E/Y583H} mutant cells containing the *siz2*^{S522A} mutation showed no enrichment of PA at the INM throughout the cell cycle (Fig. 5-8C). Cumulatively, these results directly implicate Siz2-mediated SUMOylation events in supporting the enrichment of PA at the INM.

5.2.4 Siz2-directed NE expansion is antagonized by the *pah1*^{7A} mutation.

PA levels are regulated in part by the phosphatase Pah1, which converts PA to DAG. Notably, the inhibition of Pah1 activity increases PA levels and has been shown to induce NE expansion (Han, Wu, and Carman 2006; Santos-Rosa et al., 2005; Romanauska and Köhler 2018). For example, the loss of the Pah1 activators, Spo7 and Nem1, results in NE expansion (Siniossoglou 1998; Santos-Rosa et al., 2005; Webster, McCaffery, and Cohen-Fix 2010). Moreover, the inhibition of Pah1 during mitosis by cyclin-dependent kinase (Cdk)-mediated phosphorylation has been proposed to reduce the membrane association of Pah1, leading to increased PA levels and NE expansion (Santos-Rosa et al., 2005; O'Hara et al., 2006). A *pah1*^{7A} mutation, which prevents Pah1 phosphorylation, exhibits increased membrane binding and phosphatase activity *in vitro* (O'Hara et al., 2006; Choi et

al., 2011). In agreement with this observation, the *pah1^{7A}* mutation suppresses the NE expansion phenotypes of *spo7Δ* and *nem1Δ* null mutants (Choi et al., 2011). Thus, we tested whether the expression of the *pah1^{7A}* mutation would also reduce INM associated PA and the nuclear surface area of metaphase-arrested (Cdc20-depleted) cells. As shown in Fig.5-9A,B, exogenous expression of the *pah1^{7A}* mutant, but not *PAHI* (Fig.5-10A), reduced the INM accumulation of PA and the nuclear surface area of arrested cells. Similarly, the expression of the *pah1^{7A}* mutant, but not *PAHI*, in actively growing cultures prevented mitotic increases in PA at the INM and reduced nuclear surface area throughout the cell cycle (Fig.5-10B,D).

The phenotypes arising from the constitutively active *pah1^{7A}* mutant were generally similar to those detected in cells containing the *siz^{2S522A}* mutation (Fig.5-1 and 5-7), suggesting NE SUMOylation may function to suppress the activity of Pah1 during mitosis. Therefore, we examined whether the *pah1^{7A}* mutant could suppress the NE expansion phenotype arising from increased NE SUMOylation. Introducing the *pah1^{7A}* mutant into *ulp1^{K352E/Y583H}-V5₃* mutant cells did not alter SUMOylation levels in this strain (or WT cells, Fig. 5-10E) but suppressed both the INM accumulation of PA (Fig. 5-9C) and the increased nuclear surface area phenotypes of these cells in both interphase and mitosis (5-9D). By contrast, these effects were not induced by the introduction of exogenous *PAHI* (Fig. 5-9D, 5-10C). Moreover, nuclear surface area values in WT and *ulp1^{K352E/Y583H}-V5₃* mutant cells expressing the *pah1^{7A}* mutant were indistinguishable (Fig. 5-10D). These data

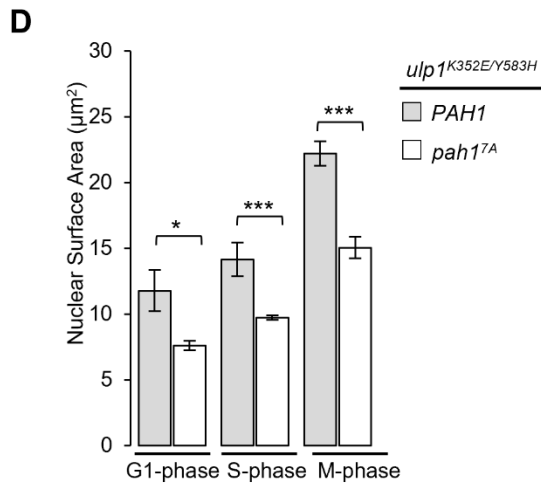
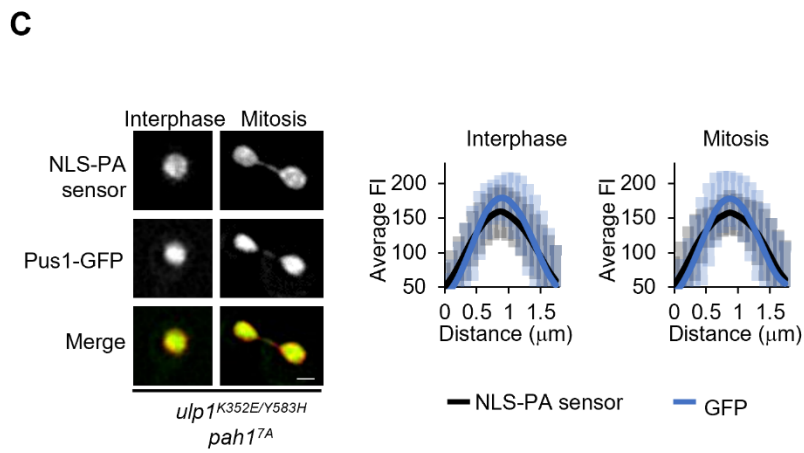
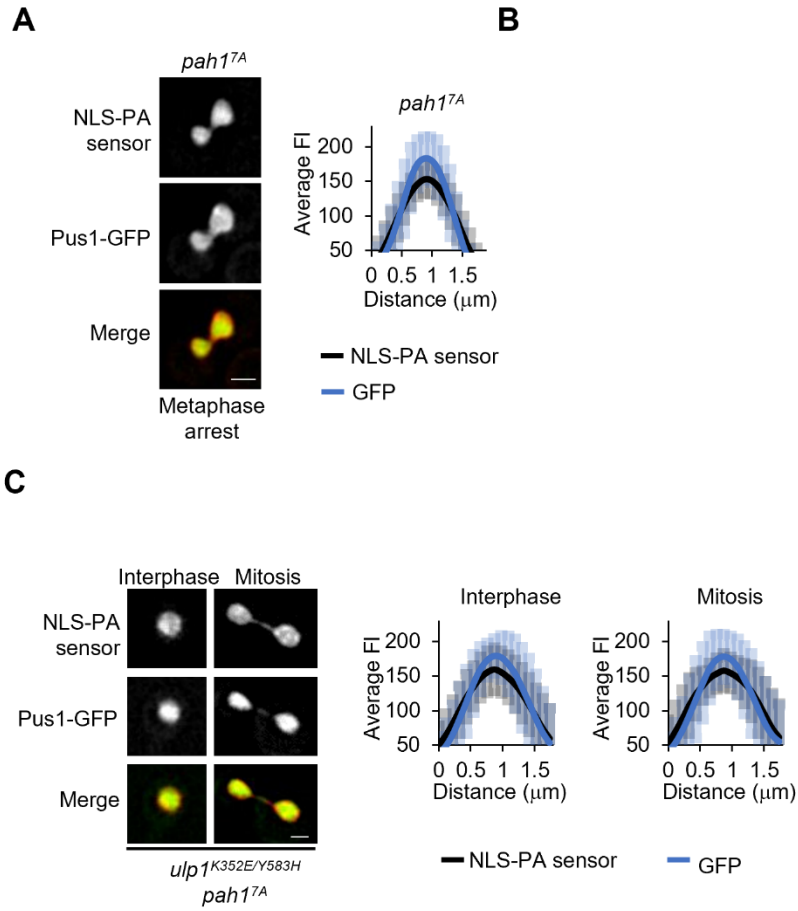


Figure 5-9. Pah1 activity antagonizes Siz2-mediated increases in nuclear surface area. **A** and **C**) Indicated strains containing the nucleoplasmic marker Pus1-GFP and a plasmid-encoded PA sensor (Opi1 Q2-mCherry) with an N-terminal nuclear localization sequence (NLS) were examined by epifluorescence. Representative epifluorescence images and corresponding nuclear fluorescence levels for the NLS-PA sensor and Pus1-GFP are shown for metaphase arrested *MET3pr-HA3-CDC20* producing cells (**A**) and asynchronously grown *ulp1* mutant cells (**C**). Nuclear levels of fluorescence were quantified using line scans as described in Fig. 5-7. n=25 nuclei. Bar- 2 μ m. Error bars- SD. FI= fluorescence intensity. **B** and **D**) The nuclear fluorescence signal of Pus1-GFP was used to calculate the nuclear surface area of the indicated cells using Imaris surface analysis. Images were acquired as a series of z-stacks. *MET3pr-HA3-CDC20* producing cells were arrested in metaphase by adding methionine for 2h before imaging (**B**). The cell cycle stage of asynchronously grown *ulp1* mutant cells was determined by bud size and nuclear morphology (**D**). Graphs show data from 3 biological replicates/sample where n=50 cells per replicate/cell cycle stage. Error bars- SD. Asterisks- significant change in the *pah1*^{7A} containing cells relative to the WT counterpart (*PAH1*) using a two-tailed student's t-test. *p \leq 0.05 ***p \leq 0.001. Note all *ulp1*^{K352E/Y583H} mutations contain a C-terminal V5₃ tag. *PAH1* and *pah1*^{7A} were expressed from a multicopy plasmid and were C-terminally tagged with PrA.

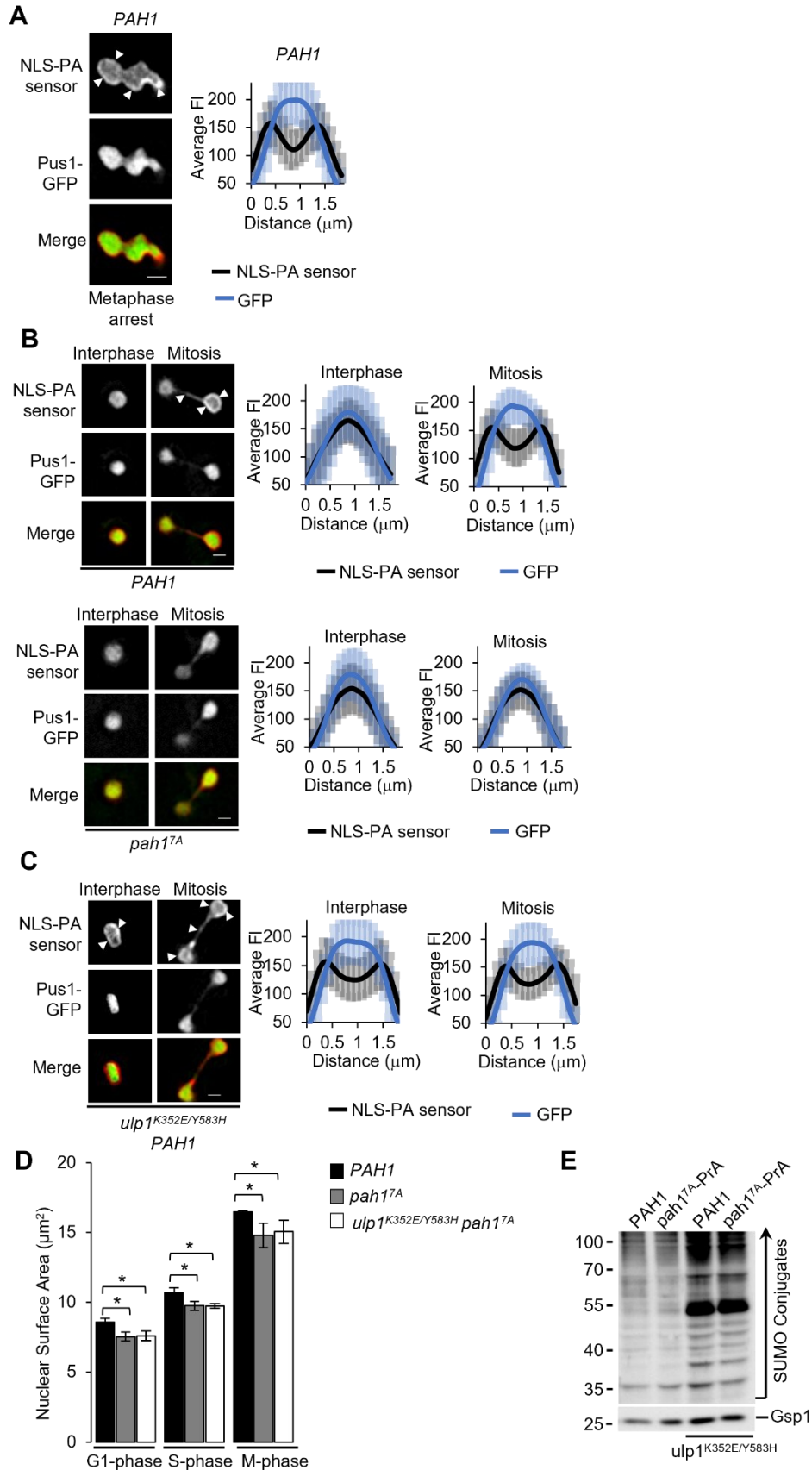


Figure 5-10. Effects of *pah1*^{7A} on PA and nuclear surface area. **A, B and C)** Indicated strains containing the nucleoplasmic marker Pus1-GFP, the plasmid-encoded *PAH1* or *pah1*^{7A}, and the plasmid-encoded PA sensor (Opi1 Q2-mCherry) with an N-terminal nuclear localization sequence (NLS) were examined by epifluorescence. Representative epifluorescence images and the corresponding nuclear fluorescence levels for the NLS-PA sensor and Pus1-GFP are shown for metaphase arrested *MET3pr-HA3-CDC20* producing cells (A), asynchronously grown WT (B) and *ulp1* mutant cells (C). Nuclear fluorescence levels were quantified using line scans as described in Fig. 5-7. n=25 nuclei. Bar- 2 μ m. Error bars- SD. FI= fluorescence intensity. Arrowheads highlight PA at the INM. **D)** The nuclear fluorescence signal of Pus1-GFP was used to calculate the nuclear surface area of the indicated cells using Imaris surface analysis. Graphs show data from 3 biological replicates/sample where n=50 cells per replicate/cell cycle stage. Error bars- SD. Asterisks- a significant change in the *pah1*^{7A} containing cells relative to the WT counterpart (*PAH1*) using a two-tailed student's t-test. *p \leq 0.05. **E)** Cell lysates derived from asynchronous cultures of indicated strains were assessed by western blotting using an anti-SUMO antibody to assess SUMO conjugate profiles. Gsp1 is a loading control. Molecular mass markers are shown in kDa. Note all *ulp1*^{K352E/Y583H} mutations contain a C-terminal V5₃ tag. *PAH1* and *pah1*^{7A} were C-terminally tagged with PrA.

support the idea that Siz2-mediated SUMOylation promotes NE biogenesis by restricting Pah1 activity.

5.2.5 Siz2 regulates the interactions of Pah1, Nem1, and Spo7.

The pah1^{7A} protein exhibits increased membrane association (Choi et al., 2011); thus, its ability to suppress membrane expansion induced by increased NE SUMOylation may reflect a role for SUMOylation in reducing the membrane association of Pah1 during mitosis. The binding of Pah1 to membranes is mediated by interactions with the Spo7/Nem1 integral membrane phosphatase complex (Karanasios et al., 2010; Dubots et al., 2014). On the basis of our results, we hypothesized that Siz2-mediated NE SUMOylation inhibits Pah1 activity by altering Pah1 association with the Spo7/Nem1 complex during mitosis. Immunoprecipitation analysis was used to assess levels of Pah1 binding to the Spo7/Nem1 complex during interphase (G1-phase) and during mitosis. For these experiments, cell cultures were synchronized by arresting in G1-phase using α -factor and then examined directly (G1-phase). Interactions during mitosis were examined by releasing α -factor arrested cells and examining interactions as cells progressed into mitosis (60 min post-release) or by examining interactions in cells following a metaphase arrest induced by Cdc20 depletion. Since Spo7 mediates Pah1 interactions with the Spo7/Nem1 complex (Siniosoglou 1998; Dubots et al., 2014), Spo7-TAP was purified under these various conditions to assess interactions of Pah1 with the Spo7/Nem1 complex. In G1-phase cells, Pah1 was detected in association with Spo7-TAP. By contrast, parallel analysis of mitotic extracts (both 60 min post α -factor release and following Cdc20 depletion) revealed a reduction

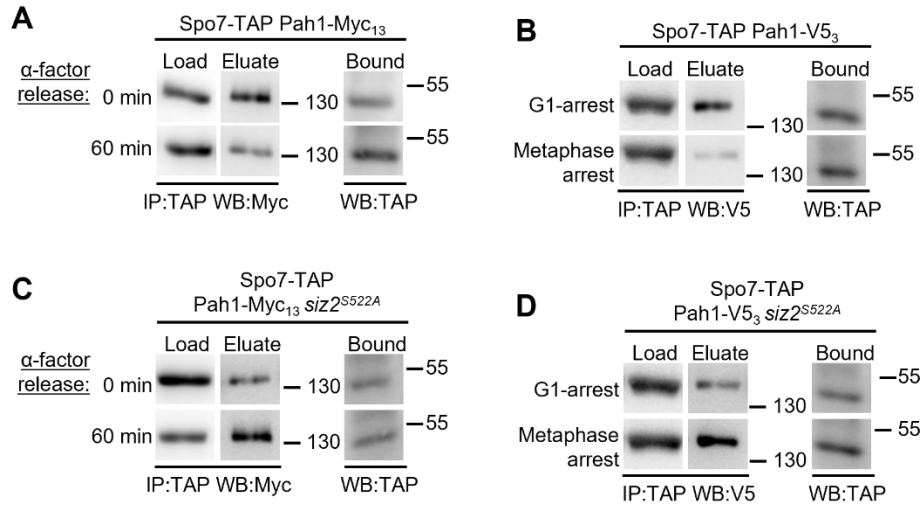


Figure 5-11. Mitotic SUMOylation events reduce Pah1 interactions with the Spo7/Nem1 complex. Spo7-TAP was affinity-purified from the indicated strains (IP) producing Pah1-V5₃ or Pah1-Myc₁₃. Equivalent portions of the indicated fractions were analyzed by western blotting (WB) to assess levels of the Myc-, V5- and TAP-tagged fusions. **A** and **C**) Indicated cells were arrested in G1-phase (0min) using α -factor. Following the release, cultures were collected at 60 min, and binding of Spo7-TAP to Pah1-Myc₁₃ was assessed. **B** and **D**) WT and *siz2*^{S522A} cells producing *MET3pr-HA₃-CDC20* were arrested in G1-phase using α -factor and arrested in metaphase by the addition of methionine. Cells were collected 2h post-arrest, and the binding of Spo7-TAP to Pah1-V5₃ was assessed. Note all Load, Elution, or Bound fractions shown in each panel were derived from the same western blot. All *ulp1*^{K352E/Y583H} mutations contain a C-terminal GFP tag. Molecular mass markers are shown in kDa on the right.

in the amount of Pah1 bound to Spo7-TAP (Fig.5-11 A,B). These observations are consistent with the proposed mitotic inhibition of Pah1 (Santos-Rosa et al., 2005). Importantly, this reduction in Pah1 association with Spo7, seen in WT cells, was not observed in *siz2^{S522A}* mutant cells. In *siz2^{S522A}* mutant cells, levels of Pah1 bound to Spo7 in the mitotic extracts were similar to, or higher than, that detected in G1-phase (Fig.5-11 C,D). These results suggest that the interaction of the Spo7/Nem1 complex with Pah1 is inhibited during mitosis, and NE SUMOylation is required to suppress their association.

Formation of the Spo7/Nem1 complex is required for the phosphatase activity of Nem1. Therefore, we also examined the assembly state of this complex during mitosis, to assess whether the activity of the Spo7/Nem1 complex was reduced. The binding of Spo7-TAP to Nem1 was assessed under the same conditions described for Spo7-TAP binding to Pah1. As shown in Fig. 5-12, WT cells progressing through mitosis or arrested in metaphase showed a reduction in the levels of Nem1 bound to Spo7 relative to that seen in G1-phase cells. The reduced association of Spo7 with Nem1 seen in mitotic WT cells (Fig. 5-12 A,B) was not observed in *siz2^{S522A}* mutant cells. In *siz2^{S522A}* mutant cells, no differences in the binding of Nem1 to Spo7 were detected in G1-phase versus mitotic cells (Fig. 5-10 C,D). On the basis of these results, we propose that Siz2-mediated mitotic SUMOylation contributes to the inhibition of Pah1 by both inhibiting the interactions of Pah1 with Spo7 as well as reducing Spo7 binding to Nem1.

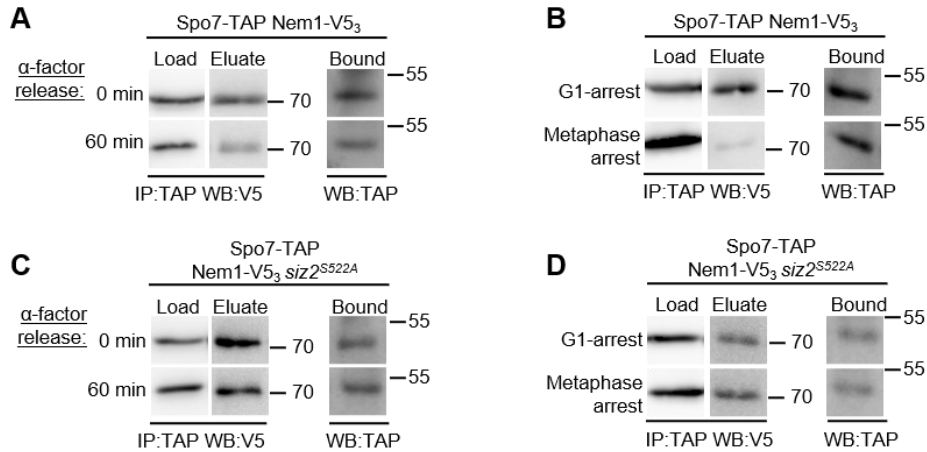


Figure 5-12. Mitotic SUMOylation events reduce interactions between Spo7 and Nem1. Spo7-TAP was affinity-purified from indicated strains (IP) producing Nem1-V5₃. Equivalent portions of the indicated fractions were analyzed by western blotting (WB) to assess levels of the V5- and TAP-tagged fusions. **A** and **C**) Indicated cells were arrested in G1-phase (0min) using α -factor. Following the release, cultures were collected at 60 min, and binding of Spo7-TAP to Nem1-V5₃ was assessed. **B** and **D**) WT and *siz2*^{S522A} mutant cells producing *MET3pr-HA3-CDC20* were arrested in G1-phase using α -factor and arrested in metaphase by the addition methionine. Cells were collected 2h post-arrest, and the binding of Spo7-TAP to Nem1-V5₃ was assessed. Note all Load, Elution, or Bound fractions shown in each panel were derived from the same western blot. All *ulp1*^{K352E/Y583H} mutations contain a C-terminal GFP tag. Molecular mass markers are shown in kDa on the right.

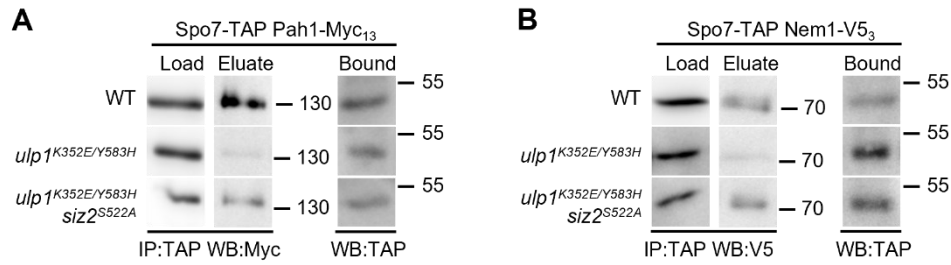


Figure 5-13. Siz2-mediated SUMOylation events reduce Spo7 interactions with Pah1 and Nem1. Spo7-TAP was affinity-purified from the indicated strains (IP) producing Pah1-V5₃ or Pah1-Myc₁₃. Equivalent portions of the indicated fractions were analyzed by western blotting (WB) to assess levels of the Myc-, V5- and TAP-tagged fusions. **A**) Binding of Pah1-Myc₁₃ to Spo7-TAP in indicated asynchronously grown cells was assessed. **B**) Binding of Nem1-V5₃ to Spo7-TAP in indicated asynchronously grown cells was assessed. Note all Load, Elution, or Bound fractions shown in each panel were derived from the same western blot. All *ulp1^{K352E/Y583H}* mutations contain a C-terminal GFP tag. Molecular mass markers are shown in kDa on the right.

If, as our data suggests, Siz2-mediated NE SUMOylation inhibits the interactions of Spo7 with Pah1 and Nem1, we would predict that the constitutively higher levels of Siz2-mediated SUMOylation observed throughout the cell cycle in *ulp1^{K352E/Y583H}* mutant cells would result in a general reduction in the interactions of Spo7 with Pah1 and Nem1. Using immunoprecipitation analysis, we detected the binding of Spo7-TAP to Pah1 and Nem1 in asynchronous cultures of WT cells (Fig.5-13). These interactions were reduced in *ulp1^{K352E/Y583H}* mutant cells and restored to WT levels in *ulp1^{K352E/Y583H} siz2^{S522A}* mutants (Fig.5-13). These observations support Siz2-mediated SUMOylation inhibiting Spo7 interactions with Pah1 and Nem1.

As our results show that the ability of Pah1 to interact with the membrane is reduced by mitotic SUMOylation events at the INM (Fig. 5-11, 5-12, 5-13), we investigated whether cells containing Pah1 constitutively associated with the INM could suppress membrane expansion phenotypes induced by increased NE SUMOylation. Using the superfolder GFP, GFP₁₋₁₀ and GFP₁₁ system (Smoyer et al., 2016), Pah1 was constitutively associated with the INM (Pah1-GFP₁₋₁₀ - GFP₁₁-mCherry-TM) in M-phase arrested cells (Fig. 5-14A) and asynchronously grown WT (Fig. 5-16A) and *ulp1^{K352E/Y583H}-V5₃* mutant cells (Fig. 5-15A). In cells where Pah1 was constitutively associated with the INM we observed that the nuclei were all spherical. Moreover, in these cells we detected a significant decrease in nuclear surface area and PA accumulation at the INM relative to the corresponding cells that positioned the GFP₁₁ fragment on the luminal side of NE/ ER membrane (mCherry-TM-GFP₁₁; Smoyer et al.,2016), which did not, as predicted, produce

GFP fluorescence at the NE (Fig.5-14, 5-15, 5-16). Collectively, these results suggest that SUMOylation prevents Pah1 phosphatase activity by preventing Pah1 association with its substrate.

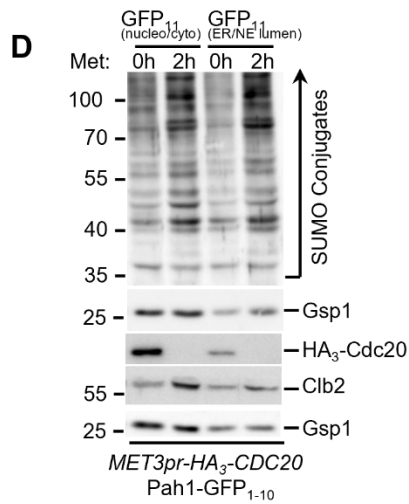
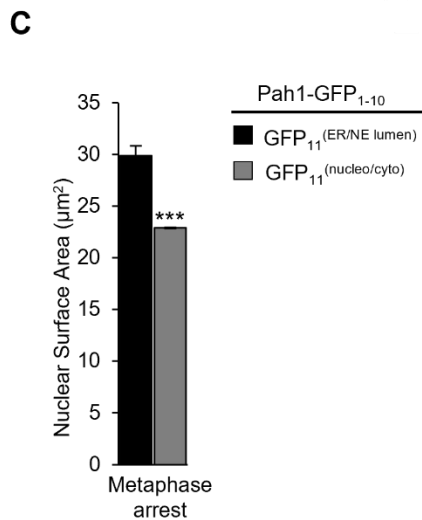
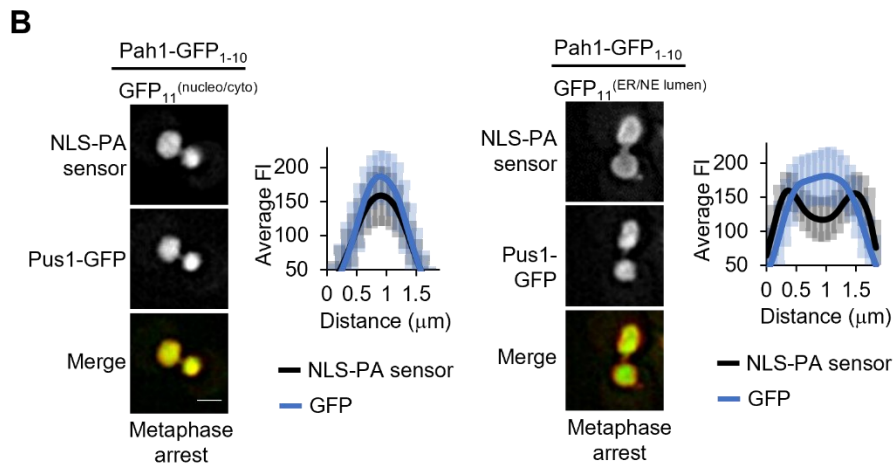
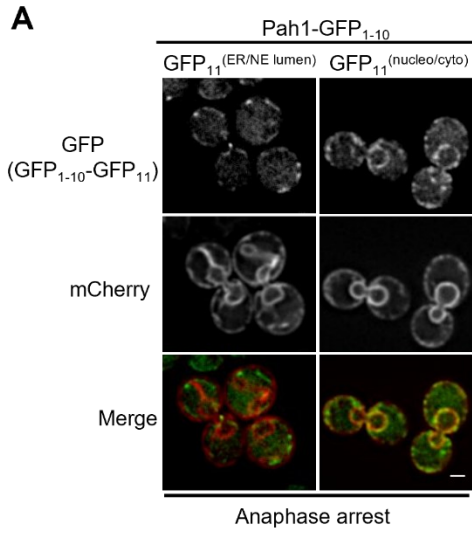


Figure 5-14. Pah1 membrane association can suppress the increased nuclear surface area of mitotically delayed cells. **A)** Epifluorescence images of cells producing Pah1-GFP₁₋₁₀ and the plasmid-encoded mCherry-scs2TM-GFP₁₁ (GFP₁₁^(NE/ER lumen)) or GFP₁₁-mCherry-scs2TM (GFP₁₁^(nucleo/cyto)) reporters which positions GFP₁₁ on the luminal or nucleo/cytosolic face of the NE/ER membrane, respectively. Membrane integration of the GFP₁₁ reporters allows visualization of NE morphology by mCherry fluorescence. Assembled GFP₁₋₁₀-GFP₁₁ dimers are visualized by GFP fluorescence when the GFP₁₁ reporter resides in the same subcellular compartment as Pah1-GFP₁₋₁₀. Bar- 2 μ m. *MET3pr-HA₃-CDC20* containing cells were arrested in metaphase by adding methionine for 2h prior to imaging. **B)** Indicated strains containing Pus1-GFP and a plasmid-encoded PA sensor (Opi1 Q2-mCherry) with an N-terminal nuclear localization sequence (NLS) were examined by epifluorescence. Representative epifluorescence images and corresponding nuclear fluorescence levels for the NLS-PA sensor and Pus1-GFP in metaphase arrested *MET3pr-HA₃-CDC20* producing cells are shown. Nuclear levels of fluorescence were quantified using line scans as described in Fig. 5-7. n=25 nuclei. Bar- 2 μ m. Error bars- SD. FI= fluorescence intensity. Note GFP₁₁ reporters utilized lacked mCherry. **C)** The nuclear fluorescence signal of Pus1-GFP was used to calculate the nuclear surface area of the indicated cells using Imaris surface analysis. Images were acquired as a series of z-stacks. *MET3pr-HA₃-CDC20* producing cells were arrested in metaphase by adding methionine for 2h before imaging. Graphs show data from 3 biological replicates where n=50 cells per replicate/cell cycle. Error bars- SD. Asterisks- significant change in GFP₁₁-mCherry-scs2TM (GFP₁₁^(nucleo/cyto)) containing cells relative to mCherry-scs2TM-GFP₁₁ (GFP₁₁^(NE/ER lumen)) counterpart using a two-tailed student's t-test. *p \leq 0.05 ***p \leq 0.001. **D)** Cell lysates derived from asynchronous (0) or metaphase arrested (2h) cultures of indicated strains were analyzed by western blotting to detect SUMO conjugates, Clb2, HA₃ tags, and the Gsp1 load control. Molecular mass markers are shown in kDa.

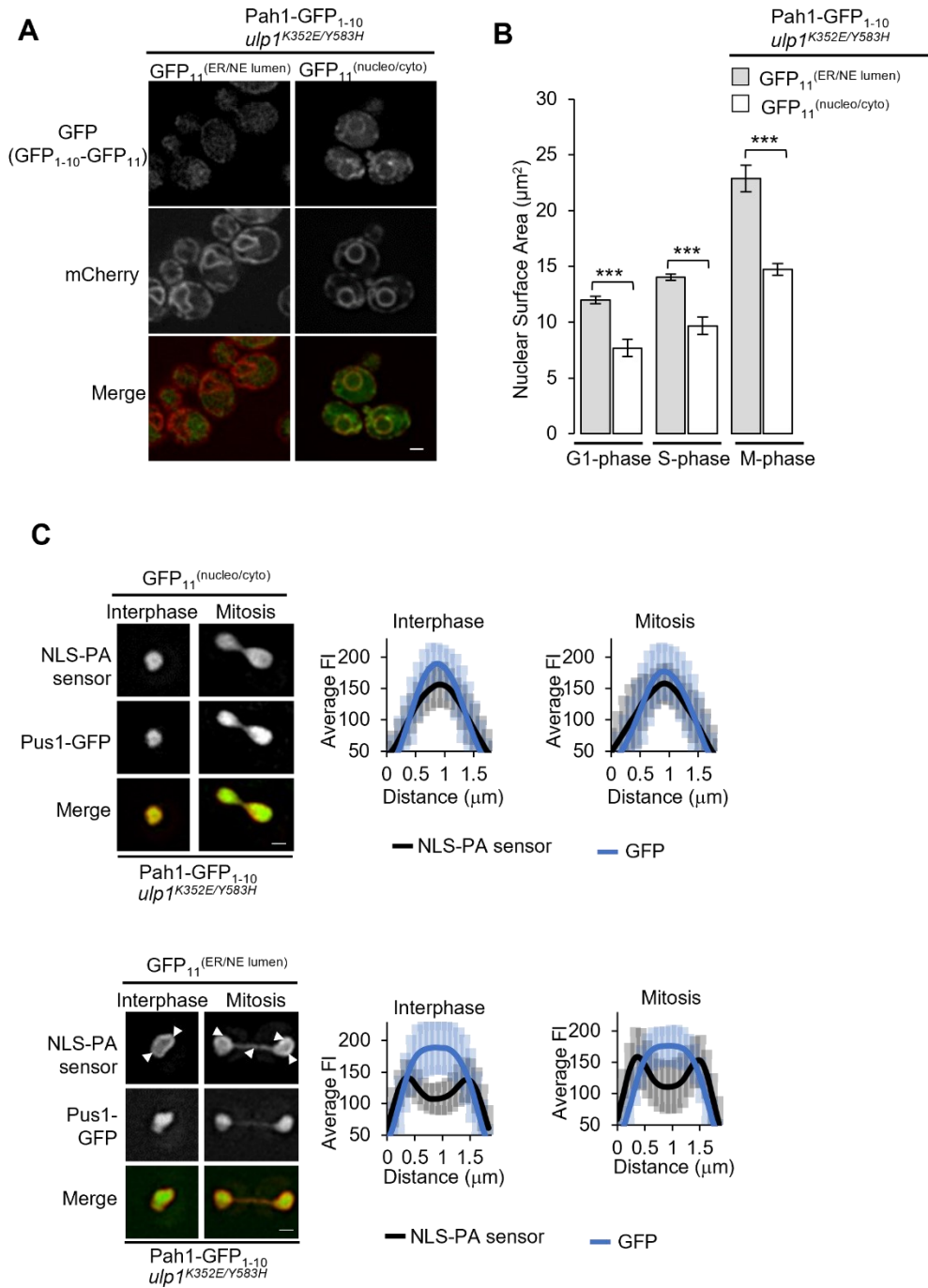


Figure 5-15. Pah1 membrane association can suppress NE expansion phenotypes of *ulp1*^{K352E/Y583H} mutant cells. A) Epifluorescence images of cells producing Pah1-GFP₁₋₁₀ and the plasmid-encoded mCherry-scs2TM-GFP₁₁ (GFP₁₁^(NE/ER lumen)) or GFP₁₁-mCherry-scs2TM (GFP₁₁^(nucleo/cyto)) reporters which position GFP₁₁ on the luminal or nucleo/cytosolic face of the NE/ER membrane, respectively. Membrane integration of the GFP₁₁ reporters allows visualization of NE morphology by mCherry fluorescence. Assembled GFP₁₋₁₀-GFP₁₁ dimers are visualized by GFP fluorescence when the GFP₁₁ reporter resides in the same subcellular compartment as Pah1-GFP₁₋₁₀. Bar- 2 μm. **B)** The nuclear fluorescence signal of Pus1-GFP was used to calculate the nuclear surface area of the indicated cells using Imaris surface analysis. Graphs show data from 3 biological replicates/sample where n=50 cells per replicate/cell cycle stage. Error bars- SD. Asterisks- significant change in GFP₁₁-mCherry-scs2TM (GFP₁₁^(nucleo/cyto)) containing cells relative to mCherry-scs2TM-GFP₁₁ (GFP₁₁^(NE/ER lumen)) counterpart using a two-tailed student's t-test. *p≤0.05 **p≤0.01. **C)** Pah1-GFP₁₋₁₀ cells containing the nucleoplasmic Pus1-GFP, plasmid-encoded PA sensor (Opi1 Q2-mCherry) with an N-terminal nuclear localization sequence (NLS) and either the plasmid-encoded GFP₁₁-scs2TM (GFP₁₁^(nucleo/cyto)) or scs2TM-GFP₁₁ (GFP₁₁^(NE/ER lumen)) reporter were examined. Representative epifluorescence images and the corresponding nuclear fluorescence levels for the NLS-PA sensor and Pus1-GFP are shown for interphase and mitotic *ulp1* mutant cells. Note all *ulp1*^{K352E/Y583H} mutations contain a C-terminal V5₃ tag.

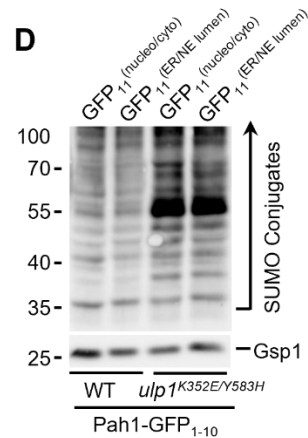
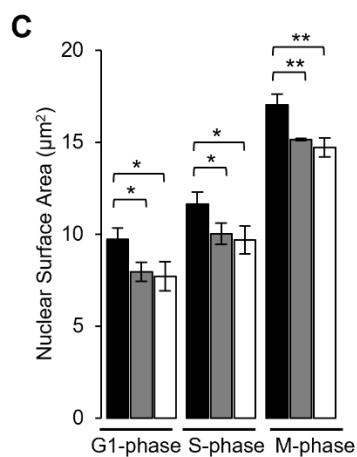
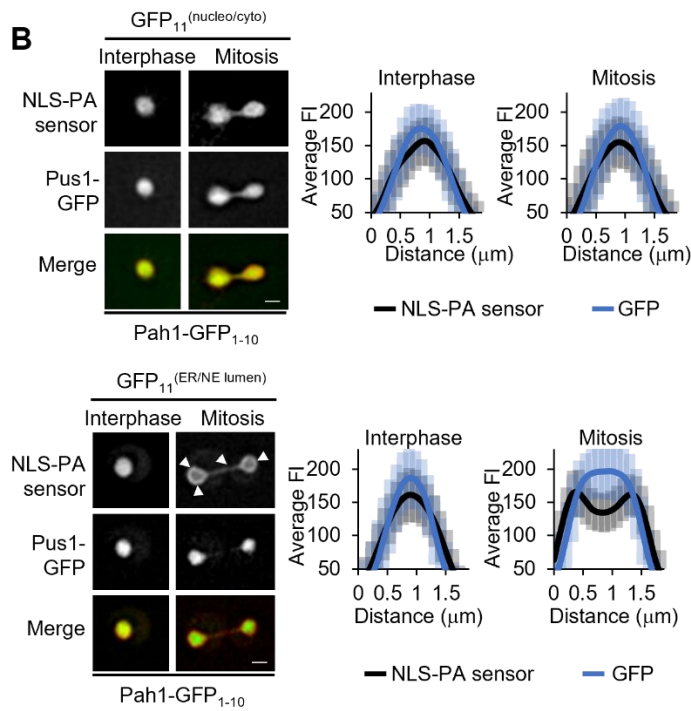
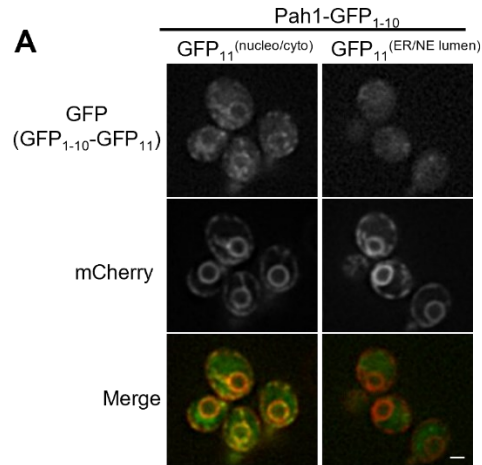


Figure 5-16. Effects of Pah1 membrane association on PA and nuclear surface area. A) Epifluorescence images of cells producing Pah1-GFP₁₋₁₀ and the plasmid-encoded mCherry-scs2TM-GFP₁₁ (GFP₁₁^(NE/ER lumen)) or GFP₁₁-mCherry-scs2TM (GFP₁₁^(nucleo/cyto)) reporters, which position GFP₁₁ on the luminal or nucleo/cytosolic face of the NE/ER membrane, respectively. Membrane integration of the GFP₁₁ reporters allows visualization of NE morphology by mCherry fluorescence. Assembled GFP₁₋₁₀-GFP₁₁ dimers are visualized by GFP fluorescence when the GFP₁₁ reporter resides in the same subcellular compartment as Pah1-GFP₁₋₁₀. Bar- 2 μm. **B)** Pah1-GFP₁₋₁₀ cells containing the nucleoplasmic Pus1-GFP, plasmid-encoded PA sensor (Opi1 Q2-mCherry) with an N-terminal nuclear localization sequence (NLS) and either the plasmid-encoded GFP₁₁-scs2TM (GFP₁₁^(nucleo/cyto)) or scs2TM-GFP₁₁ (GFP₁₁^(NE/ER lumen)) reporter were examined. Representative epifluorescence images and the corresponding nuclear fluorescence levels for the NLS-PA sensor and Pus1-GFP are shown for interphase and mitotic cells. **C)** The nuclear fluorescence signal of Pus1-GFP was used to calculate the nuclear surface area of the indicated cells using Imaris surface analysis. Graphs show data from 3 biological replicates/sample where n=50 cells per replicate/cell cycle stage. Error bars- SD. Asterisks- significant change in GFP₁₁-mCherry-scs2TM (GFP₁₁^(nucleo/cyto)) containing cells relative to mCherry-scs2TM-GFP₁₁ (GFP₁₁^(NE/ER lumen)) counterpart using a two-tailed student's t-test. *p≤0.05 **p≤0.01. **D)** Cell lysates derived from asynchronous cultures of indicated strains were assessed by western blotting using an anti-SUMO antibody to assess SUMO conjugate profiles. Gsp1 is a loading control. Molecular mass markers are shown in kDa. Note all *ulp1*^{K352E/Y583H} mutations contain a C-terminal V5₃ tag.

5.3 Discussion

During mitosis, the dividing cell increases phospholipid (PL) synthesis. PLs are increased during mitosis, in part by the inhibition of Pah1 (Santos-Rosa et al., 2005). Pah1 is the phosphatase responsible for converting PA, the central metabolite for the *de novo* synthesis of PLs, to DAG, which diverts PA away from the primary PL synthesizing pathway. The loss of Pah1 activity increases PA levels in the ER (Hassaninasab, Han, and Carman 2017) to promote PL synthesis and NE membrane expansion (Santos-Rosa et al., 2005). Recently, the INM has been shown to possess distinct lipid metabolic activities (Haider et al., 2018; Romanauska and Köhler 2018; Antonio D. Barbosa et al., 2019). In particular, enzymes involved in regulating PA levels, including Pah1 and Dgk1, have been identified at the INM (Romanauska and Köhler 2018). These observations imply that the growth of the NE during the cell cycle may rely on local lipid synthesis at the INM in addition to lipids delivered from the ER/ONM.

In support of this, we have identified SUMOylation as a spatiotemporal regulatory mechanism that facilitates the increase of PA at the INM during mitosis (Fig. 5-7). We propose that the SUMOylation-dependent increase in PA at the INM and expansion of the NE during mitosis (Fig. 5-1, 5-2, 5-3, 5-6) is due to reduced interactions between Spo7, Nem1, and Pah1 during mitosis (Fig. 5-11-, 5-12, 5-13). These observations identify SUMOylation as an important cell cycle specific regulator of NE-membrane proliferation and expand on limited analysis implicating SUMOylation in PL synthesis (Liu and Gerace 2009; Felberbaum et al., 2011).

A Siz2-mediated SUMOylation wave increases PA at the INM

In this work, we show that Siz2-mediated SUMOylation increases PA at the INM. Using a lipid biosensor with an NLS-sequence, we were able to monitor nuclear PA throughout the cell cycle. Consistent with previous observations, we show that under normal conditions, there is little PA at the INM, resulting in the PA sensor localizing throughout the nucleoplasm in interphase cells (Romanauska and Köhler, 2018; Fig. 5-7). However, as cells enter mitosis, there is an accumulation of PA at the INM, which coincides with the expansion and increased surface area of the NE (Fig. 5-1, 5-7). The inhibition of Siz2-mediated SUMOylation events reduces the mitotic accumulation of PA at the INM and the nuclear surface area of these cells (Fig. 5-1, 5-7). Conversely, increasing Siz2-mediated SUMOylation events causes aberrant PA accumulation at the INM and NE expansion (Fig. 5-3, 5-6, 5-8). Together these data support a model in which the increase in PA at the INM contributes to the expansion of the NE, as opposed to previous reports, which propose NE expansion is due to increased PA levels in the ER (Hassaninasab, Han, and Carman 2017). As the INM is capable of lipid metabolic activities (Romanauska and Köhler 2018), we propose that during mitosis, SUMOylation events promote the production of PA at the INM to facilitate the expansion of the NE. However, at this time, we cannot rule out the possibility that the PA enriched at the INM during mitosis is derived from the ER, and SUMOylation events merely facilitate the diffusion or retention of PA at the INM. Whether PA levels are globally reduced or reduced specifically at the INM will be important to discriminate between these possibilities. Testing these possibilities

will require precise tools to monitor and regulate PA such as OptoPD. OptoPD is a method that precisely generates PA at specific organelle membranes (Tei and Baskin 2020). Using this technology in the presence or absence of Siz2-mediated mitotic SUMOylation events could provide important insights into the contributions of SUMOylation in PA accumulation and/or generation at the INM. Furthermore, because the nuclear localization of Pah1 has been demonstrated (Santos-Rosa et al., 2005; Romanauska and Köhler 2018) and the INM localization of the Nem1/Spo7 complex has been predicted (Lusk, Blobel, and King 2007) preventing the nuclear localization of these proteins could also provide valuable information on the contributions of the INM in PA production and NE expansion.

Preventing the SUMOylation-dependent enrichment of PA at the INM in mitotically delayed *siz2^{S522A}* mutant cells is reminiscent of phenotypes observed for *cdc5* mutant cells (Walters et al., 2014). Analyzing whether *cdc5* mutant cells also prevent an enrichment of PA at the INM will be important for distinguishing the contributions of PA at the INM and mitotic membrane expansion. An interesting possibility is that Cdc5 and Siz2 are part of the same regulatory pathway facilitating mitotic nuclear membrane expansion. Cdc5 contains several SUMO consensus motifs (Q. Zhao et al., 2014). Cdc5 could also be responsible for the mitotic phosphorylation of Siz2, which is necessary for the enrichment of Siz2 at the INM during mitosis (Ptak et al., 2021; Chapter 4). As Cdc5 has been implicated in promoting SUMOylation events during mitosis (Baldwin et al., 2009), another possibility is that Cdc5 prevents the deSUMOylation of Siz2-mediated SUMOylation events during mitosis to promote NE expansion. More work will

need to be done to determine whether Cdc5 and Siz2 are part of the same or distinct regulatory pathways facilitating mitotic membrane expansion.

In addition to facilitating NE expansion during mitosis, the accumulation of PA at the INM during mitosis can have other important implications for the NE. PA regulates lipid-lipid and lipid-protein interactions (Zhukovsky et al., 2019). The increase in PA at the INM during mitosis may favor the formation of a “PA microdomain” that favors specific protein interactions during mitosis (Kooijman et al., 2007). As we have previously shown that Siz2-mediated SUMOylation promotes NE-chromatin interactions during mitosis (Ptak et al., 2021; Chapter 4), an interesting possibility is that PA promotes protein interactions involved in these processes. In addition, PA has been shown to function as a pH biosensor in the cytoplasm. The pH dependent binding of proteins to PA functions to link membrane biogenesis to metabolism, with PA preferentially binding to specific proteins under acidic conditions (Young et al., 2010). Interestingly, the spatiotemporal pH within the nucleus of dividing *S. cerevisiae* dramatically reduces upon entry into mitosis (H. Zhao et al., 2019). Therefore, the SUMOylation-dependent enrichment of PA at the INM may function to provide a similar function at the NE during mitosis.

A Siz2-mediated SUMOylation wave at the INM facilitates NE expansion.

We show that the enrichment of PA at the INM during mitosis is dependent on Siz2-mediated SUMOylation events (Fig. 5-7, 5-8), which functions to reduce interactions between Pah1, Spo7, and Nem1 (Fig. 5-11, 5-12, 5-13). Because the SUMOylation of a protein can inhibit protein interactions by blocking the

interaction sites of other substrates (Moldovan, Pfander, and Jentsch 2006), the SUMOylation of Pah1, Nem1, or Spo7 may function to inhibit interactions between these proteins. SUMOylation, however, more commonly mediates protein interactions by producing binding sites for proteins containing a SIM motif(s) (Psakhye and Jentsch 2012). Because Siz2-mediated SUMOylation is predicted to generate a SUMO:SIM protein network at the INM (Chapter 4), we propose that Nem1 and Spo7 interactions are reduced due to new interactions formed with SUMOylated proteins that become enriched at the INM during mitosis. We envisage that Siz2-mediated SUMOylation at the INM could enrich interacting partners to bind to Nem1 and/or Spo7 independently of SUMOylation or through SUMO:SIM interactions. Nem1, for example, has two putative SIM sites that overlap with Spo7 interaction sites (Siniosoglou 1998; Q. Zhao et al., 2014). Therefore, Nem1 interactions with Spo7 could be reduced by interactions between Nem1 and mitotic SUMOylated proteins at the INM. Another possibility for is that Siz2-mediated SUMOylation events are altering Nem1, Spo7, and Pah1 interactions in the cytosol by retaining an interacting partner at the INM during mitosis required for the formation of the Pah1-Nem1/Spo7 complex. Inhibiting the nuclear localization of Pah1 or the Nem1/Spo7 complex could provide insights between these different possibilities.

The SUMOylation dependent reduction in Pah1, Spo7, and Nem1 interactions represents a unique nuclear regulatory system facilitating a mitotic increase in PA. As mentioned above, the pH of nuclei are dramatically reduced upon entry into mitosis (H. Zhao et al., 2019). Nem1/Spo7 has optimal activity at

an acidic pH (Antonio Daniel Barbosa et al., 2015). Therefore, Siz2-mediated SUMOylation events at the INM may be required to overcome pH changes within the nucleus that would favor Nem1/Spo7 activity. Testing whether Siz2-mediated SUMOylation events alter nuclear pH levels during mitosis will be of interest to determine the contributions of pH on PA accumulation at the INM (H. Zhao et al., 2019).

Scs2 regulates lipid metabolism through interactions with multiple FFAT-containing proteins.

Scs2 is an integral ER membrane protein that interacts with the FFAT-motif of its interacting partners. Scs2 interacts with FFAT-motifs through its N-terminal MSP domain (Christopher J.R. Loewen and Levine 2005). We have previously shown that interactions between Scs2 and Siz2 are facilitated by MSP:FFAT interactions to re-establish chromatin interactions at the NE during mitosis (Ptak et al., 2021; Chapter 4). Our work here shows that Scs2^{MSP}:Siz2^{FFAT} interactions also regulate PL synthesis. These observations are reminiscent of other MSP:FFAT interactions between Scs2 and interacting partners. In the cortical ER, Scs2 interacts with the FFAT-motif of Osh3 to facilitate the formation of PI (Stefan et al., 2011) and PC (Tavassoli et al., 2013) at the plasma membrane. Whereas interactions in the peripheral ER between Scs2 and the FFAT-motif of Opi1 promotes the transcription of UAS_{INO} containing PL synthesizing genes (Christopher J.R. Loewen, Roy, and Levine 2003; J. H. Brickner and Walter 2004). Thus, Scs2 functions as an important receptor at multiple subcellular locations and with multiple FFAT-containing proteins to regulate PL metabolism. The subcellular

localization and regulation of these different interactions are essential for regulating specific aspects of lipid metabolism, including, as identified here, the temporal increase of PA at the INM.

During inositol starvation, PA at the ER increases; this causes the relocalization of Opi1 to the NE/ER, where it interacts with PA and Scs2. The interaction of Opi1 with PA and Scs2 at the NE/ER causes the derepression of UAS_{INO} containing PL synthesizing genes by preventing Opi1 from inhibiting the transcriptional activators of PL synthesizing genes (C. J.R. Loewen et al., 2004; Hofbauer et al., 2014; Gaspar et al., 2017). The mitotic increase of PA at the INM (Fig. 5-7) and INM localization of Scs2 (Ptak et al.,2021; Chapter 4) would be predicted to cause the relocalization of Opi1 to the NE. However, the relocalization of Opi1 during mitosis has not been observed (C. J.R. Loewen et al., 2004), nor has a mitotic increase in the transcription of UAS_{INO} containing PL synthesizing genes (Rowicka et al., 2007). We reason that during mitosis, the interactions of the MSP domain of Scs2 with the FFAT-like motif of Siz2 (Ptak et al.,2021; Chapter 4) outcompetes the ability of Opi1 to interact with Scs2 at the INM. Additionally, interactions of Opi1 with PA are facilitated by PA with C:16 acyl chains (Hofbauer et al., 2014). The composition of PA at the INM during mitosis may represent C:18 acyl chain-based PA, as Acc1 activity, which is increased during mitosis (Blank et al., 2017), shifts PL metabolism towards C:18 acyl chains. Therefore, Opi1 interactions with PA and Scs2 at the INM may not be sufficient to cause Opi1 enrichment at the INM and the derepression of UAS_{INO} containing genes during mitosis. Overall, these data suggest that the mitotic increase in PL biosynthesis at

the INM is independent of transcription. This is consistent with our previous observations (Chapter 3 & Chapter 4) that show Siz2-mediated SUMOylation events regulate cellular functions independently of transcription. Rather SUMOylation appears to facilitate the increase of PA at the INM for PL synthesis by reducing interactions between Pah1, Spo7, and Nem1 (Fig. 5-11, 5-12, 5-13). Collectively, these observations suggest that at the INM, interactions with Scs2, through its MSP domain, regulate lipid metabolism independently of Opi1.

Because the rapid diffusion of PLs can occur within the ER/NE membrane, specialized mechanisms must be in place to maintain the distinct PL composition of the INM. In metazoan cells, the spatial restriction of CNEP-1 (homolog of Nem1) to the NE generates a "lipid concentration gradient," where PI concentrations are highest at the plasma membrane and lowest at the NE (Bahmanyar et al., 2014). Scs2 may establish a similar "lipid concentration gradient" to maintain the unique lipid composition of the INM through its interactions with different FFAT-containing proteins at different subcellular compartments. The interaction of Scs2 with the FFAT-like motif of Siz2 facilitates PA accumulation at the INM in mitosis (Fig. 5-7). In contrast the loss of these interactions during interphase decreases PA at the INM available for PL production. At the same time, Scs2 interactions with the FFAT motif of Osh3 at the cortical ER enhances PI and PC production at the plasma membrane (Stefan et al., 2011; Tavassoli et al., 2013). In this way, Scs2 may establish lipid concentration gradients to regulate the unique lipid composition of INM throughout the cell cycle.

Overall, we have identified SUMOylation as a novel regulatory mechanism that facilitates the expansion of the NE during mitosis. We have shown that SUMOylation reduces interactions between Pah1, Spo7, and Nem1 to facilitate the mitotic increase of PA at the INM. As Siz2-mediated SUMOylation events at the INM are dependent on interactions with Scs2 at the INM, our work highlights the unique role of Scs2 in PL metabolism at the INM.

Chapter VI: Perspectives

6.1 Synopsis

Overall, our work here shows that SUMOylation at the INM regulates numerous cellular processes, including the expansion of the NE (Chapter 5) and the reassociation of chromatin to the NE (Chapter 3 & 4). The overall goal of this thesis was to identify SUMOylation events at the NE, characterize the biological functions of these events, and identify regulatory mechanisms that facilitate these events. We have identified numerous Siz2-mediated SUMOylation targets at the NE, including Scs2 and Sir4. We have identified several regulatory mechanisms that facilitate Siz2-mediated SUMOylation events at the NE, including the binding of Siz2 to the activated *INO1* locus at NPCs (Chapter 3) and the binding of Siz2 to its INM receptor, Scs2, during mitosis (Chapter 4). Importantly, we have characterized the SUMOylation machinery required for both the SUMOylation (Siz2) and deSUMOylation (Ulp1) of these targets. We show that these SUMOylation and deSUMOylation events regulate the formation of chromatin interactions with the nuclear membrane (Chapter 3 & 4) and regulate the expansion of the NE (Chapter 5). Overall, we show that SUMOylation is an important regulator of NE structure. In this chapter, the implications of our results in NE structure will be discussed.

6.2 Mitotic SUMOylation at the INM may establish the INM proteome.

Siz2-mediated SUMOylation events at the INM facilitates numerous protein interactions to generate a SUMO:SIM protein network (Chapter 4). We have shown that the formation of this SUMO:SIM protein network re-establishes chromatin interactions with the INM during mitosis to promote the proper spatial

organization of the genome in newly formed cells. The formation of these chromatin-NE interactions may also be important for establishing the INM proteome. Most integral INM proteins appear to be enriched at the INM by the diffusion-retention model (Boni et al., 2015; Ungricht et al., 2015; Smoyer et al., 2016). Within this model, integral proteins below a certain size threshold diffuse across the POMs and are retained at the INM by interactions with chromatin. Siz2-mediated SUMOylation events at the INM during mitosis may retain INM proteins by promoting their interactions with chromatin, as seen with Sir4, or by integrating these proteins into other macromolecule complexes at the INM.

In this way, Siz2-mediated SUMOylation events may act as a “glue” to capture and retain proteins at the INM during mitosis. As yeast undergo closed mitosis, the expanding NE may need to be repopulated with INM proteins. This could be enhanced by Siz2-mediated SUMO:SIM interactions. These SUMO:SIM interactions may promote the initial formation of macromolecule complexes. Once incorporated into these complexes, these proteins can be maintained at the INM following mitotic exit to become part of the INM proteome in the newly formed nuclei. Alternatively, these SUMO:SIM interactions may promote a unique INM proteome during mitosis, which are lost or reduced by deSUMOylation during mitotic exit. The formation of an INM proteome unique to mitosis may be necessary to regulate specific nuclear mitotic functions. For example, Siz2-mediated SUMOylation events may facilitate protein-lipid interactions that prevent the lateral diffusion of lipids from the INM to the ONM, allowing the mitotic enrichment of PA at the INM to occur, and thereby NE expansion (Chapter 5). The

SUMOylation-dependent retention of a protein at the INM during mitosis might also be required to regulate specific cytoplasmic functions. For example, enhancing the retention of Scs2 to the INM during mitosis by SUMOylation may be necessary for regulating the amount of Scs2 available for other mitotic functions in the cytoplasm (Christopher J.R. Loewen, Roy, and Levine 2003; Chao et al., 2014; Neller et al., 2015; Omer, Greenberg, and Lee 2018; Ng, Ng, and Zhang 2020).

Investigating whether the INM proteome is altered in a Siz2-dependent manner or throughout the cell cycle, using systems previously used to characterize the INM proteome (Smoyer et al., 2016), could have important insights into the contributions that mitotic SUMOylation events have in establishing the INM proteome and additional functions that these SUMOylation events may regulate.

6.3 Siz2-mediated SUMOylation at the INM functionally connects chromatin binding to the INM with NE expansion.

The expansion of the NE/ER membrane has been proposed to occur at the membrane adjacent to the nucleolar region (Campbell et al., 2006; Witkin et al., 2012), with the tethering of DNA to the NE outside of these regions allowing these regions to resist expansion (Campbell et al., 2006). Consistently, we show that Siz2-mediated SUMOylation events at the INM are required for chromatin association with the NE during mitosis (Chapter 4). The loss of these chromatin interactions coincides with the lack of nuclear expansion at membrane regions adjacent to the nucleolar region. Conversely, increased Siz2-mediated SUMOylation events at the INM enhance chromatin interactions with the NE

(Chapter 4) and promote NE expansion (Chapter 5). These results suggest that Siz2-mediated SUMOylation events coordinate NE-expansion and NE-chromatin interactions. One mechanism through which SUMOylation could coordinate these two processes is by producing new protein interactions and complexes at the INM with proteins involved in both processes.

Interestingly, Esc1, an INM-associated protein, has been shown to have a dual role in telomere tethering and lipid metabolism (Hattier, Andrulis, and Tartakoff 2007; Andrulis et al., 2002), with the overexpression of Esc1 promoting the expansion of the INM (Hattier, Andrulis, and Tartakoff 2007). Esc1 facilitates G1-phase telomere tethering by interacting with Sir4-associated chromatin. Because Siz2-dependent SUMOylation of Sir4 facilitates M- and G1-phase telomere tethering (Ptak et al., 2021), it is tempting to speculate that Esc1 may function as a NE anchor that facilitates interactions between proteins involved in NE expansion, such as Spo7/Nem1, and proteins involved in telomere tethering, such as SUMOylated Sir4. If Esc1 interacted with either Nem1 or Spo7, increased, Esc1 protein levels, which promote INM expansion (Hattier, Andrulis, and Tartakoff 2007), could disrupt Nem1 and Spo7 interactions similar to what is observed when SUMOylation events at the NE increase (Chapter 5). Whether these Esc1 interactions are dependent on SUMO:SIM protein networks established during mitosis is unclear, but are a possibility as Esc1 contains both a putative SIM and SUMO site (Q. Zhao et al., 2014). Interestingly, Esc1 is excluded from regions of the NE where membrane expansion occurs, and the exclusion of Esc1 from these regions is lost when Siz2 is absent (Lapetina et al., 2017). As telomeres are unable

to access these regions, normal Esc1 localization may ensure that it can interact with telomere tethering components and PL synthesizing components. The loss of Esc1 exclusion from the NE adjacent to the nucleolus would reduce the availability of Esc1 to interact with these components and could account for the loss of telomere tethering and NE expansion phenotypes that occur when Siz2 activity is absent. Determining whether Esc1 is part of the Scs2-Siz2 complex or SUMO:SIM protein interaction network at the INM will be of interest for future investigation. Identifying protein interacting partners of Spo7 and Nem1 dependent on Siz2-mediated SUMOylation, and the subcellular localization of these proteins, is also predicted to provide important insights into how SUMOylation coordinates the expansion of the NE with NE-chromatin interactions.

6.4 Scs2 is an essential receptor at different subcellular compartments.

VAP family proteins, such as Scs2, bind to FFAT (two phenylalanines in an acidic tract) motifs in interacting partners through their N-terminal MSP (major sperm protein) domain (Christopher J.R. Loewen, Roy, and Levine 2003; Christopher J.R. Loewen and Levine 2005; Kaiser et al., 2005). The function of Scs2 at different subcellular compartments is dependent on interactions with different-FFAT containing proteins (Christopher J.R. Loewen et al., 2007; Stefan et al., 2011). In the cortical ER, Scs2 interacts with the FFAT-motif of Osh3 to facilitate the formation of PI (Stefan et al., 2011) and PC (Tavassoli et al., 2013). Whereas interactions in the peripheral ER between Scs2 and the FFAT-motif of Opi1 promotes the transcription of UAS_{INO} containing PL synthesizing genes (Christopher J.R. Loewen, Roy, and Levine 2003; J. H. Brickner and Walter 2004).

Our work here shows that interactions between Scs2 and Siz2 are also facilitated by MSP:FFAT interactions at the INM. We show that phosphorylation near the FFAT-like motif of Siz2 enhances its binding to the MSP domain of Scs2 (Goto et al., 2012; Kumagai, Kawano-Kawada, and Hanada 2014; Weber-Boyvat et al., 2015; Kirmiz et al., 2018; Di Mattia et al., 2020). As a result, the mitotic phosphorylation of Siz2 regulates a cell cycle specific interaction with the MSP domain of Scs2 to facilitate NE expansion (Chapter 5) and NE-chromatin interactions (Chapter 4). It is interesting to note that in addition to the mitotic functions of Scs2 at the INM, there are also mitotic functions for Scs2 within the cytosol, including regulating the inheritance of the cortical ER and establishing an ER diffusion barrier (Christopher J.R. Loewen et al., 2007; Chao et al., 2014; Neller et al., 2015; Omer, Greenberg, and Lee 2018; Ng, Ng, and Zhang 2020). Therefore, an overarching role for Scs2 may be to facilitate the division of membranes between mother and daughter cells during mitosis. The SUMOylation of Scs2 may be necessary to coordinate the nuclear and cytoplasmic functions of Scs2 in membrane division.

Our observations that Siz2-Scs2 interactions at the INM are specific to mitosis suggest that Scs2 could interact with other nuclear FFAT-containing proteins to facilitate additional nucleoplasmic functions during interphase. Identifying the FFAT interactome of Scs2 at the INM may be critical to elucidating the mechanisms by which Scs2 facilitates NE expansion and/or NE-chromatin interactions and identifying additional functions for Scs2 in the nucleus. The position, sequence, and score of predicted FFAT-like motifs of INM proteins

(Murphy and Levine 2016) may provide important insights into the identity of these interactors.

We show that Scs2-Siz2 interactions facilitate NE expansion by causing a temporal increase of PA at the INM (Chapter 5). As Scs2 has been shown to interact with numerous PA-binding proteins (C. J.R. Loewen et al., 2004; Riekhof et al., 2014), Scs2 may function to enhance PA levels at the INM and promote PA-binding proteins' interactions with the INM during mitosis. Identifying the interactions of Scs2 at the INM could identify novel PA-binding proteins required for various nuclear specific events. Siz2 may be a PA-binding protein itself as its accumulation is coordinated with the INM increase in PA. However, as the enrichment of Siz2 at the INM in the *ulp1* mutant is not maintained (Fig. 5-4) in interphase when PA accumulation is still observed at the INM, this may not necessarily be the case. Another potential INM associated protein capable of binding PA, which may interact with INM associated Scs2, is Chm7. Chm7 has recently been shown to bind to PA at herniations that form when NPC assembly is disrupted (Thaller et al., 2021) where Chm7 is proposed to function in a nuclear surveillance mechanism that promotes NE sealing (Thaller et al., 2019; 2021). Investigating whether Scs2 interacts with Chm7 and contributes to this nuclear surveillance mechanism would represent an additional function for Scs2 at the INM. Therefore, identifying all interacting partners of Scs2 at the INM, in addition to FFAT dependent interactions, will be crucial for identifying the nuclear specific functions of Scs2 at the INM. Recent advances in proximity-labeling in yeast (Larochelle et al., 2019; Yi Li et al., 2020) may provide a feasible method to identify these INM interactions.

Overall, Scs2 and other members of the VAP (Vesicle-associated membrane (VAMP)-Associated Protein) family have a diverse interactome. Importantly, consistent with our results, this interactome is expanding to include proteins at the INM (James and Kehlenbach 2021). Future analysis of the Scs2 interactome will likely provide insights into additional functions for Scs2 at the INM and may elucidate conserved VAP protein functions within the nucleus.

6.5 SUMOylation at the INM during mitosis may be regulating other biological processes.

Our analyses have identified Scs2 and Sir4 as Siz2-mediated SUMOylation targets at the INM. The binding of Siz2 to the INM, however, also facilitates the SUMOylation of several other detectable but, as of yet, unidentified species (Fig. 4-3). As Siz2-mediated SUMOylation and interactions with SUMOylated Scs2 is predicted to generate a SUMO:SIM protein interaction network (Chapter 4), these unidentified SUMOylation species may interact with the Siz2-Scs2 complex. Mass spectrometry analysis to identify NE-proteins that interact with and are SUMOylated by Siz2 during mitosis would provide important insights into how SUMOylation regulates the biological processes described here and identify potentially additional functions for these SUMOylation events. These may include regulating other NE-chromatin interactions such as rDNA and centromeres, or as identified in Table 4-2, the regulation of retrotransposons.

Interestingly, there is an even distribution of Siz2-dependent SUMOylation conjugates at the INM during mitosis (Fig. 4-1). Although this even distribution may represent SUMOylated Scs2, we predict that it also represents other Siz2-

mediated SUMOylation targets that are likely involved in additional functions beyond those described in this thesis. For example, the SUMOylation patterns at the INM do not accumulate in foci like Sir4 or other telomere tethering components. It is tempting to speculate that these SUMOylation targets at the INM may be lamin-like structures. *S. cerevisiae* appears to lack a discernable nuclear lamina. However, lamin-like functions have been proposed for several yeast protein-interaction networks (Diffley and Stillman, 1989; Strambio-de-Castillia, Blobel and Rout, 1999; Taddei et al., 2004; Taddei and Gasser, 2012; Niepel et al., 2013; Van De Vosse et al., 2013). In metazoan cells, lamins provide the nucleus with mechanical strength and provide attachment sites for chromatin. Furthermore, the SUMOylation of lamins is important for maintaining nuclear shape (Zhang and Sarge 2008), similar to the role that Siz2-mediated SUMOylation targets at the NE regulate (Chapter 5). Lamins are also crucial for the attachment of chromatin to the nuclear periphery. Moreover, SUMO:SIM interactions in mammals are required to recruit lamin A to telophase chromosomes (Moriuchi et al., 2016; Moriuchi and Hirose 2021) in a manner analogous to those events reported here (Chapter 4). Therefore, Siz2-mediated SUMOylation events during mitosis may establish a lamin-like network that facilitates chromatin reassociation and contributes to the mechanical strength of the NE (Schreiner et al., 2015). These SUMOylated targets with lamin-like functions could include the already identified SUMOylated proteins, Scs2 and Sir4. Interestingly, Sir4 has been proposed to facilitate lamin-like interactions in yeast (Diffley and Stillman, 1989). Future work to identify other

Siz2-mitotic SUMOylation targets may identify lamin-like protein networks within yeast.

Overall, the data described in this thesis has revealed a previously unrecognized mechanism by which cells coordinate multiple events during cell division, including chromatin association with the NE (Chapter 4) and NE membrane proliferation (Chapter 5). Future work discussed here will expand on these analyses, provide insights into mechanisms that facilitate these functions, and potentially identify additional roles for Siz2-mediated SUMOylation at the INM.

References

- Ahmed, Sara, Donna G. Brickner, William H. Light, Ivelisse Cajigas, Michele McDonough, Alexander B. Froysheter, Tom Volpe, and Jason H. Brickner. 2010. "DNA Zip Codes Control an Ancient Mechanism for Gene Targeting to the Nuclear Periphery." *Nature Cell Biology* 12 (2): 111–18. <https://doi.org/10.1038/ncb2011>.
- Ai, Wandong, Paula G. Bertram, Chi Kwan Tsang, Ting Fung Chan, and X. F. Steven Zheng. 2002. "Regulation of Subtelomeric Silencing during Stress Response." *Molecular Cell* 10 (6): 1295–1305. [https://doi.org/10.1016/S1097-2765\(02\)00695-0](https://doi.org/10.1016/S1097-2765(02)00695-0).
- Aitchison, John D., and Michael P. Rout. 2012. "The Yeast Nuclear Pore Complex and Transport through It." *Genetics* 190 (3): 855–83. <https://doi.org/10.1534/genetics.111.127803>.
- Alber, Frank, Svetlana Dokudovskaya, Liesbeth M. Veenhoff, Wenzhu Zhang, Julia Kipper, Damien Devos, Adisetyantari Suprpto, et al., 2007. "The Molecular Architecture of the Nuclear Pore Complex." *Nature* 450 (7170): 695–701. <https://doi.org/10.1038/nature06405>.
- Albuquerque, Claudio Ponte De, Jason Liang, Nathaniel James Gaut, and Huilin Zhou. 2016. "Molecular Circuitry of the SUMO (Small Ubiquitin-like Modifier) Pathway in Controlling Sumoylation Homeostasis and Suppressing Genome Rearrangements." *Journal of Biological Chemistry* 291 (16): 8825–35. <https://doi.org/10.1074/jbc.M116.716399>.
- Allshire, Robin C., and Hiten D. Madhani. 2018. "Ten Principles of Heterochromatin Formation and Function." *Nature Reviews Molecular Cell Biology* 19 (4): 229–44. <https://doi.org/10.1038/nrm.2017.119>.
- Anamika, and Leo Spyropoulos. 2016. "Molecular Basis for Phosphorylation-Dependent SUMO Recognition by the DNA Repair Protein RAP80." *Journal of Biological Chemistry* 291 (9): 4417–28. <https://doi.org/10.1074/jbc.M115.705061>.
- Andrulis, Erik D., Aaron M. Neiman, David C. Zappulla, and Rolf Sternglanz. 1998. "Perinuclear Localization of Chromatin Facilitates Transcriptional Silencing." *Nature* 394 (6693): 592–95. <https://doi.org/10.1038/29100>.
- Andrulis, Erik D., David C. Zappulla, Athar Ansari, Severine Perrod, Catherine V. Laiosa, Marc R. Gartenberg, and Rolf Sternglanz. 2002. "Esc1, a Nuclear Periphery Protein Required for Sir4-Based Plasmid Anchoring and Partitioning." *Molecular and Cellular Biology* 22 (23): 8292–8301. <https://doi.org/10.1128/mcb.22.23.8292-8301.2002>.
- Aparicio, Oscar M., Barbara L. Billington, and Daniel E. Gottschling. 1991. "Modifiers of Position Effect Are Shared between Telomeric and Silent Mating-Type Loci in *S. Cerevisiae*." *Cell* 66 (6): 1279–87. [https://doi.org/10.1016/0092-8674\(91\)90049-5](https://doi.org/10.1016/0092-8674(91)90049-5).

- Ayaydin, Ferhan, and Mary Dasso. 2004. "Distinct In Vivo Dynamics of Vertebrate SUMO Paralogues." *Molecular Biology of the Cell* 15 (12): 5208–18. <https://doi.org/10.1091/mbc.e04-07-0589>.
- Azad, Gajendra Kumar, and Raghuvir Singh Tomar. 2016. "The Multifunctional Transcription Factor Rap1: A Regulator of Yeast Physiology." *Frontiers in Bioscience - Landmark* 21 (5): 918–30. <https://doi.org/10.2741/4429>.
- Bahmanyar, Shirin, Ronald Biggs, Amber L. Schuh, Arshad Desai, Thomas Müller-Reichert, Anjon Audhya, Jack E. Dixon, and Karen Oegema. 2014. "Spatial Control of Phospholipid Flux Restricts Endoplasmic Reticulum Sheet Formation to Allow Nuclear Envelope Breakdown." *Genes and Development* 28 (2): 121–26. <https://doi.org/10.1101/gad.230599.113>.
- Bahmanyar, Shirin, and Christian Schlieker. 2020. "Lipid and Protein Dynamics That Shape Nuclear Envelope Identity." *Molecular Biology of the Cell* 31 (13): 1315–23. <https://doi.org/10.1091/MBC.E18-10-0636>.
- Baldwin, Melissa L., Jeffrey A. Julius, Xianying Tang, Yanchang Wang, and Jeff Bachant. 2009. "The Yeast SUMO Isopeptidase Smt4/Ulp2 and the Polo Kinase Cdc5 Act in an Opposing Fashion to Regulate Sumoylation in Mitosis and Cohesion at Centromeres." *Cell Cycle* 8 (20): 3406–19. <https://doi.org/10.4161/cc.8.20.9911>.
- Banani, Salman F., Allyson M. Rice, William B. Peeples, Yuan Lin, Saumya Jain, Roy Parker, and Michael K. Rosen. 2016. "Compositional Control of Phase-Separated Cellular Bodies." *Cell* 166 (3): 651–63. <https://doi.org/10.1016/j.cell.2016.06.010>.
- Barbosa, Antonio D., Koini Lim, Muriel Mari, James R. Edgar, Lihi Gal, Peter Sterk, Benjamin J. Jenkins, et al., 2019. "Compartmentalized Synthesis of Triacylglycerol at the Inner Nuclear Membrane Regulates Nuclear Organization." *Developmental Cell* 50 (6): 755-766.e6. <https://doi.org/10.1016/j.devcel.2019.07.009>.
- Barbosa, Antonio Daniel, Hiroshi Sembongi, Wen Min Su, Susana Abreu, Fulvio Reggiori, George M. Carman, and Symeon Siniossoglou. 2015. "Lipid Partitioning at the Nuclear Envelope Controls Membrane Biogenesis." *Molecular Biology of the Cell* 26 (20): 3641–57. <https://doi.org/10.1091/mbc.E15-03-0173>.
- Bayer, Peter, Andreas Arndt, Susanne Metzger, Rohit Mahajan, Frauke Melchior, Rainer Jaenicke, and Jörg Becker. 1998. "Structure Determination of the Small Ubiquitin-Related Modifier SUMO-1." *Journal of Molecular Biology* 280 (2): 275–86. <https://doi.org/10.1006/jmbi.1998.1839>.
- Bernier-Villamor, Victor, Deborah A. Sampson, Michael J. Matunis, and Christopher D. Lima. 2002. "Structural Basis for E2-Mediated SUMO Conjugation Revealed by a Complex between Ubiquitin-Conjugating Enzyme Ubc9 and RanGAP1." *Cell* 108 (3): 345–56.

[https://doi.org/10.1016/S0092-8674\(02\)00630-X](https://doi.org/10.1016/S0092-8674(02)00630-X).

- Blank, Heidi M, Ricardo Perez, Chong He, Nairita Maitra, Richard Metz, Joshua Hill, Yuhong Lin, et al., 2017. “Translational Control of Lipogenic Enzymes in the Cell Cycle of Synchronous, Growing Yeast Cells.” *The EMBO Journal* 36 (4): 487–502. <https://doi.org/10.15252/embj.201695050>.
- Blobel, G. 1985. “Gene Gating: A Hypothesis.” *Proceedings of the National Academy of Sciences of the United States of America* 82 (24): 8527–29. <https://doi.org/10.1073/pnas.82.24.8527>.
- Boeke, Jef D., Joshua Trueheart, Georges Natsoulis, and Gerald R. Fink. 1987. “[10] 5-Fluoroorotic Acid as a Selective Agent in Yeast Molecular Genetics.” *Methods in Enzymology* 154 (C): 164–75. [https://doi.org/10.1016/0076-6879\(87\)54076-9](https://doi.org/10.1016/0076-6879(87)54076-9).
- Bonetti, Diego, Michela Clerici, Nicola Manfrini, Giovanna Lucchini, and Maria Pia Longhese. 2010. “The MRX Complex Plays Multiple Functions in Resection of Yku- and Rif2-Protected DNA Ends.” *PLoS ONE* 5 (11). <https://doi.org/10.1371/journal.pone.0014142>.
- Boni, Andrea, Antonio Z. Politi, Petr Strnad, Wanqing Xiang, MJ Julius Hossain, and Jan Ellenberg. 2015. “Live Imaging and Modeling of Inner Nuclear Membrane Targeting Reveals Its Molecular Requirements in Mammalian Cells.” *Journal of Cell Biology* 209 (5): 705–20. <https://doi.org/10.1083/jcb.201409133>.
- Bonnet, Amandine, Carole Chaput, Noé Palmic, Benoit Palancade, and Pascale Lesage. 2021. “A Nuclear Pore Sub-Complex Restricts the Propagation of Ty Retrotransposons by Limiting Their Transcription.” *PLoS Genetics* 17 (11): 1–27. <https://doi.org/10.1371/journal.pgen.1009889>.
- Boudreau, Émilie, Sarah Labib, Anne T. Bertrand, Valérie Decostre, Pierrette M. Bolongo, Nicolas Sylvius, Gisèle Bonne, and Frédérique Tesson. 2012. “Lamin A/C Mutants Disturb Sumo1 Localization and Sumoylation in Vitro and in Vivo.” *PLoS ONE* 7 (9): 1–9. <https://doi.org/10.1371/journal.pone.0045918>.
- Brickner, Donna G., and Jason H. Brickner. 2012. “Interchromosomal Clustering of Active Genes at the Nuclear Pore Complex.” *Nucleus (United States)* 3 (6). <https://doi.org/10.4161/nucl.22663>.
- Brickner, Donna Garvey, and Jason H. Brickner. 2010. “Cdk Phosphorylation of a Nucleoporin Controls Localization of Active Genes through the Cell Cycle.” *Molecular Biology of the Cell* 21 (19): 3421–32. <https://doi.org/10.1091/mbc.E10-01-0065>.
- Brickner, Donna Garvey, Ivelisse Cajigas, Yvonne Fondufe-Mittendorf, Sara Ahmed, Pei Chih Lee, Jonathan Widom, and Jason H. Brickner. 2007. “H2A.Z-Mediated Localization of Genes at the Nuclear Periphery Confers Epigenetic Memory of Previous Transcriptional State.” *PLoS Biology* 5 (4):

704–16. <https://doi.org/10.1371/journal.pbio.0050081>.

- Brickner, Donna Garvey, Carlo Randise-Hinchliff, Marine Lebrun Corbin, Julie Ming Liang, Stephanie Kim, Bethany Sump, Agustina D’Urso, et al., 2019. “The Role of Transcription Factors and Nuclear Pore Proteins in Controlling the Spatial Organization of the Yeast Genome.” *Developmental Cell* 49 (6): 936–947.e4. <https://doi.org/10.1016/j.devcel.2019.05.023>.
- Brickner, Donna Garvey, Varun Sood, Evelina Tutucci, Robert Coukos, Kayla Viets, Robert H. Singer, and Jason H. Brickner. 2016. “Subnuclear Positioning and Interchromosomal Clustering of the GAL1-10 Locus Are Controlled by Separable, Interdependent Mechanisms.” *Molecular Biology of the Cell* 27 (19): 2980–93. <https://doi.org/10.1091/mbc.E16-03-0174>.
- Brickner, Jason H., and Peter Walter. 2004. “Gene Recruitment of the Activated INO1 Locus to the Nuclear Membrane.” *PLoS Biology* 2 (11). <https://doi.org/10.1371/journal.pbio.0020342>.
- Buchberger, Johannes R., Megumi Onishi, Geng Li, Jan Seebacher, Adam D. Rudner, Steven P. Gygi, and Danesh Moazed. 2008. “Sir3-Nucleosome Interactions in Spreading of Silent Chromatin in *Saccharomyces Cerevisiae*.” *Molecular and Cellular Biology* 28 (22): 6903–18. <https://doi.org/10.1128/mcb.01210-08>.
- Buchwalter, Abigail, Jeanae M. Kaneshiro, and Martin W. Hetzer. 2019. “Coaching from the Sidelines: The Nuclear Periphery in Genome Regulation.” *Nature Reviews Genetics* 20 (1): 39–50. <https://doi.org/10.1038/s41576-018-0063-5>.
- Bupp, Jennifer M., Adriana E. Martin, Elizabeth S. Stensrud, and Sue L. Jaspersen. 2007. “Telomere Anchoring at the Nuclear Periphery Requires the Budding Yeast Sad1-UNC-84 Domain Protein Mps3.” *Journal of Cell Biology* 179 (5): 845–54. <https://doi.org/10.1083/jcb.200706040>.
- Bylebyl, Gwendolyn R., Irina Belichenko, and Erica S. Johnson. 2003. “The SUMO Isopeptidase Ulp2 Prevents Accumulation of SUMO Chains in Yeast.” *Journal of Biological Chemistry* 278 (45): 44113–20. <https://doi.org/10.1074/jbc.M308357200>.
- Bystricky, Kerstin, Patrick Heun, Lutz Gehlen, Jörg Langowski, and Susan M. Gasser. 2004. “Long-Range Compaction and Flexibility of Interphase Chromatin in Budding Yeast Analyzed by High-Resolution Imaging Techniques.” *Proceedings of the National Academy of Sciences of the United States of America* 101 (47): 16495–500. <https://doi.org/10.1073/pnas.0402766101>.
- Bystricky, Kerstin, Thierry Laroche, Griet Van Houwe, Marek Blaszczyk, and Susan M. Gasser. 2005. “Chromosome Looping in Yeast: Telomere Pairing and Coordinated Movement Reflect Anchoring Efficiency and Territorial Organization.” *Journal of Cell Biology* 168 (3): 375–87.

<https://doi.org/10.1083/jcb.200409091>.

- Cabal, Ghislain G., Auguste Genovesio, Susana Rodriguez-Navarro, Christophe Zimmer, Olivier Gadal, Annick Lesne, Henri Buc, et al., 2006. “SAGA Interacting Factors Confine Sub-Diffusion of Transcribed Genes to the Nuclear Envelope.” *Nature* 441 (7094): 770–73.
<https://doi.org/10.1038/nature04752>.
- Campbell, Joseph L., Alexander Lorenz, Keren L. Witkin, Thomas Hays, Josef Loidl, and Orna Cohen-Fix. 2006. “Yeast Nuclear Envelope Subdomains with Distinct Abilities to Resist Membrane Expansion.” *Molecular Biology of the Cell* 17 (4): 1768–78. <https://doi.org/10.1091/mbc.e05-09-0839>.
- Capelson, Maya, Yun Liang, Roberta Schulte, William Mair, Ulrich Wagner, and Martin W. Hetzer. 2010. “Chromatin-Bound Nuclear Pore Components Regulate Gene Expression in Higher Eukaryotes.” *Cell* 140 (3): 372–83.
<https://doi.org/10.1016/j.cell.2009.12.054>.
- Cappadocia, Laurent, Tomasz Kochańczyk, and Christopher D Lima. 2021. “DNA Asymmetry Promotes SUMO Modification of the Single-stranded DNA-binding Protein RPA.” *The EMBO Journal* 40 (22): 1–16.
<https://doi.org/10.15252/emboj.2019103787>.
- Cappadocia, Laurent, Andrea Pichler, and Christopher D. Lima. 2015. “Structural Basis for Catalytic Activation by the Human ZNF451 SUMO E3 Ligase.” *Nature Structural and Molecular Biology* 22 (12): 968–75.
<https://doi.org/10.1038/nsmb.3116>.
- Carman, George M. 2019. “Discoveries of the Phosphatidate Phosphatase Genes in Yeast Published in the Journal of Biological Chemistry.” *Journal of Biological Chemistry* 294 (5): 1681–89.
<https://doi.org/10.1074/jbc.TM118.004159>.
- Carman, George M., and Gil Soo Han. 2011. “Regulation of Phospholipid Synthesis in the Yeast *Saccharomyces Cerevisiae*.” *Annual Review of Biochemistry* 80: 859–83. <https://doi.org/10.1146/annurev-biochem-060409-092229>.
- Champion, Lysie, Sumit Pawar, Naemi Luithle, Rosemarie Ungricht, and Ulrike Kutay. 2019. “Dissociation of Membrane–Chromatin Contacts Is Required for Proper Chromosome Segregation in Mitosis.” *Molecular Biology of the Cell* 30 (4): 427–40. <https://doi.org/10.1091/mbc.E18-10-0609>.
- Chao, Jesse T., Andrew K.O. Wong, Shabnam Tavassoli, Barry P. Young, Adam Chruscicki, Nancy N. Fang, Leann J. Howe, Thibault Mayor, Leonard J. Foster, and Christopher J.R. Loewen. 2014. “Polarization of the Endoplasmic Reticulum by ER-Septin Tethering.” *Cell* 158 (3): 620–32.
<https://doi.org/10.1016/j.cell.2014.06.033>.
- Chen, Jiji, Zhengjian Zhang, Li Li, Bi Chang Chen, Andrey Revyakin, Bassam Hajj, Wesley Legant, et al., 2014. “Single-Molecule Dynamics of

- Enhanceosome Assembly in Embryonic Stem Cells.” *Cell* 156 (6): 1274–85.
<https://doi.org/10.1016/j.cell.2014.01.062>.
- Chen, Miao, and Marc R. Gartenberg. 2014. “Coordination of TRNA Transcription with Export at Nuclear Pore Complexes in Budding Yeast.” *Genes and Development* 28 (9): 959–70.
<https://doi.org/10.1101/gad.236729.113>.
- Chen, Zhaosu, Yunpeng Zhang, Qingqing Guan, Huifang Zhang, Jing Luo, Jialun Li, Wei Wei, et al., 2021. “Linking Nuclear Matrix–Localized PIAS1 to Chromatin SUMOylation via Direct Binding of Histones H3 and H2A.Z.” *Journal of Biological Chemistry* 279 (4): 101200.
<https://doi.org/10.1016/j.jbc.2021.101200>.
- Cheng, Chung Hsu, Yu Hui Lo, Shu Shan Liang, Shih Chieh Ti, Feng Ming Lin, Chia Hui Yeh, Han Yi Huang, and Ting Fang Wang. 2006. “SUMO Modifications Control Assembly of Synaptonemal Complex and Polycomplex in Meiosis of *Saccharomyces Cerevisiae*.” *Genes and Development* 20 (15): 2067–81. <https://doi.org/10.1101/gad.1430406>.
- Cheng, Jinke, Dachun Wang, Zhengxin Wang, and Edward T. H. Yeh. 2004. “SENPI Enhances Androgen Receptor-Dependent Transcription through Desumoylation of Histone Deacetylase 1.” *Molecular and Cellular Biology* 24 (13): 6021–28. <https://doi.org/10.1128/mcb.24.13.6021-6028.2004>.
- Choi, Hyeon Son, Wen Min Su, Gil Soo Han, Devin Plote, Zhi Xu, and George M. Carman. 2012. “Pho85p-Pho80p Phosphorylation of Yeast Pah1p Phosphatidate Phosphatase Regulates Its Activity, Location, Abundance, and Function in Lipid Metabolism.” *Journal of Biological Chemistry* 287 (14): 11290–301. <https://doi.org/10.1074/jbc.M112.346023>.
- Choi, Hyeon Son, Wen Min Su, Jeanelle M. Morgan, Gil Soo Han, Zhi Xu, Eleftherios Karanasios, Symeon Sinioglou, and George M. Carman. 2011. “Phosphorylation of Phosphatidate Phosphatase Regulates Its Membrane Association and Physiological Functions in *Saccharomyces Cerevisiae*: Identification of SER602, THR723, and SER744 as the Sites Phosphorylated by CDC28 (CDK1)-Encoded Cyclin-Dependent Kinase.” *Journal of Biological Chemistry* 286 (2): 1486–98. <https://doi.org/10.1074/jbc.M110.155598>.
- Chojnowski, Alexandre, Peh Fern Ong, Esther S.M. Wong, John S.Y. Lim, Rafidah A. Mutalif, Raju Navasankari, Bamaprasad Dutta, et al., 2015. “Progerin Reduces LAP2 α -Telomere Association in Hutchinson-Gilford Progeria.” *ELife* 4 (AUGUST2015): 1–21.
<https://doi.org/10.7554/eLife.07759>.
- Chubb, Jonathan R., Shelagh Boyle, Paul Perry, and Wendy A. Bickmore. 2002. “Chromatin Motion Is Constrained by Association with Nuclear Compartments in Human Cells.” *Current Biology* 12 (6): 439–45.
[https://doi.org/10.1016/S0960-9822\(02\)00695-4](https://doi.org/10.1016/S0960-9822(02)00695-4).

- Churikov, Dmitri, Ferose Charifi, Nadine Eckert-Boulet, Sonia Silva, Marie Noelle Simon, Michael Lisby, and Vincent Géli. 2016. "SUMO-Dependent Relocalization of Eroded Telomeres to Nuclear Pore Complexes Controls Telomere Recombination." *Cell Reports* 15 (6): 1242–53. <https://doi.org/10.1016/j.celrep.2016.04.008>.
- Chymkowitch, Pierre, Aurélie Nguéa P, Håvard Aanes, Joseph Robertson, Arne Klungland, and Jorrit M. Enserink. 2017. "TORC1-Dependent Sumoylation of Rpc82 Promotes RNA Polymerase III Assembly and Activity." *Proceedings of the National Academy of Sciences of the United States of America* 114 (5): 1039–44. <https://doi.org/10.1073/pnas.1615093114>.
- Cockell, M., F. Palladino, T. Laroche, G. Kyrion, C. Liu, A. J. Lustig, and S. M. Gasser. 1995. "The Carboxy Termini of Sir4 and RAP1 Affect Sir3 Localization: Evidence for a Multicomponent Complex Required for Yeast Telomeric Silencing." *Journal of Cell Biology* 129 (4): 909–24. <https://doi.org/10.1083/jcb.129.4.909>.
- Cornacchia, Daniela, Vishnu Dileep, Jean Pierre Quivy, Rossana Foti, Federico Tili, Rachel Santarella-Mellwig, Claude Antony, Geneviève Almouzni, David M. Gilbert, and Sara B.C. Buonomo. 2012. "Mouse Rif1 Is a Key Regulator of the Replication-Timing Programme in Mammalian Cells." *EMBO Journal* 31 (18): 3678–90. <https://doi.org/10.1038/emboj.2012.214>.
- Crabbe, Laure, Anthony J. Cesare, James M. Kasuboski, James A.J. Fitzpatrick, and Jan Karlseder. 2012. "Human Telomeres Are Tethered to the Nuclear Envelope during Postmitotic Nuclear Assembly." *Cell Reports* 2 (6): 1521–29. <https://doi.org/10.1016/j.celrep.2012.11.019>.
- Cremer, Thomas, Marion Cremer, Steffen Dietzel, Stefan Müller, Irina Solovei, and Stanislav Fakan. 2006. "Chromosome Territories - a Functional Nuclear Landscape." *Current Opinion in Cell Biology* 18 (3): 307–16. <https://doi.org/10.1016/j.ceb.2006.04.007>.
- Cremona, Catherine A., Prabha Sarangi, and Xiaolan Zhao. 2012. "Sumoylation and the DNA Damage Response." *Biomolecules* 2 (3): 376–88. <https://doi.org/10.3390/biom2030376>.
- Cubeñas-Potts, Caelin, and Michael J. Matunis. 2013. "SUMO: A Multifaceted Modifier of Chromatin Structure and Function." *Developmental Cell* 24 (1): 1–12. <https://doi.org/10.1016/j.devcel.2012.11.020>.
- Cuijpers, Sabine A.G., and Alfred C.O. Vertegaal. 2018. "Guiding Mitotic Progression by Crosstalk between Post-Translational Modifications." *Trends in Biochemical Sciences* 43 (4): 251–68. <https://doi.org/10.1016/j.tibs.2018.02.004>.
- D'Urso, Agustina, and Jason H. Brickner. 2017. "Epigenetic Transcriptional Memory." *Current Genetics* 63 (3): 435–39. <https://doi.org/10.1007/s00294-016-0661-8>.

- D'Urso, Agustina, Yoh Hei Takahashi, Bin Xiong, Jessica Marone, Robert Coukos, Carlo Randise-Hinchliff, Ji Ping Wang, Ali Shilatifard, and Jason H. Brickner. 2016. "Set1/COMPASS and Mediator Are Repurposed to Promote Epigenetic Transcriptional Memory." *ELife* 5 (JUN2016): 1–29. <https://doi.org/10.7554/eLife.16691>.
- Damme, Ellen van, Kris Laukens, Thanh Hai Dang, and Xaveer van Ostade. 2010. "A Manually Curated Network of the Pml Nuclear Body Interactome Reveals an Important Role for PML-NBs in SUMOylation Dynamics." *International Journal of Biological Sciences* 6 (1): 51–67. <https://doi.org/10.7150/ijbs.6.51>.
- David, Gregory, Mychell A. Neptune, and Ronald A. Depinho. 2002. "SUMO-1 Modification of Histone Deacetylase 1 (HDAC1) Modulates Its Biological Activities." *Journal of Biological Chemistry* 277 (26): 23658–63. <https://doi.org/10.1074/jbc.M203690200>.
- Dechat, Thomas, Andreas Gajewski, Barbara Korbei, Daniel Gerlich, Nathalie Daigle, Tokuko Haraguchi, Kazuhiro Furukawa, Jan Ellenberg, and Roland Foissner. 2004. "LAP2 α and BAF Transiently Localize to Telomeres and Specific Regions on Chromatin during Nuclear Assembly." *Journal of Cell Science* 117 (25): 6117–28. <https://doi.org/10.1242/jcs.01529>.
- Dechat, Thomas, Katrin Pflieger, Kaushik Sengupta, Takeshi Shimi, Dale K. Shumaker, Liliana Solimando, and Robert D. Goldman. 2008. "Nuclear Lamins: Major Factors in the Structural Organization and Function of the Nucleus and Chromatin." *Genes and Development* 22 (7): 832–53. <https://doi.org/10.1101/gad.1652708>.
- Deng, Min, and Mark Hochstrasser. 2006. "Spatially Regulated Ubiquitin Ligation by an ER/Nuclear Membrane Ligase." *Nature* 443 (7113): 827–31. <https://doi.org/10.1038/nature05170>.
- Denison, Carilee, Adam D. Rudner, Scott A. Gerber, Corey E. Bakalarski, Danesh Moazed, and Steven P. Gygi. 2005. "A Proteomic Strategy for Gaining Insights into Protein Sumoylation in Yeast." *Molecular and Cellular Proteomics* 4 (3): 246–54. <https://doi.org/10.1074/mcp.M400154-MCP200>.
- Desterro, Joana M.P., Manuel S. Rodriguez, and Ronald T. Hay. 1998. "SUMO-1 Modification of I κ B α Inhibits NF-KB Activation." *Molecular Cell* 2 (2): 233–39. [https://doi.org/10.1016/S1097-2765\(00\)80133-1](https://doi.org/10.1016/S1097-2765(00)80133-1).
- Desterro, Joana M.P., Manuel S. Rodriguez, Graham D. Kemp, and Hay Ronald T. 1999. "Identification of the Enzyme Required for Activation of the Small Ubiquitin-like Protein SUMO-1." *Journal of Biological Chemistry* 274 (15): 10618–24. <https://doi.org/10.1074/jbc.274.15.10618>.
- Dey, Prabuddha, Wen-min Su, Mona Mirheydari, X Gil-soo Han, and X George M Carman. 2019. "Protein Kinase C Mediates the Phosphorylation of the Nem1 – Spo7 Protein Phosphatase Complex in Yeast." *Journal of Biological*

- Chemistry* 294 (44): 15997–9. <https://doi.org/10.1074/jbc.RA119.010592>.
- Dieppois, Guennaëlle, Nahid Iglesias, and Françoise Stutz. 2006. “Cotranscriptional Recruitment to the mRNA Export Receptor Mex67p Contributes to Nuclear Pore Anchoring of Activated Genes.” *Molecular and Cellular Biology* 26 (21): 7858–70. <https://doi.org/10.1128/mcb.00870-06>.
- Dilworth, David J., Alan J. Tackett, Richard S. Rogers, Eugene C. Yi, Rowan H. Christmas, Jennifer J. Smith, Andrew F. Siegel, Brian T. Chait, Richard W. Wozniak, and John D. Aitchison. 2005. “The Mobile Nucleoporin Nup2p and Chromatin-Bound Prp20p Function in Endogenous NPC-Mediated Transcriptional Control.” *Journal of Cell Biology* 171 (6): 955–65. <https://doi.org/10.1083/jcb.200509061>.
- Donkor, Jimmy, Meltem Sariahmetoglu, Jay Dewald, David N. Brindley, and Karen Reue. 2007. “Three Mammalian Lipins Act as Phosphatidate Phosphatases with Distinct Tissue Expression Patterns.” *Journal of Biological Chemistry* 282 (6): 3450–57. <https://doi.org/10.1074/jbc.M610745200>.
- Drag, Marcin, and Guy S. Salvesen. 2008. “DeSUMOylating Enzymes - SENPs.” *IUBMB Life* 60 (11): 734–42. <https://doi.org/10.1002/iub.113>.
- Dreger, Mathias, Luiza Bengtsson, Torsten Schöneberg, Henning Otto, and Ferdinand Hucho. 2001. “Nuclear Envelope Proteomics: Novel Integral Membrane Proteins of the Inner Nuclear Membrane.” *Proceedings of the National Academy of Sciences of the United States of America* 98 (21): 11943–48. <https://doi.org/10.1073/pnas.211201898>.
- Duan, Zhijun, Mirela Andronescu, Kevin Schutz, Sean McIlwain, Yoo Jung Kim, Choli Lee, Jay Shendure, Stanley Fields, C. Anthony Blau, and William S. Noble. 2010. “A Three-Dimensional Model of the Yeast Genome.” *Nature* 465 (7296): 363–67. <https://doi.org/10.1038/nature08973>.
- Dubots, Emmanuelle, Stéphanie Cottier, Marie Pierre Péli-Gulli, Malika Jaquenoud, Séverine Bontron, Roger Schneiter, and Claudio De Virgilio. 2014. “TORC1 Regulates Pah1 Phosphatidate Phosphatase Activity via the Nem1/Spo7 Protein Phosphatase Complex.” *PLoS ONE* 9 (8): 1–9. <https://doi.org/10.1371/journal.pone.0104194>.
- Duval, D., G. Duval, C. Kedinger, O. Poch, and H. Boeuf. 2003. “The ‘PINIT’ Motif, of a Newly Identified Conserved Domain of the PIAS Protein Family, Is Essential for Nuclear Retention of PIAS3L.” *FEBS Letters* 554 (1–2): 111–18. [https://doi.org/10.1016/S0014-5793\(03\)01116-5](https://doi.org/10.1016/S0014-5793(03)01116-5).
- Ebrahimi, Hani, and Anne D. Donaldson. 2008. “Release of Yeast Telomeres from the Nuclear Periphery Is Triggered by Replication and Maintained by Suppression of Ku-Mediated Anchoring.” *Genes and Development* 22 (23): 3363–74. <https://doi.org/10.1101/gad.486208>.
- Eckhoff, Julia, and R. Jürgen Dohmen. 2015. “In Vitro Studies Reveal a

- Sequential Mode of Chain Processing by the Yeast SUMO (Small Ubiquitin-Related Modifier)-Specific Protease Ulp2.” *Journal of Biological Chemistry* 290 (19): 12268–81. <https://doi.org/10.1074/jbc.M114.622217>.
- Eisenhardt, Nathalie, Viduth K. Chaugule, Stefanie Koidl, Mathias Droescher, Esen Dogan, Jan Rettich, Päivi Sutinen, et al., 2015. “A New Vertebrate SUMO Enzyme Family Reveals Insights into SUMO-Chain Assembly.” *Nature Structural and Molecular Biology* 22 (12): 959–67. <https://doi.org/10.1038/nsmb.3114>.
- Ellahi, Aisha, Deborah M. Thurtle, and Jasper Rine. 2015. “The Chromatin and Transcriptional Landscape of Native *Saccharomyces Cerevisiae* Telomeres and Subtelomeric Domains.” *Genetics* 200 (2): 505–21. <https://doi.org/10.1534/genetics.115.175711>.
- Elmore, Zachary C., Megan Donaher, Brooke C. Matson, Helen Murphy, Jason W. Westerbeck, and Oliver Kerscher. 2011. “Sumo-Dependent Substrate Targeting of the SUMO Protease Ulp1.” *BMC Biology* 9 (October). <https://doi.org/10.1186/1741-7007-9-74>.
- Encinar del Dedo, Javier, Fatima Zahra Idrissi, Isabel María Fernandez-Golbano, Patricia Garcia, Elena Rebollo, Marek K. Krzyzanowski, Helga Grötsch, and Maria Isabel Geli. 2017. “ORP-Mediated ER Contact with Endocytic Sites Facilitates Actin Polymerization.” *Developmental Cell* 43 (5): 588–602.e6. <https://doi.org/10.1016/j.devcel.2017.10.031>.
- Enserink, Jorrit M. 2015. “Sumo and the Cellular Stress Response.” *Cell Division* 10 (1): 1–13. <https://doi.org/10.1186/s13008-015-0010-1>.
- Fabre, Emmanuelle, Héloïse Muller, Pierre Therizols, Ingrid Lafontaine, Bernard Dujon, and Cécile Fairhead. 2005. “Comparative Genomics in Hemiascomycete Yeasts: Evolution of Sex, Silencing, and Subtelomeres.” *Molecular Biology and Evolution* 22 (4): 856–73. <https://doi.org/10.1093/molbev/msi070>.
- Fagone, Paolo, and Suzanne Jackowski. 2009. “Membrane Phospholipid Synthesis and Endoplasmic Reticulum Function.” *Journal of Lipid Research* 50 (SUPPL.): S311–16. <https://doi.org/10.1194/jlr.R800049-JLR200>.
- Fakas, Stylianos, Yixuan Qiu, Joseph L. Dixon, Gil Soo Han, Kelly V. Ruggles, Jeanne Garbarino, Stephen L. Sturley, and George M. Carman. 2011. “Phosphatidate Phosphatase Activity Plays Key Role in Protection against Fatty Acid-Induced Toxicity in Yeast.” *Journal of Biological Chemistry* 286 (33): 29074–85. <https://doi.org/10.1074/jbc.M111.258798>.
- Falk, Martin, Yana Feodorova, Natalia Naumova, Maxim Imakaev, Bryan R. Lajoie, Heinrich Leonhardt, Boris Joffe, et al., 2019. “Heterochromatin Drives Compartmentalization of Inverted and Conventional Nuclei.” *Nature* 570 (7761): 395–99. <https://doi.org/10.1038/s41586-019-1275-3>.
- Felberbaum, R., J. Peng, M. Hochstrasser, D. Cheng, and N. R. Wilson. 2011.

- “Desumoylation of the Endoplasmic Reticulum Membrane VAP Family Protein Scs2 by Ulp1 and SUMO Regulation of the Inositol Synthesis Pathway.” *Molecular and Cellular Biology* 32 (1): 64–75.
<https://doi.org/10.1128/mcb.05878-11>.
- Ferraz, Luís, Michael Sauer, Maria João Sousa, and Paola Branduardi. 2021. “The Plasma Membrane at the Cornerstone Between Flexibility and Adaptability: Implications for *Saccharomyces Cerevisiae* as a Cell Factory.” *Frontiers in Microbiology* 12 (August): 1–11.
<https://doi.org/10.3389/fmicb.2021.715891>.
- Ferreira, Helder C., Brian Luke, Heiko Schober, Veronique Kalck, Joachim Lingner, and Susan M. Gasser. 2011. “The PIAS Homologue Siz2 Regulates Perinuclear Telomere Position and Telomerase Activity in Budding Yeast.” *Nature Cell Biology* 13 (7): 867–74. <https://doi.org/10.1038/ncb2263>.
- Feuerbach, Frank, Vincent Galy, Edgar Trelles-Sticken, Micheline Fromont-Racine, Alain Jacquier, Eric Gilson, Jean Christophe Olivo-Marin, Harry Scherthan, and Ulf Nehrbass. 2002. “Nuclear Architecture and Spatial Positioning Help Establish Transcriptional States of Telomeres in Yeast.” *Nature Cell Biology* 4 (3): 214–21. <https://doi.org/10.1038/ncb756>.
- Finlan, Lee E., Duncan Sproul, Inga Thomson, Shelagh Boyle, Elizabeth Kerr, Paul Perry, Bauke Ylstra, Jonathan R. Chubb, and Wendy A. Bickmore. 2008. “Recruitment to the Nuclear Periphery Can Alter Expression of Genes in Human Cells.” *PLoS Genetics* 4 (3).
<https://doi.org/10.1371/journal.pgen.1000039>.
- Folz, Hanne, Carlos A. Nino, Surayya Taranum, Stefanie Caesar, Lorenz Latta, François Waharte, Jean Salamero, Gabriel Schlenstedt, and Catherine Dargemont. 2019. “SUMOylation of the Nuclear Pore Complex Basket Is Involved in Sensing Cellular Stresses.” *Journal of Cell Science* 132 (7): 1–11. <https://doi.org/10.1242/jcs.224279>.
- Förstemann, Klaus, and Joachim Lingner. 2001. “Molecular Basis for Telomere Repeat Divergence in Budding Yeast.” *Molecular and Cellular Biology* 21 (21): 7277–86. <https://doi.org/10.1128/mcb.21.21.7277-7286.2001>.
- Freyre, Christophe A.C., Pascal C. Rauher, Christer S. Ejsing, and Robin W. Klemm. 2019. “MIGA2 Links Mitochondria, the ER, and Lipid Droplets and Promotes De Novo Lipogenesis in Adipocytes.” *Molecular Cell* 76 (5): 811–825.e14. <https://doi.org/10.1016/j.molcel.2019.09.011>.
- Galy, Vincent, Olivier Gadai, Micheline Fromont-Racine, Alper Romano, Alain Jacquier, and Ulf Nehrbass. 2004. “Nuclear Retention of Unspliced MRNAs in Yeast Is Mediated by Perinuclear Mlp1.” *Cell* 116 (1): 63–73.
[https://doi.org/10.1016/S0092-8674\(03\)01026-2](https://doi.org/10.1016/S0092-8674(03)01026-2).
- Galy, Vincent, Jean Christophe Olivo-Marin, Harry Scherthan, Valerie Doye, Nadia Rascalou, and Ulf Nehrbass. 2000. “Nuclear Pore Complexes in the

- Organization of Silent Telomeric Chromatin.” *Nature* 403 (6765): 108–12. <https://doi.org/10.1038/47528>.
- Gartenberg, Marc R., Frank R. Neumann, Thierry Laroche, Marek Blaszczyk, and Susan M. Gasser. 2004. “Sir-Mediated Repression Can Occur Independently of Chromosomal and Subnuclear Contexts.” *Cell* 119 (7): 955–67. <https://doi.org/10.1016/j.cell.2004.11.008>.
- Gaspar, Maria L., Yu Fang Chang, Stephen A. Jesch, Manuel Aregullin, and Susan A. Henry. 2017. “Interaction between Repressor Opi1p and ER Membrane Protein Scs2p Facilitates Transit of Phosphatidic Acid from the ER to Mitochondria and Is Essential for INO1 Gene Expression in the Presence of Choline.” *Journal of Biological Chemistry* 292 (45): 1813–18728. <https://doi.org/10.1074/jbc.M117.809970>.
- Geiss-Friedlander, Ruth, and Frauke Melchior. 2007. “Concepts in Sumoylation: A Decade On.” *Nature Reviews Molecular Cell Biology* 8 (12): 947–56. <https://doi.org/10.1038/nrm2293>.
- Ghaemmaghani, Sina, Won Ki Huh, Kiowa Bower, Russell W. Howson, Archana Belle, Noah Dephoure, Erin K. O’Shea, and Jonathan S. Weissman. 2003. “Global Analysis of Protein Expression in Yeast.” *Nature* 425 (6959): 737–41. <https://doi.org/10.1038/nature02046>.
- Gietz, R. Daniel, and Robin A. Woods. 2002. “Transformation of Yeast by Lithium Acetate/Single-Stranded Carrier DNA/Polyethylene Glycol Method.” *Methods in Enzymology* 350 (2001): 87–96. [https://doi.org/10.1016/S0076-6879\(02\)50957-5](https://doi.org/10.1016/S0076-6879(02)50957-5).
- Golden, Andy, Jun Liu, and Orna Cohen-Fix. 2009. “Inactivation of the C. Elegans Lipin Homolog Leads to ER Disorganization and to Defects in the Breakdown and Reassembly of the Nuclear Envelope.” *Journal of Cell Science* 122 (12): 1970–78. <https://doi.org/10.1242/jcs.044743>.
- Gong, Limin, Bing Li, Stefanos Millas, and Edward T.H. Yeh. 1999. “Molecular Cloning and Characterization of Human AOS1 and UBA2, Components of the Sentrin-Activating Enzyme Complex.” *FEBS Letters* 448 (1): 185–89. [https://doi.org/10.1016/S0014-5793\(99\)00367-1](https://doi.org/10.1016/S0014-5793(99)00367-1).
- González-Prieto, Román, Karolin Eifler-Olivi, Laura A. Claessens, Edwin Willemstein, Zhenyu Xiao, Cami M.P. Talavera Ormeno, Huib Ovaa, Helle D. Ulrich, and Alfred C.O. Vertegaal. 2021. “Global Non-Covalent SUMO Interaction Networks Reveal SUMO-Dependent Stabilization of the Non-Homologous End Joining Complex.” *Cell Reports* 34 (4). <https://doi.org/10.1016/j.celrep.2021.108691>.
- Gorjánác, Mátyás, and Iain W. Mattaj. 2009. “Lipin Is Required for Efficient Breakdown of the Nuclear Envelope in Caenorhabditis Elegans.” *Journal of Cell Science* 122 (12): 1963–69. <https://doi.org/10.1242/jcs.044750>.
- Goto, Asako, Xinwei Liu, Carolyn Ann Robinson, and Neale D. Ridgway. 2012.

- “Multisite Phosphorylation of Oxysterol-Binding Protein Regulates Sterol Binding and Activation of Sphingomyelin Synthesis.” *Molecular Biology of the Cell* 23 (18): 3624–35. <https://doi.org/10.1091/mbc.E12-04-0283>.
- Graves, J. Anthony, and Susan A. Henry. 2000. “Regulation of the Yeast INO1 Gene: The Products of the INO2, INO4 and OPI1 Regulatory Genes Are Not Required for Repression in Response to Inositol.” *Genetics* 154 (4): 1485–95. <https://doi.org/10.1093/genetics/154.4.1485>.
- Grégoire, Serge, Annie M. Tremblay, Lin Xiao, Qian Yang, Kewei Ma, Jianyun Nie, Zixu Mao, Zhenguo Wu, Vincent Giguère, and Xiang Jiao Yang. 2006. “Control of MEF2 Transcriptional Activity by Coordinated Phosphorylation and Sumoylation.” *Journal of Biological Chemistry* 281 (7): 4423–33. <https://doi.org/10.1074/jbc.M509471200>.
- Grimsey, Neil, Gil Soo Han, Laura O’Hara, Justin J. Rochford, George M. Carman, and Symeon Siniossoglou. 2008. “Temporal and Spatial Regulation of the Phosphatidate Phosphatases Lipin 1 and 2.” *Journal of Biological Chemistry* 283 (43): 29166–74. <https://doi.org/10.1074/jbc.M804278200>.
- Gruenbaum, Yosef, and Roland Foissner. 2015. “Lamins: Nuclear Intermediate Filament Proteins with Fundamental Functions in Nuclear Mechanics and Genome Regulation.” *Annual Review of Biochemistry* 84: 131–64. <https://doi.org/10.1146/annurev-biochem-060614-034115>.
- Gruenbaum, Yosef, Robert D. Goldman, Ronit Meyuhas, Erez Mills, Ayelet Margalit, Alexandra Fridkin, Yaron Dayani, Miron Prokocimer, and Avital Enosh. 2003. “The Nuclear Lamina and Its Functions in the Nucleus.” *International Review of Cytology* 226: 1–62. [https://doi.org/10.1016/S0074-7696\(03\)01001-5](https://doi.org/10.1016/S0074-7696(03)01001-5).
- Haider, Afreen, Yu Chen Wei, Koini Lim, Antonio D. Barbosa, Che Hsiung Liu, Ursula Weber, Marek Mlodzik, et al., 2018. “PCYT1A Regulates Phosphatidylcholine Homeostasis from the Inner Nuclear Membrane in Response to Membrane Stored Curvature Elastic Stress.” *Developmental Cell* 45 (4): 481–495.e8. <https://doi.org/10.1016/j.devcel.2018.04.012>.
- Han, Gil Soo, and George M. Carman. 2017. “Yeast PAH1-Encoded Phosphatidate Phosphatase Controls the Expression of CHO1-Encoded Phosphatidylserine Synthase for Membrane Phospholipid Synthesis.” *Journal of Biological Chemistry* 292 (32): 13230–42. <https://doi.org/10.1074/jbc.M117.801720>.
- Han, Gil Soo, Laura O’Hara, George M. Carman, and Symeon Siniossoglou. 2008. “An Unconventional Diacylglycerol Kinase That Regulates Phospholipid Synthesis and Nuclear Membrane Growth.” *Journal of Biological Chemistry* 283 (29): 20433–42. <https://doi.org/10.1074/jbc.M802903200>.
- Han, Gil Soo, Symeon Siniossoglou, and George M. Carman. 2007. “The Cellular

- Functions of the Yeast Lipin Homolog Pah1p Are Dependent on Its Phosphatidate Phosphatase Activity.” *Journal of Biological Chemistry* 282 (51): 37026–35. <https://doi.org/10.1074/jbc.M705777200>.
- Han, Gil Soo, Wen I. Wu, and George M. Carman. 2006. “The *Saccharomyces Cerevisiae* Lipin Homolog Is a Mg²⁺-Dependent Phosphatidate Phosphatase Enzyme.” *Journal of Biological Chemistry* 281 (14): 9210–18. <https://doi.org/10.1074/jbc.M600425200>.
- Hang, Lisa E, Xianpeng Liu, Iris Cheung, Yan Yang, and Xiaolan Zhao. 2011. “SUMOylation Regulates Telomere Length Homeostasis by Targeting Cdc13.” *Nature Structural & Molecular Biology* 18 (8): 920–26. <https://doi.org/10.1038/nsmb.2100>.
- Hannich, J. Thomas, Alaron Lewis, Mary B. Kroetz, Shyr Jiann Li, Heinrich Heide, Andrew Emili, and Mark Hochstrasser. 2005. “Defining the SUMO-Modified Proteome by Multiple Approaches in *Saccharomyces Cerevisiae*.” *Journal of Biological Chemistry* 280 (6): 4102–10. <https://doi.org/10.1074/jbc.M413209200>.
- Hansen, Anders S., Claudia Cattoglio, Xavier Darzacq, and Robert Tjian. 2018. “Recent Evidence That TADs and Chromatin Loops Are Dynamic Structures.” *Nucleus* 9 (1): 20–32. <https://doi.org/10.1080/19491034.2017.1389365>.
- Harris, Thurl E., Todd A. Huffman, An Chi, Jeffrey Shabanowitz, Donald F. Hunt, Anil Kumar, and John C. Lawrence. 2007. “Insulin Controls Subcellular Localization and Multisite Phosphorylation of the Phosphatidic Acid Phosphatase, Lipin 1.” *Journal of Biological Chemistry* 282 (1): 277–86. <https://doi.org/10.1074/jbc.M609537200>.
- Hassaninasab, Azam, Gil Soo Han, and George M. Carman. 2017. “Tips on the Analysis of Phosphatidic Acid by the Fluorometric Coupled Enzyme Assay.” *Analytical Biochemistry* 526 (28314): 69–70. <https://doi.org/10.1016/j.ab.2017.03.020>.
- Hasslacher, M., A. S. Ivessa, F. Paltauf, and S. D. Kohlwein. 1993. “Acetyl-CoA Carboxylase from Yeast Is an Essential Enzyme and Is Regulated by Factors That Control Phospholipid Metabolism.” *Journal of Biological Chemistry* 268 (15): 10946–52. [https://doi.org/10.1016/s0021-9258\(18\)82077-4](https://doi.org/10.1016/s0021-9258(18)82077-4).
- Hattier, Thomas, Erik D. Andrulis, and Alan M. Tartakoff. 2007. “Immobility, Inheritance and Plasticity of Shape of the Yeast Nucleus.” *BMC Cell Biology* 8: 1–17. <https://doi.org/10.1186/1471-2121-8-47>.
- Hay, Ronald Thomas. 2007. “SUMO-Specific Proteases: A Twist in the Tail.” *Trends in Cell Biology* 17 (8): 370–76. <https://doi.org/10.1016/j.tcb.2007.08.002>.
- Hecker, Christina Maria, Matthias Rabiller, Kaisa Haglund, Peter Bayer, and Ivan Dikic. 2006. “Specification of SUMO1- and SUMO2-Interacting Motifs.”

- Journal of Biological Chemistry* 281 (23): 16117–27.
<https://doi.org/10.1074/jbc.M512757200>.
- Hediger, Florence, Frank R. Neumann, Griet Van Houwe, Karine Dubrana, and Susan M. Gasser. 2002. “Live Imaging of Telomeres.” *Current Biology* 12 (24): 2076–89. [https://doi.org/10.1016/s0960-9822\(02\)01338-6](https://doi.org/10.1016/s0960-9822(02)01338-6).
- Hendriks, Ivo A., and Alfred C.O. Vertegaal. 2016. *Label-Free Identification and Quantification of SUMO Target Proteins. Methods in Molecular Biology*. Vol. 1475. https://doi.org/10.1007/978-1-4939-6358-4_13.
- Hennekes, Hartwig, Matthias Peter, Klaus Weber, and Erich A. Nigg. 1993. “Phosphorylation on Protein Kinase C Sites Inhibits Nuclear Import of Lamin B2.” *Journal of Cell Biology* 120 (6): 1293–1304. <https://doi.org/10.1083/jcb.120.6.1293>.
- Henry, Susan A., Sepp D. Kohlwein, and George M. Carman. 2012. “Metabolism and Regulation of Glycerolipids in the Yeast *Saccharomyces Cerevisiae*.” *Genetics* 190 (2): 317–49. <https://doi.org/10.1534/genetics.111.130286>.
- Herbert, Sébastien, Alice Brion, Jean-Michel Arbona, Mickaël Lelek, Adeline Veillet, Benoît Lelandais, Jyotsana Parmar, et al., 2017. “Chromatin Stiffening Underlies Enhanced Locus Mobility after DNA Damage in Budding Yeast.” *The EMBO Journal* 36 (17): 2595–2608. <https://doi.org/10.15252/embj.201695842>.
- Hetzer, Martin W. 2010. “The Nuclear Envelope.” *Cold Spring Harbor Perspectives in Biology* 2 (3): 1–16. <https://doi.org/10.1101/cshperspect.a000539>.
- Hetzer, Martin W., Tobias C. Walther, and Iain W. Mattaj. 2005. “Pushing the Envelope: Structure, Function, and Dynamics of the Nuclear Periphery.” *Annual Review of Cell and Developmental Biology* 21: 347–80. <https://doi.org/10.1146/annurev.cellbio.21.090704.151152>.
- Heun, P., T. Laroche, K. Shimada, P. Furrer, and S. M. Gasser. 2001. “Chromosome Dynamics in the Yeast Interphase Nucleus.” *Science* 294 (5549): 2181–86. <https://doi.org/10.1126/science.1065366>.
- Hietakangas, Ville, Julius Anckar, Henri A. Blomster, Mitsuaki Fujimoto, Jorma J. Palvimo, Akira Nakai, and Lea Sistonen. 2006. “PDSM, a Motif for Phosphorylation-Dependent SUMO Modification.” *Proceedings of the National Academy of Sciences of the United States of America* 103 (1): 45–50. <https://doi.org/10.1073/pnas.0503698102>.
- Hochstrasser, Mark. 2000. “Evolution and Function of Ubiquitin-like Protein-Conjugation Systems” 2 (August): 153–57.
- Hoegge, Carsten, Boris Pfander, George Lucian Moldovan, George Pyrowolakis, and Stefan Jentsch. 2002. “RAD6-Dependent DNA Repair Is Linked to Modification of PCNA by Ubiquitin and SUMO.” *Nature* 419 (6903): 135–

41. <https://doi.org/10.1038/nature00991>.
- Hofbauer, Harald F., Florian H. Schopf, Hannes Schleifer, Oskar L. Knittelfelder, Bartholomäus Pieber, Gerald N. Rechberger, Heimo Wolinski, et al., 2014. “Regulation of Gene Expression through a Transcriptional Repressor That Senses Acyl-Chain Length in Membrane Phospholipids.” *Developmental Cell* 29 (6): 729–39. <https://doi.org/10.1016/j.devcel.2014.04.025>.
- Holt, Liam J, Brian B Tuch, Judit Villén, Alexander D Johnson, Steven P Gygi, and David O Morgan. 2009. “Global Analysis of Cdk1 Substrate Phosphorylation Sites Provides Insights into Evolution.” *Science* 325 (5948): 1682–86. <https://doi.org/10.1126/science.1172867>.
- Horigome, Chihiro, Denise E. Bustard, Isabella Marcomini, Neda Delgoshai, Monika Tsai-Pflugfelder, Jennifer A. Cobb, and Susan M. Gasser. 2016. “PolySUMOylation by Siz2 and Mms21 Triggers Relocation of DNA Breaks to Nuclear Pores through the Slx5/Slx8 STUbL.” *Genes and Development* 30 (8): 931–45. <https://doi.org/10.1101/gad.277665.116>.
- Hsieh, Lu Sheng, Wen Min Su, Gil Soo Han, and George M. Carman. 2015. “Phosphorylation Regulates the Ubiquitin-Independent Degradation of Yeast Pah1 Phosphatidate Phosphatase by the 20S Proteasome.” *Journal of Biological Chemistry* 290 (18): 11467–78. <https://doi.org/10.1074/jbc.M115.648659>.
- . 2016. “Phosphorylation of Yeast Pah1 Phosphatidate Phosphatase by Casein Kinase II Regulates Its Function in Lipid Metabolism.” *Journal of Biological Chemistry* 291 (19): 9974–90. <https://doi.org/10.1074/jbc.M116.726588>.
- Huang, Lixia, Songguang Yang, Shengchun Zhang, Ming Liu, Jianbin Lai, Yanli Qi, Songfeng Shi, et al., 2009. “The Arabidopsis SUMO E3 Ligase AtMMS21, a Homologue of NSE2/MMS21, Regulates Cell Proliferation in the Root.” *Plant Journal* 60 (4): 666–78. <https://doi.org/10.1111/j.1365-313X.2009.03992.x>.
- Huffman, Todd A., Isabelle Mothe-Satney, and John C. Lawrence. 2002. “Insulin-Stimulated Phosphorylation of Lipin Mediated by the Mammalian Target of Rapamycin.” *Proceedings of the National Academy of Sciences of the United States of America* 99 (2): 1047–52. <https://doi.org/10.1073/pnas.022634399>.
- Ibarra, Arkaitz, Chris Benner, Swati Tyagi, Jonah Cool, and Martin W. Hetzer. 2016. “Nucleoporin-Mediated Regulation of Cell Identity Genes.” *Genes and Development* 30 (20): 2253–58. <https://doi.org/10.1101/gad.287417.116>.
- Ibarra, Arkaitz, and Martin W. Hetzer. 2015. “Nuclear Pore Proteins and the Control of Genome Functions.” *Genes and Development* 29 (4): 337–49. <https://doi.org/10.1101/gad.256495.114>.
- Imai, Shin-ichiro, Christopher M Armstrong, Matt Kaeberlein, and Leonard Guarente. 2000. “Transcriptional Silencing and Longevity Protein Sir2 Is an

- NAD-Dependent Histone Deacetylase.” *Nature* 403 (6771): 795–800.
<https://doi.org/10.1038/35001622>.
- Impens, Francis, Lilliana Radoshevich, Pascale Cossart, and David Ribet. 2014. “Mapping of SUMO Sites and Analysis of SUMOylation Changes Induced by External Stimuli.” *Proceedings of the National Academy of Sciences of the United States of America* 111 (34): 12432–37.
<https://doi.org/10.1073/pnas.1413825111>.
- Iouk, Tatiana, Oliver Kerscher, Robert J. Scott, Munira A. Basrai, and Richard W. Wozniak. 2002. “The Yeast Nuclear Pore Complex Functionally Interacts with Components of the Spindle Assembly Checkpoint.” *Journal of Cell Biology* 159 (5): 807–19. <https://doi.org/10.1083/jcb.200205068>.
- James, Christina, and Ralph H. Kehlenbach. 2021. “The Interactome of the VAP Family of Proteins: An Overview.” *Cells* 10 (7).
<https://doi.org/10.3390/cells10071780>.
- Jentsch, Stefan, and Ivan Psakhye. 2013. “Control of Nuclear Activities by Substrate-Selective and Protein-Group SUMOylation.” *Annual Review of Genetics* 47: 167–86. <https://doi.org/10.1146/annurev-genet-111212-133453>.
- Jentsch, Stefan, and George Pyrowolakis. 2000. “Ubiquitin and Its Kin: How Close Are the Family Ties?” *Trends in Cell Biology* 10 (8): 335–42.
[https://doi.org/10.1016/S0962-8924\(00\)01785-2](https://doi.org/10.1016/S0962-8924(00)01785-2).
- Johnson, E. S., and G. Blobel. 1997. “Ubc9p Is the Conjugating Enzyme for the Ubiquitin-like Protein Smt3p.” *Journal of Biological Chemistry* 272 (43): 26799–802. <https://doi.org/10.1074/jbc.272.43.26799>.
- Johnson, Erica S. 2004. “Protein Modification by SUMO.” *Annual Review of Biochemistry* 73: 355–82.
<https://doi.org/10.1146/annurev.biochem.73.011303.074118>.
- Johnson, Erica S., and Günter Blobel. 1999. “Cell Cycle-Regulated Attachment of the Ubiquitin-Related Protein SUMO to the Yeast Septins.” *Journal of Cell Biology* 147 (5): 981–93. <https://doi.org/10.1083/jcb.147.5.981>.
- Johnson, Erica S., and Aseem A. Gupta. 2001. “An E3-like Factor That Promotes SUMO Conjugation to the Yeast Septins.” *Cell* 106 (6): 735–44.
[https://doi.org/10.1016/S0092-8674\(01\)00491-3](https://doi.org/10.1016/S0092-8674(01)00491-3).
- Johnson, Erica S., Ingrid Schwienhorst, R. Jürgen Dohmen, and Günter Blobel. 1997. “The Ubiquitin-like Protein Smt3p Is Activated for Conjugation to Other Proteins by an Aos1p/Uba2p Heterodimer.” *EMBO Journal* 16 (18): 5509–19. <https://doi.org/10.1093/emboj/16.18.5509>.
- Kabachinski, Greg, and Thomas U. Schwartz. 2015. “The Nuclear Pore Complex - Structure and Function at a Glance.” *Journal of Cell Science* 128 (3): 423–29. <https://doi.org/10.1242/jcs.083246>.
- Kaiser, Stephen E., Jason H. Brickner, Amy R. Reilein, Tim D. Fenn, Peter

- Walter, and Axel T. Brunger. 2005. "Structural Basis of FFAT Motif-Mediated ER Targeting." *Structure* 13 (7): 1035–45. <https://doi.org/10.1016/j.str.2005.04.010>.
- Kalverda, Bernike, Helen Pickersgill, Victor V. Shloma, and Maarten Fornerod. 2010. "Nucleoporins Directly Stimulate Expression of Developmental and Cell-Cycle Genes Inside the Nucleoplasm." *Cell* 140 (3): 360–71. <https://doi.org/10.1016/j.cell.2010.01.011>.
- Kaminker, Patrick G., Sahn Ho Kim, Pierre Yves Desprez, and Judith Campisi. 2009. "A Novel Form of the Telomere-Associated Protein TIN2 Localizes to the Nuclear Matrix." *Cell Cycle* 8 (6): 931–39. <https://doi.org/10.4161/cc.8.6.7941>.
- Karanasios, Eleftherios, Gil Soo Han, Zhi Xu, George M. Carman, and Symeon Siniouoglou. 2010. "A Phosphorylation-Regulated Amphipathic Helix Controls the Membrane Translocation and Function of the Yeast Phosphatidate Phosphatase." *Proceedings of the National Academy of Sciences of the United States of America* 107 (41): 17539–44. <https://doi.org/10.1073/pnas.1007974107>.
- Katta, Santharam S., Christine J. Smoyer, and Sue L. Jaspersen. 2014. "Destination: Inner Nuclear Membrane." *Trends in Cell Biology* 24 (4): 221–29. <https://doi.org/10.1016/j.tcb.2013.10.006>.
- Kelley, Joshua B., Sutirtha Datta, Chelsi J. Snow, Mandovi Chatterjee, Li Ni, Adam Spencer, Chun-Song Yang, Caelin Cubeñas-Potts, Michael J. Matunis, and Bryce M. Paschal. 2011. "The Defective Nuclear Lamina in Hutchinson-Gilford Progeria Syndrome Disrupts the Nucleocytoplasmic Ran Gradient and Inhibits Nuclear Localization of Ubc9." *Molecular and Cellular Biology* 31 (16): 3378–95. <https://doi.org/10.1128/mcb.05087-11>.
- Kim, Youngjun, Matthew S. Gentry, Thurl E. Harris, Sandra E. Wiley, John C. Lawrence, and Jack E. Dixon. 2007. "A Conserved Phosphatase Cascade That Regulates Nuclear Membrane Biogenesis." *Proceedings of the National Academy of Sciences of the United States of America* 104 (16): 6596–6601. <https://doi.org/10.1073/pnas.0702099104>.
- Kimura, Akatsuki, Takashi Umehara, and Masami Horikoshi. 2002. "Chromosomal Gradient of Histone Acetylation Established by Sas2p and Sir2p Functions as a Shield against Gene Silencing." *Nature Genetics* 32 (3): 370–77. <https://doi.org/10.1038/ng993>.
- King, Megan C., C. Patrick Lusk, and Günter Blobel. 2006. "Karyopherin-Mediated Import of Integral Inner Nuclear Membrane Proteins." *Nature* 442 (7106): 1003–7. <https://doi.org/10.1038/nature05075>.
- Kirmiz, Michael, Nicholas C. Vierra, Stephanie Palacio, and James S. Trimmer. 2018. "Identification of VAPA and VAPB as Kv2 Channel-Interacting Proteins Defining Endoplasmic Reticulum–Plasma Membrane Junctions in

- Mammalian Brain Neurons.” *Journal of Neuroscience* 38 (35): 7562–84.
<https://doi.org/10.1523/JNEUROSCI.0893-18.2018>.
- Kirsh, Olivier, Jacob S. Seeler, Andrea Pichler, Andreas Gast, Stefan Müller, Eric Miska, Marion Mathieu, et al., 2002. “The SUMO E3 Ligase RanBP2 Promotes Modification of the HDAC4 Deacetylase.” *EMBO Journal* 21 (11): 2682–91. <https://doi.org/10.1093/emboj/21.11.2682>.
- Klug, Lisa, and Günther Daum. 2014. “Yeast Lipid Metabolism at a Glance.” *FEMS Yeast Research* 14 (3): 369–88. <https://doi.org/10.1111/1567-1364.12141>.
- Knockenbauer, Kevin E., and Thomas U. Schwartz. 2016. “The Nuclear Pore Complex as a Flexible and Dynamic Gate.” *Cell* 164 (6): 1162–71.
<https://doi.org/10.1016/j.cell.2016.01.034>.
- Köhler, Alwin, and Ed Hurt. 2007. “Exporting RNA from the Nucleus to the Cytoplasm.” *Nature Reviews Molecular Cell Biology* 8 (10): 761–73.
<https://doi.org/10.1038/nrm2255>.
- Kooijman, Edgar E., D. Peter Tieleman, Christa Testerink, Teun Munnik, Dirk T.S. Rijkers, Koert N.J. Burger, and Ben De Kruijff. 2007. “An Electrostatic/Hydrogen Bond Switch as the Basis for the Specific Interaction of Phosphatidic Acid with Proteins.” *Journal of Biological Chemistry* 282 (15): 11356–64. <https://doi.org/10.1074/jbc.M609737200>.
- Krull, Sandra, Julia Dörries, Björn Boysen, Sonja Reidenbach, Lars Magnus, Helene Norder, Johan Thyberg, and Volker C. Cordes. 2010. “Protein Tpr Is Required for Establishing Nuclear Pore-Associated Zones of Heterochromatin Exclusion.” *EMBO Journal* 29 (10): 1659–73.
<https://doi.org/10.1038/emboj.2010.54>.
- Kumagai, Keigo, Miyuki Kawano-Kawada, and Kentaro Hanada. 2014. “Phosphoregulation of the Ceramide Transport Protein CERT at Serine 315 in the Interaction with VAMP-Associated Protein (VAP) for Inter-Organellar Trafficking of Ceramide in Mammalian Cells.” *Journal of Biological Chemistry* 289 (15): 10748–60. <https://doi.org/10.1074/jbc.M113.528380>.
- Kumaran, R. Ileng, and David L. Spector. 2008. “A Genetic Locus Targeted to the Nuclear Periphery in Living Cells Maintains Its Transcriptional Competence.” *Journal of Cell Biology* 180 (1): 51–65.
<https://doi.org/10.1083/jcb.200706060>.
- Kuo, Mei Ling, Willem Den Besten, Mary C. Thomas, and Charles J. Sherr. 2008. “Arf-Induced Turnover of the Nucleolar Nucleophosmin-Associated SUMO-2/3 Protease Snp3.” *Cell Cycle* 7 (21): 3378–87.
<https://doi.org/10.4161/cc.7.21.6930>.
- Kupiec, Martin. 2014. “Biology of Telomeres: Lessons from Budding Yeast.” *FEMS Microbiology Reviews* 38 (2): 144–71. <https://doi.org/10.1111/1574-6976.12054>.

- Kwiatk, Joanna M., Gil Soo Han, and George M. Carman. 2020. "Phosphatidate-Mediated Regulation of Lipid Synthesis at the Nuclear/Endoplasmic Reticulum Membrane." *Biochimica et Biophysica Acta - Molecular and Cell Biology of Lipids* 1865 (1). <https://doi.org/10.1016/j.bbaliip.2019.03.006>.
- Laganowsky, Arthur, Eamonn Reading, Timothy M. Allison, Martin B. Ulmschneider, Matteo T. Degiacomi, Andrew J. Baldwin, and Carol V. Robinson. 2014. "Membrane Proteins Bind Lipids Selectively to Modulate Their Structure and Function." *Nature* 510 (7503): 172–75. <https://doi.org/10.1038/nature13419>.
- Lange, T. De. 1992. "Human Telomeres Are Attached to the Nuclear Matrix." *EMBO Journal* 11 (2): 717–24. <https://doi.org/10.1002/j.1460-2075.1992.tb05104.x>.
- Lapetina, Diego L., Christopher Ptak, Ulyss K. Roesner, and Richard W. Wozniak. 2017. "Yeast Silencing Factor Sir4 and a Subset of Nucleoporins Form a Complex Distinct from Nuclear Pore Complexes." *Journal of Cell Biology* 216 (10): 3145–59. <https://doi.org/10.1083/jcb.201609049>.
- Laroche, Thierry, Sophie G. Martin, Monika Tsai-Pflugfelder, and Susan M. Gasser. 2000. "The Dynamics of Yeast Telomeres and Silencing Proteins through the Cell Cycle." *Journal of Structural Biology* 129 (2–3): 159–74. <https://doi.org/10.1006/jsbi.2000.4240>.
- Larochelle, Marc, Danny Bergeron, Bruno Arcand, and François Bachand. 2019. "Proximity-Dependent Biotinylation Mediated by TurboID to Identify Protein-Protein Interaction Networks in Yeast." *Journal of Cell Science* 132 (11). <https://doi.org/10.1242/jcs.232249>.
- Lascorz, Jara, Joan Codina-fabra, David Reverter, and Jordi Torres-rosell. 2021. "Seminars in Cell and Developmental Biology SUMO-SIM Interactions : From Structure to Biological Functions," no. September.
- Leibundgut, Marc, Timm Maier, Simon Jenni, and Nenad Ban. 2008. "The Multienzyme Architecture of Eukaryotic Fatty Acid Synthases." *Current Opinion in Structural Biology* 18 (6): 714–25. <https://doi.org/10.1016/j.sbi.2008.09.008>.
- Levy, Daniel L., and Elizabeth H. Blackburn. 2004. "Counting of Rif1p and Rif2p on *Saccharomyces Cerevisiae* Telomeres Regulates Telomere Length ." *Molecular and Cellular Biology* 24 (24): 10857–67. <https://doi.org/10.1128/mcb.24.24.10857-10867.2004>.
- Lewis, Alaron, Rachael Felberbaum, and Mark Hochstrasser. 2007. "A Nuclear Envelope Protein Linking Nuclear Pore Basket Assembly, SUMO Protease Regulation, and mRNA Surveillance." *Journal of Cell Biology* 178 (5): 813–27. <https://doi.org/10.1083/jcb.200702154>.
- Li, Shang, Svetlana Makovets, Tetsuya Matsuguchi, Justin D. Blethrow, Kevan M. Shokat, and Elizabeth H. Blackburn. 2009. "Cdk1-Dependent

- Phosphorylation of Cdc13 Coordinates Telomere Elongation during Cell-Cycle Progression.” *Cell* 136 (1): 50–61.
<https://doi.org/10.1016/j.cell.2008.11.027>.
- Li, Shyr-Jiann, and Mark Hochstrasser. 2000. “The Yeast ULP2 (SMT4) Gene Encodes a Novel Protease Specific for the Ubiquitin-Like Smt3 Protein .” *Molecular and Cellular Biology* 20 (7): 2367–77.
<https://doi.org/10.1128/mcb.20.7.2367-2377.2000>.
- Li, Shyr Jiann, and Mark Hochstrasser. 1999. “A New Protease Required for Cell-Cycle Progression in Yeast.” *Nature* 398 (6724): 246–51.
<https://doi.org/10.1038/18457>.
- . 2003. “The Ulp1 SUMO Isopeptidase: Distinct Domains Required for Viability, Nuclear Envelope Localization, and Substrate Specificity.” *Journal of Cell Biology* 160 (7): 1069–81.
<https://doi.org/10.1083/jcb.200212052>.
- Li, Yi, Caiping Tian, Keke Liu, Ying Zhou, Jing Yang, and Peng Zou. 2020. “A Clickable APEX Probe for Proximity-Dependent Proteomic Profiling in Yeast.” *Cell Chemical Biology* 27 (7): 858-865.e8.
<https://doi.org/10.1016/j.chembiol.2020.05.006>.
- Li, Yunong, Xiuxing Jiang, Yanhao Zhang, Ziyi Gao, Yanxia Liu, Jinjiao Hu, Xiaoye Hu, and Lirong Li. 2019. “Nuclear Accumulation of UBC9 Contributes to SUMOylation of Lamin A / C and Nucleophagy in Response to DNA Damage” 8: 1–14.
- Liang, Ya Chen, Chia Chin Lee, Ya Li Yao, Chien Chen Lai, M. Lienhard Schmitz, and Wen Ming Yang. 2016. “SUMO5, a Novel Poly-SUMO Isoform, Regulates PML Nuclear Bodies.” *Scientific Reports* 6: 1–15.
<https://doi.org/10.1038/srep26509>.
- Light, William H., Donna G. Brickner, Veronica R. Brand, and Jason H. Brickner. 2010. “Interaction of a DNA Zip Code with the Nuclear Pore Complex Promotes H2A.Z Incorporation and INO1 Transcriptional Memory.” *Molecular Cell* 40 (1): 112–25. <https://doi.org/10.1016/j.molcel.2010.09.007>.
- Light, William H., and Jason H. Brickner. 2013. “Nuclear Pore Proteins Regulate Chromatin Structure and Transcriptional Memory by a Conserved Mechanism.” *Nucleus (United States)* 4 (5): 357–60.
<https://doi.org/10.4161/nucl.26209>.
- Lin, Donghai, Michael H. Tatham, Bin Yu, Suhkmann Kim, Ronald T. Hay, and Y. Yuan Chen. 2002. “Identification of a Substrate Recognition Site on Ubc9.” *Journal of Biological Chemistry* 277 (24): 21740–48.
<https://doi.org/10.1074/jbc.M108418200>.
- Lin, Jue, Dana L. Smith, and Elizabeth H. Blackburn. 2004. “Mutant Telomere Sequences Lead to Impaired Chromosome Separation and a Unique Checkpoint Response.” *Molecular Biology of the Cell* 15 (4): 1623–34.

<https://doi.org/10.1091/mbc.e03-10-0740>.

- Lin, Weiyang, and Gilbert Arthur. 2007. "Phospholipids Are Synthesized in the G2/M Phase of the Cell Cycle." *International Journal of Biochemistry and Cell Biology* 39 (3): 597–605. <https://doi.org/10.1016/j.biocel.2006.10.011>.
- Lin, Y. P., and G. M. Carman. 1989. "Purification and Characterization of Phosphatidate Phosphatase from *Saccharomyces Cerevisiae*." *Journal of Biological Chemistry* 264 (15): 8641–45. [https://doi.org/10.1016/s0021-9258\(18\)81840-3](https://doi.org/10.1016/s0021-9258(18)81840-3).
- Liou, Gunn Guang, Jason C. Tanny, Ryan G. Kruger, Thomas Walz, and Danesh Moazed. 2005. "Assembly of the SIR Complex and Its Regulation by O-Acetyl-ADP-Ribose, a Product of NAD-Dependent Histone Deacetylation." *Cell* 121 (4): 515–27. <https://doi.org/10.1016/j.cell.2005.03.035>.
- Liu, Guang Hui, and Larry Gerace. 2009. "Sumoylation Regulates Nuclear Localization of Lipin-1 α in Neuronal Cells." *PLoS ONE* 4 (9): 1–10. <https://doi.org/10.1371/journal.pone.0007031>.
- Livak, Kenneth J., and Thomas D. Schmittgen. 2001. "Analysis of Relative Gene Expression Data Using Real-Time Quantitative PCR and the 2- $\Delta\Delta$ CT Method." *Methods* 25 (4): 402–8. <https://doi.org/10.1006/meth.2001.1262>.
- Lo, Wan Sheng, Eric R. Gamache, Karl W. Henry, David Yang, Lorraine Pillus, and Shelley L. Berger. 2005. "Histone H3 Phosphorylation Can Promote TBP Recruitment through Distinct Promoter-Specific Mechanisms." *EMBO Journal* 24 (5): 997–1008. <https://doi.org/10.1038/sj.emboj.7600577>.
- Loewen, C. J.R., M. L. Gazpar, S. A. Jesch, C. Delon, N. T. Ktistakis, S. A. Henry, and T. P. Levine. 2004. "Phospholipid Metabolism Regulated by a Transcription Factor Sensing Phosphatidic Acid." *Science* 304 (5677): 1644–47. <https://doi.org/10.1126/science.1096083>.
- Loewen, Christopher J.R., Jesse T. Chao, Thibault Mayor, Andrew K.O. Wong, Leonard J. Foster, Barry P. Young, Adam Chruscicki, Nancy N. Fang, LeAnn J. Howe, and Shabnam Tavassoli. 2014. "Polarization of the Endoplasmic Reticulum by ER-Septin Tethering." *Cell* 158 (3): 620–32. <https://doi.org/10.1016/j.cell.2014.06.033>.
- Loewen, Christopher J.R., and Timothy P. Levine. 2005. "A Highly Conserved Binding Site in Vesicle-Associated Membrane Protein-Associated Protein (VAP) for the FFAT Motif of Lipid-Binding Proteins." *Journal of Biological Chemistry* 280 (14): 14097–104. <https://doi.org/10.1074/jbc.M500147200>.
- Loewen, Christopher J.R., Anjana Roy, and Timothy P. Levine. 2003. "A Conserved ER Targeting Motif in Three Families of Lipid Binding Proteins and in Opi1p Binds VAP." *EMBO Journal* 22 (9): 2025–35. <https://doi.org/10.1093/emboj/cdg201>.
- Loewen, Christopher J.R., Barry P. Young, Shabnam Tavassoli, and Timothy P.

- Levine. 2007. "Inheritance of Cortical ER in Yeast Is Required for Normal Septin Organization." *Journal of Cell Biology* 179 (3): 467–83. <https://doi.org/10.1083/jcb.200708205>.
- Longtine, Mark S., Amos McKenzie, Douglas J. Demarini, Nirav G. Shah, Achim Wach, Arndt Brachat, Peter Philippsen, and John R. Pringle. 1998. "Additional Modules for Versatile and Economical PCR-Based Gene Deletion and Modification in *Saccharomyces Cerevisiae*." *Yeast* 14 (10): 953–61. [https://doi.org/10.1002/\(SICI\)1097-0061\(199807\)14:10<953::AID-YEA293>3.0.CO;2-U](https://doi.org/10.1002/(SICI)1097-0061(199807)14:10<953::AID-YEA293>3.0.CO;2-U).
- Luo, Kunheng, Miguel A. Vega-Palas, and Michael Grunstein. 2002. "Rap1-Sir4 Binding Independent of Other Sir, YKu, or Histone Interactions Initiates the Assembly of Telomeric Heterochromatin in Yeast." *Genes and Development* 16 (12): 1528–39. <https://doi.org/10.1101/gad.988802>.
- Lusk, C. Patrick, Günter Blobel, and Megan C. King. 2007. "Highway to the Inner Nuclear Membrane: Rules for the Road." *Nature Reviews Molecular Cell Biology* 8 (5): 414–20. <https://doi.org/10.1038/nrm2165>.
- Luthra, Roopa, Shana C. Kerr, Michelle T. Harreman, Luciano H. Apponi, Milo B. Fasken, Suneela Ramineni, Shyam Chaurasia, Sandro R. Valentini, and Anita H. Corbett. 2007. "Actively Transcribed GAL Genes Can Be Physically Linked to the Nuclear Pore by the SAGA Chromatin Modifying Complex." *Journal of Biological Chemistry* 282 (5): 3042–49. <https://doi.org/10.1074/jbc.M608741200>.
- Mahajan, Rohit, Christian Delphin, Tinglu Guan, Larry Gerace, and Frauke Melchior. 1997. "A Small Ubiquitin-Related Polypeptide Involved in Targeting RanGAP1 to Nuclear Pore Complex Protein RanBP2." *Cell* 88 (1): 97–107. [https://doi.org/10.1016/S0092-8674\(00\)81862-0](https://doi.org/10.1016/S0092-8674(00)81862-0).
- Mahajan, Rohit, Larry Gerace, and Frauke Melchior. 1998. "Molecular Characterization of the SUMO-1 Modification of RanGAP1 and Its Role in Nuclear Envelope Association." *Journal of Cell Biology* 140 (2): 259–70. <https://doi.org/10.1083/jcb.140.2.259>.
- Maillet, Laurent, Cécile Boscheron, Monica Gotta, Stéphane Marcand, Eric Gilson, and Susan M. Gasser. 1996. "Evidence for Silencing Compartments within the Yeast Nucleus: A Role for Telomere Proximity and Sir Protein Concentration in Silencer-Mediated Repression." *Genes and Development* 10 (14): 1796–1811. <https://doi.org/10.1101/gad.10.14.1796>.
- Mak, H. Craig, Lorraine Pillus, and Trey Ideker. 2009. "Dynamic Reprogramming of Transcription Factors to and from the Subtelomere." *Genome Research* 19 (6): 1014–25. <https://doi.org/10.1101/gr.084178.108>.
- Makarova, Maria, Ying Gu, Jun Song Chen, Janel Renée Beckley, Kathleen Louise Gould, and Snezhana Oliferenko. 2016. "Temporal Regulation of Lipin Activity Diverged to Account for Differences in Mitotic Programs."

- Current Biology* 26 (2): 237–43. <https://doi.org/10.1016/j.cub.2015.11.061>.
- Makatsori, Dimitra, Niki Kourmouli, Hara Polioudaki, Leonard D. Shultz, Kelvin McLean, Panayiotis A. Theodoropoulos, Prim B. Singh, and Spyros D. Georgatos. 2004. “The Inner Nuclear Membrane Protein Lamin B Receptor Forms Distinct Microdomains and Links Epigenetically Marked Chromatin to the Nuclear Envelope.” *Journal of Biological Chemistry* 279 (24): 25567–73. <https://doi.org/10.1074/jbc.M313606200>.
- Makhnevych, Taras, Christopher Ptak, C. Patrick Lusk, John D. Aitchison, and Richard W. Wozniak. 2007. “The Role of Karyopherins in the Regulated Sumoylation of Septins.” *Journal of Cell Biology* 177 (1): 39–49. <https://doi.org/10.1083/jcb.200608066>.
- Makhnevych, Taras, Yaroslav Sydorsky, Xiaofeng Xin, Tharan Srikumar, Franco J. Vizeacoumar, Stanley M. Jeram, Zhijian Li, et al., 2009. “Global Map of SUMO Function Revealed by Protein-Protein Interaction and Genetic Networks.” *Molecular Cell* 33 (1): 124–35. <https://doi.org/10.1016/j.molcel.2008.12.025>.
- Makio, Tadashi, and Richard W. Wozniak. 2020. “Passive Diffusion through Nuclear Pore Complexes Regulates Levels of the Yeast SAGA and SLIK Coactivator Complexes.” *Journal of Cell Science* 133 (6). <https://doi.org/10.1242/jcs.237156>.
- Male, Gurranna, Pallavi Deolal, Naresh Kumar Manda, Shantam Yagnik, Aprotim Mazumder, and Krishnaveni Mishra. 2021. “Nucleolar Size Regulates Nuclear Envelope Shape in *Saccharomyces Cerevisiae*.” *Journal of Cell Science* 133 (20): 1–13. <https://doi.org/10.1242/jcs.242172>.
- Mall, Moritz, Thomas Walter, Mátyás Gorjánác, Iain F. Davidson, Thi Bach Nga Ly-Hartig, Jan Ellenberg, and Iain W. Mattaj. 2012. “Mitotic Lamin Disassembly Is Triggered by Lipid-Mediated Signaling.” *Journal of Cell Biology* 198 (6): 981–90. <https://doi.org/10.1083/jcb.201205103>.
- Manford, Andrew G., Christopher J. Stefan, Helen L. Yuan, Jason A. MacGurn, and Scott D. Emr. 2012. “ER-to-Plasma Membrane Tethering Proteins Regulate Cell Signaling and ER Morphology.” *Developmental Cell* 23 (6): 1129–40. <https://doi.org/10.1016/j.devcel.2012.11.004>.
- Manhas, Savrina, Lina Ma, and Vivien Measday. 2018. “The Yeast Tyl1 Retrotransposon Requires Components of the Nuclear Pore Complex for Transcription and Genomic Integration.” *Nucleic Acids Research* 46 (7): 3552–78. <https://doi.org/10.1093/nar/gky109>.
- Marcand, Stéphane, Benjamin Pardo, Ariane Gratiás, Sabrina Cahun, and Isabelle Callebaut. 2008. “Multiple Pathways Inhibit NHEJ at Telomeres.” *Genes and Development* 22 (9): 1153–58. <https://doi.org/10.1101/gad.455108>.
- Matic, Ivan, Joost Schimmel, Ivo A. Hendriks, Maria A. van Santen, Frans van de Rijke, Hans van Dam, Florian Gnad, Matthias Mann, and Alfred C.O.

- Vertegaal. 2010. "Site-Specific Identification of SUMO-2 Targets in Cells Reveals an Inverted SUMOylation Motif and a Hydrophobic Cluster SUMOylation Motif." *Molecular Cell* 39 (4): 641–52. <https://doi.org/10.1016/j.molcel.2010.07.026>.
- Mattia, Thomas Di, Arthur Martinet, Souade Ikhlef, Alastair G McEwen, Yves Nominé, Corinne Wendling, Pierre Poussin-Courmontagne, et al., 2020. "FFAT Motif Phosphorylation Controls Formation and Lipid Transfer Function of Inter-organelle Contacts." *The EMBO Journal* 39 (23): 1–29. <https://doi.org/10.15252/emj.2019104369>.
- Matunis, Michael J., Elias Coutavas, and Günter Blobel. 1996. "A Novel Ubiquitin-like Modification Modulates the Partitioning of the Ran-GTPase-Activating Protein RanGAP1 between the Cytosol and the Nuclear Pore Complex." *Journal of Cell Biology* 135 (6): 1457–70. <https://doi.org/10.1083/jcb.135.6.1457>.
- Matunis, Michael J., Xiang Dong Zhang, and Nathan A. Ellis. 2006. "SUMO: The Glue That Binds." *Developmental Cell* 11 (5): 596–97. <https://doi.org/10.1016/j.devcel.2006.10.011>.
- Mautsa, Nicodemus, Earl Prinsloo, Özlem Tastan Bishop, and Gregory L. Blatch. 2011. "The PINIT Domain of PIAS3: Structure-Function Analysis of Its Interaction with STAT3." *Journal of Molecular Recognition* 24 (5): 795–803. <https://doi.org/10.1002/jmr.1111>.
- Mekhail, Karim, Jan Seebacher, Steven P. Gygi, and Danesh Moazed. 2008. "Role for Perinuclear Chromosome Tethering in Maintenance of Genome Stability." *Nature* 456 (7222): 667–70. <https://doi.org/10.1038/nature07460>.
- Merta, Holly, Jake W. Carrasquillo Rodríguez, Maya I. Anjur-Dietrich, Tevis Vitale, Mitchell E. Granade, Thurl E. Harris, Daniel J. Needleman, and Shirin Bahmanyar. 2021. "Cell Cycle Regulation of ER Membrane Biogenesis Protects against Chromosome Missegregation." *Developmental Cell* 56 (24): 3364–3379.e10. <https://doi.org/10.1016/j.devcel.2021.11.009>.
- Mieczkowski, Piotr A., Joanna O. Mieczkowska, Margaret Dominska, and Thomas D. Petes. 2003. "Genetic Regulation of Telomere-Telomere Fusions in the Yeast *Saccharomyces Cerevisiae*." *Proceedings of the National Academy of Sciences of the United States of America* 100 (19): 10854–59. <https://doi.org/10.1073/pnas.1934561100>.
- Mimitou, Eleni P., and Lorraine S. Symington. 2010. "Ku Prevents Exo1 and Sgs1-Dependent Resection of DNA Ends in the Absence of a Functional MRX Complex or Sae2." *EMBO Journal* 29 (19): 3358–69. <https://doi.org/10.1038/emboj.2010.193>.
- Min, Jaewon, Woodring E. Wright, and Jerry W. Shay. 2019. "Clustered Telomeres in Phase-Separated Nuclear Condensates Engage Mitotic DNA Synthesis through BLM and RAD52." *Genes and Development* 33 (13–14):

- 814–27. <https://doi.org/10.1101/gad.324905.119>.
- Mishra, Krishnaveni, and David Shore. 1999. “Yeast Ku Protein Plays a Direct Role in Telomeric Silencing and Counteracts Inhibition by Rif Proteins.” *Current Biology* 9 (19): 1123–26. [https://doi.org/10.1016/S0960-9822\(99\)80483-7](https://doi.org/10.1016/S0960-9822(99)80483-7).
- Misteli, Tom. 2020. “The Self-Organizing Genome: Principles of Genome Architecture and Function.” *Cell* 183 (1): 28–45. <https://doi.org/10.1016/j.cell.2020.09.014>.
- Mohideen, Firaz, Allan D. Capili, Parizad M. Bilimoria, Tomoko Yamada, Azad Bonni, and Christopher D. Lima. 2009. “A Molecular Basis for Phosphorylation-Dependent SUMO Conjugation by the E2 UBC9.” *Nature Structural and Molecular Biology* 16 (9): 945–52. <https://doi.org/10.1038/nsmb.1648>.
- Moldovan, George Lucian, Boris Pfander, and Stefan Jentsch. 2006. “PCNA Controls Establishment of Sister Chromatid Cohesion during S Phase.” *Molecular Cell* 23 (5): 723–32. <https://doi.org/10.1016/j.molcel.2006.07.007>.
- Moradi-Fard, Sarah, Jessica Sarthi, Mireille Tittel-Elmer, Maxime Lalonde, Emilio Cusanelli, Pascal Chartrand, and Jennifer A. Cobb. 2016. “Smc5/6 Is a Telomere-Associated Complex That Regulates Sir4 Binding and TPE.” *PLoS Genetics* 12 (8): 1–22. <https://doi.org/10.1371/journal.pgen.1006268>.
- Moretti, Paolo, Katie Freeman, Lavanya Coodly, and David Shore. 1994. “Evidence That a Complex of SIR Proteins Interacts with the Silencer and Telomere-Binding Protein RAP1.” *Genes and Development* 8 (19): 2257–69. <https://doi.org/10.1101/gad.8.19.2257>.
- Moriuchi, Takanobu, and Fumiko Hirose. 2021. “SUMOylation of RepoMan during Late Telophase Regulates Dephosphorylation of Lamin A.” *Journal of Cell Science* 134 (17): 1–15. <https://doi.org/10.1242/jcs.247171>.
- Moriuchi, Takanobu, Masaki Kuroda, Fumiya Kusumoto, Takashi Osumi, and Fumiko Hirose. 2016. “Lamin A Reassembly at the End of Mitosis Is Regulated by Its SUMO-Interacting Motif.” *Experimental Cell Research* 342 (1): 83–94. <https://doi.org/10.1016/j.yexcr.2016.02.016>.
- Morris, Joanna R., Chris Boutell, Melanie Keppler, Ruth Densham, Daniel Weekes, Amin Alamshah, Laura Butler, et al., 2009. “The SUMO Modification Pathway Is Involved in the BRCA1 Response to Genotoxic Stress.” *Nature* 462 (7275): 886–90. <https://doi.org/10.1038/nature08593>.
- Mossessova, Elena, and Christopher D. Lima. 2000. “Ulp1-SUMO Crystal Structure and Genetic Analysis Reveal Conserved Interactions and a Regulatory Element Essential for Cell Growth in Yeast.” *Molecular Cell* 5 (5): 865–76. [https://doi.org/10.1016/S1097-2765\(00\)80326-3](https://doi.org/10.1016/S1097-2765(00)80326-3).
- Murphy, Sarah E., and Tim P. Levine. 2016. “VAP, a Versatile Access Point for

- the Endoplasmic Reticulum: Review and Analysis of FFAT-like Motifs in the VAPome.” *Biochimica et Biophysica Acta - Molecular and Cell Biology of Lipids* 1861 (8): 952–61. <https://doi.org/10.1016/j.bbalip.2016.02.009>.
- Naik, Mandar T., Che Chang Chang, Nandita M. Naik, Camy C.H. Kung, Hsiu Ming Shih, and Tai Huang Huang. 2011. “NMR Chemical Shift Assignments of a Complex between SUMO-1 and SIM Peptide Derived from the C-Terminus of Daxx.” *Biomolecular NMR Assignments* 5 (1): 75–77. <https://doi.org/10.1007/s12104-010-9271-4>.
- Nathan, Dafna, Kristin Ingvarsdottir, David E. Sterner, Gwendolyn R. Bylebyl, Milos Dokmanovic, Jean A. Dorsey, Kelly A. Whelan, et al., 2006. “Histone Sumoylation Is a Negative Regulator in *Saccharomyces Cerevisiae* and Shows Dynamic Interplay with Positive-Acting Histone Modifications.” *Genes and Development* 20 (8): 966–76. <https://doi.org/10.1101/gad.1404206>.
- Neller, Joachim, Alexander Dünkler, Reinhild Rösler, and Nils Johnsson. 2015. “A Protein Complex Containing Eplp Anchors the Cortical Endoplasmic Reticulum to the Yeast Bud Tip.” *Journal of Cell Biology* 208 (1): 71–87. <https://doi.org/10.1083/jcb.201407126>.
- Németh, Attila, and Gernot Längst. 2011. “Genome Organization in and around the Nucleolus.” *Trends in Genetics* 27 (4): 149–56. <https://doi.org/10.1016/j.tig.2011.01.002>.
- Neumann, Frank R., Vincent Dion, Lutz R. Gehlen, Monika Tsai-Pflugfelder, Roger Schmid, Angela Taddei, and Susan M. Gasser. 2012. “Targeted INO80 Enhances Subnuclear Chromatin Movement and Ectopic Homologous Recombination.” *Genes and Development* 26 (4): 369–83. <https://doi.org/10.1101/gad.176156.111>.
- Ng, Annabel Qi En, Amanda Yunn Ee Ng, and Dan Zhang. 2020. “Plasma Membrane Furrows Control Plasticity of ER-PM Contacts.” *Cell Reports* 30 (5): 1434-1446.e7. <https://doi.org/10.1016/j.celrep.2019.12.098>.
- Nie, Minghua, and Michael N. Boddy. 2015. “Pli1PIAS1 SUMO Ligase Protected by the Nuclear Pore-Associated SUMO Protease Ulp1SEN1/2.” *Journal of Biological Chemistry* 290 (37): 22678–85. <https://doi.org/10.1074/jbc.M115.673038>.
- Niepel, Mario, Kelly R. Molloy, Rosemary Williams, Julia C. Farrc, Anne C. Meinema, Nicholas Vecchietti, Ileana M. Cristea, Brian T. Chait, Michael P. Rout, and Caterina Strambio-De-Castillia. 2013. “The Nuclear Basket Proteins Mlp1p and Mlp2p Are Part of a Dynamic Interactome Including Esc1p and the Proteasome.” *Molecular Biology of the Cell* 24 (24): 3920–38. <https://doi.org/10.1091/mbc.E13-07-0412>.
- Nikolova, Vesna, Christiana Leimena, Aisling C. McMahon, Ju Chiat Tan, Suchitra Chandar, Dilesh Jogia, Scott H. Kesteven, et al., 2004. “Defects in

- Nuclear Structure and Function Promote Dilated Cardiomyopathy in Lamin A/C-Deficient Mice.” *Journal of Clinical Investigation* 113 (3): 357–69. <https://doi.org/10.1172/JCI200419448>.
- Noordermeer, Daan, Jocelyne Boulay, Michal Sobecki, Charbel Souaid, Laure Crabbe, and Vincent Guerineau. 2018. “MadID, a Versatile Approach to Map Protein-DNA Interactions, Highlights Telomere-Nuclear Envelope Contact Sites in Human Cells.” *Cell Reports* 25 (10): 2891-2903.e5. <https://doi.org/10.1016/j.celrep.2018.11.027>.
- O’Hara, Laura, Gil Soo Han, Peak Chew Sew, Neil Grimsey, George M. Carman, and Symeon Siniosoglou. 2006. “Control of Phospholipid Synthesis by Phosphorylation of the Yeast Lipin Pah1p/Smp2p Mg²⁺-Dependent Phosphatidate Phosphatase.” *Journal of Biological Chemistry* 281 (45): 34537–48. <https://doi.org/10.1074/jbc.M606654200>.
- Ohba, Tomoyuki, Eric C. Schirmer, Takeharu Nishimoto, and Larry Gerace. 2004. “Energy- and Temperature-Dependent Transport of Integral Proteins to the Inner Nuclear Membrane via the Nuclear Pore.” *Journal of Cell Biology* 167 (6): 1051–62. <https://doi.org/10.1083/jcb.200409149>.
- Okubo, Seiji, Futoshi Hara, Yuki Tsuchida, Sakurako Shimotakahara, Sakura Suzuki, Hideki Hatanaka, Shigeyuki Yokoyama, Hirofumi Tanaka, Hideyo Yasuda, and Heisaburo Shindo. 2004. “NMR Structure of the N-Terminal Domain of SUMO Ligase PIAS1 and Its Interaction with Tumor Suppressor P53 and A/T-Rich DNA Oligomers.” *Journal of Biological Chemistry* 279 (30): 31455–61. <https://doi.org/10.1074/jbc.M403561200>.
- Olins, Ada L., Gale Rhodes, David B. Mark Welch, Monika Zwerger, and Donald E. Olins. 2010. “Lamin B Receptor Multi-Tasking at the Nuclear Envelope.” *Nucleus* 1 (1): 53–70. <https://doi.org/10.4161/nucl.1.1.10515>.
- Omer, Safia, Samuel R. Greenberg, and Wei Lih Lee. 2018. “Cortical Dynein Pulling Mechanism Is Regulated by Differentially Targeted Attachment Molecule Num1.” *ELife* 7: 1–30. <https://doi.org/10.7554/eLife.36745>.
- Onischenko, Evgeny, Leslie H. Stanton, Alexis S. Madrid, Thomas Kieselbach, and Karsten Weis. 2009. “Role of the Ndc1 Interaction Network in Yeast Nuclear Pore Complex Assembly and Maintenance.” *Journal of Cell Biology* 185 (3): 475–91. <https://doi.org/10.1083/jcb.200810030>.
- Östlund, Cecilia, Teresa Sullivan, Colin L. Stewart, and Howard J. Worman. 2006. “Dependence of Diffusional Mobility of Integral Inner Nuclear Membrane Proteins on A-Type Lamins.” *Biochemistry* 45 (5): 1374–82. <https://doi.org/10.1021/bi052156n>.
- Palancade, Benoit, Xianpeng Liu, Maria Garcia-Rubio, Andrés Aguilera, Xiaolan Zhao, and Valérie Doye. 2007. “Nucleoporins Prevent DNA Damage Accumulation by Modulating Ulp1-Dependent Sumoylation Processes.” Edited by Karsten Weis. *Molecular Biology of the Cell* 18 (8): 2912–23.

<https://doi.org/10.1091/mbc.e07-02-0123>.

- Panse, V. G., Bernhard Küster, Thomas Gerstberger, and Ed Hurt. 2003. "Unconventional Tethering of Ulp1 to the Transport Channel of the Nuclear Pore Complex by Karyopherins." *Nature Cell Biology* 5 (1): 21–27. <https://doi.org/10.1038/ncb893>.
- Panse, Vikram Govind, Ulrike Hardeland, Thilo Werner, Bernhard Kuster, and Ed Hurt. 2004. "A Proteome-Wide Approach Identifies Sumoylated Substrate Proteins in Yeast." *Journal of Biological Chemistry* 279 (40): 41346–51. <https://doi.org/10.1074/jbc.M407950200>.
- Papouli, Efterpi, Shuhua Chen, Adelina A. Davies, Diana Huttner, Lumir Krejci, Patrick Sung, and Helle D. Ulrich. 2005. "Crosstalk between SUMO and Ubiquitin on PCNA Is Mediated by Recruitment of the Helicase Srs2p." *Molecular Cell* 19 (1): 123–33. <https://doi.org/10.1016/j.molcel.2005.06.001>.
- Parada, L A, P G McQueen, and T Misteli. 2004. "Genome Biology | Full Text | Tissue-Specific Spatial Organization of Genomes." *Genome Biology*, 1–9. <http://www.biomedcentral.com/1465-6906/5/R44>.
- Pardo, Benjamin, and Stéphane Marcand. 2005. "Rap1 Prevents Telomere Fusions by Nonhomologous End Joining." *EMBO Journal* 24 (17): 3117–27. <https://doi.org/10.1038/sj.emboj.7600778>.
- Pascual, Florencia, Aníbal Soto-Cardalda, and George M. Carman. 2013. "PAH1-Encoded Phosphatidate Phosphatase Plays a Role in the Growth Phase- and Inositol-Mediated Regulation of Lipid Synthesis in *Saccharomyces Cerevisiae*." *Journal of Biological Chemistry* 288 (50): 35781–92. <https://doi.org/10.1074/jbc.M113.525766>.
- Pasupala, Nagesh, Sreesankar Easwaran, Abdul Hannan, David Shore, and Krishnaveni Mishra. 2012. "The SUMO E3 Ligase Siz2 Exerts a Locus-Dependent Effect on Gene Silencing in *Saccharomyces Cerevisiae*." *Eukaryotic Cell* 11 (4): 452–62. <https://doi.org/10.1128/EC.05243-11>.
- Pennock, Erin, Kathleen Buckley, and Victoria Lundblad. 2001. "Cdc13 Delivers Separate Complexes to the Telomere for End Protection and Replication." *Cell* 104 (3): 387–96. [https://doi.org/10.1016/S0092-8674\(01\)00226-4](https://doi.org/10.1016/S0092-8674(01)00226-4).
- Peric-Hupkes, Daan, Wouter Meuleman, Ludo Pagie, Sophia W.M. Bruggeman, Irina Solovei, Wim Brugman, Stefan Gräf, et al., 2010. "Molecular Maps of the Reorganization of Genome-Nuclear Lamina Interactions during Differentiation." *Molecular Cell* 38 (4): 603–13. <https://doi.org/10.1016/j.molcel.2010.03.016>.
- Péterfy, M., J. Phan, P. Xu, and K. Reue. 2001. "Lipodystrophy in the Fld Mouse Results from Mutation of a New Gene Encoding a Nuclear Protein, Lipin." *Nature Genetics* 27 (1): 121–24. <https://doi.org/10.1038/83685>.
- Peterson, Timothy R., Shomit S. Sengupta, Thurl E. Harris, Anne E. Carmack,

- Seong A. Kang, Eric Balderas, David A. Guertin, et al., 2011. “MTOR Complex 1 Regulates Lipin 1 Localization to Control the Srebp Pathway.” *Cell* 146 (3): 408–20. <https://doi.org/10.1016/j.cell.2011.06.034>.
- Pfander, Boris, George Lucian Moldovan, Meik Sacher, Carsten Hoege, and Stefan Jentsch. 2005. “SUMO-Modified PCNA Recruits Srs2 to Prevent Recombination during S Phase.” *Nature* 436 (7049): 428–33. <https://doi.org/10.1038/nature03665>.
- Pichler, Andrea, Chronis Fatouros, Heekyoung Lee, and Nathalie Eisenhardt. 2017. “SUMO Conjugation - A Mechanistic View.” *Biomolecular Concepts* 8 (1): 13–36. <https://doi.org/10.1515/bmc-2016-0030>.
- Pichler, Andrea, Puck Knipscheer, Edith Oberhofer, Willem J. Van Dijk, Roman Körner, Jesper Velgaard Olsen, Stefan Jentsch, Frauke Melchior, and Titia K. Sixma. 2005. “SUMO Modification of the Ubiquitin-Conjugating Enzyme E2-25K.” *Nature Structural and Molecular Biology* 12 (3): 264–69. <https://doi.org/10.1038/nsmb903>.
- Pichler, Andrea, Puck Knipscheer, Hisato Saitoh, Titia K. Sixma, and Frauke Melchior. 2004. “The RanBP2 SUMO E3 Ligase Is Neither HECT- nor RING-Type.” *Nature Structural and Molecular Biology* 11 (10): 984–91. <https://doi.org/10.1038/nsmb834>.
- Pichler, Andrea, and Frauke Melchior. 2002. “Ubiquitin-Related Modifier SUMO1 and Nucleocytoplasmic Transport.” *Traffic* 3 (6): 381–87. <https://doi.org/10.1034/j.1600-0854.2002.30601.x>.
- Poleshko, Andrey, Katelyn M. Mansfield, Caroline C. Burlingame, Mark D. Andrade, Neil R. Shah, and Richard A. Katz. 2013. “The Human Protein PRR14 Tethers Heterochromatin to the Nuclear Lamina during Interphase and Mitotic Exit.” *Cell Reports* 5 (2): 292–301. <https://doi.org/10.1016/j.celrep.2013.09.024>.
- Poleshko, Andrey, Cheryl L. Smith, Son C. Nguyen, Priya Sivaramakrishnan, Karen G. Wong, John Isaac Murray, Melike Lakadamyali, Eric F. Joyce, Rajan Jain, and Jonathan A. Epstein. 2019. “H3k9me2 Orchestrates Inheritance of Spatial Positioning of Peripheral Heterochromatin through Mitosis.” *ELife* 8: 1–24. <https://doi.org/10.7554/eLife.49278>.
- Politz, Joan C. Ritland, David Scalzo, and Mark Groudine. 2013. “Something Silent This Way Forms: The Functional Organization of the Repressive Nuclear Compartment.” *Annual Review of Cell and Developmental Biology* 29: 241–70. <https://doi.org/10.1146/annurev-cellbio-101512-122317>.
- Pomorski, T., and A. K. Menon. 2006. “Lipid Flippases and Their Biological Functions.” *Cellular and Molecular Life Sciences* 63 (24): 2908–21. <https://doi.org/10.1007/s00018-006-6167-7>.
- Potts, Patrick Ryan. 2009. “The Yin and Yang of the MMS21-SMC5/6 SUMO Ligase Complex in Homologous Recombination.” *DNA Repair* 8 (4): 499–

506. <https://doi.org/10.1016/j.dnarep.2009.01.009>.
- Powell, L., and B. Burke. 1990. "Internuclear Exchange of an Inner Nuclear Membrane Protein (P55) in Heterokaryons: In Vivo Evidence for the Interaction of P55 with the Nuclear Lamina." *Journal of Cell Biology* 111 (6 I): 2225–34. <https://doi.org/10.1083/jcb.111.6.2225>.
- Psakhye, Ivan, and Stefan Jentsch. 2012. "Protein Group Modification and Synergy in the SUMO Pathway as Exemplified in DNA Repair." *Cell* 151 (4): 807–20. <https://doi.org/10.1016/j.cell.2012.10.021>.
- Ptak, Christopher, John D. Aitchison, and Richard W. Wozniak. 2014. "The Multifunctional Nuclear Pore Complex: A Platform for Controlling Gene Expression." *Current Opinion in Cell Biology* 28 (1): 46–53. <https://doi.org/10.1016/j.ceb.2014.02.001>.
- Ptak, Christopher, Natasha O. Saik, Ashwini Premashankar, Diego L. Lapetina, John D. Aitchison, Ben Montpetit, and Richard W. Wozniak. 2021. "Phosphorylation-Dependent Mitotic SUMOylation Drives Nuclear Envelope–Chromatin Interactions." *Journal of Cell Biology* 220 (12). <https://doi.org/10.1083/jcb.202103036>.
- Ptak, Christopher, and Richard W. Wozniak. 2016. "Nucleoporins and Chromatin Metabolism." *Current Opinion in Cell Biology* 40: 153–60. <https://doi.org/10.1016/j.ceb.2016.03.024>.
- Ragoczy, Tobias, M. A. Bender, Agnes Telling, Rachel Byron, and Mark Groudine. 2006. "The Locus Control Region Is Required for Association of the Murine β -Globin Locus with Engaged Transcription Factories during Erythroid Maturation." *Genes and Development* 20 (11): 1447–57. <https://doi.org/10.1101/gad.1419506>.
- Randise-Hinchliff, Carlo, and Jason H. Brickner. 2016. "Transcription Factors Dynamically Control the Spatial Organization of the Yeast Genome." *Nucleus* 7 (4): 369–74. <https://doi.org/10.1080/19491034.2016.1212797>.
- Randise-Hinchliff, Carlo, Robert Coukos, Varun Sood, Michael Chas Sumner, Stefan Zdraljevic, Lauren Meldi Sholl, Donna Garvey Brickner, Sara Ahmed, Lauren Watchmaker, and Jason H. Brickner. 2016. "Strategies to Regulate Transcription Factor-Mediated Gene Positioning and Interchromosomal Clustering at the Nuclear Periphery." *Journal of Cell Biology* 212 (6): 633–46. <https://doi.org/10.1083/jcb.201508068>.
- Rao, Monala Jayaprakash, Malathi Srinivasan, and Ram Rajasekharan. 2018. "Cell Size Is Regulated by Phospholipids and Not by Storage Lipids in *Saccharomyces Cerevisiae*." *Current Genetics* 64 (5): 1071–87. <https://doi.org/10.1007/s00294-018-0821-0>.
- Reddy, K. L., J. M. Zullo, E. Bertolino, and H. Singh. 2008. "Transcriptional Repression Mediated by Repositioning of Genes to the Nuclear Lamina." *Nature* 452 (7184): 243–47. <https://doi.org/10.1038/nature06727>.

- Regot, Sergi, Eulàlia De Nadal, Susana Rodríguez-Navarro, Alberto González-Novo, Jorge Pérez-Fernandez, Olivier Gadal, Gerhard Seisenbacher, Gustav Ammerer, and Francesc Posas. 2013. “The Hog1 Stress-Activated Protein Kinase Targets Nucleoporins to Control Mrna Export upon Stress.” *Journal of Biological Chemistry* 288 (24): 17384–98. <https://doi.org/10.1074/jbc.M112.444042>.
- Reindle, Alison, Irina Belichenko, Gwendolyn R. Bylebyl, Xiaole L. Chen, Nishant Gandhi, and Erica S. Johnson. 2006. “Multiple Domains in Siz SUMO Ligases Contribute to Substrate Selectivity.” *Journal of Cell Science* 119 (22): 4749–57. <https://doi.org/10.1242/jcs.03243>.
- Renard, Kenta, and Bernadette Byrne. 2021. “Insights into the Role of Membrane Lipids in the Structure, Function and Regulation of Integral Membrane Proteins.” *International Journal of Molecular Sciences* 22 (16). <https://doi.org/10.3390/ijms22169026>.
- Riekhof, Wayne R., Wen I. Wu, Jennifer L. Jones, Mrinalini Nikrad, Mallory M. Chan, Christopher J.R. Loewen, and Dennis R. Voelker. 2014. “An Assembly of Proteins and Lipid Domains Regulates Transport of Phosphatidylserine to Phosphatidylserine Decarboxylase 2 in *Saccharomyces Cerevisiae*.” *Journal of Biological Chemistry* 289 (9): 5809–19. <https://doi.org/10.1074/jbc.M113.518217>.
- Rodley, C. D.M., F. Bertels, B. Jones, and J. M. O’Sullivan. 2009. “Global Identification of Yeast Chromosome Interactions Using Genome Conformation Capture.” *Fungal Genetics and Biology* 46 (11): 879–86. <https://doi.org/10.1016/j.fgb.2009.07.006>.
- Rodriguez, Manuel S., Catherine Dargemont, and Ronald T. Hay. 2001. “SUMO-1 Conjugation in Vivo Requires Both a Consensus Modification Motif and Nuclear Targeting.” *Journal of Biological Chemistry* 276 (16): 12654–59. <https://doi.org/10.1074/jbc.M009476200>.
- Rodriguez Sawicki, Luciana, Karina A. Garcia, Betina Corsico, and Natalia Scaglia. 2019. “De Novo Lipogenesis at the Mitotic Exit Is Used for Nuclear Envelope Reassembly/Expansion. Implications for Combined Chemotherapy.” *Cell Cycle* 18 (14): 1646–59. <https://doi.org/10.1080/15384101.2019.1629792>.
- Romanuska, Anete, and Alwin Köhler. 2018. “The Inner Nuclear Membrane Is a Metabolically Active Territory That Generates Nuclear Lipid Droplets.” *Cell* 174 (3): 700–715.e18. <https://doi.org/10.1016/j.cell.2018.05.047>.
- Rosonina, Emanuel, Akhi Akhter, Yimo Dou, John Babu, and Veroni S. Sri Theivakadacham. 2017. “Regulation of Transcription Factors by Sumoylation.” *Transcription* 8 (4): 220–31. <https://doi.org/10.1080/21541264.2017.1311829>.
- Rosonina, Emanuel, Sarah M. Duncan, and James L. Manley. 2010. “SUMO

- Functions in Constitutive Transcription and during Activation of Inducible Genes in Yeast.” *Genes and Development* 24 (12): 1242–52. <https://doi.org/10.1101/gad.1917910>.
- . 2012. “Sumoylation of Transcription Factor Gcn4 Facilitates Its Srb10-Mediated Clearance from Promoters in Yeast.” *Genes and Development* 26 (4): 350–55. <https://doi.org/10.1101/gad.184689.111>.
- Rout, Michael P., John D. Aitchison, Adisetyantari Suprpto, Kelly Hjertaas, Yingming Zhao, and Brian T. Chait. 2000. “The Yeast Nuclear Pore Complex: Composition, Architecture, Transport Mechanism.” *Journal of Cell Biology* 148 (4): 635–51. <https://doi.org/10.1083/jcb.148.4.635>.
- Rouvière, Jérôme O., Manuel Bulfoni, Alex Tuck, Bertrand Cosson, Frédéric Devaux, and Benoit Palancade. 2018. “A SUMO-Dependent Feedback Loop Senses and Controls the Biogenesis of Nuclear Pore Subunits.” *Nature Communications* 9 (1): 1–13. <https://doi.org/10.1038/s41467-018-03673-3>.
- Rowicka, Maga, Andrzej Kudlicki, Benjamin P. Tu, and Zbyszek Otwinowski. 2007. “High-Resolution Timing of Cell Cycle-Regulated Gene Expression.” *Proceedings of the National Academy of Sciences of the United States of America* 104 (43): 16892–97. <https://doi.org/10.1073/pnas.0706022104>.
- Ryu, Joohyun, Sayeon Cho, Byoung Chul Park, and Do Hee Lee. 2010. “Oxidative Stress-Enhanced SUMOylation and Aggregation of Ataxin-1: Implication of JNK Pathway.” *Biochemical and Biophysical Research Communications* 393 (2): 280–85. <https://doi.org/10.1016/j.bbrc.2010.01.122>.
- Sachdev, Shrikesh, Laurakay Bruhn, Heidemarie Sieber, Andrea Pichler, Frauke Melchior, and Rudolf Grosschedl. 2001. “PIASy, a Nuclear Matrix-Associated SUMO E3 Ligase, Represses LEF1 Activity by Sequestration into Nuclear Bodies.” *Genes and Development* 15 (23): 3088–3103. <https://doi.org/10.1101/gad.944801>.
- Saik, Natasha O., Nogi Park, Christopher Ptak, Neil Adames, John D. Aitchison, and Richard W. Wozniak. 2020. “Recruitment of an Activated Gene to the Yeast Nuclear Pore Complex Requires Sumoylation.” *Frontiers in Genetics* 11 (March): 1–14. <https://doi.org/10.3389/fgene.2020.00174>.
- Saitoh, Hisato, and Joseph Hinchey. 2000. “Functional Heterogeneity of Small Ubiquitin-Related Protein Modifiers SUMO-1 versus SUMO-2/3.” *Journal of Biological Chemistry* 275 (9): 6252–58. <https://doi.org/10.1074/jbc.275.9.6252>.
- Sampson, Deborah A., Min Wang, and Michael J. Matunis. 2001. “The Small Ubiquitin-like Modifier-1 (SUMO-1) Consensus Sequence Mediates Ubc9 Binding and Is Essential for SUMO-1 Modification.” *Journal of Biological Chemistry* 276 (24): 21664–69. <https://doi.org/10.1074/jbc.M100006200>.
- Santos-Rosa, Helena, Joanne Leung, Neil Grimsey, Sew Peak-Chew, and Symeon

- Siniooglou. 2005. "The Yeast Lipin Smp2 Couples Phospholipid Biosynthesis to Nuclear Membrane Growth." *EMBO Journal* 24 (11): 1931–41. <https://doi.org/10.1038/sj.emboj.7600672>.
- Scaglia, Natalia, Svitlana Tyekucheva, Giorgia Zadra, Cornelia Photopoulos, and Massimo Loda. 2014. "De Novo Fatty Acid Synthesis at the Mitotic Exit Is Required to Complete Cellular Division." *Cell Cycle* 13 (5): 859–68. <https://doi.org/10.4161/cc.27767>.
- Scherthan, Harry, Susanne Weich, Herbert Schwegler, Christa Heyting, Michael Härle, and Thomas Cremer. 1996. "Centromere and Telomere Movements during Early Meiotic Prophase of Mouse and Man Are Associated with the Onset of Chromosome Pairing." *Journal of Cell Biology* 134 (5): 1109–25. <https://doi.org/10.1083/jcb.134.5.1109>.
- Schmid, Manfred, Ghislaine Arib, Caroline Laemmli, Junichi Nishikawa, Thérèse Durussel, and Ulrich K. Laemmli. 2006. "Nup-PI: The Nucleopore-Promoter Interaction of Genes in Yeast." *Molecular Cell* 21 (3): 379–91. <https://doi.org/10.1016/j.molcel.2005.12.012>.
- Schober, Heiko, Helder Ferreira, Véronique Kalck, Lutz R. Gehlen, and Susan M. Gasser. 2009. "Yeast Telomerase and the SUN Domain Protein Mps3 Anchor Telomeres and Repress Subtelomeric Recombination." *Genes and Development* 23 (8): 928–38. <https://doi.org/10.1101/gad.1787509>.
- Schreiner, Sarah M., Peter K. Koo, Yao Zhao, Simon G.J. Mochrie, and Megan C. King. 2015. "The Tethering of Chromatin to the Nuclear Envelope Supports Nuclear Mechanics." *Nature Communications* 6. <https://doi.org/10.1038/ncomms8159>.
- Scott, Robert J., Lucas V. Cairo, David W. Van De Vosse, and Richard W. Wozniak. 2009. "The Nuclear Export Factor Xpo1p Targets Mad1p to Kinetochores in Yeast." *Journal of Cell Biology* 184 (1): 21–29. <https://doi.org/10.1083/jcb.200804098>.
- Seeber, Andrew, and Susan M. Gasser. 2017. "Chromatin Organization and Dynamics in Double-Strand Break Repair." *Current Opinion in Genetics and Development* 43: 9–16. <https://doi.org/10.1016/j.gde.2016.10.005>.
- Shetty, Ameet, and John M. Lopes. 2010. "Derepression of INO1 Transcription Requires Cooperation between the Ino2p-Ino4p Heterodimer and Cbf1p and Recruitment of the ISW2 Chromatin-Remodeling Complex." *Eukaryotic Cell* 9 (12): 1845–55. <https://doi.org/10.1128/EC.00144-10>.
- Shimi, T., V. Butin-Israeli, S. A. Adam, and R. D. Goldman. 2010. "Nuclear Lamins in Cell Regulation and Disease." *Cold Spring Harbor Symposia on Quantitative Biology* 75: 525–31. <https://doi.org/10.1101/sqb.2010.75.045>.
- Sikorski, R. S., and P. Hieter. 1989. "A System of Shuttle Vectors and Yeast Host Strains Designed for Efficient Manipulation of DNA in *Saccharomyces Cerevisiae*." *Genetics* 122 (1): 19–27.

- <https://doi.org/10.1093/genetics/122.1.19>.
- Singer, Miriam S., and Daniel E. Gottschling. 1994. "TLC1: Template RNA Component of *Saccharomyces Cerevisiae* Telomerase." *Science* 266 (5184): 404–9. <https://doi.org/10.1126/science.7545955>.
- Siniooglou, S. 1998. "A Novel Complex of Membrane Proteins Required for Formation of a Spherical Nucleus." *The EMBO Journal* 17 (22): 6449–64. <https://doi.org/10.1093/emboj/17.22.6449>.
- Smoyer, Christine J., Santharam S. Katta, Jennifer M. Gardner, Lynn Stoltz, Scott McCroskey, William D. Bradford, Melainia McClain, et al., 2016. "Analysis of Membrane Proteins Localizing to the Inner Nuclear Envelope in Living Cells." *Journal of Cell Biology* 215 (4): 575–90. <https://doi.org/10.1083/jcb.201607043>.
- Song, Jing, Linda K. Durrin, Thomas A. Wilkinson, Theodore G. Krontiris, and Yuan Chen. 2004. "Identification of a SUMO-Binding Motif That Recognizes SUMO-Modified Proteins." *Proceedings of the National Academy of Sciences of the United States of America* 101 (40): 14373–78. <https://doi.org/10.1073/pnas.0403498101>.
- Song, Jing, Ziming Zhang, Weidong Hu, and Yuan Chen. 2005. "Small Ubiquitin-like Modifier (SUMO) Recognition of a SUMO Binding Motif: A Reversal of the Bound Orientation." *Journal of Biological Chemistry* 280 (48): 40122–29. <https://doi.org/10.1074/jbc.M507059200>.
- Sorger, D., and G. Daum. 2003. "Triacylglycerol Biosynthesis in Yeast." *Applied Microbiology and Biotechnology* 61 (4): 289–99. <https://doi.org/10.1007/s00253-002-1212-4>.
- Soullam, Bruno, and Howard J. Worman. 1995. "Signals and Structural Features Involved in Integral Membrane Protein Targeting to the Inner Nuclear Membrane." *Journal of Cell Biology* 130 (1): 15–27. <https://doi.org/10.1083/jcb.130.1.15>.
- Srikumar, Tharan, Megan C. Lewicki, and Brian Raught. 2013. "A Global *S. Cerevisiae* Small Ubiquitin-Related Modifier (SUMO) System Interactome." *Molecular Systems Biology* 9 (668): 1–9. <https://doi.org/10.1038/msb.2013.23>.
- Starr, Daniel A., and Min Han. 2003. "ANChors Away: An Actin Based Mechanism of Nuclear Positioning." *Journal of Cell Science* 116 (2): 211–16. <https://doi.org/10.1242/jcs.00248>.
- Stefan, Christopher J., Andrew G. Manford, Daniel Baird, Jason Yamada-Hanff, Yuxin Mao, and Scott D. Emr. 2011. "Osh Proteins Regulate Phosphoinositide Metabolism at ER-Plasma Membrane Contact Sites." *Cell* 144 (3): 389–401. <https://doi.org/10.1016/j.cell.2010.12.034>.
- Stehmeier, Per, and Stefan Muller. 2009. "Phospho-Regulated SUMO Interaction

- Modules Connect the SUMO System to CK2 Signaling.” *Molecular Cell* 33 (3): 400–409. <https://doi.org/10.1016/j.molcel.2009.01.013>.
- Steinacher, Roland, and Primo Schär. 2005. “Functionality of Human Thymine DNA Glycosylase Requires SUMO-Regulated Changes in Protein Conformation.” *Current Biology* 15 (7): 616–23. <https://doi.org/10.1016/j.cub.2005.02.054>.
- Stellwagen, Anne E., Zara W. Haimberger, Joshua R. Veatch, and Daniel E. Gottschling. 2003. “Ku Interacts with Telomerase RNA to Promote Telomere Addition at Native and Broken Chromosome Ends.” *Genes and Development* 17 (19): 2384–95. <https://doi.org/10.1101/gad.1125903>.
- Stoops, James K., and Salih J. Wakil. 1978. “The Isolation of the Two Subunits of Yeast Fatty Acid Synthetase.” *Biochemical and Biophysical Research Communications* 84 (1): 225–31. [https://doi.org/10.1016/0006-291X\(78\)90286-3](https://doi.org/10.1016/0006-291X(78)90286-3).
- Strambio-de-Castillia, Caterina, Günter Blobel, and Michael P. Rout. 1999. “Proteins Connecting the Nuclear Pore Complex with the Nuclear Interior.” *Journal of Cell Biology* 144 (5): 839–55. <https://doi.org/10.1083/jcb.144.5.839>.
- Strambio-De-Castillia, Caterina, Mario Niepel, and Michael P. Rout. 2010. “The Nuclear Pore Complex: Bridging Nuclear Transport and Gene Regulation.” *Nature Reviews Molecular Cell Biology* 11 (7): 490–501. <https://doi.org/10.1038/nrm2928>.
- Strunnikov, Alexander V., L. Aravind, and Eugene V. Koonin. 2001. “*Saccharomyces Cerevisiae* SMT4 Encodes an Evolutionarily Conserved Protease with a Role in Chromosome Condensation Regulation.” *Genetics* 158 (1): 95–107. <https://doi.org/10.1093/genetics/158.1.95>.
- Su, Wen Min, Gil Soo Han, and George M. Carman. 2014. “Yeast Nem1-Spo7 Protein Phosphatase Activity on Pah1 Phosphatidate Phosphatase Is Specific for the Pho85-Pho80 Protein Kinase Phosphorylation Sites.” *Journal of Biological Chemistry* 289 (50): 34699–708. <https://doi.org/10.1074/jbc.M114.614883>.
- Su, Wen Min, Gil Soo Han, Prabuddha Dey, and George M. Carman. 2018. “Protein Kinase A Phosphorylates the Nem1-Spo7 Protein Phosphatase Complex That Regulates the Phosphorylation State of the Phosphatidate Phosphatase Pah1 in Yeast.” *Journal of Biological Chemistry* 293 (41): 15801–14. <https://doi.org/10.1074/jbc.RA118.005348>.
- Suka, Noriyuki, Kunheng Luo, and Michael Grunstein. 2002. “Sir2p and Sas2p Oppositely Regulate Acetylation of Yeast Histone H4 Lysine16 and Spreading of Heterochromatin.” *Nature Genetics* 32 (3): 378–83. <https://doi.org/10.1038/ng1017>.
- Sun, Huaiyu, and Tony Hunter. 2012. “Poly-Small Ubiquitin-like Modifier

- (PolySUMO)-Binding Proteins Identified through a String Search.” *Journal of Biological Chemistry* 287 (50): 42071–83. <https://doi.org/10.1074/jbc.M112.410985>.
- Suzuki, Rintaro, Heisaburo Shindo, Akira Tase, Yoshiko Kikuchi, Mitsuhiro Shimizu, and Toshimasa Yamazaki. 2009. “Solution Structures and DNA Binding Properties of the N-Terminal SAP Domains of SUMO E3 Ligases from *Saccharomyces Cerevisiae* and *Oryza Sativa*.” *Proteins: Structure, Function and Bioinformatics* 75 (2): 336–47. <https://doi.org/10.1002/prot.22243>.
- Sydorsky, Yaroslav, Tharan Srikumar, Stanley M. Jeram, Sarah Wheaton, Franco J. Vizeacoumar, Taras Makhnevych, Yolanda T. Chong, Anne-Claude Gingras, and Brian Raught. 2010. “A Novel Mechanism for SUMO System Control: Regulated Ulp1 Nucleolar Sequestration.” *Molecular and Cellular Biology* 30 (18): 4452–62. <https://doi.org/10.1128/mcb.00335-10>.
- Taddei, Angela, and Susan M. Gasser. 2004. “Multiple Pathways for Telomere Tethering: Functional Implications of Subnuclear Position for Heterochromatin Formation.” *Biochimica et Biophysica Acta - Gene Structure and Expression* 1677 (1–3): 120–28. <https://doi.org/10.1016/j.bbaexp.2003.11.014>.
- . 2012. “Structure and Function in the Budding Yeast Nucleus.” *Genetics* 192 (1): 107–29. <https://doi.org/10.1534/genetics.112.140608>.
- Taddei, Angela, Florence Hediger, Frank R. Neumaan, Christoph Bauer, and Susan M. Gasser. 2004. “Separation of Silencing from Perinuclear Anchoring Functions in Yeast Ku80, Sir4 and Esc1 Proteins.” *EMBO Journal* 23 (6): 1301–12. <https://doi.org/10.1038/sj.emboj.7600144>.
- Taddei, Angela, Griet Van Houwe, Florence Hediger, Veronique Kalck, Fabien Cubizolles, Heiko Schober, and Susan M. Gasser. 2006. “Nuclear Pore Association Confers Optimal Expression Levels for an Inducible Yeast Gene.” *Nature* 441 (7094): 774–78. <https://doi.org/10.1038/nature04845>.
- Taddei, Angela, Heiko Schober, and Susan M. Gasser. 2010. “The Budding Yeast Nucleus.” *Cold Spring Harbor Perspectives in Biology* 2 (8). <https://doi.org/10.1101/cshperspect.a000612>.
- Takahashi, Y., J. Mizoi, A. Toh-e, and Y. Kikuchi. 2000. “Yeast Ulp1, an Smt3-Specific Protease, Associates with Nucleoporins.” *Journal of Biochemistry* 128 (5): 723–25. <https://doi.org/10.1093/oxfordjournals.jbchem.a022807>.
- Takahashi, Yoshimitsu, Masayuki Iwase, Mineko Konishi, Masato Tanaka, Akio Toh-e, and Yoshiko Kikuchi. 1999. “Smt3, a SUMO-1 Homolog, Is Conjugated to Cdc3, a Component of Septin Rings at the Mother-Bud Neck in Budding Yeast.” *Biochemical and Biophysical Research Communications* 259 (3): 582–87. <https://doi.org/10.1006/bbrc.1999.0821>.
- Takahashi, Yoshimitsu, Akio Toh-e, and Yoshiko Kikuchi. 2003. “Comparative

- Analysis of Yeast PIAS-Type SUMO Ligases in Vivo and in Vitro.” *Journal of Biochemistry* 133 (4): 415–22. <https://doi.org/10.1093/jb/mvg054>.
- Tan-Wong, Sue Mei, Hashanthi D. Wijayatilake, and Nick J. Proudfoot. 2009. “Gene Loops Function to Maintain Transcriptional Memory through Interaction with the Nuclear Pore Complex.” *Genes and Development* 23 (22): 2610–24. <https://doi.org/10.1101/gad.1823209>.
- Tange, Yoshie, Aiko Hirata, and Osami Niwa. 2002. “An Evolutionarily Conserved Fission Yeast Protein, Ned1, Implicated in Normal Nuclear Morphology and Chromosome Stability, Interacts with Dis3, Pim1/RCC1 and an Essential Nucleoporin.” *Journal of Cell Science* 115 (22): 4375–85. <https://doi.org/10.1242/jcs.00135>.
- Tanny, Jason C, Gustave J Dowd, Julie Huang, Helmuth Hilz, and Danesh Moazed. 1999. “An Enzymatic Activity in the Yeast Sir2 Protein That Is Essential for Gene Silencing That Are Inserted within the Ribosomal DNA (RDNA) Re-PEATs, Suggesting That a Silencing-Based Mechanism Regulates RDNA Chromatin Structure (Bryk et al.,1997.” *Shore Und Molekularbiologie and Nasmyth* 99: 735–45.
- Tavassoli, Shabnam, Jesse T. Chao, Barry P. Young, Ruud C. Cox, William A. Prinz, Anton I.P.M. De Kroon, and Christopher J.R. Loewen. 2013. “Plasma Membrane - Endoplasmic Reticulum Contact Sites Regulate Phosphatidylcholine Synthesis.” *EMBO Reports* 14 (5): 434–40. <https://doi.org/10.1038/embor.2013.36>.
- Tei, Reika, and Jeremy M. Baskin. 2020. “Spatiotemporal Control of Phosphatidic Acid Signaling with Optogenetic, Engineered Phospholipase Ds.” *Journal of Cell Biology* 219 (3). <https://doi.org/10.1083/jcb.201907013>.
- Teixeira, M. Teresa, Milica Arneric, Peter Sperisen, and Joachim Lingner. 2004. “Telomere Length Homeostasis Is Achieved via a Switch between Telomerase- Extendible and -Nonextendible States.” *Cell* 117 (3): 323–35. [https://doi.org/10.1016/S0092-8674\(04\)00334-4](https://doi.org/10.1016/S0092-8674(04)00334-4).
- Texari, Lorane, Guennaëlle Dieppois, Patrizia Vinciguerra, Mariana Pardo Contreras, Anna Groner, Audrey Letourneau, and Françoise Stutz. 2013. “The Nuclear Pore Regulates GAL1 Gene Transcription by Controlling the Localization of the SUMO Protease Ulp1.” *Molecular Cell* 51 (6): 807–18. <https://doi.org/10.1016/j.molcel.2013.08.047>.
- Thaller, David J., Matteo Allegretti, Sapan Borah, Paolo Ronchi, Martin Beck, and C. Patrick Lusk. 2019. “An Escrt-Lem Protein Surveillance System Is Poised to Directly Monitor the Nuclear Envelope and Nuclear Transport System.” *ELife* 8: 1–36. <https://doi.org/10.7554/eLife.45284>.
- Thaller, David J, Danqing Tong, Christopher J Marklew, Nicholas R Ader, Philip J Mannino, Sapan Borah, Megan C King, Barbara Ciani, and C Patrick Lusk. 2021. “Direct Binding of ESCRT Protein Chm7 to Phosphatidic Acid – Rich

Membranes at Nuclear Envelope Herniations” 220 (3).

- Tham, Wai Hong, and Virginia A. Zakian. 2002. “Transcriptional Silencing at *Saccharomyces* Telomeres: Implications for Other Organisms.” *Oncogene* 21 (4 REV. ISS. 1): 512–21. <https://doi.org/10.1038/sj/onc/1205078>.
- Therizolsa, Pierre, Tarn Duong, Bernard Dujon, Christophe Zimmer, and Emmanuelle Fabre. 2010. “Chromosome Arm Length and Nuclear Constraints Determine the Dynamic Relationship of Yeast Subtelomeres.” *Proceedings of the National Academy of Sciences of the United States of America* 107 (5): 2025–30. <https://doi.org/10.1073/pnas.0914187107>.
- Tseng, Shun Fu, Jing Jer Lin, and Shu Chun Teng. 2006. “The Telomerase-Recruitment Domain of the Telomere Binding Protein Cdc13 Is Regulated by Mec1p/Tel1p-Dependent Phosphorylation.” *Nucleic Acids Research* 34 (21): 6327–36. <https://doi.org/10.1093/nar/gkl786>.
- Ungricht, Rosemarie, Michael Klann, Peter Horvath, and Ulrike Kutay. 2015. “Diffusion and Retention Are Major Determinants of Protein Targeting to the Inner Nuclear Membrane.” *Journal of Cell Biology* 209 (5): 687–704. <https://doi.org/10.1083/jcb.201409127>.
- Varejão, Nathalia, Jara Lascorz, Ying Li, and David Reverter. 2020. “Molecular Mechanisms in SUMO Conjugation.” *Biochemical Society Transactions* 48 (1): 123–35. <https://doi.org/10.1042/BST20190357>.
- Vosse, David W. Van De, Yakun Wan, Diego L. Lapetina, Wei Ming Chen, Jung Hsien Chiang, John D. Aitchison, and Richard W. Wozniak. 2013. “A Role for the Nucleoporin Nup170p in Chromatin Structure and Gene Silencing.” *Cell* 152 (5): 969–83. <https://doi.org/10.1016/j.cell.2013.01.049>.
- Vosse, David W. Van de, Yakun Wan, Richard W. Wozniak, and John D. Aitchison. 2011. “Role of the Nuclear Envelope in Genome Organization and Gene Expression.” *Wiley Interdisciplinary Reviews: Systems Biology and Medicine* 3 (2): 147–66. <https://doi.org/10.1002/wsbm.101>.
- Wälde, Sarah, and Ralph H. Kehlenbach. 2010. “The Part and the Whole: Functions of Nucleoporins in Nucleocytoplasmic Transport.” *Trends in Cell Biology* 20 (8): 461–69. <https://doi.org/10.1016/j.tcb.2010.05.001>.
- Walters, Alison D., Christopher K. May, Emma S. Dauster, Bertrand P. Cinquin, Elizabeth A. Smith, Xavier Robellet, Damien D’Amours, Carolyn A. Larabell, and Orna Cohen-Fix. 2014. “The Yeast Polo Kinase Cdc5 Regulates the Shape of the Mitotic Nucleus.” *Current Biology* 24 (23): 2861–67. <https://doi.org/10.1016/j.cub.2014.10.029>.
- Wan, Yakun, Ramsey A. Saleem, Alexander V. Ratushny, Oriol Roda, Jennifer J. Smith, Chan-Hsien Lin, Jung-Hsien Chiang, and John D. Aitchison. 2009. “Role of the Histone Variant H2A.Z/Htz1p in TBP Recruitment, Chromatin Dynamics, and Regulated Expression of Oleate-Responsive Genes.” *Molecular and Cellular Biology* 29 (9): 2346–58.

<https://doi.org/10.1128/mcb.01233-08>.

- Wang, Huajin, Michel Becuwe, Benjamin E. Housden, Chandramohan Chitraju, Ashley J. Porras, Morven M. Graham, Xinran N. Liu, et al., 2016. “Seipin Is Required for Converting Nascent to Mature Lipid Droplets.” *ELife* 5 (AUGUST): 1–28. <https://doi.org/10.7554/eLife.16582>.
- Wang, Renjie, Alain Kamgoue, Christophe Normand, Isabelle Léger-Silvestre, Thomas Mangeat, and Olivier Gadal. 2016. “High Resolution Microscopy Reveals the Nuclear Shape of Budding Yeast during Cell Cycle and in Various Biological States.” *Journal of Cell Science* 129 (24): 4480–95. <https://doi.org/10.1242/jcs.188250>.
- Wang, Yonggang, Debaditya Mukhopadhyay, Smita Mathew, Takashi Hasebe, Rachel A. Heimeier, Yoshiaki Azuma, Nagamalleswari Kolli, Yun Bo Shi, Keith D. Wilkinson, and Mary Dasso. 2009. “Identification and Developmental Expression of *Xenopus Laevis* SUMO Proteases.” *PLoS ONE* 4 (12). <https://doi.org/10.1371/journal.pone.0008462>.
- Weber-Boyvat, Marion, Henriikka Kentala, Johanna Lilja, Terhi Vihervaara, Raisa Hanninen, You Zhou, Johan Peränen, Tuula A. Nyman, Johanna Ivaska, and Vesa M. Olkkonen. 2015. “OSBP-Related Protein 3 (ORP3) Coupling with VAMP-Associated Protein A Regulates R-Ras Activity.” *Experimental Cell Research* 331 (2): 278–91. <https://doi.org/10.1016/j.yexcr.2014.10.019>.
- Webster, Micah T., J. Michael McCaffery, and Orna Cohen-Fix. 2010. “Vesicle Trafficking Maintains Nuclear Shape in *Saccharomyces Cerevisiae* during Membrane Proliferation.” *Journal of Cell Biology* 191 (6): 1079–88. <https://doi.org/10.1083/jcb.201006083>.
- Wilhelmsen, Kevin, Mirjam Ketema, Hoa Truong, and Arnoud Sonnenberg. 2006. “KASH-Domain Proteins in Nuclear Migration, Anchorage and Other Processes.” *Journal of Cell Science* 119 (24): 5021–29. <https://doi.org/10.1242/jcs.03295>.
- Wilson, Joshua D., Sarah L. Thompson, and Charles Barlowe. 2011. “Yet1p-Yet3p Interacts with Scs2p-Opi1p to Regulate ER Localization of the Opi1p Repressor.” *Molecular Biology of the Cell* 22 (9): 1430–39. <https://doi.org/10.1091/mbc.E10-07-0559>.
- Wilson, Van G. 2017. *Advances in Experimental Medicine and Biology - SUMO Regulation of Cellular Processes*.
- Witkin, Keren L., Yolanda Chong, Sichen Shao, Micah T. Webster, Sujoy Lahiri, Alison D. Walters, Brandon Lee, et al., 2012. “The Budding Yeast Nuclear Envelope Adjacent to the Nucleolus Serves as a Membrane Sink during Mitotic Delay.” *Current Biology* 22 (12): 1128–33. <https://doi.org/10.1016/j.cub.2012.04.022>.
- Wohlschlegel, James A., Erica S. Johnson, Steven I. Reed, and John R. Yates.

2004. "Global Analysis of Protein Sumoylation in *Saccharomyces Cerevisiae*." *Journal of Biological Chemistry* 279 (44): 45662–68. <https://doi.org/10.1074/jbc.M409203200>.
- Wykoff, Dennis D., and Erik K. O'Shea. 2005. "Identification of Sumoylated Proteins by Systematic Immunoprecipitation of the Budding Yeast Proteome." *Molecular and Cellular Proteomics* 4 (1): 73–83. <https://doi.org/10.1074/mcp.M400166-MCP200>.
- Yamaguchi, Masashi, Yuichi Namiki, Hitoshi Okada, Yuko Mori, Hiromitsu Furukawa, Jinfang Wang, Misako Ohkusu, and Susumu Kawamoto. 2011. "Structome of *Saccharomyces Cerevisiae* Determined by Freeze-Substitution and Serial Ultrathin-Sectioning Electron Microscopy." *Journal of Electron Microscopy* 60 (5): 321–35. <https://doi.org/10.1093/jmicro/dfr052>.
- Yang, Qing, Michael P. Rout, and Christopher W. Akey. 1998. "Three-Dimensional Architecture of the Isolated Yeast Nuclear Pore Complex: Functional and Evolutionary Implications." *Molecular Cell* 1 (2): 223–34. [https://doi.org/10.1016/S1097-2765\(00\)80023-4](https://doi.org/10.1016/S1097-2765(00)80023-4).
- Yang, Shen Hsi, Alex Galanis, James Witty, and Andrew D. Sharrocks. 2006. "An Extended Consensus Motif Enhances the Specificity of Substrate Modification by SUMO." *EMBO Journal* 25 (21): 5083–93. <https://doi.org/10.1038/sj.emboj.7601383>.
- Young, Barry P, John J H Shin, Rick Orij, Jesse T Chao, Shu Chen Li, Xue Li Guan, and Christopher J R Loewen. 2010. "Phosphatidic Acid Is a PH Biosensor." *Science* 329 (August): 1085–88.
- Yunus, Ali A., and Christopher D. Lima. 2009. "Structure of the Siz/PIAS SUMO E3 Ligase Siz1 and Determinants Required for SUMO Modification of PCNA." *Molecular Cell* 35 (5): 669–82. <https://doi.org/10.1016/j.molcel.2009.07.013>.
- Zhang, Yu Qian, and Kevin D. Sarge. 2008. "Sumoylation of Amyloid Precursor Protein Negatively Regulates A β Aggregate Levels." *Biochemical and Biophysical Research Communications* 374 (4): 673–78. <https://doi.org/10.1016/j.bbrc.2008.07.109>.
- Zhao, Hang, Yu Zhang, Mingming Pan, Yichen Song, Ling Bai, Yuchen Miao, Yanqin Huang, Xiaohong Zhu, and Chun Peng Song. 2019. "Dynamic Imaging of Cellular PH and Redox Homeostasis with a Genetically Encoded Dual-Functional Biosensor, PHaROS, in Yeast." *Journal of Biological Chemistry* 294 (43): 15768–80. <https://doi.org/10.1074/jbc.RA119.007557>.
- Zhao, Qi, Yubin Xie, Yueyuan Zheng, Shuai Jiang, Wenzhong Liu, Weiping Mu, Zexian Liu, Yong Zhao, Yu Xue, and Jian Ren. 2014. "GPS-SUMO: A Tool for the Prediction of Sumoylation Sites and SUMO-Interaction Motifs." *Nucleic Acids Research* 42 (W1): 325–30. <https://doi.org/10.1093/nar/gku383>.

- Zhao, Xiaolan, and Günter Blobel. 2005. "A SUMO Ligase Is Part of a Nuclear Multiprotein Complex That Affects DNA Repair and Chromosomal Organization." *Proceedings of the National Academy of Sciences of the United States of America* 102 (13): 4777–82. <https://doi.org/10.1073/pnas.0500537102>.
- Zhao, Yingming, Sung Won Kwon, Anthony Anselmo, Kiran Kaur, and Michael A. White. 2004. "Broad Spectrum Identification of Cellular Small Ubiquitin-Related Modifier (SUMO) Substrate Proteins." *Journal of Biological Chemistry* 279 (20): 20999–2. <https://doi.org/10.1074/jbc.M401541200>.
- Zheng, Xiaobin, Jiabiao Hu, Sibiao Yue, Lidya Kristiani, Miri Kim, Michael Sauria, James Taylor, Youngjo Kim, and Yixian Zheng. 2018. "Lamins Organize the Global Three-Dimensional Genome from the Nuclear Periphery." *Molecular Cell* 71 (5): 802-815.e7. <https://doi.org/10.1016/j.molcel.2018.05.017>.
- Zhou, Shanggen, Junling Si, Tong Liu, and James W. DeWille. 2008. "PIASy Represses CCAAT/Enhancer-Binding Protein δ (C/EBP δ) Transcriptional Activity by Sequestering C/EBP δ to the Nuclear Periphery." *Journal of Biological Chemistry* 283 (29): 20137–48. <https://doi.org/10.1074/jbc.M801307200>.
- Zhu, Xuefeng, and Claes M. Gustafsson. 2009. "Distinct Differences in Chromatin Structure at Subtelomeric X and Y' Elements in Budding Yeast." *PLoS ONE* 4 (7). <https://doi.org/10.1371/journal.pone.0006363>.
- Zhukovsky, Mikhail A., Angela Filograna, Alberto Luini, Daniela Corda, and Carmen Valente. 2019. "Phosphatidic Acid in Membrane Rearrangements." *FEBS Letters* 593 (17): 2428–51. <https://doi.org/10.1002/1873-3468.13563>.
- Zimmer, Christophe, and Emmanuelle Fabre. 2011. "Principles of Chromosomal Organization: Lessons from Yeast." *Journal of Cell Biology* 192 (5): 723–33. <https://doi.org/10.1083/jcb.201010058>.
- Zuleger, Nikolaj, Michael I. Robson, and Eric C. Schirmer. 2011. "The Nuclear Envelope as a Chromatin Organizer." *Nucleus* 2 (5). <https://doi.org/10.4161/nucl.2.5.17846>.